# PROGNOSTICS AND HEALTH MANAGEMENT OF LIGHT EMITTING DIODES

UNIVERSITY
*of*
GREENWICH

## THAMOTHARAMPILLAI SUTHARSSAN

A thesis submitted in partial fulfilment of the

requirement of the University of Greenwich

for the Degree of Doctor of Philosophy

September 2012

# DECLARATION

*"I certify that this work has not been accepted in substance for any degree, and is not concurrently being submitted for any degree other than that of Doctor of Philosophy being studied at the University of Greenwich. I also declare that this work is the result of my own investigations expect where otherwise identified by references and that I have not plagiarised the work of others".*

_____          _____

*Thamotharampillai Sutharssan*                    *Date*


_____          _____

*Professor Chris Bailey*                              *Date*


_____          _____

*Dr Stoyan Stoyanov*                               *Date*

Dedicated to my brother Thamotharampillai Sugeenthan.

# ACKNOWLEDGEMENTS

# ABSTRACT

Prognostics is an engineering process of diagnosing, predicting the remaining useful life and estimating the reliability of systems and products. Prognostics and Health Management (PHM) has emerged in the last decade as one of the most efficient approaches in failure prevention, reliability estimation and remaining useful life predictions of various engineering systems and products. Light Emitting Diodes (LEDs) are optoelectronic micro-devices that are now replacing traditional incandescent and fluorescent lighting, as they have many advantages including higher reliability, greater energy efficiency, long life time and faster switching speed. Even though LEDs have high reliability and long life time, manufacturers and lighting systems designers still need to assess the reliability of LED lighting systems and the failures in the LED.

This research provides both experimental and theoretical results that demonstrate the use of prognostics and health monitoring techniques for high power LEDs subjected to harsh operating conditions. Data driven, model driven and fusion prognostics approaches are developed to monitor and identify LED failures, based on the requirement for the light output power. The approaches adopted in this work are validated and can be used to assess the life of an LED lighting system after their deployment based on the power of the light output emitted. The data driven techniques are only based on monitoring selected operational and performance indicators using sensors whereas the model driven technique is based on sensor data as well as on a developed empirical model. Fusion approach is also developed using the data driven and the model driven approaches to the LED. Real-time implementation of developed approaches are also investigated and discussed.

# Contents

# List of Figures

# List of Tables

# Nomenclature

**Greek Symbols**

$\pi$     $\simeq 3.14\ldots$

**Acronyms**

$ALT$   Accelerated Life Test

$ED$    Euclidean Distance

$FMMEA$ Failure Modes, Mechanisms, and Effect Analysis

$FPGA$ Filed Programmable Gate Array

$KF$    Kalman Filter

$LED$   Light Emitting Diode

$LRKF$   Logistic Regression and Kalman Filter

$MD$    Mahalanobis Distance

$NGLIA$ Next Generation Lighting Industry Alliance

$NI$     National Instruments

$NNKF$ Neural Network and Kalman Filter

$PHM$   Prognostics and Health Management

$RUL$   Remaining Useful Lifetime

# Chapter 1

# Introduction

Prognostic and health management (PHM) is a process of diagnosing, predicting the remaining useful lifetime (RUL) and estimating the reliability of systems and products. PHM has emerged in the last decade as one of the most efficient processes in failure prevention, predicting engineering reliability and useful life time of various engineering systems and products. Prognostics of engineering systems and products have become very important as malfunction or failure may cause severe damage to the system, environment and users, and may result in significant costly repairs. Prognostics process depends on the continuous monitoring of the key performance parameters and detecting anomalies in their "normal" values. It will be more accurate if the parameters are monitored in real-time, especially in the case of safety critical and emergency applications.

Modern engineering systems and products increasingly depend on some sort of electronics such as control systems, sensors, communications, etc. These electronic components play a crucial role to control, monitor and interact. For example a modern automotive car uses engine control unit (ECU) which is a microprocessor and software, for its main operations such as ignition timing, fuel control, engine oil management, etc. Some systems such as modern aircraft is completely dependent on electronics for every single operation (i.e., engine control, autopilot, environmental monitoring, landing gear, etc.,). Malfunctions, failures, and reliability of any individual electronic hardware and software components independently affect the systems and product as a whole. Hence it is important to assess reliability of these individual electronic components to ensure the safety of

the operation and increase the maintainability of the systems and products.

Traditional critical systems used a special device called fail-safe components to protect the systems and personnel from a failure. Some critical systems such as avionic systems and computer servers use redundant systems to continue the normal operation in the event of failures. This increases the reliability and survivability of the system. But the growing demand for high reliability, survivability and maintainability, and shortage of skilled labours lead to the development of fault-tolerant control (FTC) systems and PHM which is a proactive FTC system [19; 20; 21]. In addition, increasing sophistication and multi-mode functionality of many units that limit the usefulness of the functional trouble shooting, provisions for output regulation that prevent observation of the decreasing performance and hardware/software interaction are other motivating factors for the development of PHM for electronic systems [20; 21]. As the complexity of electronics increases, maintenance workload, required skill level for troubleshooting, and maintenance cost will increase. PHM can help to reduce the maintenance requirement and convert the need for unscheduled maintenance into a predictable and controllable activity [20; 21].

## 1.1 Research Motivation

Compared to the traditional light sources, applications of high power light emitting diodes (LED) lighting systems are continuously increasing as they have many advantages including high reliability, greater energy efficiency, long lifetime, small in size, no mercury and faster switching speed. Even though high power LEDs have high reliability and long life time, manufacturers and lighting systems designers still need to assess the reliability of LED lighting systems and the failures in the LED. This is very important with respect to the maintainability of the LED lighting systems after their deployments. In particular assessing the reliability of the LED lighting systems which are used for safety critical and emergency applications is a requirement to ensure the light output meets the standards all the time. In this case, lighting systems designers and users face challenges in assessing the quality of the light of high power LEDs subjected to harsh operating conditions such as high and low temperature, etc.

One of the main challenges is measuring optical characteristics of LEDs which directly indicates the failure of the high power LEDs (i.e., luminance and chromaticity). This is very difficult in the field and prevents accurate assessment of the reliability and estimation of the remaining useful lifetime of the high power LEDs after it is deployed. However the identification of failure precursors, which are driving the failure and degradation in the light output, is possible. Electrical characteristics can be used to estimate or predict the light output power of an LED lighting system as there is a close correlation between degradation of the light output power and degradation of electrical characteristics [22]. Sensors are available to monitor these parameters in real-time and therefore assessing the reliability and estimating the remaining useful lifetime are possible using appropriate PHM tools and approaches. Hence developing a real-time health monitoring system for high power LEDs improve the overall quality of the lighting systems and improve the lifetime. In addition to the overall reliability and remaining useful lifetime (RUL) estimation, PHM approach to the high power LEDs will enable to issue advance failure warnings, provide fault detection capability, avoid unscheduled maintenance via evidence based scheduled maintenance, and help to improve future designs.

Environmental conditions such as high and low temperature affect electrical and optical properties of the LEDs [23]. It implies that environmental conditions have direct impact on the reliability and lifetime of an LED lighting systems. This makes huge impact on the lifetime and reliability of the LED lighting systems which are used in many different temperature ranges such as aircraft exterior lighting systems, automobile lighting systems etc. Assessing the reliability and predicting the reliability of such LED systems needs real-time monitoring of the LED electrical characteristics.

## 1.2 Problem Description

LED lighting systems are identified as the future lighting source because of its several advantages. Although the lifetime of the LED light sources is very high, typical lifetime is 50000 hours (approximately 11.5 years for a 50% calendar time usage), half of the LED light sources will fail before that period and half of the LED light sources will operate well over that period. It is observed that the failed LED light sources continue to emit light but their light output goes below a required level after a certain period. Research shows how different commercial LEDs performed under similar operating conditions [24]. Six arrays of white LED packages form different manufacturers were tested under their rated conditions (350 mA drive current and 35°C ambient temperature) and results showed that the different commercial white LEDs degrade at different rates hence demonstrated different life values [24]. These behaviours of the LED light sources indicate the difficulties in assessing and maintaining LED lighting systems particularly in the case of safety critical, emergency and harsh environment applications. Main problems identified for the LED health monitoring and maintenance are as follows:

1. Light sensors are required to identify the failures in the LED lighting systems hence labour and additional equipment are required for the maintenance;

2. Lumen degradation of the LED lighting systems cannot be represented by a specific model;

3. Colour shift of the LED lighting systems cannot be represented by a specific model;

4. Although LED engine exhibited very long lifetime with high reliability, LED lighting systems have significantly less lifetime and less reliability since the LED lighting systems reliability depends on components such as power supply and driver, and housing;

5. Placing a light sensor inside the luminaries to monitor the luminance or colour shift (i.e., chromaticity) is difficult.

## 1.3  Objectives of the Research

Primary objective of this research is to develop a real-time PHM approach to assess the reliability and predict the failures and remaining useful lifetime (RUL) of a LED light source in the field after their deployment. Develop a real-time PHM approach for the LED following research objective is identified:

1. Develop a methodology for accelerated life test (ALT) – Since LED packages have very long lifetime, it is useful to have accelerated testing methodology which can be used to test the LED degradation within a short period of time. ALT can also be used to test the developed PHM approaches and their capabilities under developed accelerated conditions. ALT can also be used to provide failure data for the development of the PHM approaches.

2. Develop data driven approach – Data driven approach can be easily developed without having any specific knowledge about the product or systems although they do require certain failure data. In addition, data driven approach can be easily implemented in low cost microcontroller based real-time systems to monitor the health of LEDs.

3. Develop model driven approach – Although it is difficult to establish a mathematical model to represent the light degradation, some of the p-n characteristics can be derived from the first principle or from the empirical data sets. The model represents the p-n junction characteristics which can be used to assess the p-n junction for any anomalies and hence can be used to monitor the health or assess the reliability of the LEDs.

4. Develop fusion approach – Fusion approach can be used to incorporate remaining useful lifetime (RUL) predictions from data driven and model driven approaches. This will improve the overall performance of the PHM approach.

5. Validate the developed approaches – Further similar ALT tests can be carried out to collect the data for validate the developed techniques. These test data can be used to validate the developed approaches for LED prognostics and health monitoring.

6. Compare the developed techniques for LED health monitoring and identify the suitable approach for LED health monitoring application.

7. Investigate the implementation strategies in different real-time hardware platforms. For this work LabVIEW real-time platform and LabVIEW FPGA platform can be used to investigate the implementation strategies.

## 1.4   Novelty and Contribution

The proposed real-time PHM approaches will provide robust assessment of the reliability and predict the failures and remaining useful lifetime (RUL) for LEDs based on the sensor data. Thesis presents novel approaches that can be used in real-time health monitoring and RUL prediction applications for LED packages and products. Some of the main novelties and contributions are:

1. Strategy for LED life test under accelerated voltage condition is investigated. Accelerated voltage test is used to provide data for the PHM approach development, testing and validation. Two different accelerated voltage tests are investigated:

    (a) Forward voltage is increased in steps from typical minimum voltage to typical maximum voltage;

    (b) Forward voltage is kept constant at the typical maximum voltage.

    Accelerated voltage test is used to elevate forward current and junction temperature which are key damaging parameters of the LED.

2. A novel methodology based on distance measure techniques for data driven PHM approach for LEDs is investigated under the accelerated voltage condition. Diagnostics and prognostics capability of two distance metrics:

    (a) Euclidean; and

    (b) Mahalanobis Distance;

    have been investigated and a comparative analysis on their performance is undertaken. Diagnostics and prognostics parameters are developed for

distance measure techniques based on developed accelerated test conditions. Primary advantage of the developed distance metrics based approach is that they can be implemented using low cost microcontrollers with minor/no modifications for LED health monitoring. In addition, distance metrics can reduce the higher dimensional data into one dimensional value which can be easily monitored and used for PHM purposes.

3. Logistic regression and Kalman filter (LRKF) is investigated for the real-time health monitoring of LED packages and products. None of the current data driven approach uses both logistic regression and Kalman filter for data driven PHM approach of electronic systems or products. Compared to other existing techniques, proposed LRKF approach not only uses range of monitoring parameters that can indicate degradation or failures but also makes very accurate consistence predictions. Primary disadvantage of this approach is that the logistic function needs to be approximated in order to be implemented in a microcontroller based real-time system.

4. A novel approach based on neural network and Kalman filter (NNKF) is investigated for the real-time PHM of the LED packages and products. This approach makes similar prediction as the LRKF approach. Single hidden layer with two hidden neuron is investigated in this work and it is obvious NN can be further developed by increasing the neurons and hidden layers. Primary advantage of this approach is that activation functions for the NN can be selected as linear or logistic functions. Linear activation function NN can be more suitable for the microcontroller based real-time health monitoring systems for LED packages and products.

5. An empirical model driven approach is investigated for the health monitoring of the LEDs. Diagnostics and prognostics capability of the developed empirical model shows empirical model can be used to predict the system behaviour and hence use to monitor the health. The main advantage of the investigated empirical model is that it can be easily programmed into a low cost microcontroller based real-time monitoring system.

6. LED accelerated voltage test data is used to evaluate the developed ap-

proach. This thesis also gives a comparative study of different novel approaches developed for the real-time PHM of other electronic systems or products.

## 1.5 Outcome and Impact

Increasing use of LED packages and products for the lighting applications and uncertainty of their failures identification make the manufacturers and lighting system designers difficult to design and maintain reliable LED lighting systems. In particular lighting systems used in safety and emergency applications and lighting systems used under harsh environmental conditions. Undertaken research proposes a real-time health monitoring and prognostics system for LED packages based on different approaches. In addition, undertaken research proposes an accelerated voltage test to collect the data to train, validate and test the developed approaches for LED health monitoring. This research allows manufacturers and lighting system designers to enhance their design by embedding temperature and current sensors, and real-time health monitoring and prognostics component with LED driver to monitor the health of LED packages and products. The following papers have been published as a result of the undertaken research programme:

1. Sutharssan, T.; Stoyanov, S.; Bailey, C.; Rosunally, Y.; 'Data Analysis Techniques for Real-Time Prognostics and Health Management of Semiconductor Devices', in Proceeding of 18th European Microelectronics and Packaging Conference (EMPC), Brighton, UK, 12-15 September 2011

2. Sutharssan, T.; Bailey, C.; Stoyanov, S.; Rosunally, Y.; 'Prognostics and Reliability Assessment of Light Emitting Diode Packaging', in Proceeding of 12th International Conference on Electronic Packaging Technology and High Density Packaging (ICEPT-HDP), Shanghai, China, 8-11 August 2011

3. Sutharssan, T.; Stoyanov, S.; Bailey, C.; Rosunally, Y.; 'Prognostics and Health Monitoring of High Power LEDs', Micromachines 2012, 3, 78-100

4. Sutharssan, T.; Bailey, C.; Stoyanov, S.; 'A Comparison Study of the Prognostics Approaches to Light Emitting Diodes under Accelerated Ageing',

in Proceeding of 13th International Conference on Thermal, Mechanical, and Multi-Physics Simulation and Experiments in Microelectronics and Microsystems, Lisbon, Portugal, 16-18 April, 2012

## 1.6    Structure of the Thesis

This thesis is organised into 9 chapters. Literature reviews of prognostics and health management approaches, real-time PHM, PHM applications for high power light emitting diodes, and accelerates life test for LEDs are given in chapter 2. Review of PHM is based on three main approaches and related work carried out under each approach is discussed in this chapter. Work carried out based on real-time aspect is discussed under real-time PHM. Only few researches reported in LED prognostics and most of the suitable publications and the outcomes are presented under PHM for high power light emitting diodes. Reported accelerated life tests for LEDs are also discussed in this chapter.

Chapter 3 presents the development of the high power light emitting diodes, their market growths, applications, LED lamp configurations, lifetime, and failure modes and mechanisms.

Detail review of algorithms for PHM approaches is presented in chapter 4. Review is presented under three different approaches for PHM. Statistical and machine learning algorithms are investigated and presented in under data driven approach. System models and physics of failure models are investigated and presented under model driven approach. Methodologies for fusion approach is also investigated and presented.

In chapter 5 proposed approaches to the high power white LED light source are given. Identification of the failure precursors using the failure mode and three different approaches to the real-time PHM of the LED are explained.

Accelerated life test is selected as the testing methodology to collect the data for this research. Detailed explanation of the accelerated life test, experimental setup and data collections under two different testing conditions (normal and accelerated) are given under chapter 6.

Chapter 7 discusses the results with validation examples for each approach. Real-time implementation of the developed approaches are discussed and ex-

plained in chapter 8 using National Instruments PXI systems as the real-time platform and LabVIEW FPGA. Conclusion and future work direction of this work are discussed in chapter 9.

# Chapter 2

# Literature Review

## 2.1 Introduction

A review of Prognostics and Health Management (PHM) and real-time PHM, and review of PHM application to high power LEDs are given here. This chapter is organised into four sections. Second section describes the development of the PHM technology and general overview of the researches carried out in the field of PHM connected to many different fields and applications. Based on the approaches to PHM technology, PHM is divided into three different categories and literature reviews were also done based on these approaches. Third section describes the work carried out related to the real-time aspect of the diagnostics, prognostics and health management. Fourth section describes the research carried out with regard to LED reliability assessment and application of the PHM technology to high power light emitting diodes.

## 2.2 Prognostics and Health Management (PHM)

### 2.2.1 Data Driven Approach

Prognostics and health management is a technology used to monitor degradation in engineering systems, understand when failure may occur, and provide a cost effective strategy for scheduled maintenance. Prognostics and health management of engineering systems or products has become very important as failures

may cause severe damage to the system, environment and users, and may result in significant costly repairs. Adopting PHM techniques require continuous monitoring of key performance parameters and detecting any anomalies in these parameters. There are three different approaches to PHM applications and numerous researches have been carried out for many different systems, products and in many different fields. Three different approaches to PHM system are:

1. Data driven approach

2. Model driven approach

3. Fusion approach

Concept of PHM was initially developed to monitor failures and diagnose the cause of failures in the safety critical systems. Nowadays it has become an essential part of many different systems and products. Numerous research papers have been published and numerous applications have been developed on PHM technology. Most of the real PHM applications use fusion approach as they are based on both data driven and model driven approaches i.e., generally data driven approach is used to predict the anomalies and then combined with model driven technique to predict the life time. However this review is divided into three sections based on PHM approaches. Selected suitable publications are used for the literature reviews of the different approaches.

## 2.2.2   Data Driven Prognostics Approach

Since data driven approach has many advantages: it is easy to implement, it does not require systems specific knowledge, considerably cheap, etc., many PHM research studies carried out are based on data driven approach. There are many data driven techniques available and some of the research work carried out based on different data driven techniques are reviewed for this thesis.

Data driven approach is used to detect the anomalies, diagnose the failures and estimate the remaining useful lifetime (RUL) using historical data and operational data. Most of the existing data driven PHM applications use the extent of deviation or degradation from its expected typical operating performance as the

health measure [25] or failure precursors [26]. Health measure or failure precursor is a parameter which used to indicate the state of the system. By monitoring operating performance data, degradation from the normal operating performance can be estimated. This helps to issue early warning of failures, forecast necessary maintenance, avoid scheduled maintenance and extend maintenance cycles, assess the potential life extensions, reduce the amount of redundancy, provide guidance for system re-configuration and self-healing, provide efficient fault detection and identification, and improve future designs and qualification methods [25].

Anomaly detection in any operational performance data is the first step in the diagnostics and failure prognostics. Most of the anomaly detection techniques use the sensor data collected from the system or product. An anomaly detection technique has been developed in the case of absence of unhealthy data and based on one class (healthy data) support vector machine (SVM) [27]. It is called $CALCE_{SVM}$ and it was used to test and validate the result. Lockheed Martin server data and another simulated correlated data set, consisting of three random variables were used to test the developed $CALCE_{SVM}$. Results were compared with the open source SVM software $LibSVM$ which is developed by Chih-Chung Chang and Chih-Jen Lin [27]. For both data sets (i.e. Lockheed Martin server data which is real data and the simulated data set), $CALCE_{SVM}$ performed better than the $LibSVM$. $CALCE_{SVM}$ novelty anomaly detection capabilities are limited and it depends on user specified threshold value if the number of training samples are too small and the choice of the decomposition detail [27].

Celaya et al., presented an accelerated life testing system for Power MOS-FETs[1] under power cycling to induce the die-attach degradation due to thermal over stress [28]. Drain to source ON-resistance ($R_{DS(on)}$) was established as a precursor for the die-attach failure mechanism. It was established that the $R_{DS(on)}$ and the junction temperature has a quadratic relationship and $R_{DS(on)}$ is proportional to the damage magnitude of the device. Hence junction temperature could be used for a data driven prognostics approach for an in-situ health monitoring of the power MOSFETs [26]. Using collected data for the ON-resistance ($R_{DS(on)}$) data driven approach based on Gaussian Process Regression (GPR) was developed and compared with model driven approach. Although the GPR approach

---

[1]Metal oxide semiconductor field effect transistors

does not have the benefit of a model for the degradation, the prediction made by GPR approach becomes more accurate at a considerably later time compared with model driven techniques [28].

A comparison study of three different data driven techniques were discussed using a set of time series data obtained from rotating equipment in an aerospace setting [29]. Relevance Vector Machine (RVM) which is a Bayesian treatment of Support Vector Machine (SVM), Gaussian Process Regression (GPR) and Neural Network (NN) were studied in this work and reported by Goebel et al. Although the general prediction accuracy was within the acceptable limit, remaining useful lifetime estimations varied considerably. Unstable prediction resulted due to the sensitivity to state estimation in the NN approach and due to sensitivity to training coherence in the RVM approach [29].

Many of the existing data driven prognostics systems were developed based on the Artificial Neural Network (ANN) [30; 31]. Roy and Ganguli developed and analysed neural network filters to reduce the noise in the health monitoring signals [32]. A weighted recursive median (WRM) filter and a radial basis function (RBF) neural network filter were developed and tested for helicopter rotor blade damage detection. 54-76% and 59-75% noise reduction were achieved by the optimally WRM filter and RBF neural network filter, respectively. Performances were compared with unweighted recursive median filter and finite impulse response (FIR) filter, and established that much better performances were achieved by the developed WRM and RBF filters based on soft computing methods [32].

Sohn et al., presented a novelty detection technique for computer hard disk under changing environmental and operational conditions based on auto-associative neural network [33]. Technique is demonstrated using a simplified computer hard disk model from MathWorks. From the simplified computer hard disk model, discrete transfer function of the model was obtained using Laplace transformation and discretising the continuous transfer function. The auto-associative neural network was trained using coefficients of the discrete transfer function of the computer hard disk model under different environmental and operational conditions. Novelty index (NI) was defined as the distance between the target output and output of the auto-associative neural network. Although no threshold values were presented in the paper and several issues needed to be addressed, the presented

work demonstrated some progress in the anomaly detection under changing environmental and operational conditions using proposed novelty index (NI) and auto-associative neural network [33].

A systematic data driven approach using the knowledge from the signal processing and statistical domain had been developed to detect and diagnose the faults in automotive engines [34; 35]. Experiment was conducted and data for five different faults under various operating conditions was collected from the engine. This data was used to test the applicability of the data driven diagnostic approach. This approach had been applied to a Toyota Camry engine with manual transmission and experimental result has been reported [34; 35].

Degree of randomness (DoR) measure and Laplace test were used to develop a diagnostics and prognostics method for roller bearing based on the vibration signal [36]. Shannon entropy was used to estimate the DoR. Any trends associated with the estimated DoR was demonstrated as the abnormal event in the systems. Laplace test statistic was applied to the abnormal event detected from the DoF estimate to predict the failure of the roller bearing systems. Roller bearing data from the NASA prognostic data repository was used to test the approach. Predicted result illustrated that the proposed approach can predict the failures 10 days before they occur [36].

### 2.2.3 Model Driven Prognostics Approach

The model driven prognostics approach is based on accurate mathematical models. It is used in many different applications where the system model can be derived from first principles or an empirical model represents the system dynamics and damage accumulation. Such models can be determined from test data. Numerous papers have been published based on the model driven technique for PHM [28; 37; 38; 39; 40]. Luo et al., presented a step by step approach to develop a model driven prognostics technique for an automotive suspension system adopted from a half-car two degree of freedom model [41; 42]. The system models were simulated with a standard 4th order variable-step-size Runge-Kutta algorithm and Monte-Carlo algorithm for three different road conditions. Simulated results presented in the paper showed that fair and very good road conditions

produced 35% and 80% increase in the life time compared to the severe road conditions. Expected life of a suspension for a 10% calendar time usage under severe, fair and good road conditions were estimated at 4.5, 6 and 8 years, respectively. An interacting multiple model (IMM) estimator was used to estimate the degradation measure and the time-averaged mode probabilities were used to predict the remaining useful lifetime of the automotive suspension system with a drifting parameter. Accuracy of this model was not reported. It was reported however that the implementation of this model in a real automotive suspension system would be achieved in the future [41; 42].

Vichare et al., monitored following parameters of a notebook to develop a model driven PHM techniques for the notebook computer based on thermal loads [25]: central processing unit (CPU) heat sink temperature; hard disk drive (HDD) temperature; ambient temperature; percentage of CPU utilised; and fan condition (on/off). The absolute temperature data then processed by 3-parameter Rainflow Counting method to identify the complete and half cycles, amplitude, mean temperature and ramp rate of each cycle. Collected data and stress and damage models were used to estimate the degradation and remaining useful lifetime of the notebook computer. Data reduction and load parameter extraction algorithms were used to utilise the less on-board storage and power consumption. More than 90% data reduction produced less than 1% error in damage accumulation in the notebook in-situ health monitoring [25]. Details of the stress and damage model were not discussed in the paper. Accuracy of this in-situ health monitoring based on model driven approach was not reported in the publication.

Saha et al., developed a framework for estimating the remaining useful lifetime (RUL) of batteries based on an empirical model [43]. Battery model was adopted from a lumped parameter model of a battery cell. Batteries internal parameters of the battery model were estimated from the sensor data comprising of voltage, current, power, impedance electro-chemical impedance spectrometry (EIS), frequency and temperature readings and applying relevance vector machine (RVM) regression. Estimated parameters then fed into extended Kalman filter (EKF) and particle filter (PF) algorithms to estimate the remaining useful lifetime of lithium-ion battery. In the case of EKF, constant model parameters were considered throughout the estimation. In the case of PF, constant model parameters

were incorporated with the internal battery parameters as components of the state vector and values learned from the RVM were used as the initial values for the constant model parameters. A purely data driven technique Autoregressive integrated moving average (ARIMA) was also studied based on the capacity of the battery which is derived from the sensor data. The Bayesian statistical approach, RVM-PF framework demonstrated significant advantage over both ARIMA and EKF [43].

Celaya et al., presented an empirical model based prognostics approach to electrolytic capacitors based on electrical overstress accelerated aging [44]. Empirical degradation process model for the capacitor was developed from the percentage loss in the capacitance. The percentage loss in the capacitance established as the precursor of the failure from the lumped parameter model for a real capacitor and the frequency response of the capacitor impedance measured with electro-impedance spectroscopy. Constant model parameters were estimated from the accelerated aging experiments. A nonlinear least-square regression algorithm was used to estimate the model parameters from the test data for five different capacitors. The model description then fed into the Kalman filter framework to predict the remaining useful lifetime (RUL) of the capacitor. The results presented in the paper were based on the accelerated life time conditions and on the accelerated life timescale and RUL prediction were within the acceptable limit [44].

### 2.2.4 Fusion Approach

Many of the real world prognostics system are based on fusion approach. Fusion approach is the combination of both data driven and model driven approaches. Typical sensor PHM systems use data driven approach as a first level of anomaly detection based on the sensor data and then use both model and data driven approaches to predict the remaining useful lifetime.

Cheng and Pecht developed a step by step approach to implement the fusion prognostics approach to multilayer ceramic capacitors (MLCCs) [45]. Failure modes, mechanisms, and effect analysis (FMMEA) was used to identify the failure precursors of the MLCCs. Insulation resistance was established as the main failure precursors based on the silver migration and overall degradation of the

dielectric of MLCCs as both caused a lowering of insulation resistance. Capacitance and dissipation factor of the MLCCs were also monitored based on the function of the capacitor. Multivariate state estimation technique (MSET) was used to estimate values for each monitored parameter (i.e. insulation resistance, capacitance and dissipation factor) and residual was calculated from the estimated values and observed values. Statistical probability ratio test (SPRT) was used to detect the anomalies in the calculated residuals. When an anomaly was detected, RUL was estimated. Physics of failure approach was used to identify the failure mechanisms and data driven approach was used to detect the anomalies in the residual. Linear extrapolation technique was used to estimate the RUL and reasonable prediction was made [45].

A fusion approach for insulated gate bipolar transistors (IGBTs) was presented by Nishad et al. FMMEA analysis was performed to identify the failure precursors [46]. IGBT threshold voltage ($V_{GE(th)}$), transconductance ($g_m$) and gate leakage current ($I_{ge}$) were established as the failure precursors for the dielectric breakdown and hot electron failure mechanisms. Collector-emitter saturation current ($I_{CES}$) and collector-emitter ON voltage ($V_{CE(ON)}$) were established as the failure precursors for the latch-up failure mechanism. Collector-emitter ON voltage ($V_{CE(ON)}$) was established as the failure precursors for the failures related to the wire bond flexure and solder die attach. Physics of failure models for time dependent dielectric breakdown and solder die attach fatigue model were developed. Rainflow counting method was used to analyse the loading profile and output of the analysis was used to predict the remaining life in real-time. Data driven approach was proposed based on trending of the collector-emitter ON voltage ($V_{CE(ON)}$) drop to failure threshold. Fusion approach was proposed in the paper based on discussed physics of failure models and data driven approach [46].

Xu and Xu proposed a fusion based PHM approach for avionic systems. Fusion approach was developed from an optimal linear combination forecast model and three different approaches were used to predict the remaining useful lifetime of the avionic systems. Data driven, model driven and knowledge based approaches were used as the baseline prognostics approaches. Fusion approach was developed based on avionic systems conceptual health management architecture and under the post flight condition. RUL estimation was achieved through the following

step by step approach [47].

1. Parameter selection

2. In-situ monitoring and data acquisition

3. Threshold creation

4. Health assessment

5. Parameter isolation

6. Diagnostics and failure definition

7. Prognostics and fusion

Autoregressive moving average (ARMA), support vector machine (SVM) and fuzzy neural network (FNN) were used to represent the three approaches. A case study was carried out based on the collected time to failure data values of fifty avionic radar magnetrons. Comparison study was made between individual approaches as well as fusion approach based on prediction error indexes such as sum of squared error (SSE), mean square error (MSE), mean absolute error (MAE), mean absolute percentage error (MAPE) and mean squared percentage error (MSPE). Predictions based on the fusion approach were improved significantly and all the prediction error index measures indicated better values for fusion approach compared with individual approach. Detail explanations of model developments for baseline approaches (i.e. model driven, data driven and knowledge based) were not given in the paper [47].

## 2.3 Real-Time Prognostics and Health Management

Real-time prognostics and health management are used to predict the remaining useful lifetime in real-time using in-situ sensors for health monitoring. Most of the safety critical and mission critical systems have some sort of health monitoring systems based on sensors and will be able to issue early warnings, predict

and diagnose the failures in advance. For example modern cars have on-board health monitoring systems to monitor the health and reliability of the various components using sensor data.

A neural network real-time predictive maintenance system was developed by Bansal et al. Experiment was carried out to collect motion signatures to classify five distinct motor loads [48]. Five readings of motion signatures were collected for a unique configuration. The p-gain (proportional gain) and i-gain (integral gain) were used to change the configurations. Altogether 5000 readings were collected with a sample size of 900. Collected data grouped into training data (1/2 patterns), validation data (1/6 patterns) and testing data (1/3 pattern). These group data were then normalised to zero mean and unit variance. Based on the principal component analysis (PCA), neural network with 14 inputs, 15 hidden units and 5 outputs was selected. The confusion matrix which is used as an evaluation tool, showed 97.59% of the test data classified correctly. Implementation of this approach or real-time system requirements (i.e. CPU or microcontroller) for the implementation was not discussed in the paper [48].

Raptis and Vachtsevanos developed an adaptive particle filtering framework for real-time fault diagnosis and failure prognostics of environmental control systems [49]. Evaporator modelling was carried out based on mass balance and energy balance equations. Refrigerant leakage model was developed based on the mass flow rate at the crack surface. Particle filter (PF) algorithm was selected and non-linear time growth model (i.e. refrigerant leakage model) was implemented using PF to predict the expected leaked mass flow rate. A prognostic of the environmental control system was achieved through recursive Bayesian estimation techniques from the information for fault growth model and real-time data from the sensors. This approach was tested with numerical simulations and result showed this approach provided very accurate estimate of the fault progression, crack growth and RUL prediction. A real-time systems requirement to implement this approach was not discussed in the paper [49].

Health monitoring approach for lithium-ion batteries in the electrical vehicles was developed based on on-board internal resistance estimation by Remmlinger et al. Data collected from inner-city driving of a hybrid vehicle was analysed for degradation index [50]. Suitable features were selected as degradation index

for the lithium-ion batteries. These features were then used to test the batteries in a laboratory battery testing system inside a climate chamber to control the environmental temperature from -20°C to 50°C. A battery model also adopted from the general equivalent circuit of a battery and internal resistance values were identified for several different temperatures with reference current pulse excitation. Processing power and the memory capacity of the engine control unit (ECU) were considered as limiting factors for deciding the algorithm to estimate the internal resistance. Regressive formulation of the linear least square algorithm was used to estimate the internal resistance [50].

Prognostic of ball grid array (BGA) is a hot topic of research as the use of BGA is increasing as they have many advantages which include lead free and smaller in size, and modern electronic design requires high reliability, less package size and small interconnection height. Particularly, in-situ monitoring and built in test (BIT) were discussed in recent publications. Voutilainen et al., proposed a prognostic method for embedded health monitoring of BGA interconnections with 1149.4 test bus architecture [51]. Test modules (15mm x 15mm) with 9x9 matrix and 1.5mm pitch were fabricated using standard multilayer low-temperature co-fired ceramic (LTCC) processing with thick-film screen-printed conductors. These ceramic BGA modules were attached on a FR-4[1] printed circuit board (PCB). A measurement system was developed using traditional Wheatstone bridge measurement technique. Prognostics corner balls, centre ground ball, and external resistors (100) were together used to build an embedded measurement circuit for in-situ monitoring. Thermal cycling test (TCT) was carried out using the temperature range of -40°C to 125°C, one cycle per hour, with a ramp rate of 11°C/min. DC voltage was applied to the embedded circuit and voltage measurement was performed in every 3 min using a data logger. During the thermal cycling break electrical measurements were performed using a IEEE 1149.4[2] compliant component. Unbalancing voltage reading was observed and due to crack in a corner ball. This unbalance voltage level was increasing as the corner ball crack was increasing with the thermal cycling process. Such an unbalance was established as the

---

[1]A grade designation assigned to glass-reinforced epoxy laminate sheets, tubes, rods and printed circuit boards

[2]An IEEE standard for mixed-signal test bus

precursor of the solder interconnect breakdown. Scanning acoustic microscopy and X-ray measurements were also made in addition to the in situ monitoring. Solder interconnect breakdown was observed with developed approach well earlier than the actual breakdown occurred [51].

## 2.4   PHM for High Power Light Emitting Diodes (LEDs)

Even though typical life time of a high light emitting diode (LED) is very high, typically specified in the order of 50000 hours, statistics show that half of the light emitting diodes fail before this limit is reached. The reason for this is that this specification is not based on individually measured characteristics of LEDs. Therefore, manufacturers and lighting system designers still need to monitor the health of assembled LEDs and predict their failures, especially for safety emergency critical applications in sectors such as aerospace, medical, energy and others.

Numerous papers have been published that characterise the reliability and thermal behaviour of LEDs [24; 52; 53; 54; 55; 56; 57; 58; 59; 60]. Recent publications have detailed the importance of temperature on the reliability of LEDs and the need for suitable packaging to ensure that appropriate heat is extracted [24]. Physics of Failure Models for high power LEDs have also been developed where thermomechanical models have been used to characterise a number of failure modes [61]. At present there is no reported work on real-time monitoring of LED degradation and the use of data driven or physics of failure or fusion models to predict degradation and remaining useful life of the LEDs in real-time. And there are few high temperature (or accelerated) LED tests [23; 62], some accelerated humidity test [63], some accelerated humidity and accelerated temperature test [64] and some accelerated electrical stress based on DC and DC pulsed [65; 66] were reported in the literature. But there are no work reported on accelerated life test for LED packaging based both on current (electrical overstress) and temperature (thermal overstress).

List of recommendations were developed to assess the LED lifetime for general

lighting by the Alliance of Solid-State Illumination Systems and Technologies (ASSIST) [58]. LED lifetime was defined based on two performance criteria:

1. $L_{70\%}$ – Time to 70% lumen maintenance (i.e., 30% depreciation in the light output power) for general lighting applications;

2. $L_{50\%}$ – Time to 50% lumen maintenance (i.e., 50% depreciation in the light output power) for the applications where light output is not critical.

Within this period the LED system should not exhibit greater chromatic shift bounded by a four-step MacAdam ellipse [58]. Lifetime measurements should be taken after a seasoning period of 1000 hours of operation at the rated operating conditions. Since the LEDs have a very long life time, the LED should be monitored for minimum of 5000 hours of operation at rated conditions after the seasoning period (1000 hours) under three different temperature conditions. Temperature measurements should be taken at a nearest point to the junction and manufacture should indicate the point where the temperature was measured. Recommended temperatures for the test are 45°C, 65°C and 85°C for the high power LEDs (rated current above 100mA), and 35°C, 45°C and 55°C for the low power LEDs (rated current below 100mA). A functional fit to data between 1000 and 6000 hours can be used to extrapolate to 70% and 50% lumen maintenance. Since LED's light output increases in the initial period were observed for most of the LEDs, the initial 1000 hours operation should not be used to find the functional fit. A common data sheets format for high power and low power LEDs, and LED systems were also provided [58; 59].

Failure analysis of white LEDs was reported by Narendran et al. Experiment was carried out to understand the long term performance of white LEDs and establish the relationship between the degradation of light output power and junction temperature, and the amplitude of short-wavelength radiation [53]. It was established that the yellowing of the epoxy was caused by the junction temperature and the amplitude of short-wavelength radiation and hence the light output degradation rate of the white LEDs also affected. Presented experimental results showed that the junction temperature had more influence in the light output degradation rate of the white LEDs than the amplitude of short-wavelength radiation. Results presented also showed that the lumen maintenance of the white

LEDs could be enhanced by removing the heat from the junction more efficiently by using the epoxy materials which have lower photodegradation characteristics [53].

Experimental assessment of the life of white LED was presented by Narendran and Gu. First experiment was carried out for the LED from the same manufacturer for their rated current 350mA and for different ambient temperatures [24]. Test was run for several thousand hours. The failure mode was selected as the 30% reduction in the light output from the initial light level. As the LEDs require several years to reach this criterion, collected data was used to extrapolate further to estimate the lifetime of the LEDs. It was observed the light output decreases and follows the exponential decay curve, and also is a function of temperature i.e. the life decreased with the temperature. Lifetime of this type of white LEDs was established as more than 50 000 hours at room temperature 25°C. Since there are many different manufacturers for the LEDs, a second experiment was carried out to compare the lifetime of the white LEDs from different manufacturers. All LEDs were operated at the rated current of 350mA and ambient temperature of 35°C. For the same operating conditions, all the LEDs indicated different temperature readings at their T-point, the point where the temperature measured in the LEDs. Although the light output decrease followed the exponential decay curve, the lifetimes of the LEDs were much different from each other [24].

High temperature storage effects on degradation of Gallium nitride based high brightness LED was reported by Meneghini et al. Two different families of devices were selected for the temperature stress test ranging from 180 to 230° C which is significantly higher than the maximum recommended by the manufacturer [62]. In order to detect the pure thermal effects, no bias was applied during the accelerated test period. Device electrical and optical measurements were made at each step of the storage test. Presented results showed that the applied thermal stress induced an optical power decrease and an operating voltage increase. Spectral characteristics of the light output showed that the thermal stress induced a worsening of the chromatic properties of the device. Presented microscopic analysis showed that the thermal stress induced the carbonization of the white plastics which reflected as a reduction in the package reflective properties (i.e. darkening of top contact layer) [62].

Humidity effects on the degradation of high power white LEDs was reported by Tan et al. High temperature-humidity (85° C – 85% RH) ageing test based on IPC/JEDEC[1] industry standard was carried out and non-destructive failure analysis tools were used to analyse the data [63]. Physics of failure used to verify the failure mechanism obtained by the non-destructive failure analysis tools. Results indicated a degradation of optical power when the LEDs subjected to high temperature-humidity ageing test (accelerated test). Non-destructive failure analysis tools showed that the degradation rate of two failure mechanisms (related to chip failure and degradation of phosphor) followed log-normal distribution. Based on the physics of failure analysis tools failure mechanism related to chip failure was caused by high reverse saturation current due to the mechanical damage of the GaN[2] based LED. Failure mechanism related to degradation of phosphor was caused by diffusion of Zn activator and dissolution of phosphor [63].

A new concept of metal package was proposed by Kang et al., to estimate the lifetime of GaN based blue LED chips (i.e. LED die) with high accuracy [22]. Since the degradation rate of the surrounding components of the chip such as pate, silicone-gel, phosphor and package body are different and typically higher than the chips, accurate estimation of the degradation rate of the chips was difficult. To overcome this, metal package was introduced based on the materials which have less degradation rate and have high thermal conductivity and efficient heat dissipation characteristics. Accelerated life test was carried out to test the proposed metal package to estimate the lifetime of the GaN based blue LED chips. Three chambers with three different temperature (40, 60 and 80° C) were used to test the metal package and in each chamber, three different metal packages with three different operating drive currents (500, 700 and 1000 mA) were placed. Measurements of light output power and package temperature were made for an ageing time of 5000 hours with the interval of 100 hours and 500 hours. Three different chips from three different manufacturers were investigated in this work. Only chip from a manufacturer produced light output power with enough degra-

---

[1]Association Connecting Electronics Industries and Joint Electron Devices Engineering Council standard for microelectronics and connecting electronics

[2]Gallium Nitride

dation to estimate the lifetime and not enough degradation of the light output power was observed in the other two chips within the ageing period of 5000 hours. Degradation about 20-40% was observed in all three control groups (from three manufacturers) of LED chips with conventional plastics packages. It indicated that metal package could be used to estimate the lifetime of the GaN based blue LED chips with high accuracy, excluding other degradation factors which have higher rate of degradation than the LED chips. Estimated lifetime of the chips which showed enough degradation was 45000 hours based on extrapolation of the exponential decay function [22].

Fan et al., developed physics of failure based prognostics approach for the high power white LEDs. Failure modes, mechanisms and effective analysis (FMMEA) was used to identify the failure modes and mechanisms [61]. System circuit open (i.e. lighting off), lighting chromatic changes and power efficiency degradation (i.e. luminous flux degradation) were identified as the failure modes. Failure mechanisms were divided into three main categories:

1. Chip level degradation;

2. Package level degradation;

3. System level degradation.

Chip level degradation was caused by the increasing non-radiative recombination process. Defects in the active layer (i.e. die) of the LEDs and diffusion of dopants were established as the main contributors to the chip level degradations. Interface delamination failures, epoxy lens and silicone glue darken failure, and phosphor coating degradation were established as the key failure mechanisms in the package level. Degradation in SMT (surface mount technology) module and degradation in the active cooling systems were identified as the main cause for the system level degradation of a LED lighting system. Empirical model for lumen maintenance for thermal induced luminous degradation was established as a function of the junction temperature and junction temperature-dependent light output degradation rate. Linear relationships between junction temperature and input power, and junction temperature and input current were established

using finite element method simulations for the junction temperature under different driving powers. Coffin-Manson-Basquin model which is a plastic and elastic strain driven model for the fatigue failures and Engelmaier model for cyclic frequency effects, temperature effects and elastic-plastics strain were proposed for the thermal cycle induced solder interconnect failures [61].

A detailed review of failure mechanisms and reliability study of the high power LEDs was carried out by Chang et al. Analysis presented in the study was based on three different groups of failures [67]. Failure mechanisms related to three groups are given below:

1. Semiconductor related

    (a) Defect and dislocation generation, and movements
    (b) Die cracking
    (c) Dopant diffusion
    (d) Electromigration

2. Interconnect Related

    (a) Electrical contact metallurgical inter-diffusion
    (b) Electrostatic discharge

3. Package Related

    (a) Carbonization of the encapsulant
    (b) Delamination
    (c) Encapsulant yellowing
    (d) Lens cracking
    (e) Phosphor thermal quenching
    (f) Phosphor thermal quenching
    (g) Solder joint fatigue

High temperature and low temperature effect on degradation of high power LED's characteristics were studied and reported by Weling et al. High power LEDs based on InGaN[1] (blue) and AlGaInP[2] (red) were selected for the test [23]. These LEDs were driven at rated conditions and placed into an oven. Oven temperature was increased from -30 to 100°C with the step on 10°C and forward voltage, relative light intensity, wavelength and spectral bandwidth were measured. Results showed that the temperature has great influence in both GaN[3] based blue and AlGaInP based red LEDs. When the environment temperature was low (i.e. junction temperature low), relative light intensity and forward voltage were increased and peak wavelength was blue-shifted. On the other hand when the temperature was high (high junction temperature) relative light intensity and forward voltage were dropped and peak wavelength was red-shifted. Properties of AlGaInP based red LEDs were more affected by the temperature increases compared with GaN based blue LEDs [23].

Accelerated life test of high power white LEDs based on package failure mechanisms was reported by Chan et al. Commercially available high power LED (peak wavelength 455nm, rated current 350 mA and rated power 1W) from a leading manufacturer was selected for the test [64]. The LED specimen composed of a chip, a phosphor layer, a reflector, a metal ring and an optical lens. Silicone encapsulant was used to fill the gap between LED chip and optical lens. This LED specimens were subjected to an unbiased highly accelerated temperature and humidity test. Based on the IPC/IEC[4] standard, 110° C – 85% RH and 130° C – 85% RH were set as the test conditions. Normal operating conditions was set at 25° C – 50% RH. Results indicated light output of both accelerated life test degraded faster than the light output of normal operating condition and induced similar degradation mechanisms in terms of following failure modes:

1. Light output decay;

2. Spectral property modification;

---

[1]Indium gallium nitride

[2]Aluminium gallium indium phosphide

[3]Gallium nitride

[4]Association Connecting Electronics Industries and International Electrotechnical Commission standard for microelectronics and PCB

3. Discolouration of the encapsulating material and bubble in the package;

4. Increased thermal resistance due to the yellow-brown of phenyl silicon resin in package [64].

## 2.5   Accelerated Life Test for LED

LED has a very long life time and high reliability. Testing LEDs for failure is a hot topic of research and only few work carried out. Accelerated test using different accelerated parameters is one of the best option to test LED within a short period of time.

Accelerated life test is applied to LEDs by different researchers for different purposes. ALT based on high current electrical test with pulse amplitudes between 1–7 A and voltage between 10–70 V with a pulse width of 100 ns and 1 KHz repetition rate is used to perform a degradation study of AlGaN[1]/InGaN/GaN green high brightness LEDs [65]. X. A. Cao et al., reported an ALT under high injection current (150 A/cm$^2$) and reverse bias (-20 V) conditions to investigate the electrical and optical degradation of GaN/InGaN single quantum well LEDs [68]. M. Meneghini et al., used ALT based on high DC (direct current), pulse current and high temperature conditions to analyse the electro-optical degradation of high brightness GaN based LEDs [62; 66]. LED backlight module used for the front display in the refrigerator was tested based on high temperature cycle and humidity by J -S Jeong et al. Low power LEDs with 5 mA typical forward current were used in this test [69]. Using ALT based on temperature and humidity E. Nogueira et al., reported main failure mechanisms for the lower power LEDs with typical forward current of 20 mA, which are frequently used in many outdoor applications. Pressure cooker was used as climate chamber for the test. Additionally high temperature accelerated tests with different forward current were also performed to identify the failure mechanisms [70]. Degradation of GaN based high power (1 W) white LEDs caused by humidity was investigated using humidity ALT [63]. Degradation of AlInGaP based low power red LEDs with typical forward current of 20 mA, was investigated using different levels

---

[1]Aluminium gallium nitride

temperature and current [71].

## 2.6   Summary

The detail literature review on undertaken research on different PHM approaches for different applications, real-time PHM, PHM for high power LED and ALT for high power LEDs have been conducted and reported in this chapter. Many data driven techniques are used to develop PHM applications. Some research work are based on more than one data driven techniques. Classification techniques are used to detect the anomalies in the system and then forecasting techniques are used to predict the remaining useful lifetime. Support vector machine and neural network demonstrated better performance as anomaly detection techniques. Gaussian process regression is one of the best forecasting for remaining useful lifetime estimation. Although models are used in model driven approach to estimate the damage, data driven techniques are also used to forecast the remaining useful lifetime. Kalman filters and Particle filters are identified as the other best forecasting techniques.

It is established from the conducted review that there are no evidence of an existing real-time prognostics and health monitoring systems for LEDs currently available. Two problems are identified to solve. The first problem is to test the LEDs in a short period so that the algorithm can be developed, tested and deployed within an acceptable period of time. The second problem is to identify the suitable approach for the real-time health monitoring for the LEDs. Chapter 5 will present the approaches taken into account for the health monitoring of LEDs.

# Chapter 3

# High Power Light Emitting Diodes (LEDs)

## 3.1    Introduction

A high power LED is an optoelectronic device which consists of a p-type region, n-type region and a p-n junction. For many years LEDs were only used as indicator lights after introduced to the market as electronic components which emit light, in early 1962 by Nick Holonyak Jr. Early LEDs emitted light with limited colours and intensity. LEDs have evolved from indicator lights to a high brightness light source as modern LEDs produce lights in all colours with high brightness. A high power LED, sometime referred as power LED and high brightness LED, is defined as an LED with electrical power equal or greater than 1 Watt or as an LED driven by 350mA or higher current. Figure 3.1 shows the electrical notation of an LED.

Anode/ (+)                                    Cathode/ (-) Terminal
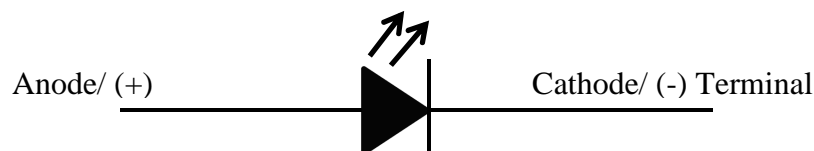
Figure 3.1: Electronic representation of an LED

When the current passes through the p-n junction (i.e., forward biased con-

dition), electrons recombine with holes and release energy in the form of photons and this process is referred as radiative recombination process. This process sometimes referred as electroluminescence or luminescence in which light is produced. This light is not produced due to heating. Like other semiconductor devices, p-n junction in an LED is created by doping impurities into intrinsic semiconductor material. Introduction of impurity atoms into an intrinsic semiconductor changes the concentration of electron and hole as they add more valence electrons into the semiconductor. This allows the semiconductor to conduct the current from anode to cathode when there is a voltage difference between anode and cathode terminals. A schematic cross-section of a LED assembly with typical construction is shown in Figure 3.2.
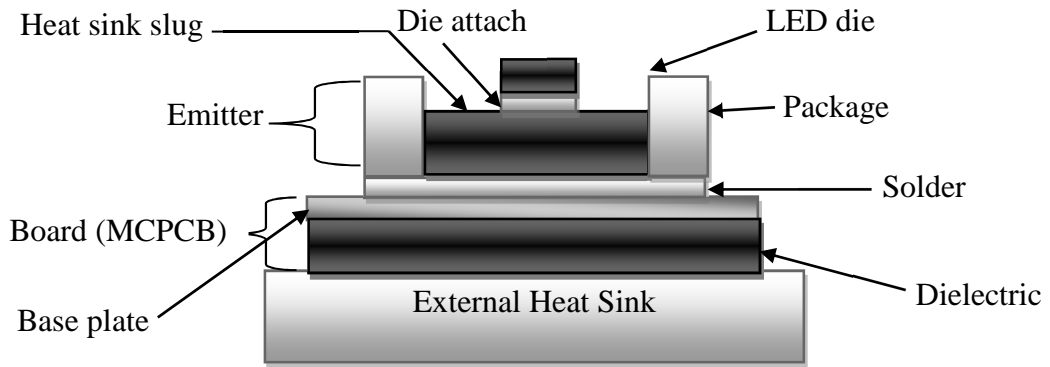


Figure 3.2: Cross section of LED assembly

LED devices undergo three different processes until light comes out of the devices. First, LEDs undergo injection or excitation process when the LEDs are connected to a forward voltage. During the injection process carrier's energy is increased by the forward voltage. In other words, carriers in p-n junction are injected by an external energy. After that a recombination process takes place. In the recombination process most of the energised carriers emit their excess energy gained through injection or excitation process. This emitted energy is in the form of photons or light. Finally emitted photons are removed from the devices and it is called extraction process. Each of these processes has their own efficiency based on the devices structure and package types. Overall device

32

efficiency depends on these individual processes and their efficiency. The overall efficiency can be estimated using the following equation:

$$\eta_{ov} = \eta_{in}\eta_{re}\eta_{ex} \qquad (3.1)$$

where $\eta_{in}$, $\eta_{re}$ and $\eta_{ex}$ are the efficiency in the process of injection, recombination and extraction, respectively, and $\eta_{ov}$ is the overall efficiency of the device.

## 3.2 Semiconductor Materials for LEDs

Since the first invention of red LED based on GaAsP semiconductor material by Holonyak in 1962, semiconductor material research became a hot topic and many developments took place. First red LED demonstrated very low luminous efficiency of about 0.1 lm/W. Exponential growths in the semiconductor material developments improved the luminous efficiency and light output power of the LEDs exponentially. Figure 3.3 [1] illustrates the graph of the historical development of the LEDs. The graph also illustrates the luminous efficiency of different LEDs based on different material and other light sources.

Figure 3.4 [1] demonstrates the band-gap energy, corresponding wavelength and forward voltage for different materials. Visible spectrum of the light wavelength is between 0.35 and 0.70 m which corresponds to the band-gap energy between 3.5 and 1.8 eV. Most of the LEDs are made of III-V compound semiconductor materials (i.e., elements which have 3 electrons in the last orbit such as Boron, Aluminium, Gallium, Indium etc., and elements which have 5 electrons in the last orbit such as Nitrogen, Phosphorus, Arsenic, Antimony, Bismuth etc.,) such as AlGaAs, AlGaInP, GaInN, etc., [72]. Some LEDs are made of II-VI and IV semiconductor materials such as ZnCdSe[1], ZnTeSe[2] etc., [72].

---

[1]Zinc cadmium selenium
[2]Zinc tellurium selenium
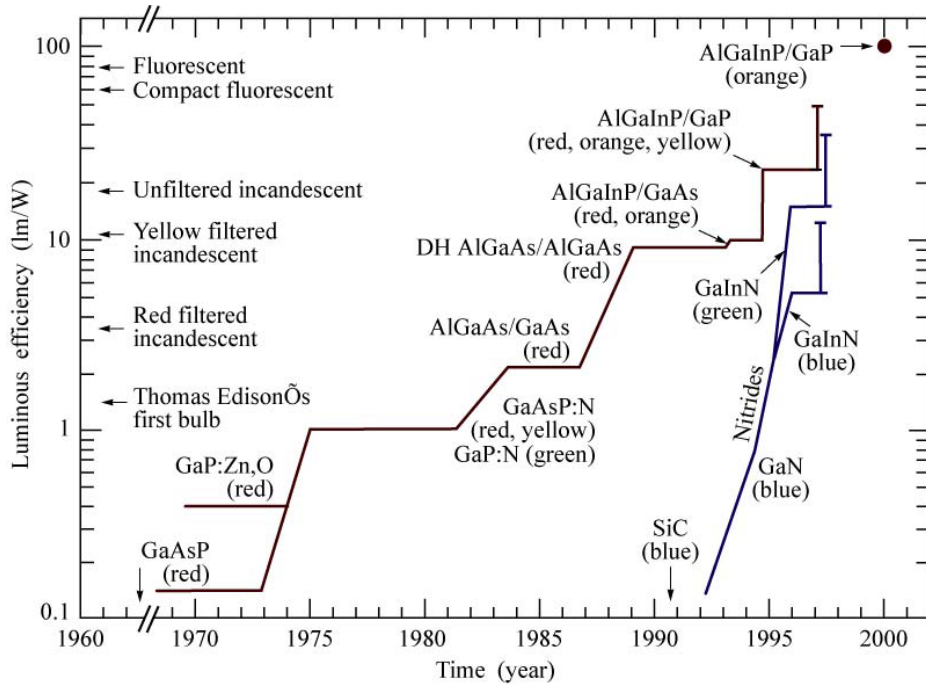
Figure 3.3: Luminous efficiency of visible-spectrum LEDs and other light sources with time [1]
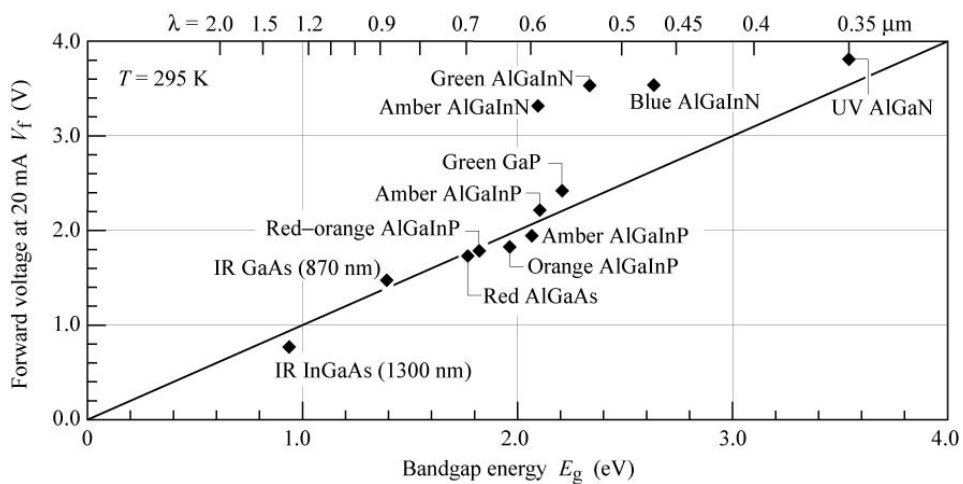


Figure 3.4: Diode forward voltage with bandgap energy for LEDs made from different materials [1]

## 3.3 Market of High Power LEDs

Market for LED lighting is growing rapidly as the LED becomes a promising candidate for the future lighting. Many different positive attributes of the LED such as long lifetime, versatility, power efficiency, robustness, high reliability, small in size, design freedom and stylish attribute, faster switching speed and durability are the motivation factors for future lighting. The LED lighting started capturing strong market positions in many applications such as automotive, industrial, aviation, commercial etc. Market for white LEDs accounted for just over 50% of the total LED lighting market [73] and white LED lighting into general illumination application will increase if high performance white LEDs are available at affordable price. According to the Strategies Unlimited, an LED market research company, market forecast in 2009, LED lighting market will exceed $5 billion by 2012 and will have a growth rate of 28% from 2008 to 2012. But the global market of the LED reached $5.6 billion in 2009 and almost doubled in 2010 to $10.8 billion. According to the latest report of Strategies Unlimited and iSuppli in 2011, the total global LED market has been forecast to $90 billion in 2011.

Governments' strict policies and regulations are effectively motivating the replacement of the LEDs as the modern world faces energy crisis and global warming. Governments all over the world are forced to look for alternative energy sources as well as to use the available energy more effectively. This scenario is worsening as the global population and standard of living increases, and as the natural resources such as fossil fuel run out. Therefore the demand for the energy efficient lighting such as high power LED will increase further in future. Mass production of LEDs will bring the cost down and also the revolutions in the LED technology will enhance the efficiency of the LED lighting further. R Haitz et al predicted the LED's future market and future development in 1999 for the first time in a comprehensive manner [2]. This forecast triggered the development as well as the investment in the LED lighting industries. Figure 3.5 [2] illustrates the Haitz prediction in 1999 for the LED technology and it is widely known as Haitz' law similar to the Moore's law for the integrated circuit technology. Two curves are shown in Figure 3.5. One shows LED technology developments (flux/package - lm) increases almost 30 times every decade. Another curve indicates almost 10

times cost reduction every decade (cost/Lumen - $/lm).
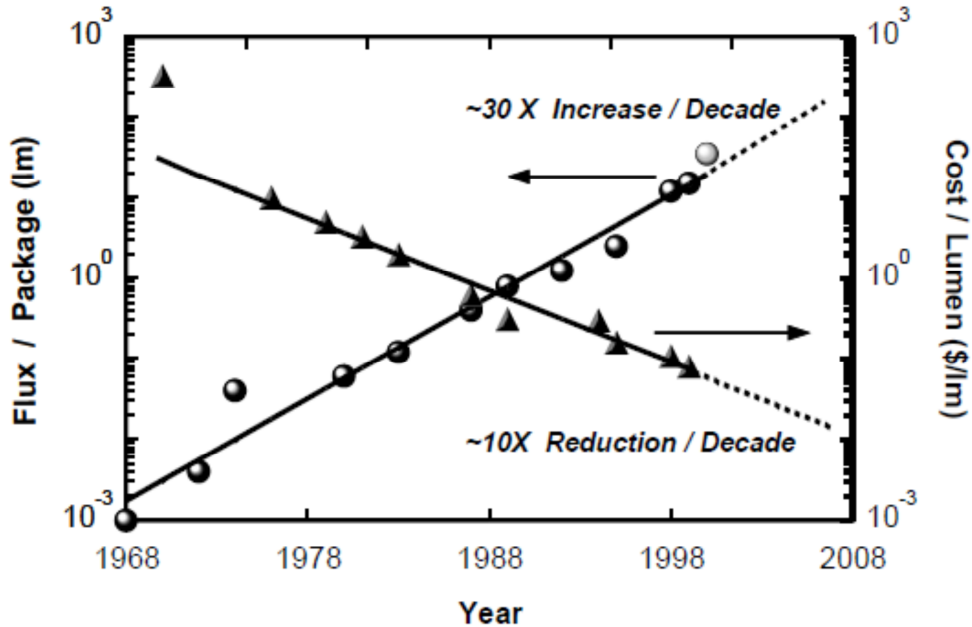


Figure 3.5: Haitz' law [2]

Latest update version of the Haitz law as of early 2010 is shown below in Figure 3.6 [3]. Red points represent the data for the red LED and white data points represent the data for the white LED. Based on the Haitz law the flux per lamp increased from 10 lm in 1999 to 6 klm in 2010 and cost per lumen dropped from $150/klm in 2000 to $5/klm in 2010 for cool white LEDs. LED technology needs significant further development to supply the same flux and quality of the light with energy efficient at low cost. Haitz also predicted that power lamps in the 0-10 klm range with an efficacy of 150-200 lm/W are necessary to supply the same flux and quality of the light at a better efficiency [2; 3].

Early 2011 Cree Inc., reported a white LED die component with best efficacy of 231 lm/W and test was carried out at the standard room temperature and 350 mA drive current conditions [74]. This proved that the LED technology will further develop and become an ultimate light source of the next generation.
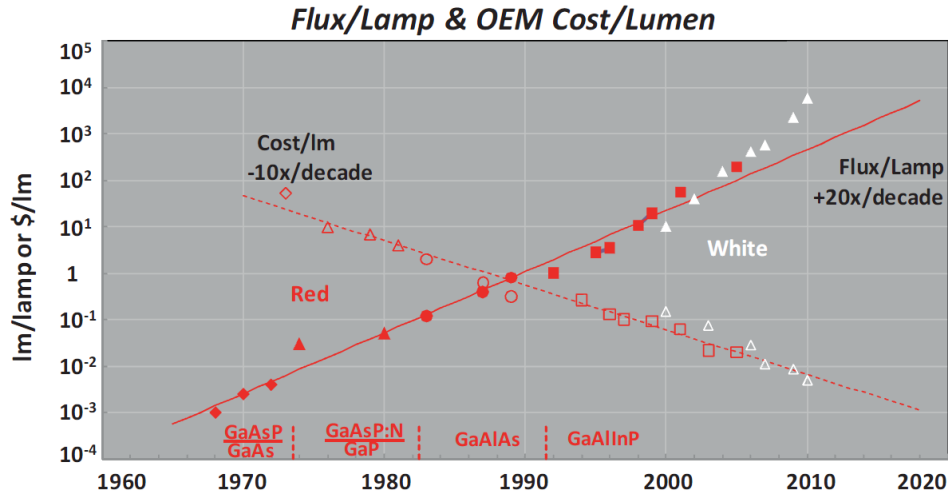
Figure 3.6: Latest version of the Haitz' law [3]

## 3.4 LED Applications

Applications of high power LEDs are continuously increasing as they are energy efficient (typically 85%), green (e.g. no mercury), have demonstrated longer life than traditional lighting sources, and emits low UV radiation [67]. Single colour LEDs are over ten time more efficient than the incandescent lamps and white LEDs are more over two times more efficient than the incandescent lamps [67]. LED lighting systems are already replacing the lighting applications in many sectors such as automobile, aviation, retail, medical, traffic signals, street lightings, machine vision applications, interior and decorative lightings etc., where incandescent and fluorescent were used for many years.

### 3.4.1 Automobile Lighting

Automotive signal, break and interior lights were successfully replaced with high power LEDs in many automotive vehicles more than ten years ago. Required colours and lumen for these applications were achieved successfully [75]. High power LEDs attributes such as fast switching speed, smaller size, high reliability, energy efficient, long lifetime, robustness and stylist design are the main driving

factors of the widespread adoption of LEDs into automotive signalling and interior lighting. However applying the high power LED to the head lamp was under study for few years and successfully deployed in the Lexus LS and Audi R8 in 2007 and 2008 respectively [76]. Although the advantages of the high power LEDs are understood, required light levels, thermal management and cost of the LED head lamps for an automotive vehicle are the main limiting factors. Compared to the signal lights, head lamps require high level of light output and operation for long hours, which results in increase of the heat generated in the lamps. In addition, LED head lamps need to operate in high temperature environment and require additional design consideration for the heat sink or the cooling systems. Figures 3.7 to 3.10 illustrate the Audi R8 head lamp, Audi Q5 headlight assembly, Audi Q5 rear lamp assembly and Audi Q5 head lamp, respectively. Figure 3.11 shows a Lexus LS head lamp.



Figure 3.7: Audi R8 head lamp [4]

### 3.4.2 Aviation Lighting

Adoption of the high power LEDs for both civil and military aviation has been taking place for long time in many different applications such as cabin interior, aircraft exterior and ground lighting applications. High power LED lights are successfully replacing commercial aircraft interiors lights since they are more flexible for design as they are small in size, very stylish and available in different colours. In addition, higher power efficiency of the LEDs allows less power consumption and therefore less fuel energy for interior lights. Perfect dimmable characteristics

**Audi Q5**

**Scheinwerfer des Audi Q5, Elektrische Komponenten**
Audi Q5 headlight, electrical components
07/08

1 LED
2 LED Steuergerät
3 LED Kühlkörper
4 Xenon-Projektionsmodul
5 elektronisches Xenon-Vorschaltgerät
6 Shutterelektronik für Fernlicht
7 Leistungsmodul
8 Lichtquellenmodul für Blinker

1 LED
2 LED control unit
3 LED heat sink
4 Xenon projection module
5 Electronic xenon ballast unit
6 High-beam shutter electronics
7 Power module
8 Light-source module for flashing turn indicators

Figure 3.8: Audi Q5 head lamp assembly [4]



**Audi Q5**

**LED-Heckleuchte**
LED rear light
07/08
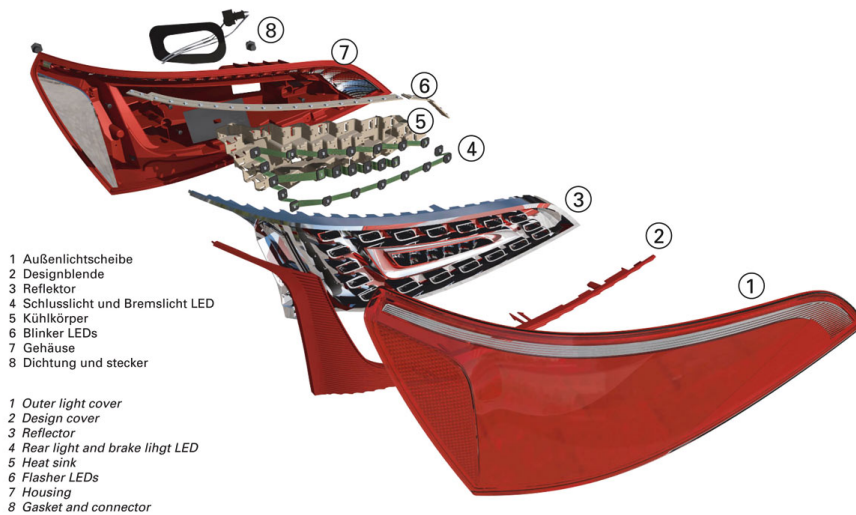
1 Außenlichtscheibe
2 Designblende
3 Reflektor
4 Schlusslicht und Bremslicht LED
5 Kühlkörper
6 Blinker LEDs
7 Gehäuse
8 Dichtung und stecker

1 Outer light cover
2 Design cover
3 Reflector
4 Rear light and brake lihgt LED
5 Heat sink
6 Flasher LEDs
7 Housing
8 Gasket and connector

Figure 3.9: Audi Q5 rear lamp assembly [4]

Figure 3.10: Audi Q5 head lamp [4]



Figure 3.11: Lexus LS head lamp [5]

of the LED lighting systems further enhance the customer in-cabin experience. Commercial aircraft manufacturers such as Airbus and Boeing are using the current LED technology to enhance the aircraft interiors. Figures 3.12 to 3.14 show the interior lighting of Airbus A320, Boeing 747-8 intercontinental, and Boeing 737, respectively. These interiors are developed based on high power LEDs.
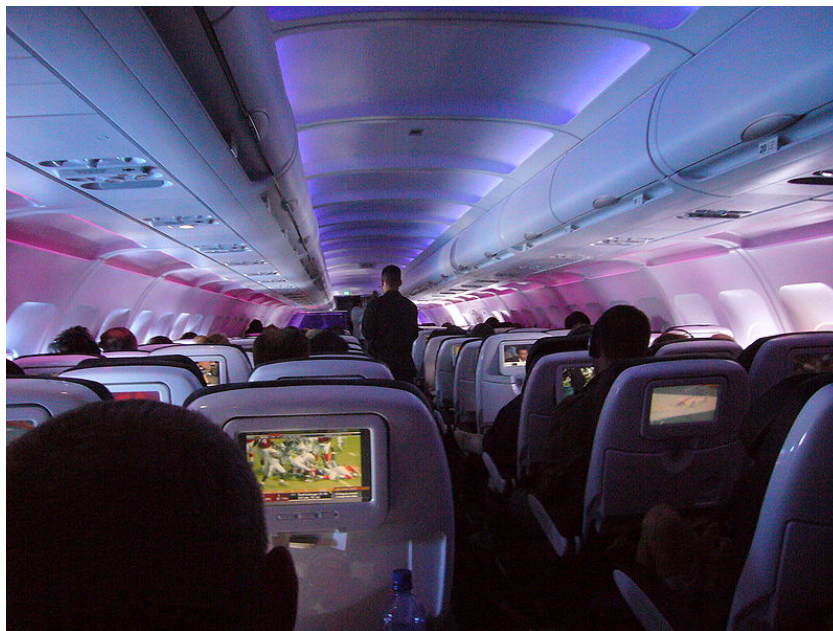


Figure 3.12: Airbus A320 economy class enhanced cabin with LED lighting [6]

In addition to the interior and exterior lighting of the aircraft, there are many lighting applications used in aviation such as runway lights, taxiway lights and signalling. Main attributes that motivate the LED replacement in the aviation lightings are versatility, reliability, durability, long lifetime and low power consumption. Some of the typical ground lighting (air traffic control room and runway) of the aviation applications are shown in Figures 3.15 and 3.16.

### 3.4.3 Retail Lighting

Retail applications are the other main application of the high power LEDs. LED technology is demonstrated how the lighting systems can be used attractively to enhance the business using less power consumption. In particular, LEDs are very

Figure 3.13: Interior lighting effect by the LED in the Boeing 747-8 interconti-
nental [7]
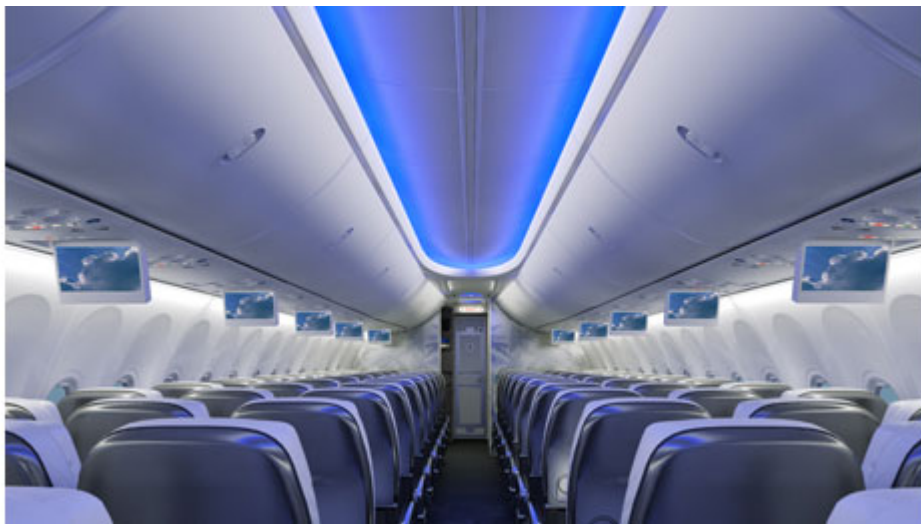


Figure 3.14: 737 Boeing sky interior a soft blue "sky" created with LEDs [8]

Figure 3.15: Airport ground lighting systems [9]



Figure 3.16: Airport runway lighting systems [9]

efficient and have very long lifetime in low temperature environment. August 2009, a retail store in Lianhua, Shanghai replaced the refrigerators lights by T8 LED tube and saved up to 60% of electricity in refrigeration lighting [10]. Figure 3.17 shows the implemented refrigeration lighting in the retail store in Lianhua, Shanghai. UK's biggest two retailers, Sainsbury's and Tesco PLC, have switched to Philips LED cooling and freezer systems and reported 75% and 60% energy saving respectively and 150% improvement in lighting effects [11]. Implemented refrigerator lighting systems in Sainsbury's is shown in Figure 3.18. Further high power LEDs are used for billboard and display board lighting to attract the customers using less energy.



Figure 3.17: Refrigeration lighting [10]

### 3.4.4 Medical Lighting

Surgical operation requires highest quality and quantity of light throughout the operation. LED technology is the right candidate for the operating room. Nowadays most of the medical lighting equipment is successfully replaced by the LED based power source as the LED can provide brighter, cold and cooler lights with very less power compared with traditional halogen lights. Other advantage is LED lights can be controlled by microprocessor precisely to get the accurate

Figure 3.18: Sainsbury's freezer lighting [11]

level of the light output required for the operating theatre environment. Most of the equipment can be controlled 0-100% of their light output. Freedom of design flexibility allows the designer to arrange the individual LEDs to achieve a good design. For example iLED provides shadow free lights which cleverly focus the light on the surgical area. Since the LED lighting systems have the design flexibility, smooth surface for the lights can be achieved and therefore equipment can be cleaned easily. iLED system for operating theatre is shown below in Figure 3.19.

### 3.4.5 Traffic Lighting

Traffic lights, road signs and traffic message boards are some of the most typical application fields for the LED lighting technology. LED traffic lights are developed from arrays of LEDs spread around a circle or area which result in better visibility and higher brightness from long distance compared to the traditional lighting systems. In addition, LED lighting systems take less energy to operate, have high reliability and very long lifetime. This significantly reduces the operational, and maintenance cost, and reduces the down time considerably. Fast switching speed of the LED lighting systems provides better performance to a fast moving traffic situation. Figure 3.20 shows the traffic signals lights based on LEDs. Figures 3.21 and 3.22 show the traffic message boards created from the

Figure 3.19: iLED the first operating light with LED technology [12]

LED lighting systems.



Figure 3.20: Traffic signals using LEDs [13]

Figure 3.21: Traffic message board using LEDs [14]



Figure 3.22: Traffic message [15]

| Measures | Before | After |
|---|---|---|
| Total Nominal Watts | 6,244 KW | 2,648 KW |
| Estimated Energy Saving | 40% | 57.6% |
| Annual CO2 Reduction | 0 | 8,674 MTons |
| Annual Energy Saving | 0 | 14,688 MWh |
| Annual Energy Saving | 0 | $ 1, 297, 173 |

Table 3.1: Project evaluation results for the city of Los Angeles LED street light replacement project

### 3.4.6 Street Lighting

There are lots of energy wasted every day by street lights all over the world. Street lighting is one of the main areas where the LED replacement is taking place very slowly. City of Los Angeles LED street light replacement project was identified as the first project in the world which will replace high number of street lights (140,000) in 2013 by LED lights [16]. Table 3.1 illustrates the project evaluation summary. At the time of the evaluation in February 2011, 36,500 lights were replaced successfully and total estimated cost of the project is $57 million. Figure 3.23 shows the implemented LED street lights in the City of Los Angeles.

This trial project clearly demonstrates the benefit of replacing the street lights with modern LED technology. There are three other trial projects reported in China where more than 8800, 8700 and 5200 street lights are successfully replaced by the LED lights so far [17]. Figure 3.24 shows the LED street implementation in Australia.

### 3.4.7 Machine Vision Applications

Machine vision applications required to have a homogeneous and bright light to capture the features clearly so that it can be processed easily. High power LEDs are frequently used for these type of application as the LEDs can provide a homogeneous and bright light. Robustness of LEDs give designers great flexibility and array of LEDs can be manufactured in any shape and size to focus the light exactly where it should focus. This design flexibility is not available with other lighting systems such as fluorescent and incandescent. Many machine vision applications

Figure 3.23: Implemented LED street lights in the city of Los Angeles [16]



Figure 3.24: Implemented LED street lights in Australia [17]

require cold light which will not change or affect the appearance or property of the objects which need to be captured. LEDs emit cold lights and this attribute provides better lighting solution to machine vision applications. In addition to the LED's high efficiency and long lifetime, less maintenance requirement is the other promoting factor for the LEDs in the machine vision applications. Figure 3.25 shows a sample machine vision application which uses LED lights.



Figure 3.25: A machine vision system using LED lighting systems

### 3.4.8 Interior and Decorative Lighting

LED lighting systems are used as interior and decorative lighting systems increasingly nowadays as LEDs provide many advantages. Introduction of the LEDs to the interior and decorative market provide very high flexibility with the lighting systems design and enhance the development of the new architectural designs such as variety of designs in wall mounted, celling mounted etc., in many different colours. Less power consumption and the long lifetime with high reliability are the main motivating factors of the LEDs for the interior and decorative lighting applications.

## 3.5 High Power LED Drivers

Single power LED requires direct current (DC) to operate and in many cases the amount of direct current should be very specific to drive the LED perfectly. Hence LEDs require an electronic driver circuit to achieve that. LED driver circuit generally convert AC power into required DC power which can be controlled very accurately. Different applications may have very different requirements and there is no specific LED driver to achieve that. For example an automobile rear light may have 20 LEDs whereas a front light may have 15 LEDs. Both of these lights require very different electrical power supply and hence need different types of LED drivers to match the requirement of the LED lighting systems. There are many aspects that need to be considered when designing a LED driver and some of the important factors are listed below:

1. Available input power source (i.e., AC main, Battery, etc.,);

2. Required voltage output of the driver;

3. Required power output;

4. Special requirements such as controllable lights (dimmer), colour changeable, etc.

One simplest and cheapest way to drive the LEDs is to use a rectifier to convert the alternating current (AC) into direct current (DC) and then use a voltage divider to get the required voltage output. A full wave rectifier with smoothing capacitor and LEDs is shown in Figure 3.26. Figure 3.27 shows the simple potential divider which can be used to power the LED.

However, in order to get required performance, different applications require unique driver designs with specific configurations. There are various LED drivers available to achieve specific electrical output from an input source. Some of the frequently used configurations are listed below:

1. Buck configuration;

2. Boost configuration;

3. Buck-Boost configuration.
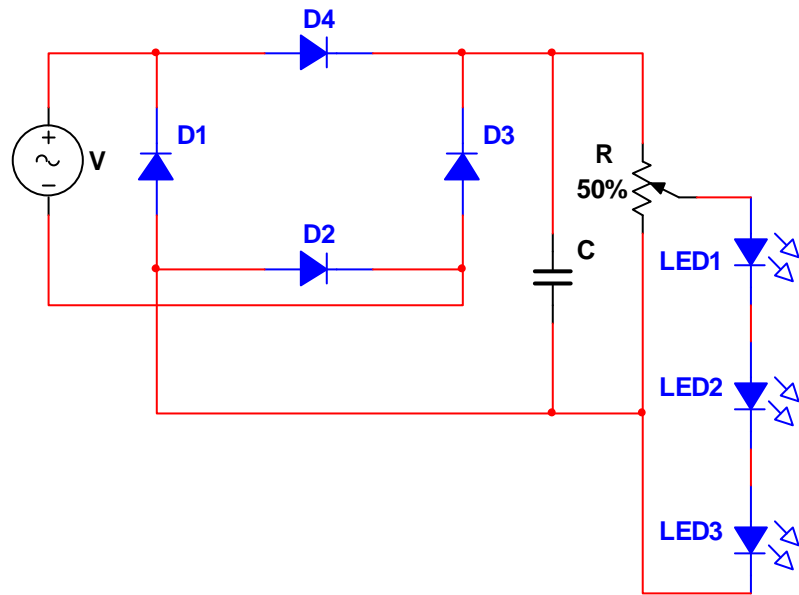
Figure 3.26: Full-wave rectifier with smoothing capacitor for LED application
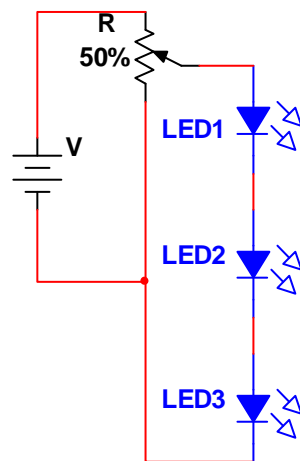


Figure 3.27: Voltage/potential divider with LEDs

### 3.5.1 Buck Configuration

Buck configuration is an efficient voltage converter which converts a high voltage into a low output voltage. Pulse width modulation (PWM) switching technique between voltage source and ground is used to convert the high voltage into a low voltage. When the switch is connected to the voltage source, high current is achieved in the circuit. This current is used to charge the capacitor and some energy stored in the inductor as magnetic field because of the high current. When the switch is connected to the ground, the current starts to reduce to zero using the energy stored in the inductor. When the current reaches zero, switch is connected to the voltage source. The smoothing capacitor converts the full-wave rippled output into a smooth DC output voltage. When the current from the voltage source goes below certain level, capacitor starts to discharge and keeps the load current almost constant. Based on the different PWM speed, inductance and capacitance, various output currents are achieved. Figure 3.28 illustrate a basic buck configuration driver circuit. PWM switching speed is mostly controlled by the microcontrollers precisely. This simple buck configuration driver circuit can be used to power the LEDs.
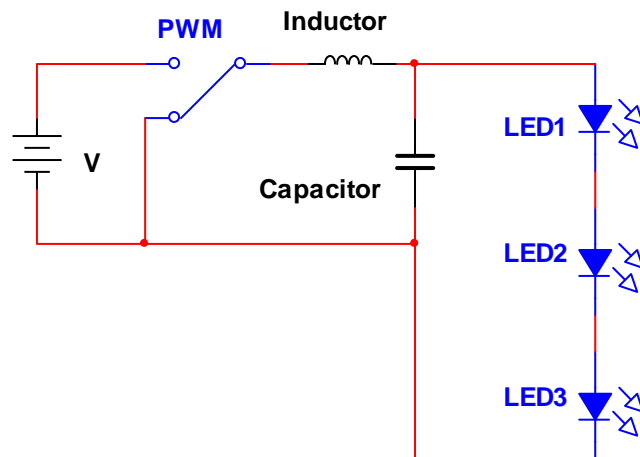


Figure 3.28: A simple buck configuration to power the LEDs

### 3.5.2 Boost Configuration

Boost configuration is used to step up the lower voltage into a high voltage. PWM technique is used as the switching method to achieve the high voltage from a low voltage input. In the boost configuration inductor is used to store the energy when the PWM switch is connected to the ground and LED will be powered by the capacitor. When the PWM switch is connected to the load, battery and stored energy in the inductor are used to power the load as well as recharge the capacitor. To achieve a steady state operation the energy removed from the capacitor during the discharge period must be replaced during the recharge period. Boost configuration driver is shown below in Figure 3.29. PWM switching operation is controlled by a microcontroller accurately.
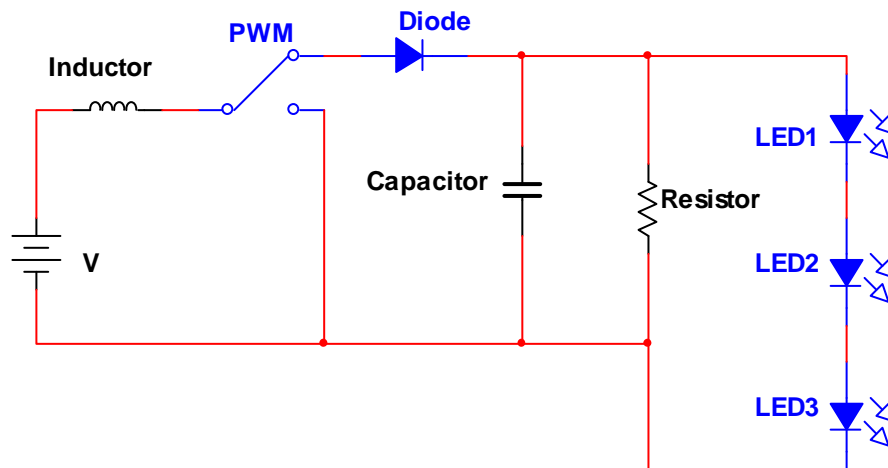


Figure 3.29: A boost configuration

### 3.5.3 Buck-Boost Configuration

Buck-boost configuration is used if the available supply voltage is above or below the required power supply for the LEDs. A general configuration of a buck-boost driver is shown in Figure 3.30. Like buck and boost drivers, buck-boost driver's switching is controlled by a microcontroller accurately.
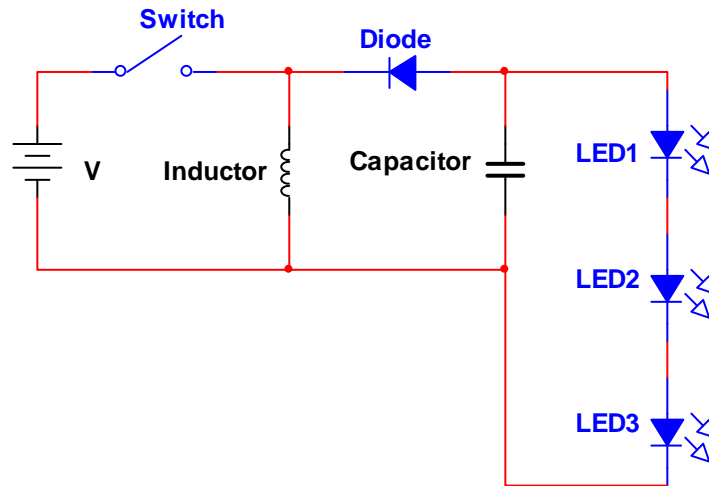
Figure 3.30: A buck-boost configuration

## 3.6 LED Lamps

A single LED is not enough to create an LED lamp. Most of the LED lamps
consists of many individual LEDs connected together. These LEDs are connected
in many different configurations and powered using LED drivers. There are var-
ious ways to power these LEDs from a LED driver. Some of the frequently used
configurations are discussed below.

### 3.6.1 Series/String Connection Lamps

This is the simplest way to power the LEDs from constant current LED driver.
LEDs are connected in series with each other to make a string connection. In this
case required output of the LED driver is determined by the number of LEDs
which are connected in series. Same current flows through each LED. Primary
disadvantage of this configuration is an open circuit in the string because of the
open LED (i.e., LED failed and circuit becomes open) or failure in the connection
causes the complete failure in the LED lamp. Another disadvantage is if an LED

fails short, current through the other LEDs will increase and accelerate the failures in other LEDs. In addition, required output voltage of the LED driver for large number of LEDs is very high hence this has become a safety issue. Achievable maximum LED driver output voltage is the deciding factor of the number of LEDs which can be connected in series. A typical string connection of the LEDs is shown in Figure 3.31.
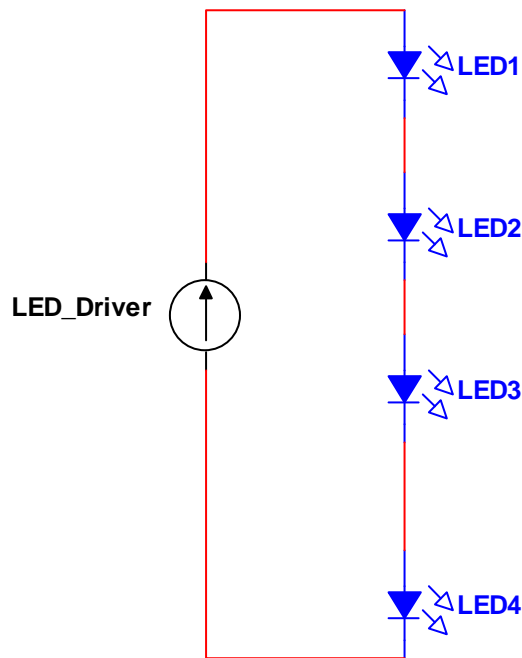


Figure 3.31: Series/String configuration of LEDs

## 3.6.2 Parallel String Connection Lamps

Parallel string connection overcomes the maximum string voltage limit and increases the reliability of the LED lamp overall. In particular required LED driver output voltage reduces in factor of number of parallel strings and if an LED is failed open or any open connection in one string will not affect the operation of the lamp completely rather affects the brightness of the lamp. A parallel string connection of LEDs is shown in Figure 3.32. Parallel string connection introduces current imbalance between strings i.e., current is divided between strings based

LEDs in each strings. Generally a resistor in each string is introduced to correct the current imbalance in the parallel strings. These resistors affect the overall energy efficiency of the LED lamp. In addition if an LED failed short, current through the particular string will increase and lead to accelerated failures in other LEDs.
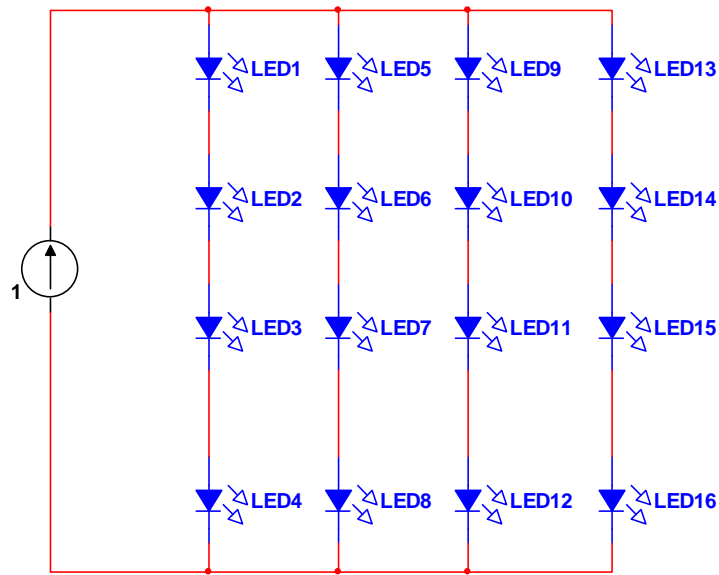


Figure 3.32: A parallel string connection

### 3.6.3   Matrix Connection Lamps

A typical matrix connection of LEDs is shown in Figure 3.33. Matrix connection introduces more connections between LEDs and creates parallel connections between the LEDs in same rows, i.e., all the LEDs in the same rows are operating parallel in addition to the parallel string connection. The LEDs are in fact arranged into a matrix form i.e., rows and columns. This configuration reduces the current imbalance between strings and increases the overall reliability of the LED lamp. Primary disadvantage of this configuration is if an LED fail short, all the LEDs in the same row will not operate as the effective voltage across the row is zero. Hence brightness of the lamp will reduce. On the other hand if an LED failed open, all the other LEDs in the matrix connection will operate as normal.
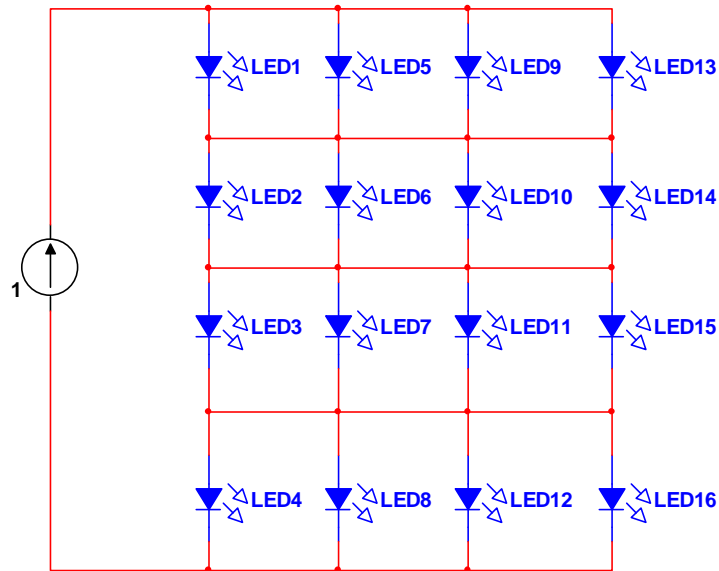
Figure 3.33: A matrix configuration

### 3.6.4 Multi-Channel Connection Lamps

In multi-channel connection, complexity of the driver is increased as individual string of LEDs powered by independent constant current drivers. This feature adds more sophistication to the LED lamp in terms of preciously controlled current to the individual strings. Multi-channel connection overcomes the current imbalance problem in the parallel string connection. A typical multi-channel connection configuration circuit is shown in Figure 3.34.

## 3.7 Lifetime of High Power LEDs

Lifetime of the LEDs is defined based on the light output power depreciation and colour shift. For example, when an LED starts to operate below the acceptable limit of the light output power or outside the colour spectrum, then the LED will be defined as failed LED. The time it takes to reach one of the limits (light power output or colour spectrum) is the lifetime of the particular LED. For the first time, ASSIST[1] developed comprehensive recommendations for the manufacturers and

---

[1]The alliance for solid-state illumination systems and technologies
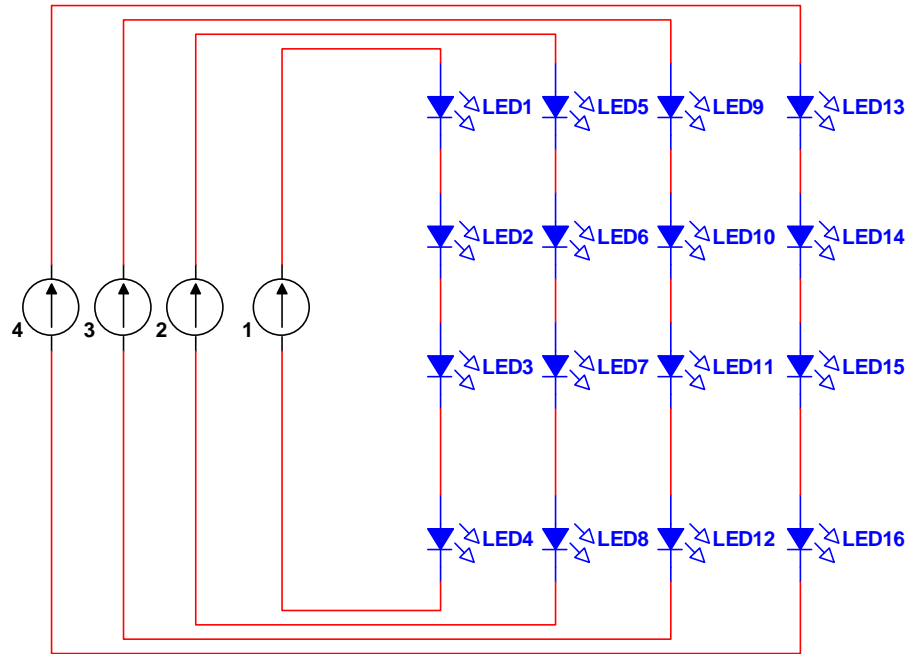
Figure 3.34: A multi-channel configuration

lighting systems designers to assess and document the lifetime of LEDs. Although different applications require different light output power, for general lighting light output power should not get below 70% of the initial light output power of the LED. For decorative lighting light output power should not get below 50% of the initial light output of the LED. These two performance criteria are defined as $L_{70\%}$ (i.e., time to 70% lumen maintenance) and $L_{50\%}$ (i.e., time to 50% lumen maintenance) hours by the ASSIST. Hence, the useful life of a LED for general lighting is given by the time which it takes for the luminance to reduce by 30% from its initial value. For some safety critical and emergency applications, the amount of luminance reduction allowed may be less than 30%.

Lifetime of high power LEDs is very high compared to traditional lighting sources such as fluorescent, halogen and incandescent light sources. For example, typical LEDs can operate for 50,000 hours (approximately 11.5 years for a 50% calendar time usage) provided the drive current and p-n junction temperature remain within the limits specified by the manufacturer. In particular, for the Philips Luxeon Star warm white LEDs, the maximum values recommended for

the DC forward current and junction temperature are 350 mA and 135°C respectively. Although this information is available to the customers, it is based on very little data. Generally, these typical operating conditions specified by the manufacturers are not tested for other environmental and stress conditions. Different manufacturers report different lifetimes for their LED and these reports also show their lifetime estimations are based on few hard facts, very little published data and also little consistency. Reputable manufacturers have thousands of hours data under varying conditions for their LED packages, hence package level reliability and lifetime information can be derived but not based on enough data set [77].

It should also be noted that the lifetime specified by the manufacturer is the average life time of LEDs, and some LEDs would fail before this specified life time due to variations in individual characteristics, manufacturing quality and environmental conditions. Hence the actual reliability and lifetime of individual LED lighting systems cannot be assessed exactly for many reasons. The true reliability and lifetime generally do not depend only on lumen depreciation. LED lighting systems consist of a number of other interdependent components and parts which demonstrated different reliability and lifetime [77]. A typical LED lighting system has LED engine or package alone with power supply, control circuit and housing. Generally, these components and parts have less reliability and lifetime values compared to the individual LED package or LED engine. Failures in any of these components or parts will lead to total failure in LED lighting systems. Hence the LED lighting systems require maintenance that involving labour and the use of measuring instruments.

Since LEDs started to replace the traditional lighting systems there is a huge interest in developing standards defining the failure of an LED light sources and luminaries, measurement procedures etc. Illumination Engineering Society (IES) have developed some standard documents for LED packages and luminaries. IES LM-79[1] is an approved standard for electrical and photometric measurements of solid state lighting products (SSL) such as luminaries and integrated LED lamps. This document covers the measurements of luminous flux (lumen - lm), luminous

---

[1]IES standard for electrical and photometric measurements of solid-state lighting products

efficacy (lm/W), chromaticity and luminous intensity distribution. IES LM-80[1] is an approved standard for measuring lumen maintenance for LED light sources such as packages, arrays and modules. Purpose of this standard is to make the manufacturers follow the same standard procedures for the life prediction of their product. IES TM-21[2] is the standard for lifetime prediction on an LED light source such as package, array and module. This standard describes how the collected data can be used to project the lifetime of an LED light sources. All these standards need to be followed and tests need to be carried out by an independent laboratory to get the Energy star approval from Department of Energy in United States.

## 3.8  Failure Modes

Light emitting diodes have very limited failure mechanisms and generally LEDs are not subjected to sudden failures. The most common mode of failure is the depreciation of the light output power or lumen, because of failure mechanisms of the LED chip and surrounding components. Typically individual LED package or LED engine is considered as failed based on the light requirement for the particular application. In particular general applications require less than 30% depreciation, decorative applications require less than 50% depreciation and some special application such as safety critical or emergency application may require less than 10% or 20% depreciation. Hence the failure mode based on light output power or lumen depends on the required light output power of the application.

In addition to gradual light depreciation, discolouration of the LEDs or LED die encapsulate is another mode of failure. In this mode of failure, specified light colour of the LED light changes with the time before the light output of an LED depreciates to a certain level which is discussed as above (i.e., 30% depreciation or 50% depreciation). This colour shift in the light output is called as chromaticity shift. Maximum allowable limit of this chromaticity shift for both $L_{70\%}$ and $L_{50\%}$ performance criteria is recommended by the boundary of a four-step MacAdam ellipse [58; 78]. Even though for some application colour shift

---

[1]IES standard for measuring lumen maintenance of LED light sources
[2]IES standard projecting long term lumen maintenance of LED light sources

might be a failure, there is no standard or document which provides a recognised way to project the failure based on colour shift in the light output. IES LM-80 only provides requirements for the test report to include chromaticity shift during the recommended test period. In addition, system colour shift is not very well-understood, well-studied, or even commonly used as a metric, even for incumbent technologies. Great progress has been made by the LED manufacturer to improve the colour stability [77]. Hence, failures in LED lighting system can be defined as the overall lumen output degradation as measured by IES LM-80.

The third failure mode is the catastrophic failures i.e., LED is stopped emitting the light suddenly. These types of failure are very rare and generally occur because of the mechanical breakdown or permanent damage in the device. This affects the other LEDs in the circuit as the failed LED may act as an open circuit or closed circuit because of the damage.

## 3.9 Failure Mechanisms

Failure mechanisms of LED lighting systems can be classified into three different groups:

1. Failures related to driver;

2. Failures related to housing;

3. Failures related to the LED engine.

Figure 3.35 [77] shows the causes of the failure in 29 failed lighting systems out of installed 5400 outdoor LED lighting systems reported by Appalachian Lighting Systems [77]. Figure 3.35 indicates 59% of failures identified in the driver, and 31% failures identified in housing and only 10% of failures actually identified in the LED engine.

This information indicates that most of the failures in LED lighting systems are not related to the LED engine. Although the LED engine's failures are normally distributed with the mean of 50,000 hours, LED lighting systems failure are mainly driver and housing related. A sample failure probability of LED lighting systems based on LED engine and driver is shown in Figure 3.36 [77]. In
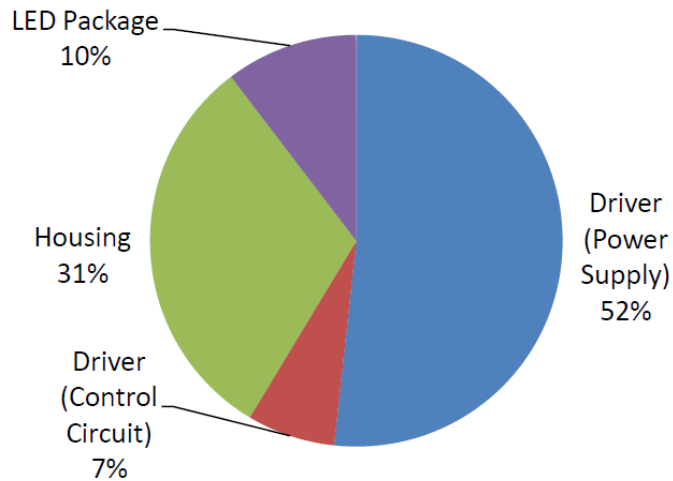
Figure 3.35: Percentage of failures

this case, the LED engine has lower failure rate compared to the driver. Since lighting systems depend on driver and LED engine, system failure rate becomes a combination of the LED driver and LED engine.

This section intends to discuss the failure mechanisms related to LED engine. LED engine failures can be divided into three main categories:

1. Failure related to semiconductor;

2. Failure related to interconnects;

3. Failure related to package. [67]

Semiconductor related failure mechanisms are defects and diffusion in the active region, and electro-migration. Interconnect related failure mechanisms are fractures in the bond wires and die attach, diffusions on the bond wires and electrostatic discharge. Package related failure mechanisms are lens damage, solder joint damage, encapsulant yellowing, carbonisation in the encapsulant, delamination, etc., [67].
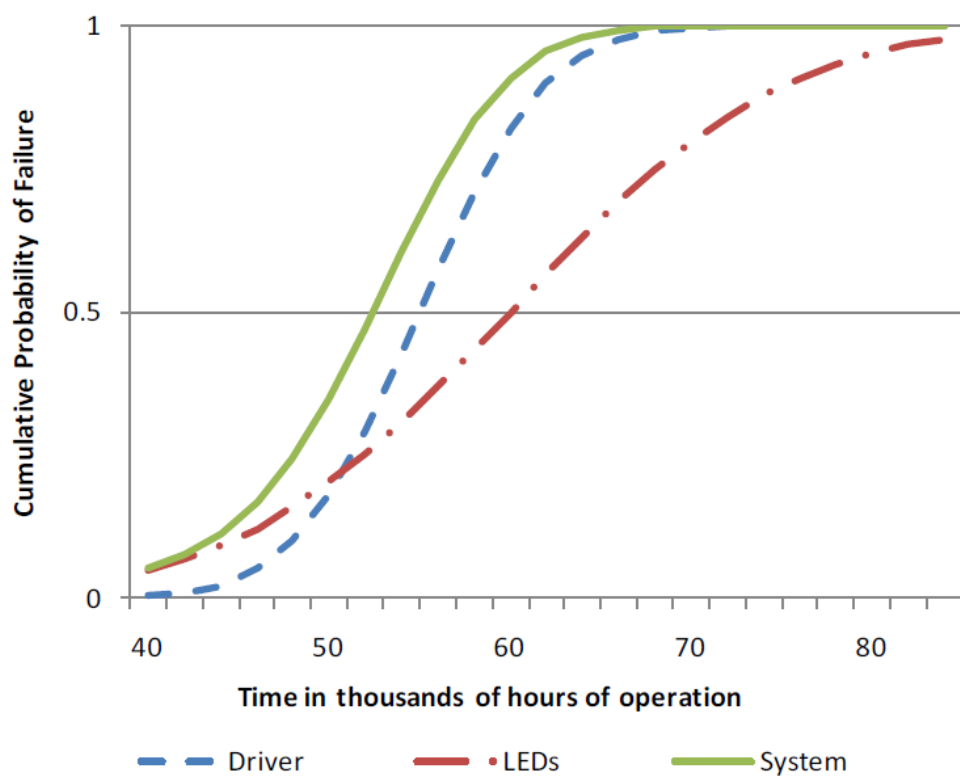
Figure 3.36: Simple example of LED system failure probability based on driver and LED engine

### 3.9.1 Semiconductor Related Failure Mechanisms

Semiconductor related failure mechanisms are usually related to the property of the material used in the active region (i.e., p-type and n-type). Carrier generation and recombination are the processes in the active region of a semiconductor LED leading to generation of energy in the form of light. Although there are different recombination processes, Radiative recombination is the process which emits energy in the form of light. Other recombination processes such Shockley-Read-Hall (SRH) recombination and Auger recombination do not only emit photons but also reduce the rate of radiative recombination processes because of some failure mechanisms related to the semiconductor. These recombination are also sometimes referred as non-radiative recombination processes. In SRH recombination energy is exchanged in the form of lattice vibration or thermal energy and in Auger recombination energy is exchanged to a third carrier. Figure 3.37 (a) [1] shows a radiative recombination and Figure 3.37 (b) shows a non-radiative recombination.
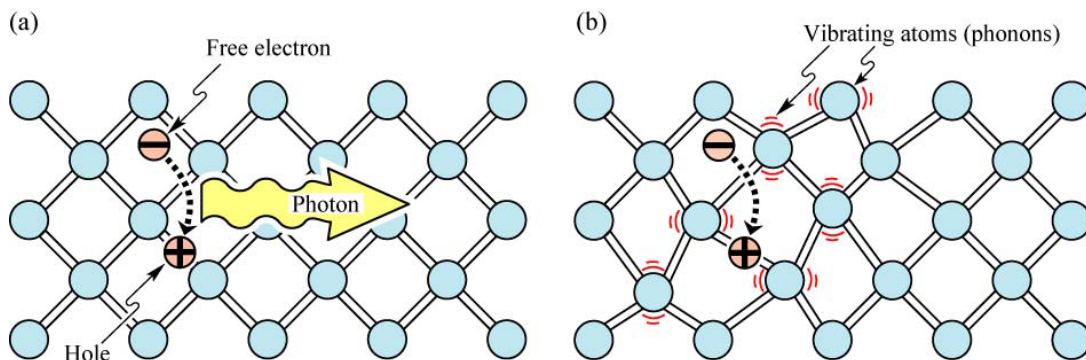


Figure 3.37: (a): Radiative recombination (b): Non-radiative recombination

Crystal defects are one of the main failure mechanisms in the semiconductor. Crystal defects have two forms (1) dark line defect (DLD) and (2) dark spot defect (DSD) in the active region. These defects are caused by the dislocation network and created in the process of the manufacturing because of the contamination, dislocation, etc., [79]. When the LED starts to operate this defect grows and creates new defect and finally damage the die/LED engine completely. Defects

lead to other failure mechanisms such as current crowding and diffusion, and hence accelerate the LED failures. When the junction temperature increases, defects start to increase and lead to trigger other failure mechanisms. Finally this will lead to complete failure in the die. Defects are also one of the reasons for the increase of non-radiative recombination which emits heat instead of photons or light. This failure mechanism is reported in many articles [18; 61; 67; 79]. Figure 3.38 [18] shows a sectioned image of a LED with a large die crack which causes the catastrophic failures in LEDs. Figure 3.39 [18] illustrates a crack in LED dies which causes failure in LEDs.
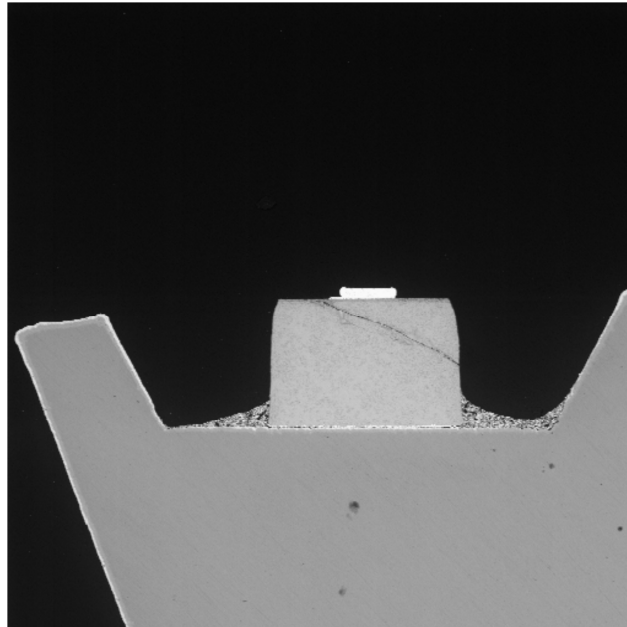


Figure 3.38: A large die crack causing a catastrophic failure in LED [18]

Diffusion in the active region is another mechanism which increases the non-radiative recombination process. High temperature accelerates the process of the diffusion in the active region [61; 67]. High temperatures cause many semiconductor related failures in LED, such as Shockley-Read-Hall (SRH) recombination and carrier leakage from the active region [80]. Defects and diffusion in the active region further increase the SRH recombination and carrier leakage from the active region. Light output power reduction (23.4%) is reported by Meyaard et al.,
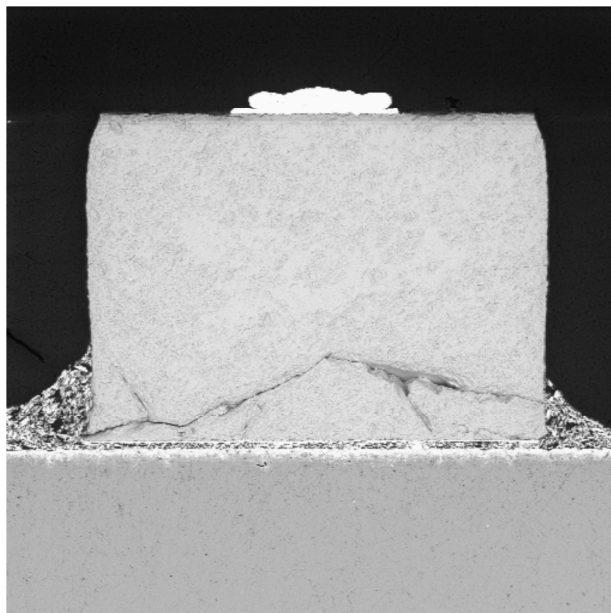
Figure 3.39: A die crack as the cause of the catastrophic LED failure [18]

based on SRH recombination (accounts for 10.4%) and carrier leakage (accounts for 13%) at high temperature (450K).

Another failure mechanism which is related to the semiconductor is the electro-migration. It is an electrically induced movement of the metal atoms in the active region. Electro-migration causes the current crowding and thermal runway. Current crowding and thermal runway increase the junction temperature to very high levels and hence reduce the light output power. Poor thermal management increase the electro-migration [67].

### 3.9.2 Interconnect Related Failure Mechanisms

Failures related to interconnects are well-known in electronic packages. An interconnect is the part which connects two different micro-structures of an electronic package. Sometimes these failures are referred to as delamination at the interconnect. There are many layers of micro-structures from board to LED die (see Figure 3.2 in page 32) and interconnect wires which connect the LED die with cathode and anode terminals of the LEDs. These layers and interconnect are

made from different materials with considerably different properties. When the operating condition is changed the materials used in the devices respond to the conditions differently. In particular, they undergo different thermo-mechanical or mechanical stresses and lead to failures driven by different forces associated with the individual parts of the structures. Poor thermal and electrical management of the device causes thermo-mechanical stress and failures. Interconnect related failures create a short circuit or open circuit in the device which cause the device to stop operating completely. Failures related to interconnect are reported in many articles [18; 61; 67]. Figure 3.40 [18] shows a bright-field optical image illustrating a broken bond wire at the wedge bond. Figure 3.41 [18] shows a die attach failed due to mechanical stress caused by a lead bending operation.
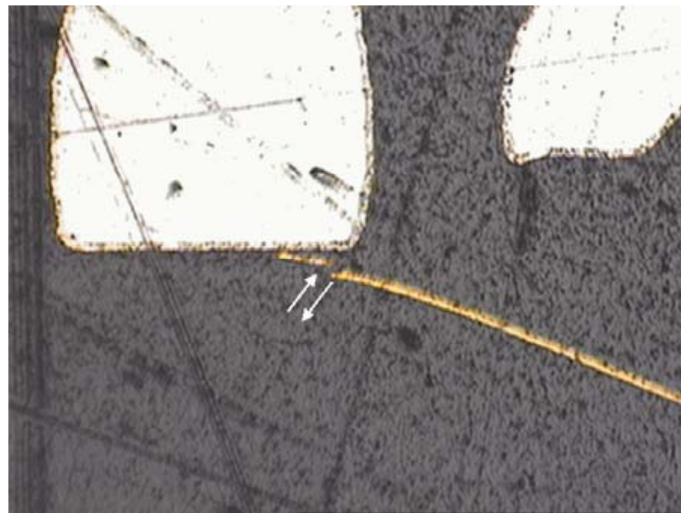


Figure 3.40: A broken bond wire at the wedge bond [18]

Figure 3.42 [18] shows a custom LED package with significant lead (bending) strain and associated damage to the glass feed-through seals. This caused the die attach to fail [18]. Figure 3.43 [18] shows a LED which exhibited degradation in light output power after humidity and rapid decompression testing. It shows damage to the die/die-attach interface [18]. Figure 3.44 [18] shows very fine crack in the lens material. The wire bond apparently failed in shear at the heel of the wedge bond. This explains the intermittent nature of the failure [18].

Some of the identified problems at interconnect level are illustrated in Figures
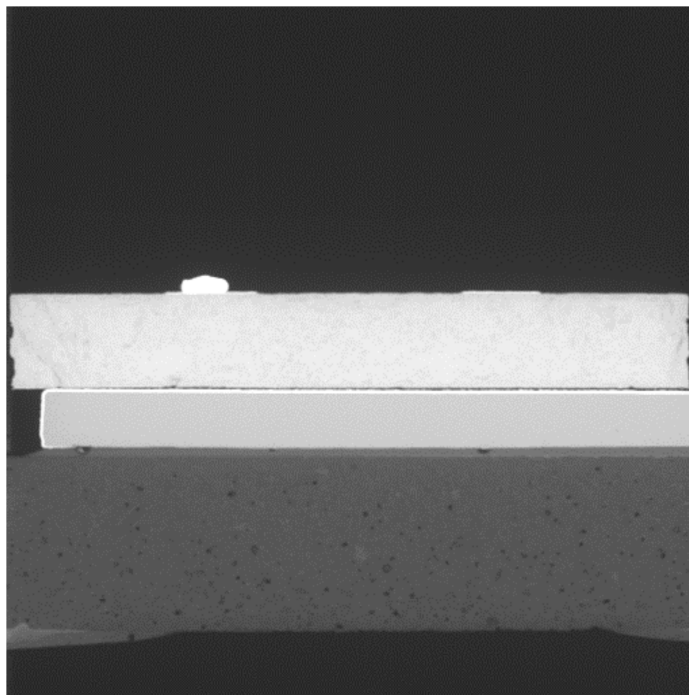
Figure 3.41: A die attach failure due to mechanical stress caused by a lead bending operation [18]
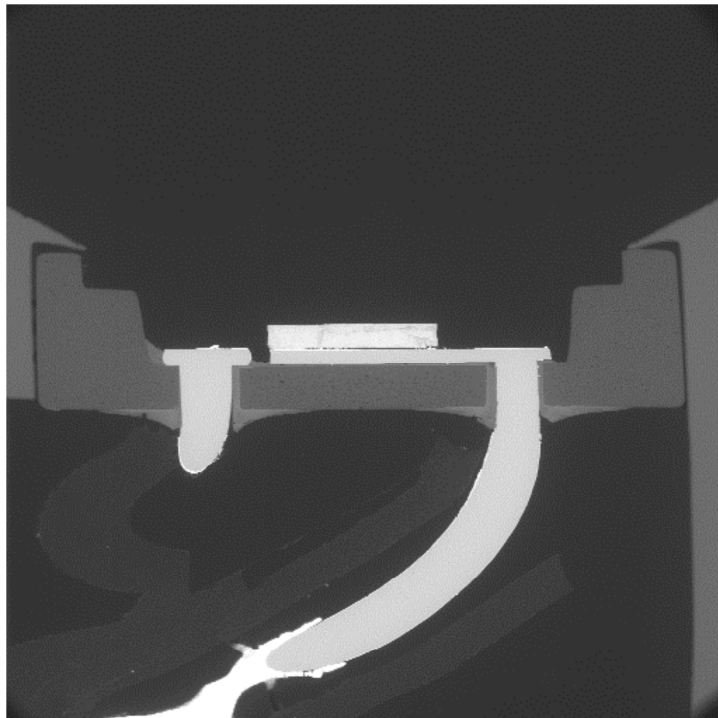
Figure 3.42: A die attach failure [18]
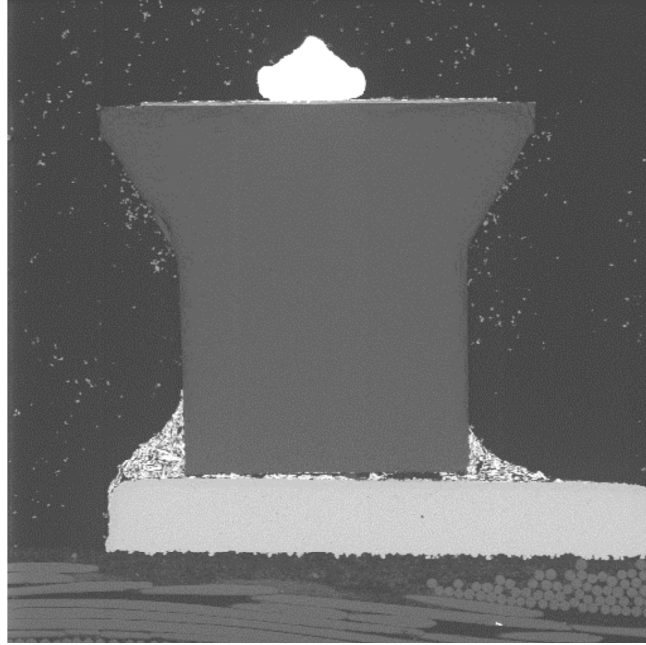
Figure 3.43: A damage to the die/die-attach interface [18]
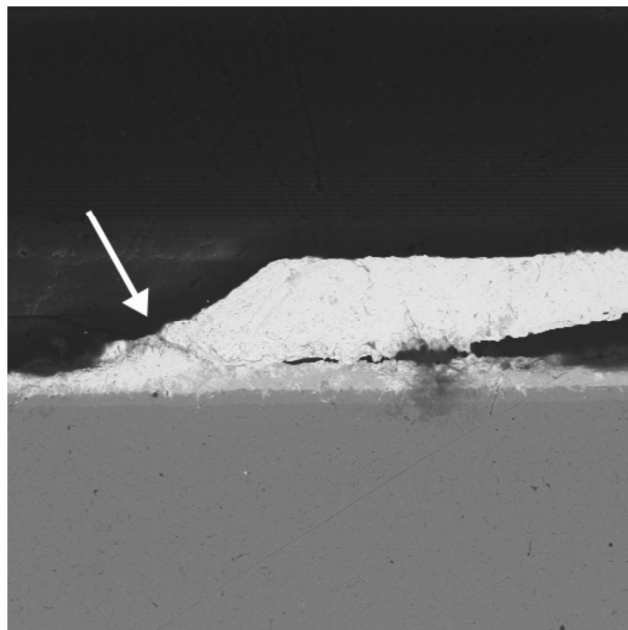


Figure 3.44: A wire bond failure in shear at the heel of the wedge bond [18]

3.45 and 3.46 [18]. Figure 3.45 shows a poor bond alignment to the pad. The probe marks on the post (right) suggest that a problem was identified prior to encapsulation [18]. Figure 3.46 shows a picture of an LED which verified as dim on the test fixture. The dark area on the die surface is an area of delamination of the encapsulant from the die. The delamination is evidence of displacement and is likely related to a high resistance bond [18].
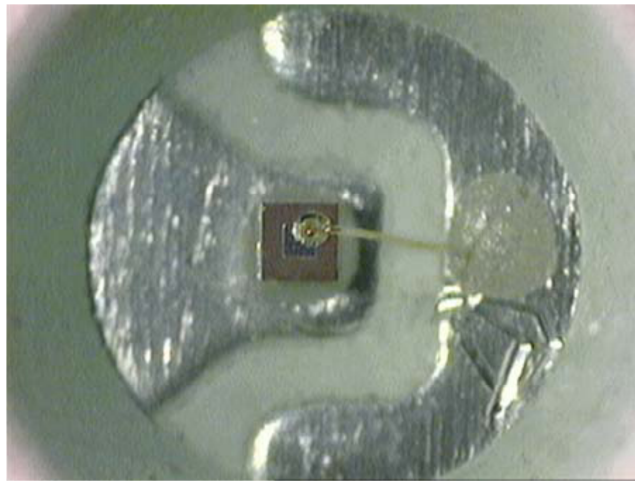


Figure 3.45: A poor bond alignment to the pad [18]
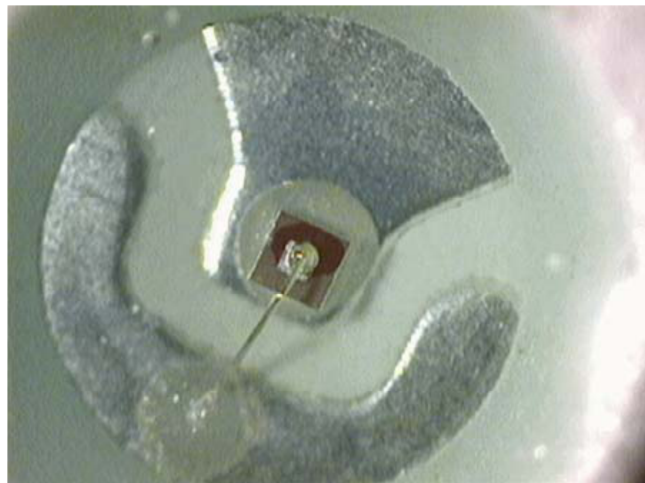


Figure 3.46: A dark area on the die which is delamination [18]

### 3.9.3 Package Related Failure Mechanisms

LED package plays critical role in removing the heat from the junction and extracting the emitted light from the semiconductor surface. Encapsulants are designed to extract the emitted light efficiently from the surface of the semiconductor. Figure 3.47 [1](a) shows a planar LED without an epoxy dome. Figure 3.47(b) shows a planar LED with an epoxy dome. Figure 3.47(c) shows a graph of extraction efficiency ratio versus refractive index of encapsulating epoxy material. Encapsulant also designed to protect the LED from the mechanical and thermal shock and humidity-induced corrosion. Transparent epoxy resins are used to design the encapsulant [67]. This encapsulant is exposed to the environmental conditions such as humidity and temperature, and other harsh operating conditions such high temperatures and thermal cycling. Hence encapsulant undergoes degradation based on these different conditions. Some of the failure mechanisms associated with the encapsulant are carbonisation and yellowing. These failure mechanisms reduce the amount of light output extracted from the surface of the active region and reduce the amount of heat removed from the active region.

Delamination can also occur at package level, between the package materials. Thermal cycles and electrical overstress can cause the materials to separate from each other. This will increase the thermal resistance and increase the temperature in the active region. High temperature in the active region will induce other failure mechanisms such as semiconductor and interconnect related failures. Delamination can also lead to permanent breakdown of the devices [67]. Figure 3.48 [18] shows a high magnification view of a ball bond failure caused by delamination of the encapsulant from the die surface [18].
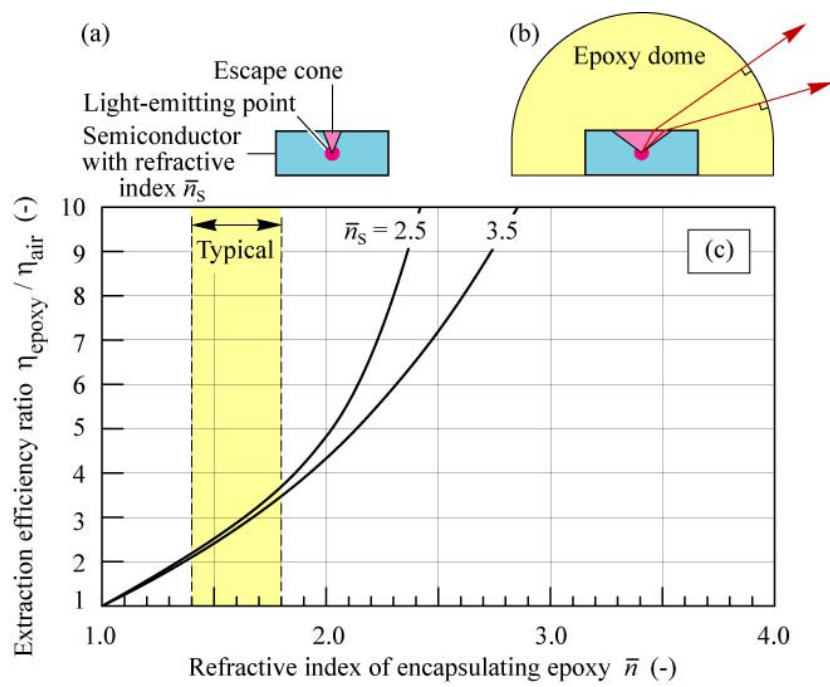
Figure 3.47: (a) LED without and (b) with dome-shaped epoxy encapsulant and (c) Calculated ratio of light extraction efficiency emitted through the top surface of a planar LED with and without an epoxy dome [1]
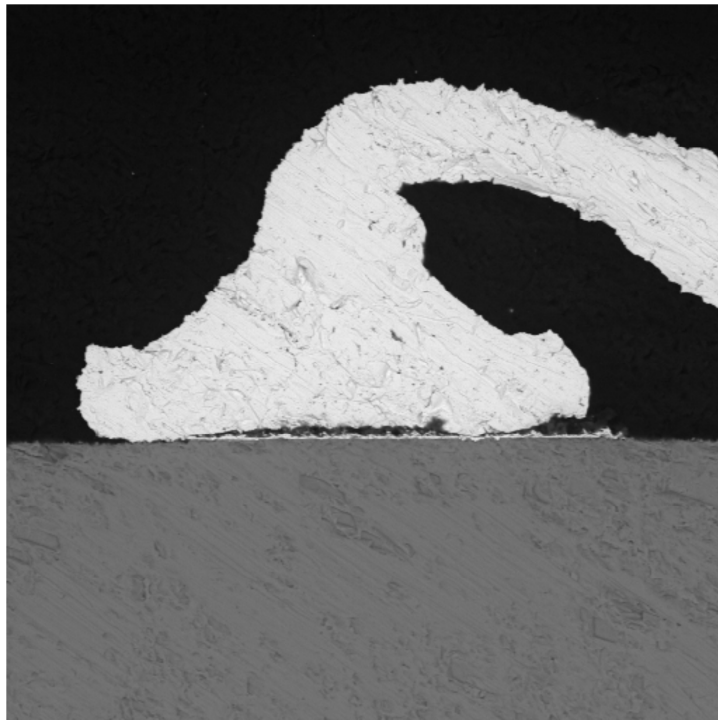
Figure 3.48: A ball bond failure caused by delamination of the encapsulant from the die surface [18]

## 3.10 Summary

This chapter has presented a detailed review on LEDs and their market, application domains, driver configurations, lamp configurations, lifetime, failure modes and mechanisms. It is evident that the market penetration of the LEDs is increasing exponentially since many lighting applications benefit form the LEDs and their advantages compared to the traditional light sources. It is also predicted that the price of the LED lighting systems will decrease with time. This will further increase the market for the LEDs.

LEDs do not stop emitting light, rather their light output power (lumen) degrade with time. Hence the failures in the LEDs are very difficult to identify. Therefore LED lighting systems need to be monitored for their failures, even though they have very long lifetime and very high reliability. As a new technology, LEDs have evolved from the simple indicator into a more advanced form of lighting systems recently, there is a need for research on their reliability, lifetime etc. In particular, there is a need for real-time health monitoring of LED lighting systems which are used in emergency, safety applications and under harsh operating conditions.

# Chapter 4

# Prognostics and Health Management Approaches and Algorithms

## 4.1 PHM Classification

Prognostics and health management (PHM) is an engineering process of failure prevention, and predicting reliability and remaining useful life-time. It has emerged in the last few years as one of the most efficient approaches in failure prevention and predicting reliability and useful life time of various engineering systems and components. PHM of engineering systems have become very important as a malfunction or failure may cause severe damage to the system, environment and users, and may result in significant repair on un-scheduled maintenance costs. Severe damages can be prevented by providing advance warning message and alarm. Repair and maintenance costs can be reduced by converting the scheduled maintenance tasks into evidence based un-scheduled maintenance tasks. Evidence based un-scheduled maintenance strategy will reduce the inspection cost, required number of skilled labours, system down time, life-cycle cost of the system and emergency un-scheduled maintenance [81]. PHM is identified as the best candidate to improve the maintenance cycle, reduce the maintenance cost and extend the overall life time through evidence based un-scheduled main-

tenance strategies. PHM can also provide support to improve the qualification approach and improve the design of the future systems [81].

PHM applications can be classified into two main categories based on how the PHM is applied to the system or product:

1. Real-time PHM (sometimes referred as online PHM);

2. Off-line PHM.

Most of the safety critical and mission critical applications require real-time PHM (refereed to as on-board health monitoring). Modern aircrafts, automobiles, etc., have a large range of on-board monitoring that is based on the use of real-time sensors. For example, an electric car provides the range distance which can be achieved with battery operation based on real-time PHM of the battery. Another example is autonomous unmanned vehicles which have embedded real-time on-board PHM, use to re-plan the mission and reconfigure the controls based on the health diagnostic and prognostic information. This includes the current state of the health and predicted state of the health [19].

Off-line PHM is deployed where the system safety is not critical and likelihood of failures is very small. Data are collected from the system and then used off-line to predict the remaining useful lifetime and to perform the maintenance. One main advantage of the off-line PHM is that complex systems models can be used to perform the PHM using computer simulations whereas, in real-time PHM, computer simulations may not be achievable as there might be limitation in the available on-board computational power and efficiency. Main advantage of the real-time PHM relates to the capability to detect failures and anomalies in the systems in a fraction of second whereas in the off-line PHM this is not possible. Real-time PHM for electronic systems is sometimes known as built-in test (BIT) or self-scanning where the electronic system tests itself. Such embedded diagnostics and prognostics allow to perform test to verify if all parts of the electronic systems work as expected.

PHM is also applied in development and deployment stages of a systems or product. PHM methodology can be applied in the design stage to optimise the design and to get the expected performance from the systems or products given certain reliability requirements. Physics of Failure (PoF) based models are used

to optimise the product design based on failure modes, mechanisms and effects analysis (FMMEA). Products and systems undergo different life-cycle loads such as thermal, electrical, mechanical, chemical, etc. These life-cycle loads vary at different stages and under different conditions of the product life such as manufacturing, storage, shipment, harsh operating, non-operating, etc. These parameters are considered at the product design stage to optimise the product design and get the best performance from the product for a certain period of time without failure. These life-cycle loads are also monitored, and used with the PoF based damage models to assess the reliability and degradation of the product in the field after it has been deployed [82]. Anomaly detection is the starting point of the PHM in the field. Anomaly detection and failure prevention can be achieved effectively by monitoring the life-cycle loads and performance parameters of the system. It will be more accurate if the life-cycle loads and parameters are monitored in real-time, especially in the case of critical applications. Many safety critical systems and mission critical systems consist of electronic hardware and software that control the electronic hardware and also interacts with the user. Most of these electronic hardware devices use thousands of individual semiconductor components to perform their operation. Malfunction or failure of any individual semiconductor component, electronic hardware or software module independently affects the system as a whole.

Health of a system is defined as the extent of deviation or degradation from its expected typical operating performance [27]. This extent of deviation or degradation of the expected typical operating performance has to be determined accurately to prevent the failures. It is also necessary to determine the parameters which operating parameters are contributing to this extent of deviation or degradation. There are two different approaches available. They are: (1) Data-driven approach and (2) Model-driven approach. Fusion approach incorporates the advance features from both data-driven and model-driven approach to perform the PHM. Most of the real world PHM applications are based on the fusion approach. Figure 4.1 illustrates the different prognostic approaches and their relationships.

Based on the techniques used for data-driven and model-driven approaches, PHM can be further classified into different approaches. For example, data-
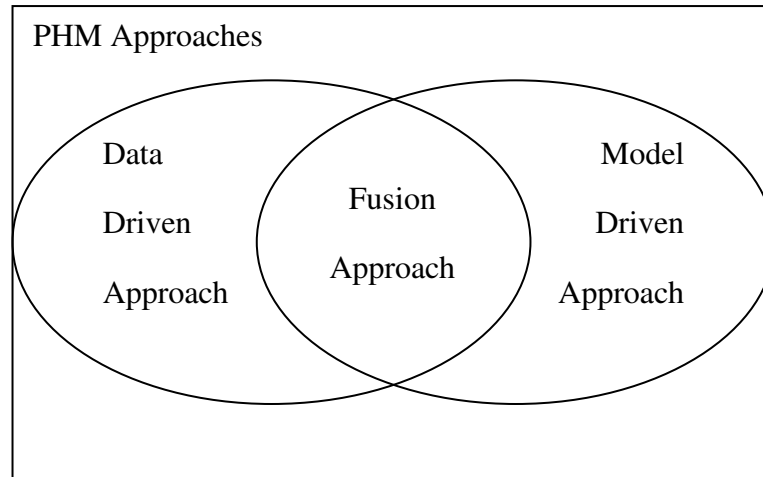
Figure 4.1: Prognostics and health management approaches

driven approach can be classified into statistical based approach and machine learning approach. Model-driven approach can be classified into Physics of failure approach and system model based approach. Figure 4.2 shows the classification of the PHM approaches.
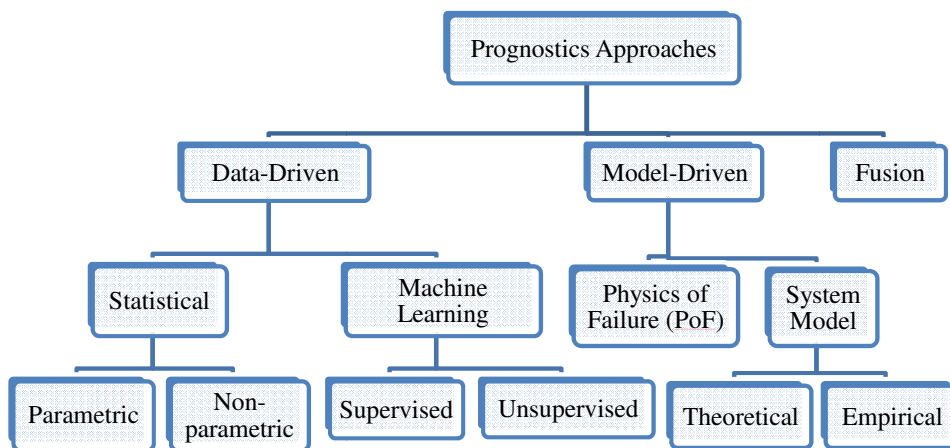


Figure 4.2: Classification of PHM approaches

This chapter divided into three main sections where data driven, model driven and fusion approaches are discussed. In this thesis PHM techniques for LEDs are investigated. Main focus of the research is to investigate suitable data driven technique for real-time health monitoring of LEDs after their deployment. Distance measure techniques such as Euclidean distance (ED) and Mahalanobis distance (MD), logistic regression (LR), neural network (NN) and Kalman filter (KF) are investigated for data driven approach. Detail investigation of these techniques in the context of LED health monitoring are discussed in next chapter. Equivalent circuit model of LED for model driven approach and Kalman filter for fusion approach are also discussed in next chapter.

## 4.2 Data Driven Approach

Data driven approach is considered as a black box approach to PHM as it does not require system models or system specific knowledge to start the prognostics [82]. Monitored and historical data are used to learn the system behaviour and to perform the prognostics. Hence the data driven approach is suitable for the systems which are complex and whose behaviour cannot be assessed and derived from first principles. The implementation of data driven techniques for the purpose of health monitoring and prognostics is generally based on the assumption that the statistical characteristics of system performance will not change until fault occurs [82]. Therefore, the main advantage of data driven approach is that the underlying algorithms are quicker to implement and computationally more efficient to run compared to other techniques. However, it is necessary to have historical data and knowledge of typical operational performance data, the associated critical threshold values and their margins. Data driven techniques rely completely on the analysis of data obtained from sensors and exploit operational or performance related signals that can indicate the health of the monitored system. Data driven strategies for diagnostics and prognostics have been applied in a number of different Prognostics and Health Management (PHM) applications [28; 29; 36; 83; 84; 85; 86; 87].

The principal disadvantage of the data driven approach is that the confidence level in the predictions depends on the available historical and empirical data (i.e.,

healthy and failure data). Availability of run-to-failure data sets for a particular system or component is the main issue of data-driven PHM, as running a system or a component to failure might be time consuming and expensive [88]. These data are required in the data-driven approach to define the respective threshold values. In some instances it is difficult to obtain or have historical data available, for example in the case of a new system or device that may require long time and/or expensive tests to failure to generate this data. However, there are techniques and procedures available that can be used to achieve this [26; 89; 90]. Three of the strategies which can be used to address this challenge are based on the use of:

1. Hardware-in-the-Loop simulations (HiL):- Hardware-in-the-Loop is a computer simulation which is used to test a real product or system by connecting its hardware that applies simulated loads as in real application. It is very fast and cheap to implement. In addition, several failure parameters (i.e., operational and environmental) can be controlled independently. HiL can also be used to algorithm development, testing and validation, benchmarking and development of metrics for prognostics [89; 90].

2. Accelerated Life Test (ALT):- Accelerated load test is designed to cause the product to fail more quickly than under normal conditions by applying accelerated (elevated) stress conditions resulting in the same failure mechanisms. ALT becomes an important methodology in the development of the PHM for electronics. Several environmental and loading conditions can be applied independently to accelerate the failure [26].

3. Online Training:- Online training is based on the assumption that a new system performance data defines the healthy system and they do not fail for a certain period of time. This type of approach can also be called semi supervised learning as only healthy data is available. Reinforcement learning approach is also suitable for this strategy.

Data-driven approach for PHM can be classified into (1) Statistical approach and (2) Machine learning approach [87]. Statistical approach uses statistical parameters such as mean, variance, median, etc., to make prediction based on the

known or unknown underlying probabilistic distributions. Statistical approach might be simple if the underlying statistical property (i.e., probability distribution) is known and this type of approach is called parametric approach. Statistical parameter estimation techniques and hypothesis testing that belong to that probabilistic class can be applied to detect the anomalies in the data [91]. Statistical distance measure is another simple way to estimate the deviation of the new sample data from the expected mean data (i.e., how many standard deviations away from the mean) [91]. Outlier rejection technique is another way to detect data anomalies based on the box plot parameters such as lower extreme and upper extreme [91]. Unfortunately, most of the reliability data and their statistical properties are unknown and hence probability functions representing these data need to be constructed first. This type of approach is called non-parametric approach and it introduces more flexibility into the computations. Therefore a non-parametric approach can be viewed as a generalised approach. One of the widely used techniques for non-parametric approach is histogram analysis. A better way to estimate the probability density function is to use kernel methods [91].

Machine learning approach makes predictions based on acquired data (such as healthy and failure data) by converting the acquired data into useful information which then can be used in conjunction with sensor data to achieve the future predictions. Machine learning approach is more data-driven and typically no statistical assumptions are made. One of the well-known approaches in the field of machine learning is the neural network [92]. Another machine learning approach is support vector machine (SVM) which separates the data into different classes using hyper-planes, after they are transformed by a kernel function [93]. SVM uses linear combination of kernel functions centred on the subset of the training data which is known as support vectors [94]. PHM application may require more than one algorithm for different tasks such as anomaly detection, parameter isolation, parameter trending, damage estimation, life time estimation, etc. Hence different types of algorithms can be used to achieve these individual tasks based on the performance of those algorithms.

### 4.2.1 Statistical Approach

Statistical approach is based on the underlying statistical property of the data. If a new observation is not representing the statistical property of the data then the observation is considered as an anomaly. Statistical techniques fit the typical expected operating condition data and then apply statistical inference test to determine if the new observation belongs to the fitted statistical model. For example, if the data representing the normal operating condition is modelled as the probability density function (PDF) $p(x)$ then new observation data can be tested against the developed PDF (i.e., if $P(x_{new}) < \varepsilon$ flag anomaly and if $P(x_{new}) \geq \varepsilon$ flag normal). There are two different ways available to fit the data into a statistical model (i.e., develop a PDF, $p(x)$) (1) parametric approach and (2) non-parametric approach [95]. Statistical models have different computational complexity and require different computational powers based on the complexity of the statistical models.

Main advantage of the statistical approach is, if the assumed statistical characteristics are true, then the result from the statistical inference test for the new observation will be statistically valid. In addition, statistical approach can provide a confidence interval and this can be used in the decision making in relation to the new observation data. Statistical approaches can be based on an unsupervised technique which does not require labelled training data, thus offering a robust statistical approach [95]. On the other hand, statistical approach completely depends on the assumed statistical characteristics of the data and hence if the assumption is not true, they will not detect the anomalies accurately. Typically the assumption may not be true in particular for high dimensional real data sets. In addition, even if the assumed statistical characteristics are true, there are many statistical inference tests available and selecting the suitable one might be difficult [95].

#### 4.2.1.1 Parametric Approach

Parametric approaches are based on assumed underlying statistical properties (typically normal, Weibull, exponential, etc.,) of the expected data. Based on the assumed underlying probability distribution of the data, parameters associ-

ated with that probability distribution are calculated from the data. Typically these data will represent a healthy system performance under expected typical operating conditions. Healthy or normal operating data then will be defined by these parameters assuming a probability distribution. This model can be used to detect the anomalies and predict the remaining useful life. Once the system healthy or normal operating data are defined by a probability distribution and parameters associated with that probability distribution are estimated, new monitored data can be gathered and analysed. The new data can be classified using different methods and different probability distributions. Some of the methods available are listed below:

1. Distance Measures – These techniques are based on the assumption that the variables follow the normal distribution. Namely, there are many different distance measure techniques available. Distance measure techniques have been considered for this research work as one of the data driven PHM approach to LED prognostics. In particular, Mahalanobis distance and Euclidean distance are investigated for this research program. The Mahalanobis distance have been reported in some research work related to PHM [96; 97; 98]. Detail information about these methods has been reported in next chapter and is based on the work reported by R. De Maesschalck et al., [99].

2. Hypothesis Testing – Hypothesis testing is one of the simplest statistical procedures which can be used to test the data whether they come from the same population as the training data or not [91]. It can also be used to test if the mean of a sample is equal to $\mu$ when the standard deviation $\sigma$ is known [100]. Hypotheses are always statements about the sample population parameters instead of sample population data. There will be two types of error which may occur in the hypothesis testing (1) Type I Error and (2) Type II Error. Type I Error (false positive – $\alpha$) is defined as rejecting the null hypothesis when null hypothesis is actually true. Type II Error (false negative – $\beta$) is defined as the accepting the null hypothesis when the hypothesis is actually false. It is not possible to eliminate these errors completely. Typically the hypothesis test decision is taken by fixing

an acceptable value for $\sigma$ and by minimising the $\beta$. Standardised difference between the population and sample statistics is compared with the decision rules before making the decision. Most of the hypothesis tests use underlying probability density function as normal. Figures 4.3 and 4.4 illustrate the normal and Weibull fits respectively to a sample current data. Figures 4.5 and 4.6 illustrate example of normal and Weibull fits to a sample temperature data.
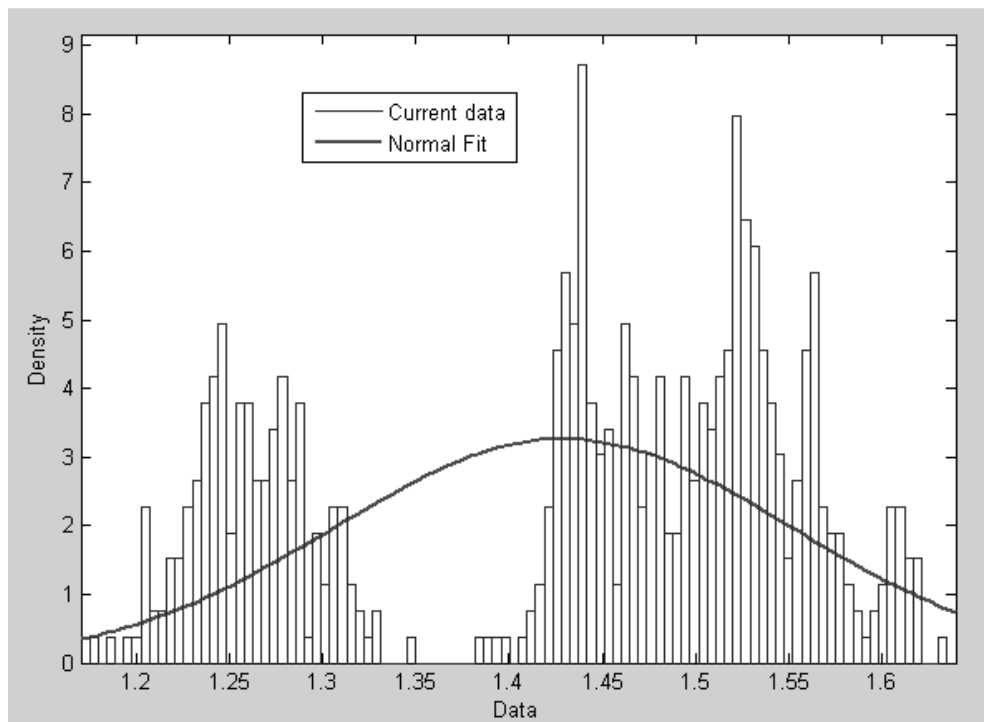


Figure 4.3: Normal fit to sample data set

3. Analysis of Variance (ANOVA) – It is a method to analyse the means of several groups of samples which can be affected by different types of factors. Simplest form is one-way analysis and it is an extension of the t-test. Simple form of ANOVA can be used to compare different groups of sample data [100]. ANOVA can be applied to groups of data based on the following assumptions: (1) values are normally distributed in every group and (2) variance are equal. Decision will be made based on the variability among
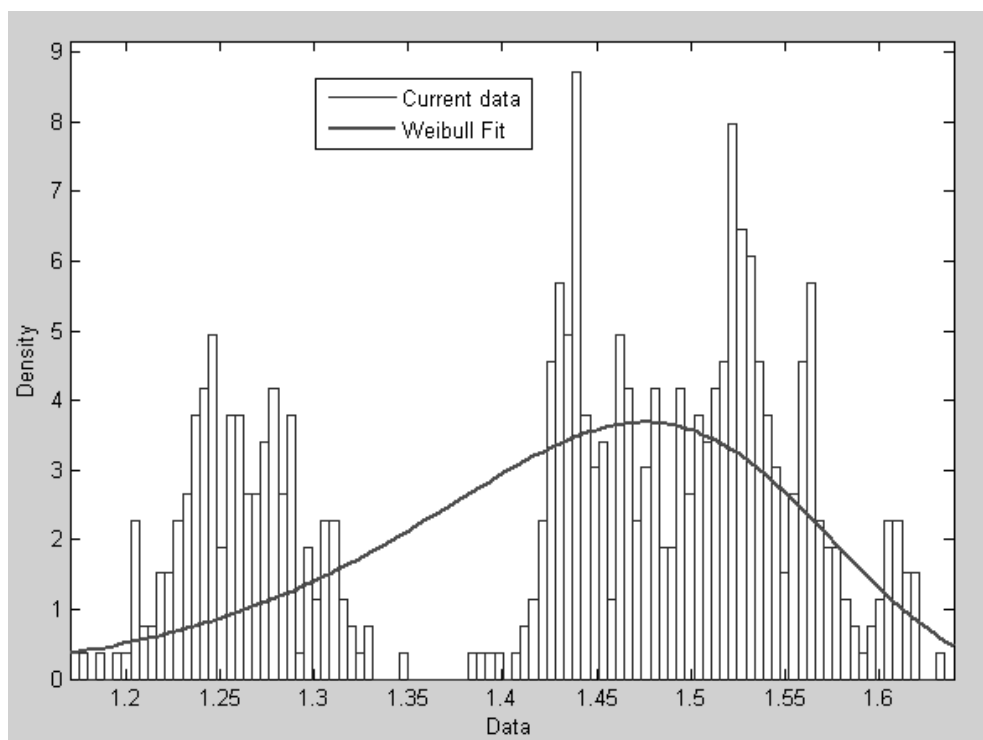
Figure 4.4: Weibull fit to sample data set
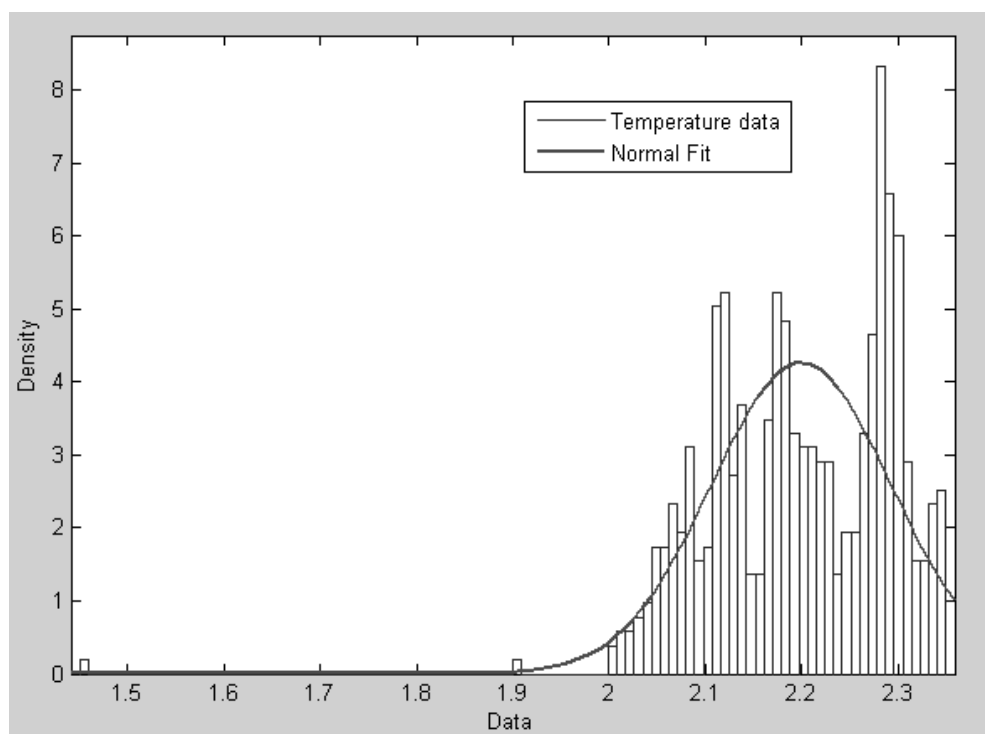
Figure 4.5: Normal fit to another sample data set
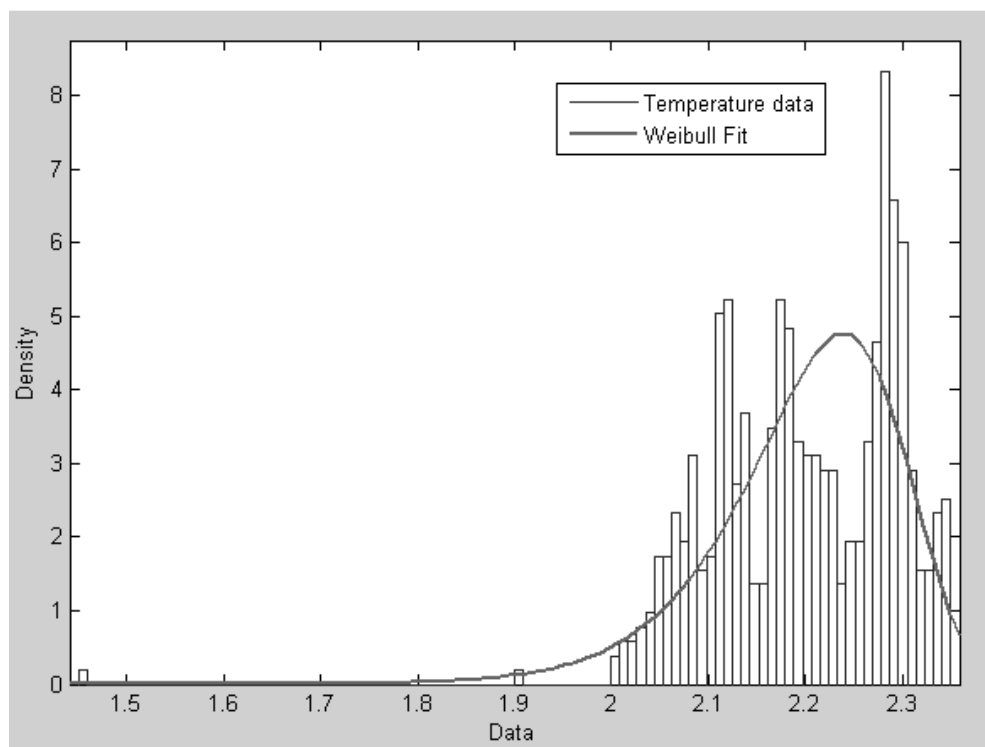
Figure 4.6: Weibull fit to another sample data

the groups. If the variability among the group is small compared to the variability within the group, then this will lead to the decision that groups can be treated as identical. If the variability among the groups is large compared to the variability within the groups, then the groups can't be treated as identical.

4. Extreme Value Theory – Extreme Value Theory (EVT) is a branch of statistics and analysis for data belonging to the tails of the distribution. EVT can be used to set the threshold values for anomaly detection where EVT explicitly models the tails of the distribution of normal data [92; 101; 102].

5. Maximum Likelihood (ML) Estimation – It is an approach to estimate the most likely value related to other values in the population data. Log-likelihood which is the logarithm of the likelihood function is typically used to estimate the MLE by maximising the log-likelihood [87]. If the maximum likelihood is the mutually-independent observations $x = \{x_1, x_2, x_3, \ldots, x_n\}$ which is an instance of the random sample $\{X_1, X_2, X_3, \ldots, X_n\}$, the joint probability density function (PDF) equals to the product of marginal PDF. Therefore the likelihood $L$ and the maximum likelihood for a parameter $\theta$ will be estimated as follows [103]

$$L\left(\theta|x\right) = P\left(x|\theta\right) \tag{4.1}$$

$$L(\theta|x) = P(X_1 = x_1, X_2 = x_2, X_3 = x_3, \ldots, X_n = x_n) \tag{4.2}$$

$$L(\theta|x) = \prod_{i=1}^{n} P_{X_i}(x_i|\theta) \tag{4.3}$$

$$\theta^* = \arg\max_{\theta} L(\theta|x) \tag{4.4}$$

6. Maximum-A-Posteriori (MAP) Estimation – MAP estimation is considered as a Bayesian version of ML estimation [87]. This estimation technique can

be used to estimate the parameters of a process or system based on prior knowledge of the system. This prior knowledge typically comes from the historical data of this system. Such prior information can be included in the estimation in the form of probability density function (PDF). Parameter $\theta$ which need to be estimated are considered as random variable and the associate probability $P(\theta)$ is called the prior probability. Bayes' theorem can be applied to incorporate the prior information into the estimation [103]:

$$P\left(\theta|x\right) = \frac{P\left(x|\theta\right)P(\theta)}{P(x)} \tag{4.5}$$

The term on the left hand side of the equation is called the posterior and represent the predicted probability. On the right hand side, the numerator is the product of the likelihood term and the prior term. The denominator serves as a normalization term so that the posterior PDF integrates to unity. Therefore, Bayesian inference produces the maximum-a-posteriori (MAP) estimate [103]:

$$\arg\max_{\theta} \mathrm{P}(\theta|\mathrm{x}) = \arg\max_{\theta} P(x|\theta)P(\theta) \tag{4.6}$$

7. Expectation-Maximisation (EM) Algorithm – EM algorithm is used to estimate the ML or MAP of parameters using an interactive process. These parameters are from a statistical model which depends on some hidden variable. The iterative process switches between two different steps in the process: (1) estimating the expectation (E-step) and (2) maximisation (M-step). The E-step is used to compute the expectation of the log-likelihood based on the current estimate for the parameters. The M-step is used to compute parameters which maximise the computed log-likelihood in the E-step. Estimated parameters values are used to compute the expectation of the log-likelihood in the next E-step and this have to be repeated until the log-likelihood of the parameter remains constant [87; 103].

8. Gaussian Mixture Modelling (GMM) – It is widely used for density estima-

tion and to form the hidden space of radial-basis function networks [101]. GMM uses fewer kernels than the number of pattern in the training set and model parameters are estimated by maximising the log likelihood of the training set with respect to the model. Optimisation algorithms such as conjugate gradients are used to maximise the log-likelihood of the training set with respect to the model. One of the disadvantages is in the very large number of the samples that are necessary to train the model if the dimensionality of the data is high [91].

#### 4.2.1.2    Non-Parametric Approach

Non-parametric approach is not based on any assumption of underlying statistical property of the population data. Non-parametric approach gives more flexibility than the parametric approach and can be used to fit the data more accurately. Non-parametric approach is more suitable where the underlying probability distribution is not known or not a standard distribution. Most of the real world data may require a non-parametric approach to estimate the density function as they do not follow a standard density function. There are many approaches available to solve non-parametric problems. Some of the approaches based on non-parametric approach are listed below:

1. Parzen-Window Density Estimation – This non-parametric probability density function estimation technique was introduced by Emanuel Parzen. Probability density is estimated such that all the observation data belong to a window function that can contribute to the density estimation based on selected window kernel function which is a weighting function used in non-parametric techniques [87; 91; 104]. For a given data set $D = \{x_1, x_2, \ldots, x_n\}$ of n independent and identically distributed (i.i.d) example drawn from $p(x)$ which is the density function that needs to be estimated, the Parzen-window estimate of $p(x)$ based on the $n$ example in the $D$ is given by [104]:

$$p(x) = \frac{1}{n} \sum_{i=1}^{n} \delta_n(x - x_i) \qquad (4.7)$$

where $\delta_n\left(.\right)$ is the kernel function and its exact form depends on $n$. Typically Gaussian kernel is used in many situations as they are: (1) very smooth and (2) symmetrical about the centre. Hence the estimated density function will also be smooth and can be a mixture of radially symmetrical Gaussian kernel with a common variance $\sigma^2$ [104].

$$p\left(x\right) = \frac{1}{n(2\pi)^{d/2}\sigma^d} \sum_{i=1}^{n} exp\left\{-\frac{\|x - x_i\|^2}{2\sigma^2}\right\} \qquad (4.8)$$

where $d$ is the dimensionality of the feature space. For example in PHM, $d$ can be represented by the number of sensors which are used to monitor health of a system. There are many different kernel functions and some of the commonly used functions are Gaussian, uniform, box, triangle, Epanechnikov, etc. Kernel functions are generally selected based on the required property of the function and the available computational power [81]. Non-parametric fitting for temperature sample data is shown below. Figures 4.7, 4.8 and 4.9 illustrate the non-parametric fitting to current sample data using Gaussian, box and triangle kernel window functions, respectively.

2. Histogram Based Approach – The simplest non-parametric approach is the histogram based approach. It involves two steps: (1) building the histogram based on available data typically under normal operating conditions and (2) test the new observation data against the developed histogram. If the data does not belong to any of the bin of the histogram then observed data is an anomaly. Size of the bins plays a critical role in this approach. If the size of the bins are small then many normal test instances will fall in empty or rare bins, which lead to a high rate of false alarm. If the size of the bins is large then many fault instances will fall in frequent bins which lead to high false negative rate. An optimum size for the bin is necessary to construct the histogram which will maintain a low false alarm rate and a low false negative rate [95]. Accuracy of the histogram based approach can
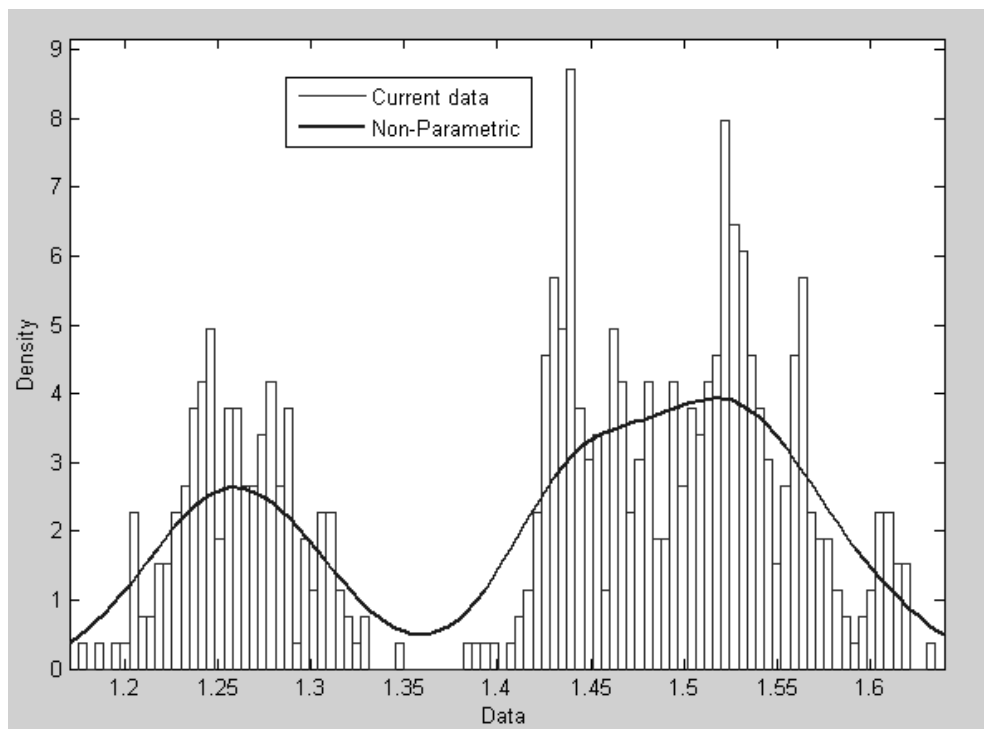
Figure 4.7: Non-parametric fit using Gaussian kernel
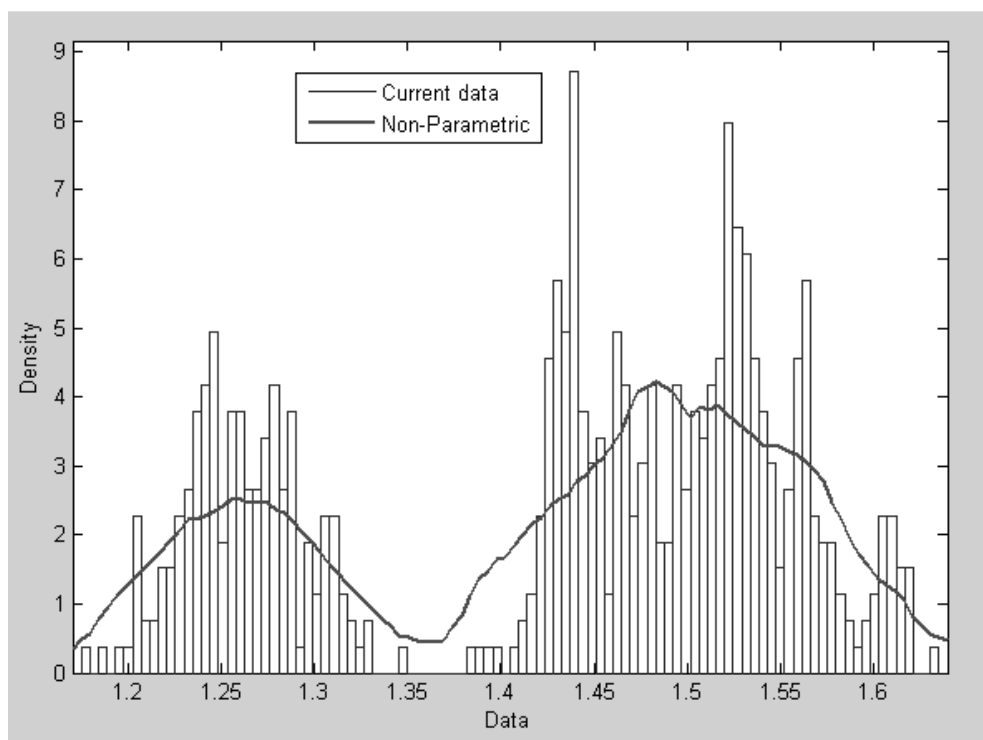
Figure 4.8: Non-parametric fit using box kernel
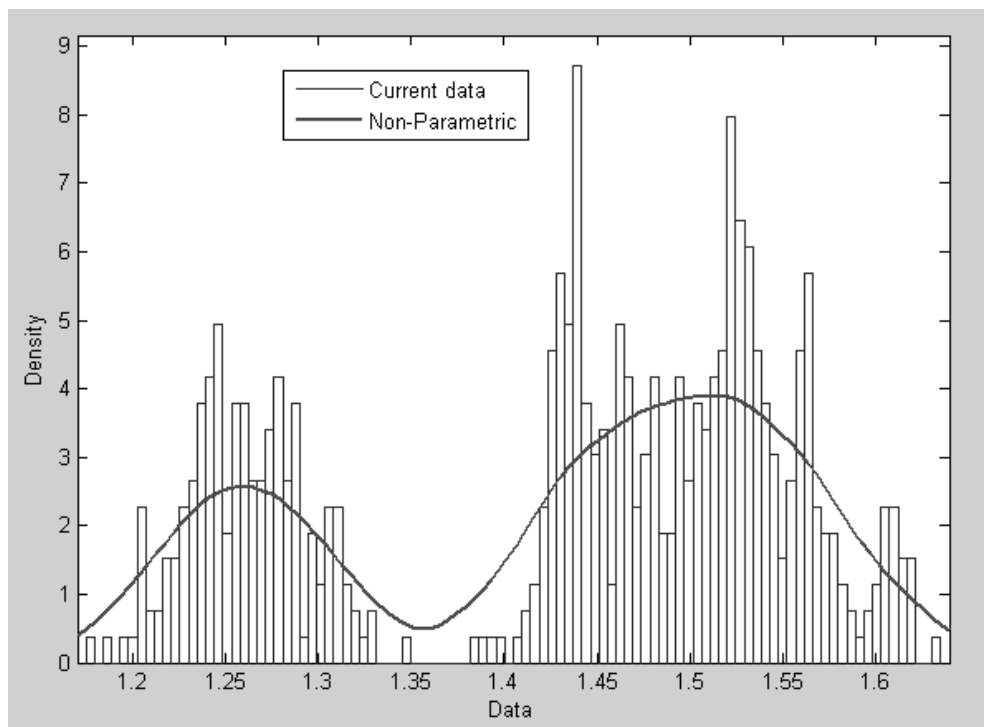
Figure 4.9: Non-parametric fit using triangle kernel

be estimated using integrated square mean error (ISME) as follows [81].

$$IMSE = \int E[g(x) - f(x)]^2 dx \qquad (4.9)$$

where $g(x)$ is the estimated density and $f(x)$ is the true density. Optimum bin size was estimated by Scott in 1979 [81].

$$h_n^* = \left[ 6^{\frac{1}{3}} \left( \int_{-\infty}^{\infty} f'(x)^2 dx \right)^{-\frac{1}{3}} \right] n^{-\frac{1}{3}} \qquad (4.10)$$

Since this equation requires the derivative of the unknown PDF $f(x)$, an estimate of $f(x)$ (i.e., $g(x)$) can be used to estimate the $h_n^*$. Optimal bin size for the Gaussian density estimation is [81]:

$$h_n^* = 3.49 \ s n^{-1/3} \qquad (4.11)$$

where $s$ is the standard deviation and $n$ is the sample size. For non-Gaussian density estimation Freedman and Diaconis suggested another bin size [81].

$$h_n^* = 2 \left( IQR \right) n^{-1/3} \qquad (4.12)$$

where $IQR$ is inter-quartile rage of the data. If the bins size is estimated then the histogram can be defined as [81]:

$$g(x) = \frac{1}{nh} (number \ of \ X_i \ in \ the \ same \ bin \ as \ x) \qquad (4.13)$$

3. k-Nearest Neighbour (k-NN) Approach – It is another technique which can be used to estimate the density function. It does not require a smoothing parameter. It requires however a width parameter which sets the position of the data point in relation to other data points. Main disadvantage of this method is that it requires large number of computations [87; 91]. k-NN approach assumes the normal operating instances occur in the dense neighbourhoods, while the anomalies occur far from their closest neighbourhoods [95]. This approach requires a similarity or distance measure between

two data points. This distance or similarity can be calculated in many different ways such as Euclidean distance, Mahalanobis distance, Manhattan distance, cosine angle distance, etc. Distance measure is also used in many other tasks such as clustering (k-mean), distance-based outlier detection, classification (SVM) and several other machine learning techniques [105]. k-NN anomaly detection approach can be divided into two groups: (1) approach which uses the distance of a data instance to its $k^{th}$ nearest neighbour as the anomaly and (2) approach which computes the relative density of each data instance [105]. The basic k-NN approach is based on the assumption that the anomaly score of a data instance is defined as its distance to its $k^{th}$ nearest neighbour in a given data set. k-NN approach based on relative density estimates the density of the neighbourhood of all data instances. New data instance (observation) with low density is marked as anomaly and data instance with high density is marked as normal [105]. Main disadvantage of k-NN approach is computational complexity which is $O(n^2)$. Although sampling techniques try to address the computational complexity by considering nearest neighbours within a limited sample of the data set, they might end up in incorrect anomaly scores if the sample size is very limited [95]. Main advantage of this approach is the k-NN does not make any assumption about the distribution of the data.

4. Wilcoxon-Mann-Whitney Test – The test is used to compare two groups of sample data. Wilcoxon-Mann-Whitney test is also called as Wilcoxon rank sum test [87; 106]. This is a hypothesis test on the two different samples. Main advantage of this rank test is that rank can be estimated in advance hence run time computation will be less. In addition, noise effects will be reduced using the rank instead of the raw data [87].

## 4.2.2   Machine Learning Approach

Although there is no explicit definition for machine learning, Arthur Samuel defines the machine learning as a field of study that gives computers the ability to learn without being explicitly programmed [107]. Tom Mitchell defines the machine learning problem as a computer program which is said to learn from

experience E with respect to some task T and some performance measure P, if its performance on T, as measured by P, improve with experience E [108]. Machine learning is a proved approach in many different fields such as speech recognition, computer vision (i.e., face, hand writing and object recognitions), information retrieval, robotics, medical diagnosis, financial prediction, target tracking, biological predictions, etc. There are mainly three types of learning approaches: (1) Supervised learning (2) Unsupervised learning and (3) Reinforcement learning. Machine learning approaches can be used in the PHM applications to learn the behaviours of the systems and make predictions based on the learned models. Since PHM problems can be formulated as classification or clustering techniques of a machine learning approach, it can be used to classify or cluster the data into different groups (i.e., healthy, anomaly, etc.,). Hence, with the help of machine learning new data can be classified into healthy or anomaly and then can be used to isolate the anomalies and faults. Further this information can be fed into prediction algorithm to predict the reaming useful life time of a system [87].

### 4.2.2.1 Supervised Learning Approach

If the algorithm is given with the labelled outputs for a set of input, then the learning is called supervised learning. Its goal is to predict a correct output for a new input data. Most of the PHM problems can be treated as a supervised learning problem where the sets of healthy and failure data are available. Some of the frequently used supervised learning techniques are discussed below.

1. Linear Regression – Linear regression is the simplest way to model a relationship between input variable and output variable. Generally the linear regression coefficient are estimated by minimising the squared error function for a set of training data [109].

$$y(x, w) = w_0 + w_1 x_1 + ... + w_n x_n \qquad (4.14)$$

where $x_0$, $x_1$, ..., $x_n$ are the input variables, $y(x, w)$ is the output variable and $w_0$, $w_1$, ..., $w_n$ are the regression coefficients. Gradient decent algorithm is generally used to estimate the regression coefficient by minimising the

99

mean squared error function. Mean square error function sometimes is referred as cost function in machine learning.

2. Logistic Regression – Logistic regression is another simplest approach to model the relationship between the input variables and output variable. This is similar to the linear regression but provides the output between 0 and 1. Hence logistics regression is used a classification technique. This approach is discussed in chapter 5 in detail. Logistic regression is used in medical diagnosis and also in industrial diagnosis [109; 110].

3. Neural Networks – Many data-driven PHM approaches are based on artificial neural networks [29; 30; 31]. Neural network is a graph based on some interconnected numerical values attached to each node. It also has set of input nodes, output nodes and hidden layers. Neural networks are trained with a set of training data to optimise the network parameters to get the desired output. This can be achieved by minimising the output error. For the PHM application, a neural network can be used as a statistical modelling and prediction algorithm which can be achieved in two different ways: (1) density estimation and prediction, and (2) classification and regression. For a statistical modelling and prediction problem the neural network can be trained to produce a statistical model which can be used to predict the output for a new input data. Density estimation is achieved by modelling the unconditional distribution of the training data. In the case of an input vector , neural network is trained to model the density function $(X)$. Based on the labelled target variable threshold value of the probability of anomalies will be determined. Classification is achieved by arranging the input data into different groups based on the output classes. In the case of an input vector , a neural network classifies the input vector into one of the different classes $C_1, C_2, \ldots, C_n$ represented by the labels of the output variable [111].

For example in the case of PHM application the labels of the output variable can be healthy, anomaly, etc. Then the regression can be used to extrapolate the damage or failure precursor to estimate the remaining useful life time of a system. Main advantage of the neural network is that a very small

number of parameters need to be optimised for training networks and no
prior assumptions on the property of the data are made. There are many
different types of architectures available for neural networks such as multi-
layer perceptron (MLP) networks, self-organised maps (SOM), radial basis
function (RBF) networks, support vector machines (SVM), Hopfield net-
works, oscillatory networks, etc., [91]. Figure 4.10 [111] illustrates a neural
network for density estimation. Figure 4.11 [111] shows a neural network
for classification problem.
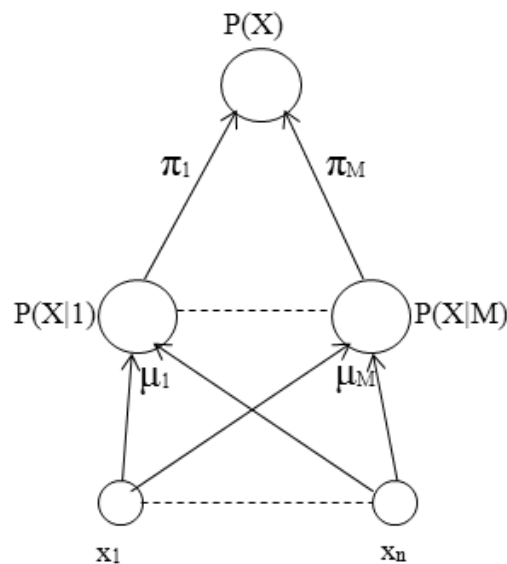


Figure 4.10: Neural network for density estimation problem

4. Support Vector Machines (SVM) – Support Vector Machine was introduced
   by Vapnik in 1998. SVM is described as a function estimation problem for
   a given set of measurement data with noise. Idea behind the approach is to
   map the low dimensional data (input space vector $X$) into high dimensional
   vectors of the features space (feature space $Z$) such that the input vectors
   can be grouped based on the label of the target variable by an optimal
   unique hyper plane [93]. Initially SVM was applied for pattern recognition
   problems but became a popular approach in many different fields because
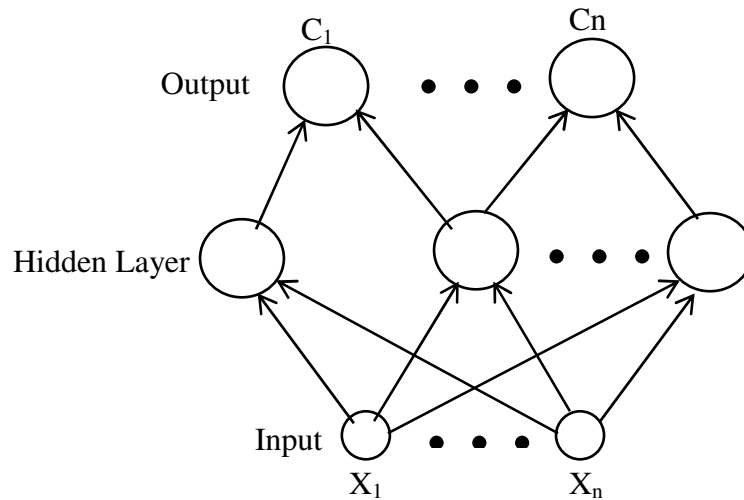
Figure 4.11: Neural network for classification problem

of its performance. SVM has been applied to anomaly detection problems as a one class learning technique. Set of normal data are used to learn a region using kernel functions. This region can be defined as a normal operating region. If the new observation data belongs to the normal region, it is flagged as normal or otherwise it is flagged as anomaly [95].

For a set of training data $x_i, y_i$, $i = 0, 1, \ldots, n$, $y_i \in -1, 1\}$, $x_i \in \mathbf{R}^d$, there are some hyper-planes which separate the positive (+1) from the negative (-1) training data. Figure 4.12 illustrates some of the hyper-planes which can be used to separate two classes of the sample data. Shortest distances to the closest negative and closest positive points from the hyper-plane are $d_-$ and $d_+$ and this distance will be defined as the margin of separating hyper-plane. In the case of linearly separable, the hyper-plane with the largest margin will be selected by the SVM. The closest points from the hyper-plane are called the support vectors [112]. Figure 4.13 shows the hyper-plane with the largest margin and the support vectors.
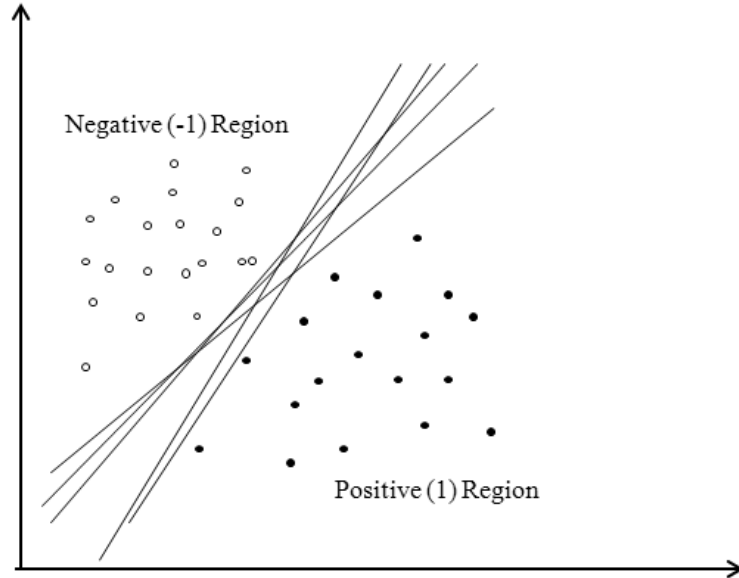
Figure 4.12: Linearly separable data with several hyper-planes

Linear support vector machine can be formulated as follows [112]:

$$x_i.\mathbf{w} + b \; \geq \; +1 \qquad\qquad for \; y_i = \; +1 \qquad\qquad (4.15)$$

$$x_i.\mathbf{w} + b \; \leq \; -1 \qquad\qquad for \; y_i = \; -1 \qquad\qquad (4.16)$$

These two constrains can be combined together as one inequality:

$$y_i \left( x_i.\mathbf{w} + b \right) - 1 \; \geq 0 \qquad\qquad for \; all \; i \qquad\qquad (4.17)$$

Largest margin will be $\frac{2}{\|\mathbf{w}\|}$ (i.e., in the above case, $d_- + d_+$). Hence pair of hyper-planes which gives the largest margin can be obtained by minimising $\|\mathbf{w}^2\|$ subject to the constraints [112].

Relevance Vector Machine (RVM) is a Bayesian treatment model of identical functional form of the SVM. RVM overcomes a number of practical disadvantages faced by the SVM. In particular, RVM uses dramatically
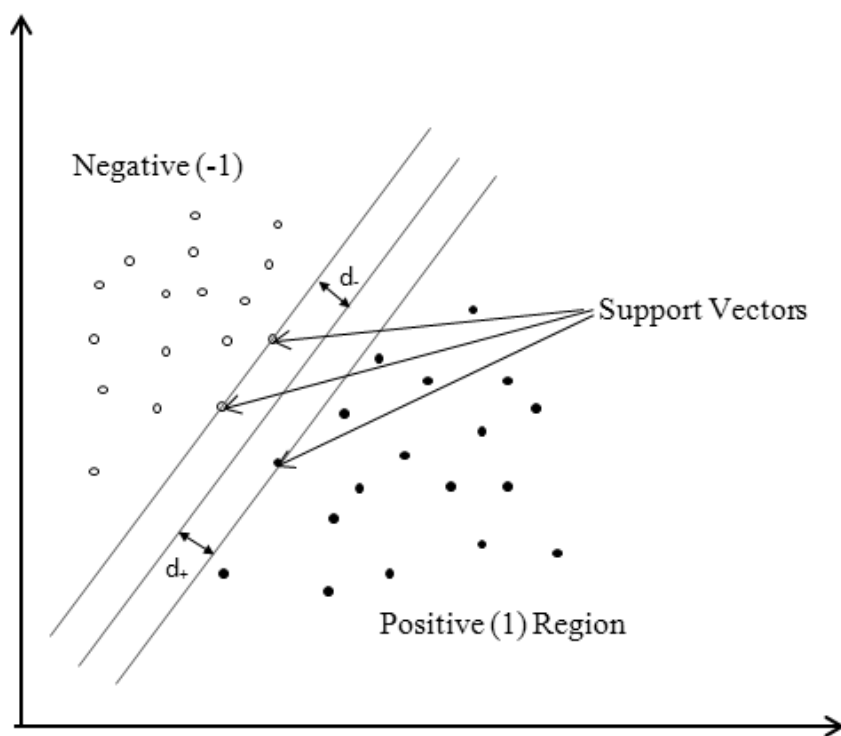
Figure 4.13: Linearly separable data with support vectors and hyper-plane with largest margin

fewer kernel functions, in the meantime the performance comparable to an equivalent SVM model [29; 113].

5. Gaussian Process Regression (GPR) – A Gaussian process (GP) is a collection of random variables, any finite number of which have (consistent) a joint Gaussian distributions [114]. Gaussian process can be used with more flexibility for the non-linear regression problem. A set of $n + 1$ random variables $(Z_1, Z_2, \ldots, Z_n, Z_n ew)$ has a joint Gaussian distribution with mean 0 and covariance matrix $K_+$ and covariance matrix $K_+$ is partitioned as follows [115]:

$$K_+ = \begin{pmatrix} K & k \\ k^T & k_{new} \end{pmatrix} \tag{4.18}$$

where $K$ is $n \times n$ matrix, $k$ is $n \times 1$ matrix and $k_{new}$ is a scalar. After first $n$ observations, i.e., $Z_1 = z_1, \ldots, Z_n = z_z$, the conditional distribution for new observation $Z_{new}$ is a Gaussian with [115]:

$$E[Z_{new}] = k^T K^{-1} z \tag{4.19}$$

$$Var[Z_{new}] = k_{new} - k^T K^{-1} k \tag{4.20}$$

where $z^T = (z_1, z_2, \ldots, z_n)$. Covariance matrix plays a critical role in the GPR as GPR requires a prior knowledge in the form of covariance matrix [29]. Figure 4.14 shows Gaussian process regression to a sample set of light output data at four different times.

6. Bayesian Networks (BN) – Bayesian networks is a directed acyclic graph which represents the joint probability distribution of the variables [109]. In other words a directed graph which does not have any closed paths within the graph such that following the direction we will not end up in the starting node again. In the example graph (Figure 4.15), there are three nodes which represent three events (example . Node $c$ has two parent nodes (i.e., $a, b$), node $b$ has only one parent (i.e., $a$) and node $a$ does not have any parents
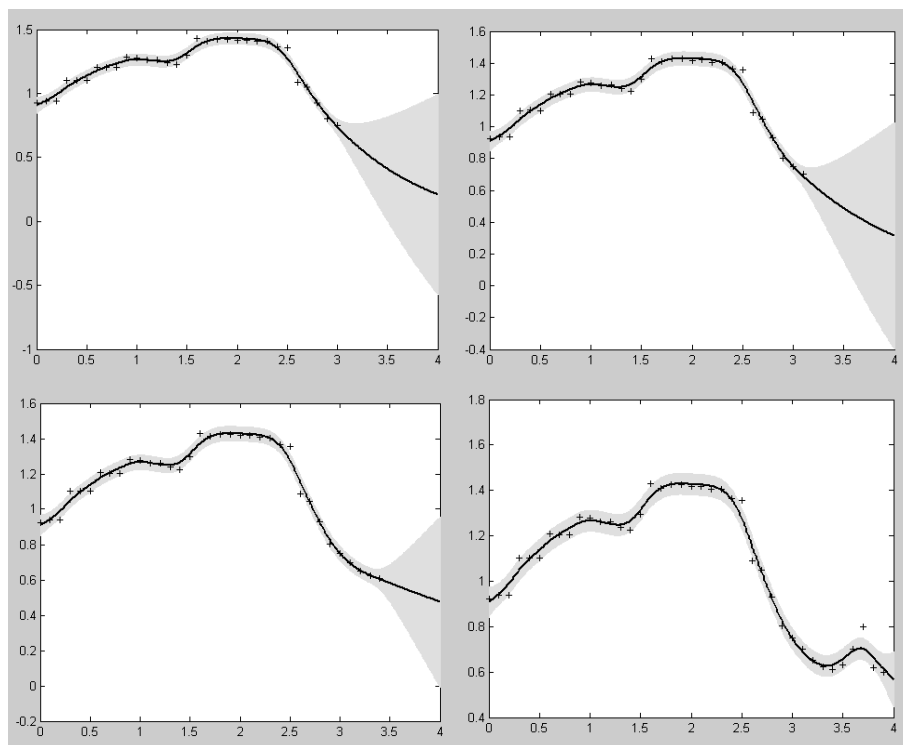
Figure 4.14: Gaussian process regression to sampled data set

nodes.
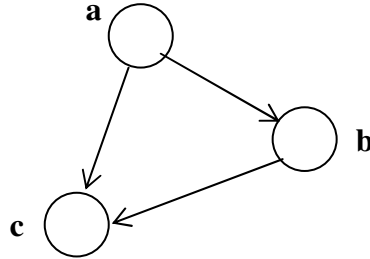


Figure 4.15: A Bayesian network with three events

Joint distribution for the above BN can be formulated using the product rule of probability as follows [109]:

$$p\left(a, b, c\right) = p\left(c|a, b\right) p\left(a, b\right) \tag{4.21}$$

$$p\left(a, b, c\right) = p\left(c|a, b\right) p\left(b|a\right) p(a) \tag{4.22}$$

In general for a graph with $K$ nodes, joint distribution is given as follows [109]:

$$p\left(\mathbf{x}\right) = \prod_{k=1}^{K} p(x_k|pa_k) \tag{4.23}$$

where $pa_k$ denotes the set of parents of $x_k$, and $\mathbf{x} = \{x_1, x_2, \ldots, x_K\}$. The above equation for the Bayesian network shows the factorisation property of the joint distribution.

Generally BN is used to estimate the conditional probability of one node, given values for other nodes. Since BN is used to estimate the posterior probability of one node given the values for other nodes, BN can be used as a classifier. Nodes represent the dataset attributes when BN learns from the datasets [45]. Nave-Bayes (NB) classifier is a simple Bayesian network where the classification node represented by the parent node to all the other

nodes and no other connections are allowed in the Nave-Bayes classifier. Main advantages of the NB classifier are easy to construct and classification process is very efficient, hence NB has been used as an effective tool for many classification problems [45]. A general Nave-Bayes network is shown in Figure 4.16 [109].
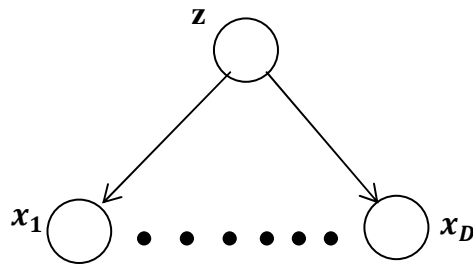


Figure 4.16: A graphical representation of Nave-Bayes classifier

7. Hidden Markov Model (HMM) – Markov models (MM) assume the future predictions are independent of all but the most recent observations [109]. Hidden Markov models are one of Markov models in which latent variable are discrete. HMM is widely used to model sequential data [116]. Figure 4.17 [109] shows a HMM as specific instance of the state space model where the latent variables are discrete. It can be viewed as a mixture model with component densities given by $p(x|z)$. State of the latent variable depends on the state of the previous latent variable and therefore $p(z_n|z_{n-1})$. Initial latent node has specialty as it does not have a parent node and therefore it has a marginal distribution $p(z_1)$. Other important distribution is the conditional distribution of the observed variables $p(x_n|z_n)$. Sometime these are known as emission probabilities. This is a special case of Bayesian network called as dynamic Bayesian network (DBN).

#### 4.2.2.2 Unsupervised Learning Approach

Unsupervised learning is used where there are no labelled data available (i.e., target variable). It is used to discover the similar groups within the data based
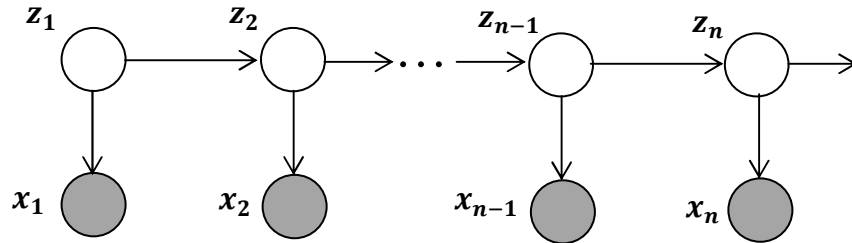
Figure 4.17: A graphical structure of hidden Markov model

on clustering techniques or estimate the distribution of the data within the input space or maps the high dimensional input space into a low dimensional space for the purpose of visualisation [109]. In the case of PHM application unsupervised learning approach can be used to classify the data into different groups and identify the healthy and normal data or learn the healthy systems or learn the failure data based on what types of data available. For most of the new systems, only normal operating data will be available and these data can be used to learn a healthy system under different settings. Then this learned information can be used to detect the anomalies in the new observation and predict the reliability and the life-time. Some of the supervised learning approaches can also be used under unsupervised setting. Some of the frequently used techniques for unsupervised learning approach are listed below:

1. Principal Component Analysis (PCA) – PCA is a widely used method for dimensionality reduction, data compression, feature extraction and data visualisation via mapping the data into a lower dimensional linear space also called principal subspace. The goal of this approach is to map the higher dimensional data into a lower dimension while maximising the variance of the mapped data. Alternatively PCA can be performed by minimising the sum-of-squares of the projection errors [109]. Figure 4.18 illustrates the mapping of two dimensional data into a one dimension.

2. $K$-means Clustering – $K$-mean clustering is to group the data into $K$ number of clusters such that the inter-point distance are small compared to the distance to the points outside of the cluster. Every cluster centres around a
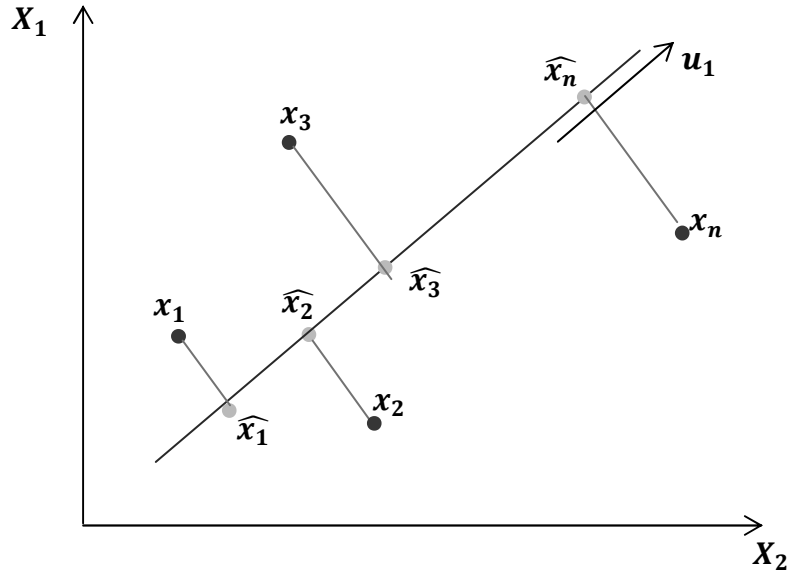
Figure 4.18: Principal component analysis for 2-D data set

centre point $\mu_k$ where $k = 1,\ 2,\ \ldots,\ K$. Data point needs to be assigned to these clusters such that the sum of the squares of the distances of each data point to its closest centre is minimum [109].

3. Neural Networks – Neutral network can also be used in the unsupervised setting where labelled data is not available. Self-organising Maps (SOM) are the type of neural network used for unsupervised learning and it was proposed by Kohonen. It is an alternative approach to the statistical clustering. In most of the SOM, every cluster is identified by a threshold value and based on these threshold data points are assigned to the particular cluster [91]. This technique can be used for the PHM of a new system or product.

4. Kalman Filters (KF) – R E Kalman proposed a technique to solve the problems such as (1) Prediction of random signal (2) Separate the random signal from the random noise and (3) Detection of signals of known form (i.e., pulses, sinusoids, etc.,) in the presence of random noise [117].

The Kalman filter is based on the assumption that the posterior density at every time step is Gaussian and hence parameterised by the mean and covariance [118]. The Kalman filter (KF) is frequently used as an optimised estimation technique for systems state. It is a recursive approach to estimate the system state based on the prior knowledge of the state of the system and the measured information. The Kalman filter is also used to fuse the measurements for same variable from different sensors. The KF is used in PHM application of electrical components based on changes in resistance [44; 119]. Figure 4.19 shows sample measured sensor data and filtered data using the Kalman filter.
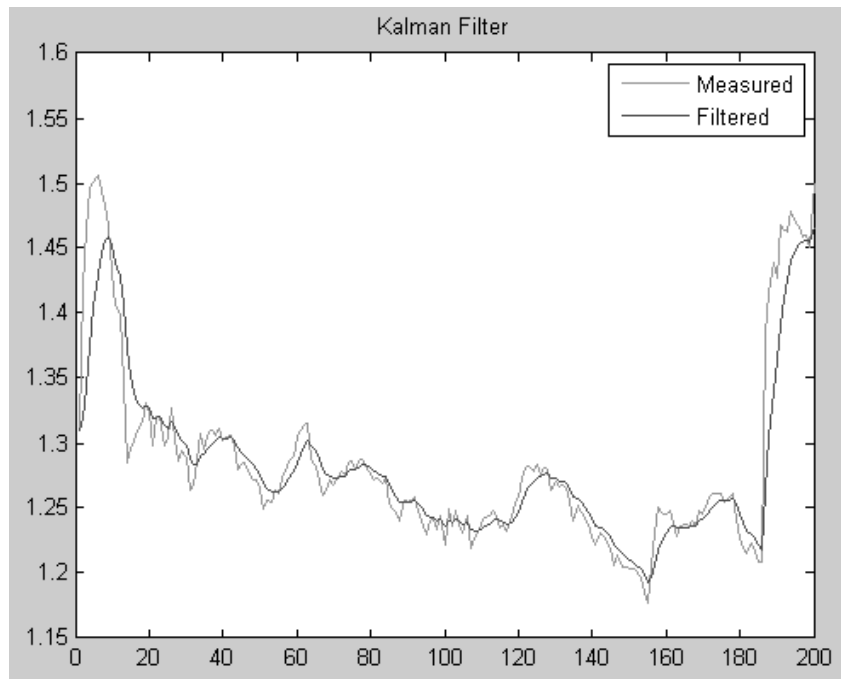


Figure 4.19: Kalman filter for sample data set

5. Particle Filter (PF) – Particle filters also referred as sequential Monte Carlo (SMC) are used to handle model non-linearity or non-Gaussian process or observation noise [120]. PF was developed based on the concept of sequential important sampling (SIS) and Bayesian theory. PF has been applied

111

in many fields such as economics, biostatistics, target tracking, time series analysis, signal processing, etc., [118].

There are many different particle filters based on different sampling techniques such as sampling important resampling (SIR) particle filter, auxiliary particle filter, regularised particle filter, etc. PF have been applied successfully in number of PHM applications [89; 90; 121; 122].

## 4.3   Model Driven Approach

The model driven approach uses mathematical equations that predict the physics governing failures and therefore is sometimes referred to as the Physics-of-Failure (PoF) approach. It requires knowledge of the failure mechanisms, geometry of the system, material properties and the external loads being applied to the system. An accurate mathematical model can benefit the prognostics process, where the difference between the output from a mathematical model and the real output of the system can be used to find the anomalies, malfunctions, disturbance, etc., [44]. Using the difference between model and data values for a performance parameter, the early warnings for failures and remaining useful life can be predicted. PHM research based on model-driven approach has been undertaken in recent years for a number of different applications [28; 38; 39; 40; 44; 85; 86; 87; 123].

A block diagram of a typical model based approach is shown in Figure 4.20. Fault is identified and diagnosed using the model and sensor data. Sensors are used to assess the actual state of the system and then compared to the output of the model. The different between the model output and sensor data is called residual which then used to estimate the damage in the system. Appropriate extrapolation technique is used to predict the useful life. Estimated damage and remaining useful life are then used for the purpose of maintenance.

Physics-of-Failure (PoF) approach is developed based on underlying physical behaviour which causes the failure (physics-based degradation model) or is based system models which represent the dynamic of the systems (sometime referred as state space models). These models are often developed from first principles. An empirical model is developed when it is difficult to derive a model from first
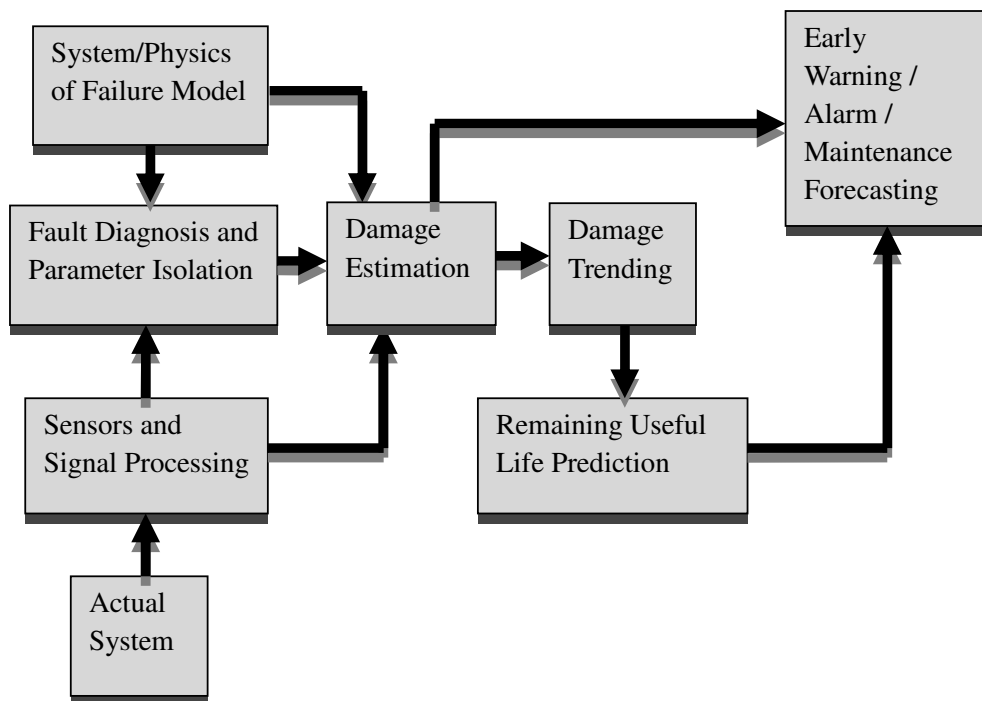
Figure 4.20: Block diagram of model driven approach

principles.

### 4.3.1  System Models

System model represent the system dynamic accurately and sometimes is referred to as a state space model. System models have many different subsystems and individual components. System models are derived by assembling the subsystem models and component models. Subsystems and individual components are need to be modelled. For example most of the electronic components have equivalent circuit models which are used to represent their operation/dynamic. Figure 4.21 shows three different equivalent circuit models for a capacitor. Figure 4.21 (a) represents a capacitor model with an equivalent series resistance (ESR) and it ignores the parallel resistance associated with the capacitor. Figure 4.21 (b) represents a capacitor model with an equivalent parallel resistance (EPR) and it ignores the serial resistance of the capacitor. Figure 4.21 (c) represents a capacitor model with an equivalent parallel resistance (EPR) and an equivalent series resistance (ESR) and it can be used to represent a capacitor more accurately. A lumped parameter model which is shown in Figure 4.21 (c), for a real capacitor has been used by J R Celaya et al as a model for model-driven PHM for electrolytic capacitors under electrical overstress accelerated ageing.

An important task in the modelling process is the estimation of the model parameters accurately. For example, in the case of the capacitor models, model parameters are $R_c$, $X_c$, and $C$. This can be achieved in two different ways: (1) estimate from the first principle or (2) from empirical data. Values of these model parameters depend on the type of material, geometry, size of the device, etc. Therefore it might be difficult to estimate the values for these parameters from first principles. In principle, it is easier to estimate parameters from empirical data which are collected from a test designed for that purpose.

Another example is a simple equivalent circuit model for lithium-ion battery (LIB) cell as reported by B Y Liaw et al. This is based on equivalent circuit model for Ni-MH cells which is developed by Verbrugge and Conell [37]. Figure 4.22 shows the equivalent circuit model for LIB cell. Typically model parameters are estimated from the empirical data collected from the experiments.
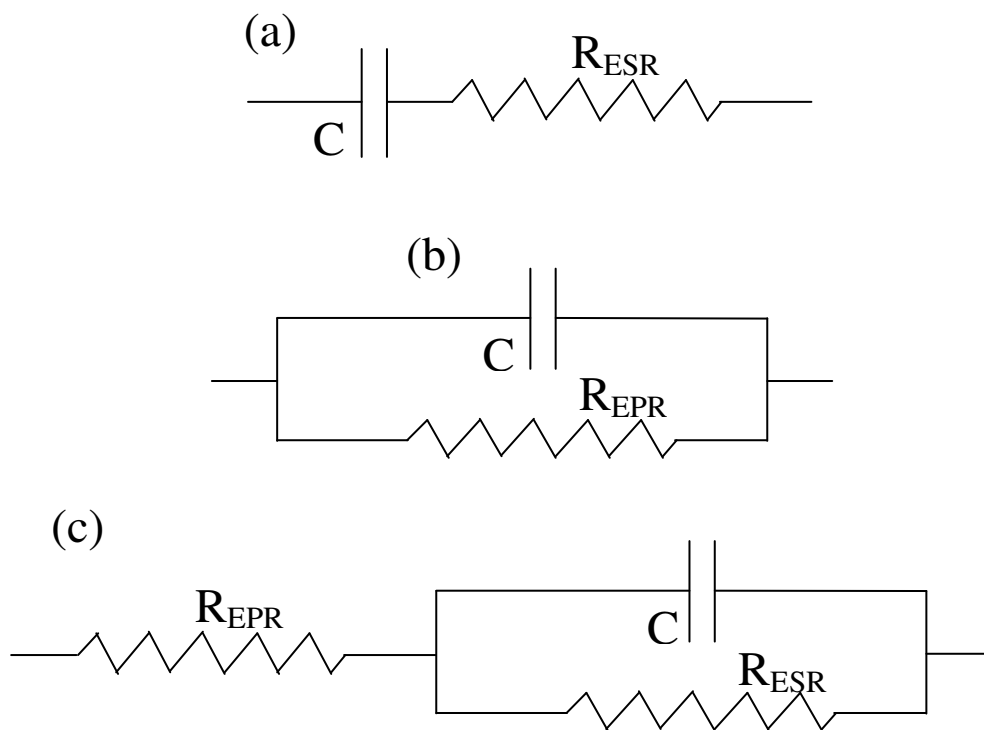
Figure 4.21: Equivalent circuit models of an electrolytic capacitor
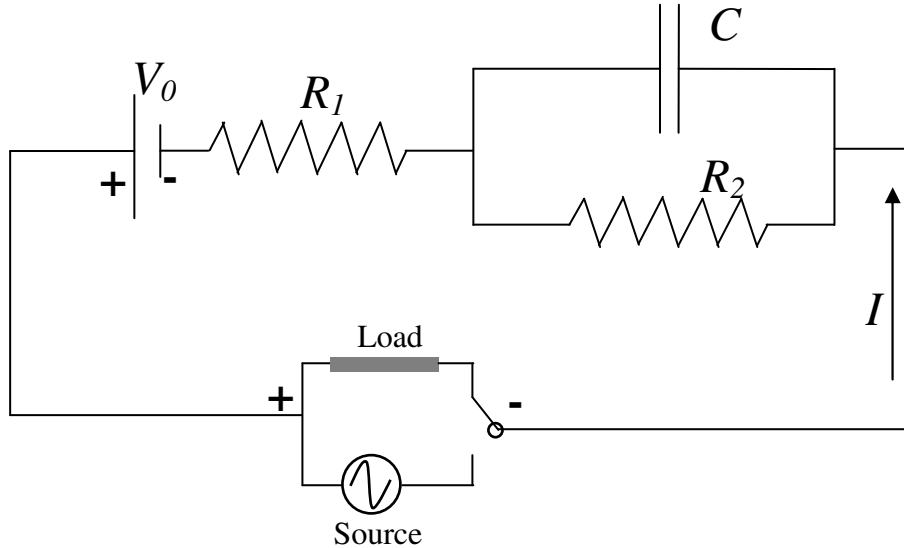
Figure 4.22: Equivalent circuit model for a Lithium-ion battery cell

System models can be used to do the prognostics with the help of sensors or measuring equipment. Based on the sensor or measured data and output from the model data, potential damage can be estimated. Estimation techniques such as Kalman filters (KF) and particle filters (PF) are typically used to estimate the damage from the sensor output and model out [82]. Fault can be diagnosed by isolating the parameter which causes the failure. Then the estimated damage is used to forecast the remaining useful life time as shown in block diagram for model driven approach in Figure 4.20.

### 4.3.2 Physics-of-Failure Models

Physics-of-Failure (PoF) approach is developed based on Failure Modes, Mechanisms and Effects Analysis (FMMEA) of the device [82; 87]. Potential failure modes and corresponding failure mechanisms based on different life-cycle loading conditions need to be identified to develop a PoF approach. The maximum stress for each failure mechanisms that a device can withstand is obtained as a function of life-cycle loading. This information is then fed into an appropriate

damage model to estimate the RUL. Some of the frequently used damage models are listed below:

1. Arrhenius Relationship Based Models – Arrhenius relationship is a relationship between a chemical reaction and temperature. In reliability, Arrhenius relationship is used to establish the time to failure ($T_{failure}$) of a semiconductor device for which a failure is based on temperature assuming all other parameters are constant [124].

$$T_{failure} \propto e^{\frac{E_a}{kT}} \tag{4.24}$$

where $E_a$ is the activation energy of the failure mechanisms in electron volts (eV), $k$ is the Boltzmann's constant and $T$ is the operating temperature in Kelvin. Activation energy $E_a$ will vary based on the failure mechanisms and Arrhenius model is valid only for the failure mechanisms which depend on the temperature while all the other parameters are constant.

2. Black's Equation – J R Black developed an empirical relationship to estimate the time to failure of a wire because of electro-migration. Electro-migration is one of the important failure mechanisms in the semiconductor devices. Black's equation was developed further and widely used to estimate the time to failure of semiconductor devices because of the failure mode caused by the electro-migration [124].

$$T_{failure} = A_{EM} \ (J - \ J_{crit})^{-n} \ e^{\frac{E_a}{kT}} \tag{4.25}$$

where $A_{EM}$ is an empirically determined constant, $J$ is the current density in the interconnect, $J_{crit}$ is the critical current density required for the electro-migration, $E_a$ is the activation energy for the electro-migration in electron volts (eV), $k$ is the Boltzmann's constant ($8.62 \ \times 10^{-5} \frac{eV}{K}$), $T$ is the operating temperature in Kelvin and $n$ is an empirically determined constant which typically depends on the interconnect material. $n = 1.1$ is used for copper interconnect. Activation energy $E_a$ depends on the material used in the interconnect.

3. Stress Migration Model – Stress migration is the process of migration of the atoms in the interconnect due to the thermo-mechanical stress. Damage model for stress migration is given as follows [124]:

$$T_{failure} = A_{SM} \ \sigma^{-n} \ e^{\frac{E_a}{kT}} \qquad (4.26)$$

where $A_{SM}$ is an empirically determined constant, $\sigma$ is the mechanical stress caused due to different expansion rate, $n$ is an empirically determined constant and $E_a$ is the activation energy for the stress migration. Activation energy $E_a$ depends on the material used in the interconnect. Since the mechanical stress $\sigma$ is proportional to the changes in the temperature from the stress free temperature, damage model based on operating temperature is given as follows [124]:

$$T_{failure} \propto \ |T_0 - T|^{-n} \ e^{\frac{E_a}{kT}} \qquad (4.27)$$

4. Coffin-Manson Model – Coffin-Manson model initially developed to model the damage in the aircraft frame due to large thermal cycles. It has been modified and used frequently in the semiconductor industries to assess the reliability of semiconductor devices. The Coffin-Manson equation for the thermal cycle is given by [124]:

$$N_f = C_0 \ (\delta T)^{-q} \qquad (4.28)$$

where $N_f$ is the number of thermal cycle to failure, $C_0$ is an empirically determined constant which depends on the material, $\delta T$ is the temperature range experienced by the device and $q$ is the Coffin-Manson constant which needs to be determined empirically.

## 4.4 Fusion Approach

The fusion approach is based on the advanced features of the both data driven and model based approach. This approach will require an accurate mathematical

model of the system for physics based failure approach and enough historical data and knowledge of typical operational performance data for data driven approach. The aim of the fusion approach is to overcome the limitations of both the model and data driven approaches to estimate the remaining useful life (RUL) [87]. Therefore the accuracy of the fusion approach should be high, although for real-time analysis it may not be suitable due to the computational resource required. Fusion approach to PHM has been demonstrated for a number of applications but remains an open research area [45; 47; 125].

A block diagram of a typical fusion approach is shown in Figure 4.23. Data driven approach is added to detect the anomalies and then extrapolate the anomalous data to predict the remaining life. Model driven approach predicts the remaining life based of the system or failure model and sensor data. Remaining useful life predicted from model driven and data driven approaches are then fused together to make a better prediction.

A typical PHM application consists of many different tasks, from sensing to prediction. Each task benefited from different techniques hence the real world PHM application does not necessarily depend on a single approach. Many model-driven approaches use data-driven techniques for the RUL prediction based on the state-space or PoF models. Some data-driven techniques such as Kalman Filter and Particle Filter can be used to sequentially estimate the system state based on a model and sensor data. In particular, they are capable of correcting the predictions based on their outer feedback correction loops. Particle Filter demonstrated its robustness in online (real-time) estimation of the remaining useful lifetime of a system [121].

## 4.5 Summary

This chapter has presented detail review of many different techniques available for data driven, model driven and fusion PHM approaches. Generally PHM problem cab be formulated as anomaly detection and extrapolation (prediction) problems. To detect the anomalies in the system, it is required to have latest data about the system. Anomalies can be detected using probability of an event or using suitable threshold. Prediction problem requires some previous data to make prediction or
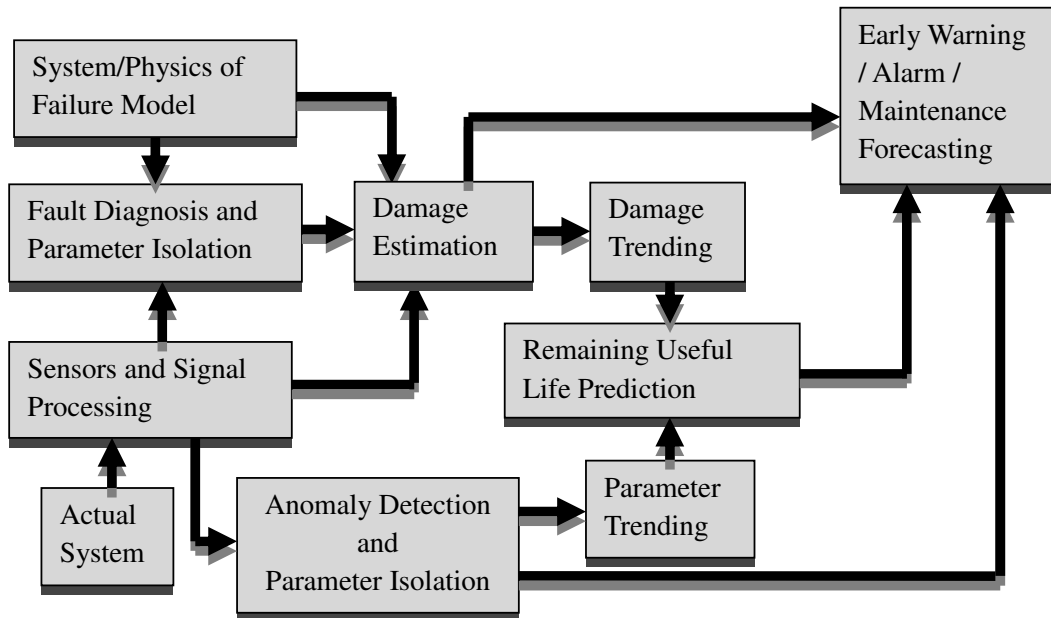
Figure 4.23: Block diagram of fusion approach

extrapolate the data to estimate future state of the systems.

PHM also requires different techniques to achieve different tasks such as signal conditioning, noise reduction, damage estimation, parameter trending, RUL prediction etc. Data driven techniques achieve most of these tasks. Model driven and fusion approaches often benefit from data driven techniques such as Kalman filter, regression etc., for noise reduction, extrapolation etc.

This research investigates suitable techniques for real-time PHM. In particular, this programme investigates suitable techniques which can be easily implemented in low cost microcontrollers.

# Chapter 5

# PHM Approaches to High Power LEDs

## 5.1  Introduction

Light emitting diodes are identified as future light sources since they have many advantages such as high reliability, long lifetime, faster switching speed, energy efficient, small in size etc., compared to traditional lighting systems. A high power LED is defined as an LED with power equal or greater than 1 Watt. When the LED is forward biased and current passes through the p-n junction, electrons in the n-region get sufficient energy to move across the p-n junction into the p-region and holes are injected into the n-region from the p-region through the p-n junction [67]. Some of the electrons and holes recombine in the active region (p-n junction) where electrons move one energy band to another. This process is known as the radiative recombination process. When the radiative recombination takes place, energy is released in the form of photons with the wavelength related to the change in the energy band. This process is illustrated in Figure 5.1. Light output power of an LED light source is determined by the radiative recombination process. When the efficiency of the radiative recombination process reduces (i.e., rate of non-radiative recombination process increases), degradation of the LED performance starts taking place.

Reliability and lifetime of LED lighting systems are established as very high
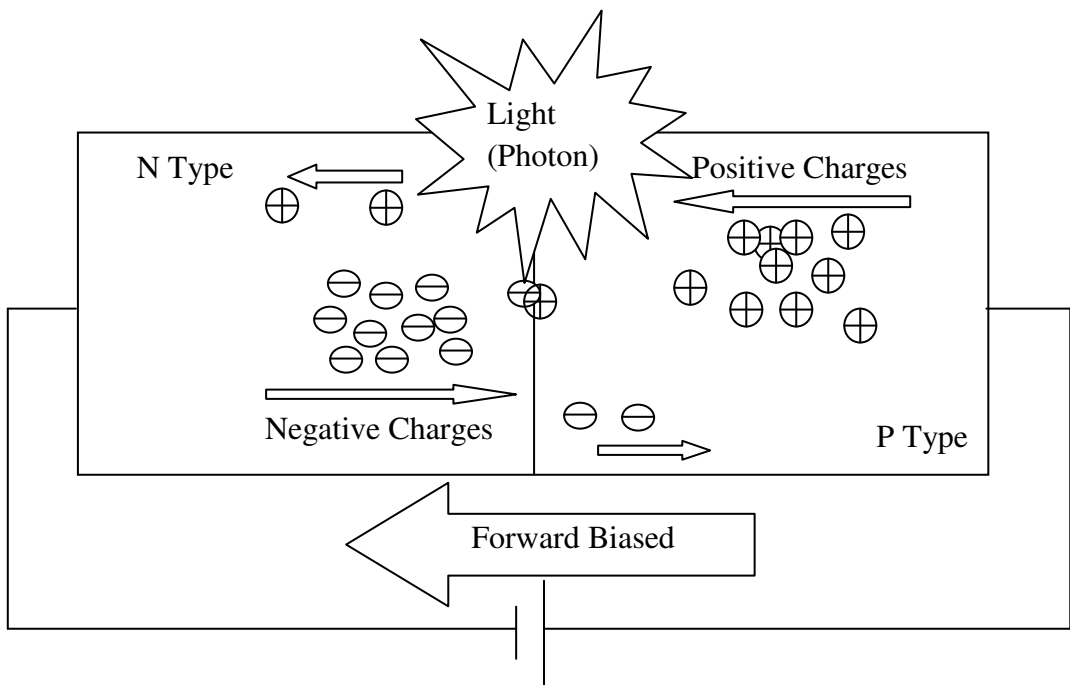
Figure 5.1: Radiactive recombination process in the p-n junction (LED die) where the photon emitted in the form of light

under normal operating conditions. Lifetime specified by the manufacturers is typically based on the average lifetime of a group of individual LED packages. This average reliability might vary from the reliability of an individual LED package. When the operating conditions change the reliability and lifetime of the LEDs also change. In particular, reliability and lifetimes of the LEDs greatly influenced by the heat generated in the junction and the drive current. Although the reliability and life time of LED packages are very high, LED lighting systems show considerably lower reliability compared with the individual LED packages. The reason is that LED lighting systems reliability depends on other parts such as driver and housing.

Most of the manufacturers perform reliability tests and publish these data for their products. These reliability tests are conducted under a controlled environment specified by the current available standards such as LM-79[1], LM-80[2], and IES TM-21[3] etc. Lifetimes of the LEDs are estimated based on these reliability tests data. Generally, lifetime is statistically estimated time of average or median useful lifetime. Real application environments and operating conditions are very different and vary compared to the tested conditions. Lifetime of different LEDs and from different manufacturers have different reliability and lifetime as their individual characteristics such as die structure, chemical composite of the die and the encapsulant, mechanical structure of the device, quality of manufacturing practice etc., vary.

Monitoring the reliability of the light of LED lighting systems in the field requires light sensors and labour. This maintenance task can be converted into a predictable evidence based maintenance strategy using PHM techniques in real-time if they are embedded with the LED controller. Applying PHM techniques to LED lighting systems requires additional sensors and real-time computational power. Real-time PHM to LED lighting systems can be implemented in two different ways: (1) measure the light output power using a light sensor in real-time and forecast the maintenance task based on light sensor reading or (2) measure other parameters such as forward voltage, forward current and temperature using

---

[1]IES standard for electrical and photometric measurements of solid-state lighting products
[2]IES standard for measuring lumen maintenance of LED light sources
[3]IES standard for projecting long term lumen maintenance of LED light sources

specialised sensors and do the forecasting. The first approach is very straight-forward since the exact light output power is known; it can be used to schedule the maintenance activity. Although the light sensors are available in the market, placing the sensors into the luminaries is very difficult. The second approach is based on other parameters such as forward voltage, forward current and board temperature. Prediction and maintenance forecast need to be made from these parameters. This work is carried out based on sensor data for forward voltage, forward current and board temperature measurements to perform the prognostics and health monitoring of the LEDs, and based on the lifetime recommendation for LED lighting systems by Next Generation Lighting Industry Alliance (NGLIA), in 2011. NGLIA recommends lifetime of LED lighting systems can be estimated using only light output power reduction since colour shift of any lighting systems is not well-understood and there is no accepted standard to define the lifetime based on colour shift. In this research, the 30% reduction in the light output is used as the failure criteria, and any LED which operates below this limit (i.e., 70%) is defined as a failed LED.

There is no life time model developed and reported in the literature so far for LEDs [78; 126; 127]. Manufacturers need to work toward understanding the issues surrounding true lifetime and reliability, and also need to develop models for the underlying failure mechanisms [77]. The main cause of the failure in the LEDs is the heat generated at the p-n junction [24]. Under the forward bias condition the p-n junction carries a current which is almost an exponential function of the applied voltage which means if there is an increase in the applied voltage, the current through the p-n junction increases exponentially. This characteristic is explained by the Shockley's Equation [128]. The modified version Shockley's equation for the p-n junction characteristics is given in equation 5.1. An increase in the current will cause the temperature to increase dramatically which means the heat generated in the p-n junction increases.

$$J_f = J_s \left[ \exp \left( \frac{eV_f}{n_{ideal}kT} \right) - 1 \right] \tag{5.1}$$

where $J_f$ is the forward current density, $J_s$ is the saturation current density, $V_f$ is the junction voltage, $k$ is the Boltzmann constant, $T$ is the absolute temperature

of the pn junction and $n_{ideal}$ is the diode ideality factor or quality factor. The saturation current density $J_s$ is not constant for given devices and it increases with temperature $T$. Hence the forward current density $J_f$ increases with temperature increase.

## 5.2 LED Health Monitoring

Measuring the light output of an LED in real-time (i.e., in the field) is difficult. Instead, performance indicators of the LEDs such as forward current, and the p-n junction temperature, can be used to measure any deviations in performance and to realise any prognostics assessment. Forward current can be measured using power resistors (i.e., current sensor) as the ordinary resistors cannot handle the typical expected current through the LEDs which is 350mA. Forward voltage across the LED can also be measured. It is impossible to measure the p-n junction temperature directly as it is impossible to reach the p-n junction. However, it is possible to estimate this value by measuring the temperature at a nearest point to the p-n junction, and then use the following one-dimensional heat conduction equation to estimate the junction temperature [56; 57]:

$$T_j = T_b + R\theta_{jb} \times V \times I \tag{5.2}$$

where $T_j$ is the p-n junction temperature, $T_b$ is the board temperature, $R\theta_{jb}$ is the p-n junction to board thermal resistance coefficient, $V$ is the input voltage and $I$ is the input current. Thermal resistance coefficient depends on the power dissipation at the junction, ambient temperature, amount of heat sink and the orientation of the heat sink [56; 57].

For the purpose of real-time health monitoring and prognostics, we assume the average power dissipation of the LED remains constant and ambient temperature, amount of heat sink and orientation of the heat sink remain the same. If the power dissipation, ambient temperature and heat sink remain same, board temperature and junction temperature will vary linearly [57]. In addition a large heat sink is used in the experiment and hence the junction temperature can be estimated with the board temperature [57]. Y Xi et al also showed that the junction temperature

and input power for GaInN UV LED and AlGaN UV LED have linear fit for the experimental data [129]. It implies the thermal resistance coefficient remain constant for these particular LEDs. For the Philips Luxeon star, the LED used in this research study, the thermal resistance co-efficient is 20°C/W which can be assumed as a constant. This allows us to monitor the board temperature and use this temperature to train the investigated data driven PHM approach instead of the p-n junction temperature.

The real-time health monitoring and prognostics approach adopted in this study is based on the output from both thermocouple data for board temperature and current sensor data for forward current. This data is then fed into the data driven techniques to predict the anomalies in LED performance. The test data was obtained using a National Instruments' (NI) PXI[1] real-time platform which gathered data for the studied high power Luxeon star LEDs under accelerated voltage conditions.

## 5.3  Data Driven Approach

The health of a product or system is defined as the extent of deviation or degradation from its expected typical operating performance. This extent of deviation or degradation from the expected typical operating performance has to be determined accurately to assess the reliability of a product and predict its remaining useful life.

In the case of High power LEDs which are semiconductor devices, overall reliability depends on several factors such as properties of p-n junction, band gap energy, internal quantum efficiency (i.e., product of current injection efficiency and radiative efficiency), light extraction efficiency, cavities or defects in the active region etc. Modeling these individual LED characteristics for the purpose of prognostics and health monitoring is difficult. Data-driven approach for PHM has been identified as the best strategy as they do not require system specific knowledge. However, in this case there is a requirement for historical and failure data. Data-driven approach is also easy to implement, in particular in a real-time environment.

---

[1]The peripheral controller interface (PCI) eXtensions for instrumentation

Light output power degradation is caused by high temperature at the p-n junction due to the heat generated at the p-n junction. Heat generated depends on the current through the p-n junction. Injection current (current through the p-n junction) and the p-n junction temperature can be used as the performance indicators of the LEDs. Monitoring the current and temperature at the p-n junction and relating them to the drop in output lumens (i.e., power) will provide the ability to monitor the degradation of the LED in real time. To achieve this, two distance measure techniques have been assessed (1) Euclidean Distance and (2) Mahalanobis Distance. Logistic regression technique has also been investigated based on sensor data for the forward current and the board temperature. Neural network (NN) is used to predict the light output based on the sensor data for the forward current and the board temperature.

## 5.3.1 Distance Measures

Distance measures are used in many classification and clustering techniques. Each cluster can be defined by a center point and a threshold distance (i.e., outlier). In the case of PHM application for LED lighting systems, we define a healthy region by a cluster with center point as the typical operating data and the outlier as threshold value. This cluster defines a healthy operating region for LEDs and LED operating beyond this region can be considered as being abnormal condition.

The strategy which is followed here is to train the algorithms first off-line for a certain number of training data sets in order to identify the healthy and failure threshold values, regression coefficients etc. These identified values and equations can be then programmed into a real-time system (i.e., LED driver) to assess the reliability and predict the remaining useful lifetime.

### 5.3.1.1 Euclidean Distance

Euclidean distance (ED) is the physical distance between two data points and it is the most commonly used distance measure in many different fields. It is defined as the distance that examines the root of square differences between any data sets i.e., it can be in any dimension. For a data matrix $X$ which contains $n$ objects measured by p variables (i.e., $n \times p$ matrix), ED can be calculated in the

vector space as follow:

$$ED_i = \sqrt{(X_i - \bar{X})(X_i - \bar{X})^T} \tag{5.3}$$

Here $\bar{X}$ is the mean vector. In the case of prognostics and health monitoring of high power LEDs, $\bar{C}$ and $\bar{T}$ are the mean values of current through the p-n junction and p-n junction temperature under typical operating conditions respectively. $C_i$ and $T_i$ are the new observation data. $ED_i$ will be computed for the new observation data as follows (i.e., two dimensional data):

$$ED_i = \sqrt{(C_i - \bar{C})^2 + (T_i - \bar{T})^2} \tag{5.4}$$

The ED value will give an estimate of LED's deviation or the degradation from the typical healthy LED. Higher values for the ED will indicate anomalies in the performance and prognostics of LED can be achieved by monitoring the ED values. Figure 5.2 shows Euclidean distance for random data generated from multivariate normal distribution with same standard deviation in both directions.

### 5.3.1.2  Mahalanobis Distance

Mahanobis distance (MD) is another physical distance measure. Although similar to the Euclidean distance, the Mahalanobis distance takes into account the actual correlations of the data sets hence having a potential advantage over ED. Since the health of the system is defined as the deviation from expected typical operating performance, Mahalanobis distance is useful in determining the similarity/distance between the typical operating performance and monitored operating performance. For a data matrix X which contain n objects measured by p variables as above MD can be estimated in the vector space as follows:

$$MD_i = \sqrt{(X_i - \bar{X})Cov_X^{-1}(X_i - \bar{X})^T} \tag{5.5}$$

Here $\bar{X}$ is the mean vector and $Cov_x$ is the variance-covariance matrix of data matrix X. In the case of prognostics and health monitoring of LEDs, $\bar{C}$ and $\bar{T}$ are
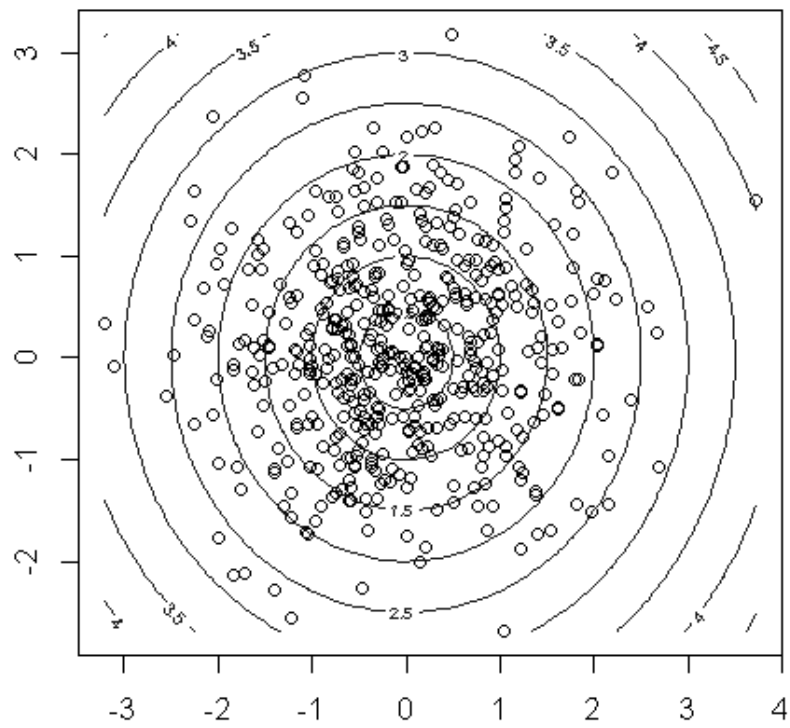
Figure 5.2: Euclidean distance for random data

the mean values of current through the p-n junction and p-n junction temperature, and $Cov_{CT}$ is the variance-covariance matrix of current and temperature under the typical operating conditions.

$C_i$ and $T_i$ are the new observation data. MD for two dimensional data can be calculated whenever new data becomes available as follows:

$$MD_i = \sqrt{(C_i - \bar{C})Cov_{CT}^{-1}(T_i - \bar{T})^T} \qquad (5.6)$$

In the case of 2 monitored parameters, the MD formula for two dimensional data is using the following variance-covariance matrix:

$$Cov_{CT} = \begin{bmatrix} \sigma_C^2 & \rho_{CT}\sigma_C\sigma_T \\ \rho_{CT}\sigma_C\sigma_T & \sigma_T^2 \end{bmatrix} \qquad (5.7)$$

where $\sigma_C^2$ and $\sigma_T^2$ are the variance of current and temperature and $\rho_{CT}\sigma_C\sigma_T$ is the covariance of current and temperature under the typical operating conditions. Using these variables MD can be derived as follows:

$$MD_i = \sqrt{\left(\frac{C_i - \bar{C}}{\sigma_C}\right)^2 + \left[\left\{\left(\frac{T_i - \bar{T}}{\sigma_T}\right) - \rho_{CT}\left(\frac{C_i - \bar{C}}{\sigma_T}\right)\right\}\frac{1}{\sqrt{1 - \rho_{CT}^2}}\right]^2} \qquad (5.8)$$

The MD value will give an estimate of LED's deviation or the degradation from the typical healthy LED. Higher values for the MD will indicate anomalies in the performance and by tracking the MD values prognostics of LED can be achieved. Figure 5.3 shows Mahalanobis distance for random data generated from multivariate normal distribution with different standard deviation in both directions.

The advantage of the above techniques is that they transform multi-dimensional sensor readings into a single performance parameter. In addition, fault parameters can also be isolated in the event of faults or anomalies in the ED or MD estimate by monitoring the individual sensors data. This can be used to analyse the fault and to find the root cause of the anomaly or the fault. Using MD or ED techniques for the purpose of health monitoring and prognostics of LEDs require historical data to establish the threshold values representing when the LED is
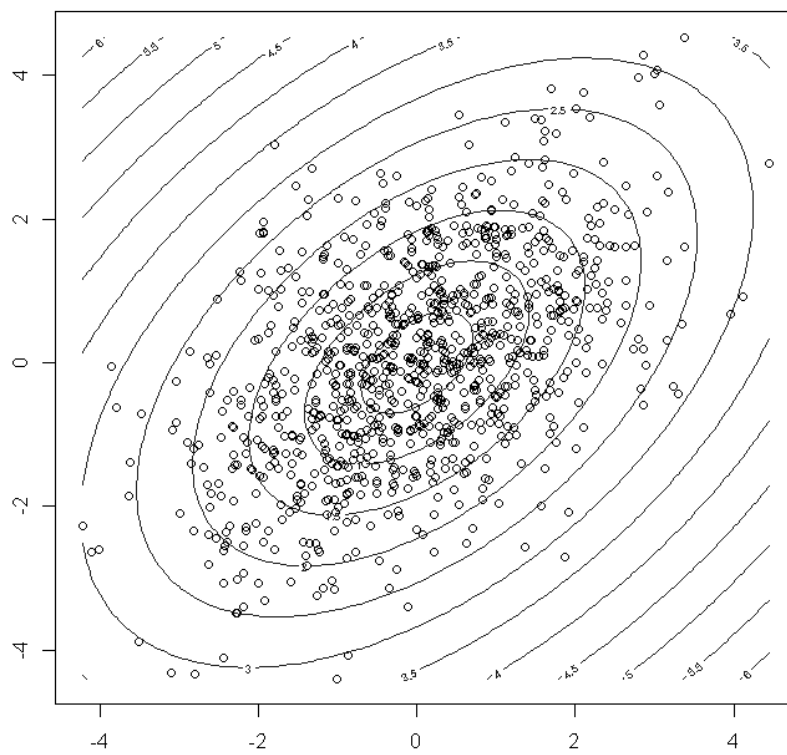
Figure 5.3: Mahalanobis distance for random data

performing outside its safe limits. To generate this data we use an accelerated voltage as condition to stress the components to failure. As a result of this, the current and the temperature also increase.

## 5.3.2 Logistic Regression

Logistic regression is used to predict the probability of occurrence of an event based on the parameters the event depends on. Logistic sigmoid function is investigated and used to fit the parameters which control the occurrence of the event. Logistic sigmoid function is given by the following equations:

$$f(z) = \frac{1}{1 + \exp(-z)} \tag{5.9}$$

where $z = \beta_0 + \beta_1 x_1 + \ldots + \beta_n x_n$, $x_1, x_2, \ldots, x_n$ are the parameters which control the occurrence of the event $z$ and $\beta_0$, $\beta_1$, ..., $\beta_n$ are the regression coefficient of the parameters. In the case of LED's health monitoring, forward current and board temperature are identified as the key parameters which control the LED reliability and health. Hence the parameter $z$ in the logistic regression equation is reduced to $z = \beta_0 + \beta_1 I + \beta_2 T$. Regression coefficient $\beta_0, \beta_1$ and $\beta_2$ need to be determined from the training data set and this can be achieved using the following formulation and subsequent derivation of the result:

$$\exp(-z) = \frac{1 - f(z)}{f(z)} \tag{5.10}$$

$$z = \log\left(\frac{f(z)}{1 - f(z)}\right) \tag{5.11}$$

$$\beta_0 + \beta_1 I + \beta_2 T = \log\left(\frac{f(z)}{1 - f(z)}\right) \tag{5.12}$$

Equation 5.12 is in the form of a linear equation and it can be written as:

$$bX = y \tag{5.13}$$

where $b$ is the regression coefficient column vector with $\beta_0, \beta_1, \beta_2$ elements, $X$ is the input matrix with columns of $[1IT]$ data and $y$ is the output column vector. For a given set of data set $X$ and $y$, the coefficient vector $b$ can be solved using following equation:

$$b = (X^T X)^{-1} X^T y^T \tag{5.14}$$

where $b$ is the regression coefficient matrix $(3{\times}1)$, $X$ is the input matrix $(3{\times}n)$ and $y$ is the output matrix $(1{\times}n)$. For a set of healthy data and failure data regression coefficients can be determined. Then logistic regression function can be used to classify the new sensor data into healthy or failure i.e., if the logistic regression returns 1, LED is healthy and probability of the failure is 0. If the logistic regression return 0 for a new set of sensor data, LED is failed and probability of failure is 1. If the output from logistic function starts to reduce, that indicates the start of the degradation and hence the probability of failure will increase while the probability of healthy state will decrease. Figure 5.4 shows a logistic regression function for random input data.

### 5.3.3 Neural Network

The exploitation of neural network for the purpose of PHM in this research is motivated by the advantages of this technique discussed in chapter 4. Neural network is used here to classify the light output values based on the sensor data for the forward current and board temperature. In this case neural network is optimised for the training data such that the mean square error is minimum. Sensor data for the forward current and board temperature are used as the input data. A simple neural network consists of three layers of neurons, namely input, hidden and output. Typical output of a neuron in the hidden layer can be expressed using the following equation, if the neuron has $n$ inputs:

$$h_j = \ f(\sum_1^n w_i x_i + b_j) \tag{5.15}$$
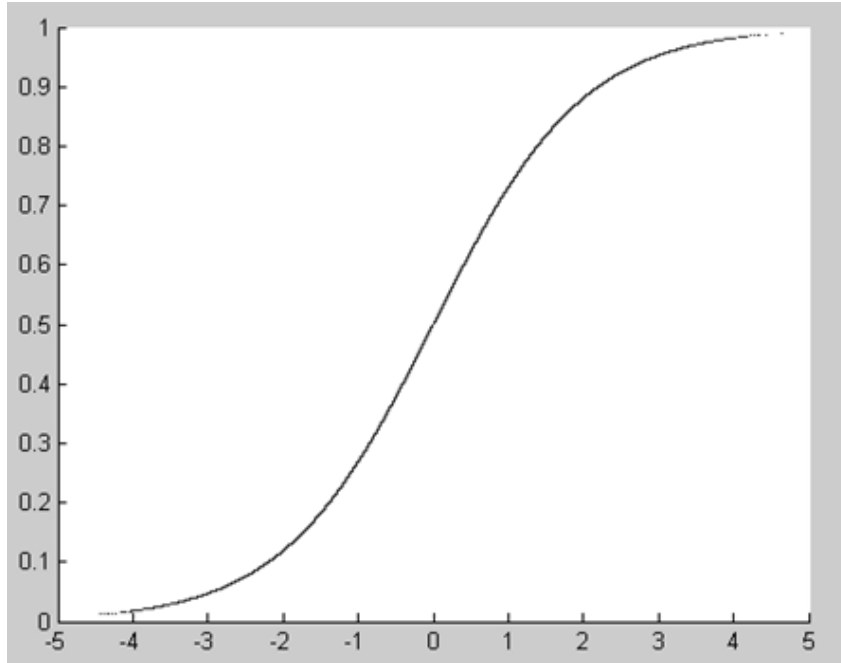
Figure 5.4: Logistic regression plots for random data

where $f$ is called activation function, $w_i$ is the weight of the $i^{th}$ input $x_i$, $x_i$ is the $i^{th}$ input to the $j^{th}$ neuron in the hidden layer, and $b_j$ is the bias to the $j^{th}$ neuron in the hidden layer. Output of the neurons in the hidden layer will act as the input to the neurons in the output layer. Output of a neuron in the output layer can be expressed using the following equation, if the neuron has $m$ inputs:

$$y_k = f(\sum_{1}^{m} m_j h_j + b_k) \tag{5.16}$$

where $f$ is called activation function, $m_j$ is the weight of the $j^{th}$ input, $h_j$ is $j^{th}$ input to the $k^{th}$ neuron in the output, and $b_k$ is the bias to the $k^{th}$ neuron in the output layer. For the purpose of prognostics and health monitoring of LED, a simple neural network with five neurons is investigated. The output value from the neural network can be used to diagnose the LEDs. This approach is similar to the logistic regression technique approach. Each node can be represented by the logistic regression function if the activation function of the neural network is a

134

sigmoid function. If the output of the neural network is 1 then the LED is healthy and if the output of the neural network is 0 then the LED is defined as failed. Output of the neural network can also be interpreted as the healthy probability of an LED. Figure 5.5 shows the simple neural network for LED prognostics.

In this neural network $h_1$ and $h_2$ represent the two neurons in the hidden layer. Inputs from the input layers are multiplied by the weight parameters and fed into the neurons in the hidden layer. For example, current and temperature sensor data are multiplied by $w_{1,1}$ and $w_{1,2}$, respectively and fed into the neuron $h_1$ where these data then used as input of the logistic function (i.e. activation function of this case). Output of this neuron $m_1$ is the output from the logistic function. Finally outputs from both neurons (i.e. $m_1$ and $m_2$) is fed into output neuron $y$ where logistic function is used. Output from this layer then is used as the probability of failure.
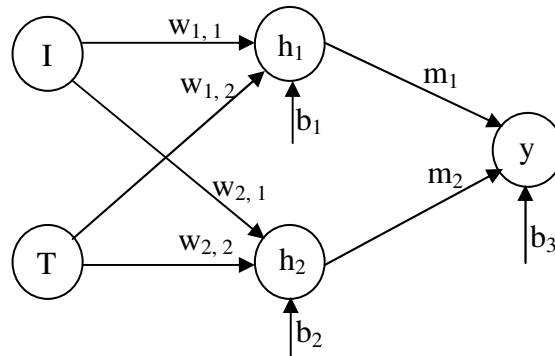


Figure 5.5: A simple neural network for the prognostics of LEDs

## 5.4   Model Driven Approach

Model driven approach can be adopted different ways as discussed in chapter 4. For the purpose of the LED health monitoring, we developed an empirical model in this work. This model is based on voltage-current characteristics and is developed with data obtained under accelerated life conditions. Figure 5.6 shows the linear model of the LEDs for small signal simulations.
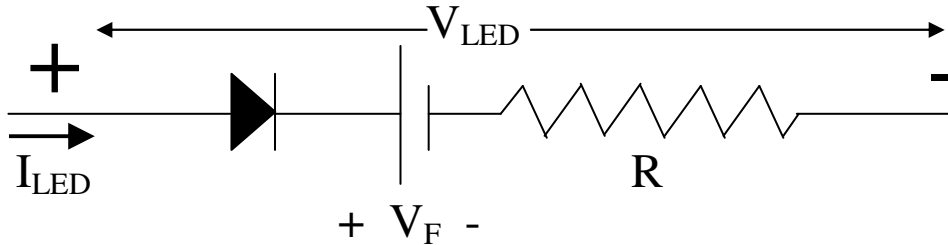
Figure 5.6: A linear model for LED

The above linear model shown in Figure 5.6 can be represented by the following equation:

$$V_{LED} = V_F + I_{LED} \times R \tag{5.17}$$

where $V_{LED}$ is the voltage across the LED (forward voltage), $V_F$ is the forward junction potential, $I_{LED}$ is the current through the LED (forward current) and $R$ is forward resistance of the LED. Typically the forward resistance of the LED is infinity until the forward voltage reaches the forward junction potential i.e., no current flows, after that the current rapidly increases as the forward resistance is very small i.e., small increase in the voltage results in high increase in current. Figure 5.7(a) shows V-I characteristics of an ideal LED with no forward junction potential and forward resistance, Figure 5.7(b) shows V-I characteristics of a LED model with only forward junction potential and Figure 5.7(c) shows the V-I characteristics of a LED model with forward junction potential and forward resistance. The empirical model developed in this work is based on the V-I characteristics shown in Figure 5.7(c). Test data is used to determine the model parameters $R$ and $V_F$.
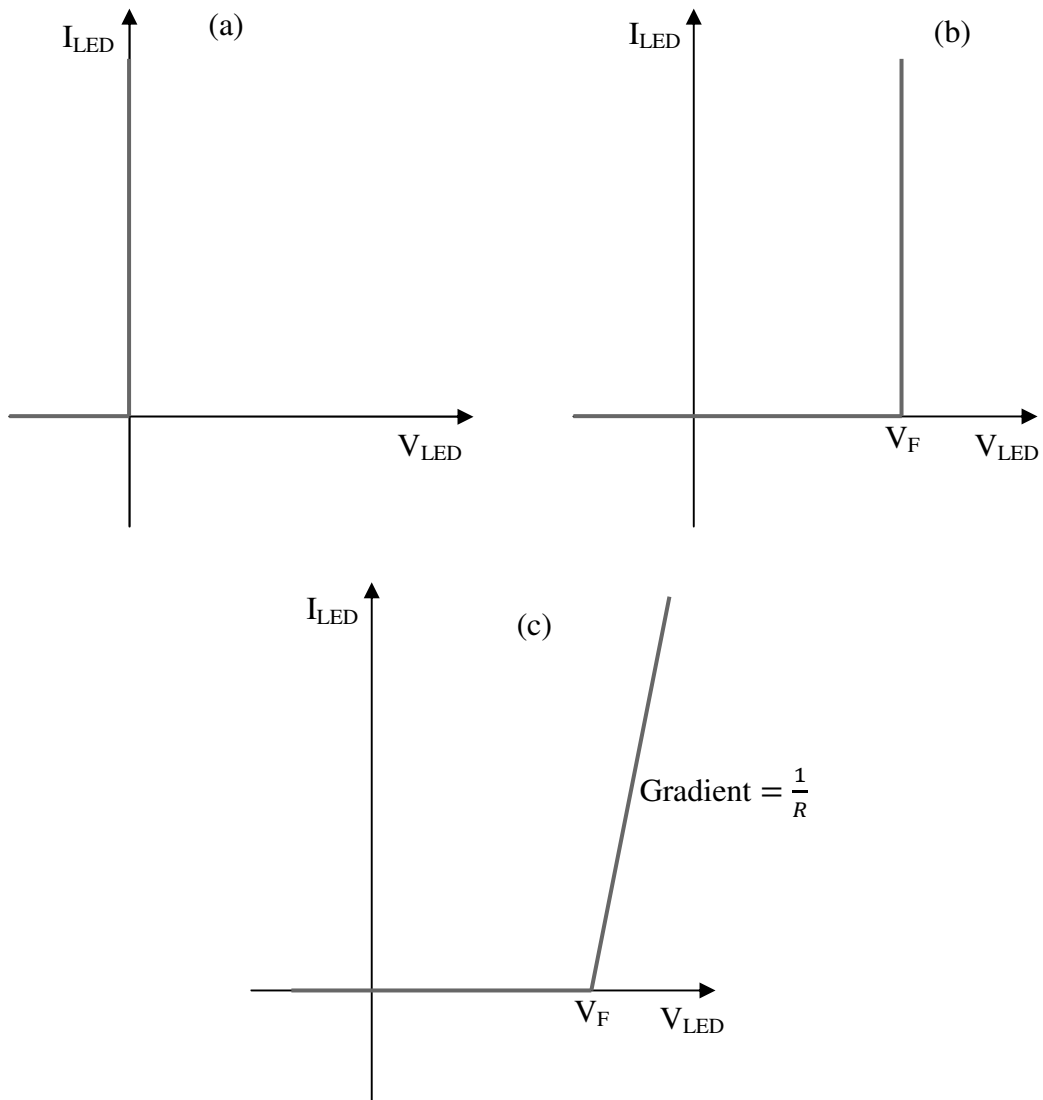
Figure 5.7: (a) An ideal V-I characteristics (b) V-I characteristics with froward junction potential (c) V-I characteristics with forward junction potential and forward resistance

## 5.5 Fusion Approach

We propose a fusion approach based on one of the developed data driven approach and the empirical model driven approach. We also propose to estimate the RUL using Kalman filter. In this case, we assume the data driven approach estimate has an error and it follows Gaussian distribution with mean $\mu_1$ and standard deviation $\sigma_1$. Similarly we assume the model driven approach has an error and it also follows the Gaussian distribution with mean $\mu_2$ and standard deviation $\sigma_2$. We use Kalman filter to estimate a single RUL by combining data driven and model driven approach RUL estimation. For example, if the RUL values from data driven and model driven approaches are equally good (i.e., $\sigma_1 = \sigma_2$), we can take average of the estimated RULs from data driven and model driven approaches. If data driven approach is far more accurate than the model driven approach we should give more weight to the RUL estimated from the data driven approach. Kalman filter is an estimation technique which uses previous data and estimate best value for RUL based on assign error parameters for data driven and model driven approaches (i.e., $\sigma_1$ and $\sigma_2$). Sometimes these error parameters are called accuracy of the models used for the fusion.

## 5.6 Summary

This chapter has presented developed PHM approaches to the LED health monitoring and prognostics. Euclidean distance, Mahalanobis distance, logistic regression and Kalman filter (LRKF) and neural network and Kalman filter (NNKF) approaches have been proposed and developed for the data driven PHM of the LEDs. An empirical model based approach for the model driven PHM has been developed and discussed. A fusion approach is proposed and developed based on Kalman filter to estimate best RUL from the estimated RULs from the data driven and model driven approaches.

# Chapter 6

# Experimental Setup and Data Collection

## 6.1 Introduction

There are standards developed by the Illuminating Engineering Society of North America (IES/IESNA) to test the LED lighting systems for the purpose of qualifications. IES LM-79-08[1] is developed as a standard to measure electrical and photometric characteristics of solid state lighting products such as LED luminaries and integrated LED lamps. IES LM-80-08[2] is developed as a standard to test the solid state light sources such as LED packages, arrays and modules (not luminaries) for lumen maintenance. IES TM-21-11[3] is developed to estimate the lifetime of the LED packages, arrays and modules based on the test procedures set out by the LM-80-08. TM-21-11 is a technical memorandum which specifies the approach to extrapolate the test data beyond the LM-80-08 test time. Purpose of these standards is to allow all the manufacturers to follow a common measuring procedure so that the users can compare the performance of the different products in the market. These tests need to be carried out and reported for the products by an independent laboratory. This is also a requirement of the Energy Star which is international standard for energy efficient products.

---

[1]IES standard for electrical and photometric measurements of solid-state lighting products
[2]IES standard for measuring lumen maintenance of LED light sources
[3]IES standard projecting long term lumen maintenance of LED light sources

The Alliance for Solid State Illumination Systems and Technology (ASSIT) has also developed standard for life test of the LED based on 50% light output degradation ($L_{50}$) and 30% light output degradation ($L_{70}$). Manufacturers are performing tests and producing the result based on these standards and tests. These standards and testing procedures provide the data for comparing the life expectancy of the different solid state lighting products but does not provide detailed information on the failure modes and mechanisms hence it will not help to estimate the life time of an LED in the field. Test times set out by these standards (i.e., ASSIST and IES) are generally too long. Therefore the use of accelerated life test (ALT) is investigated in this work to test the LEDs for the failure and collect data to develop an approach to assess degradation and predict the remaining useful lifetime of LEDs in the field.

## 6.2   Accelerated Life Test (ALT)

Accelerated life tests are widely used to assess the reliability, and develop and test the prognostics approach for electronic systems, mechanical systems etc. ALT is designed to elevate the stress conditions individually or as a combination to accelerate the failure. ALT is also used for various tasks in the process of PHM. For example, ALT is used to generate the failure data set for different failure modes or mechanisms and normal data set etc. under different normal operating conditions. In addition, ALT is used to develop and test the PHM algorithms under the ALT conditions. Published research work on ALT for LEDs or LED lighting systems is discussed in chapter 2 section 5.

In this work ALT is used to accelerate the failures based on both drive current and junction temperature. In particular, this test is designed to accelerate the failures which are caused by power supply breakdown or driver breakdown. If the power supply or driver breaks, LEDs in the circuit will undergo electrical overstress. This electrical overstress will induce the thermal overstress since the electrical overstress increases the junction temperature of the LEDs. When the LEDs are deployed in the field, there are many known and unknown factors which affect the performance of the LED lighting systems and increase the possibility of catastrophic failures. For example LED lighting systems under the harsh op-

erating environments such as automobile exterior lighting, lighting applications in the factories etc., need to operate under extreme environmental temperature conditions. Such systems will have a short lifetime and in many case they have to be monitored. The experiment below is designed to capture such failures caused by voltage and current fluctuations, driver break down, temperature increases, etc.

The objective of adopting the ALT here is to develop and assess the performance of the proposed PHM for high power LEDs. In the experiments detailed below, the current through the p-n junction and the p-n junction temperature can be defined as the performance indicators of the LED. Therefore, any accelerated test can use the current or the temperature as the stress parameter of the LED. Generally LEDs are controlled by controlling constant current through the sense voltage (analogue dimming) or pulse width modulated switching (digital diming). In this experiment, the constant current required to operate the LED is controlled by controlling the forward voltage across the LED and the experiment is designed to test a single LED at a time. Since the failures based on current and the temperature need to be accelerated, the forward/applied voltage is used as an accelerating damage condition in the experiments. The acceleration of the applied voltage results in the elevation of both stress parameters (e.g. the drive current and the junction temperature). Test strategy based on forward voltage is shown in Figure 6.1.

Figure 6.2 (a) shows a Luxeon star LED from Philips Lumileds lighting and Figure 6.2 (b) shows a fitted LED on a holder that represents the LED test set up. Figure 6.3 details the experimental test setup, which consists of a data acquisition system (National Instruments PXI), a voltage regulator and sensors, and a single High Power Philips Luxeon Star LED. For the purpose of light measurement, the LED is placed within a semi spherical enclosure which also contains a photodiode light sensor.

The National Instruments PXI platform can be connected to both analog and digital input modules providing the ability to measure voltage levels for different types of signals. For this experiment we use a 24-bit universal analog input module (NI 9219) to measure the applied voltage, and the voltage across the three sensors (current, temperature, and light).
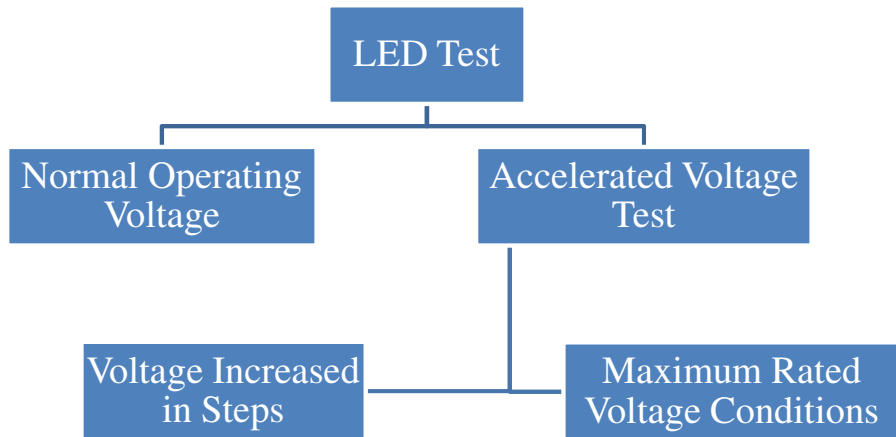
Figure 6.1: LED test strategy
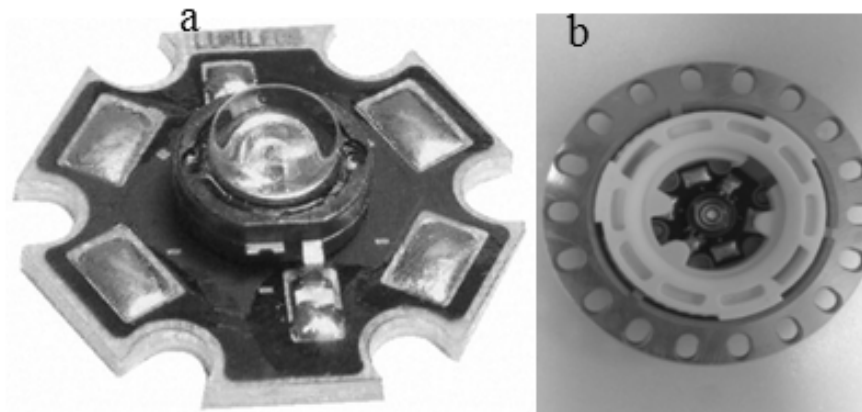


Figure 6.2: (a) Luxeon star LED from Philips (b) Luxeon star LED with holder
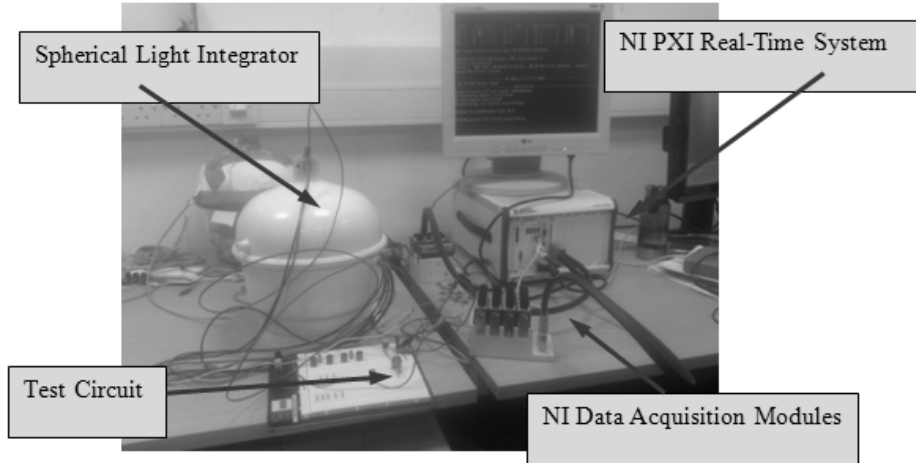
Figure 6.3: Test bench – Experiment setup with NI PXI systems

The applied voltage is measured by connecting the anode and cathode terminals of the LED and sensors for current, light and temperature are connected to the data acquisition platform. Voltage is measured for all three sensors, for example to measure light output we use a photodiode which converts light into voltage and is calibrated to convert the light into voltage in a proportional manner. To measure temperature we use a thermocouple which generates very small voltage (mV) related to the temperature on the board. For current we measure the voltage across the power resistor and this is converted into current. Figure 6.4 shows all three sensors used in this experiment. Figure 6.4 (a) is the light sensor (Photodiode TSL250R-LF) which converts the light proportionally into volts. Figure 6.4 (b) is the thermocouple (NI readymade J type thermocouple) which converts the temperature into millivolts. Figure 6.4 (c) is the current sensor (Power resistor, MHP 100-0.25 $\Omega$) which converts the current into voltage. Therefore the measured sensor data from the sensors for current, light and temperature reported in the remaining part of the this these is given in row format and in units of volts or millivolts (V or mV). For the purpose of PHM algorithms, it is not required to post process into the relevant parameter specific units (e.g, A for current, °C for temperature etc.,).
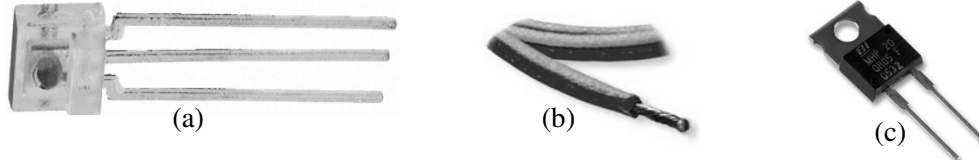
Figure 6.4: (a) Photodiode TSL250R-LF (b) NI readymade J type thermocouple (c) Current sensor (Power resistor, MHP 100-0.25 $\Omega$)

## 6.3 Data Collection – Normal Operating Condition

Although normal operating values for voltage, forward current and junction temperature are given in the LED manufacturer's data sheet, these values are based on the test carried out under control environment. For example, the technical datasheet DS23 for power light source Luxeon Star gives the optical and electrical characteristics data based on the junction temperature 25°C. In real world applications, it is difficult to maintain the junction temperature at 25°C. It is also necessary to establish the corresponding sensor values (i.e, in V or mV) for normal operation of the LED. Therefore it is necessary to run a test under normal operating condition.

The sensor data obtained under normal operating condition specified by the LED manufacturer, is used to determine the mean values of the voltage readings for the three sensors (current, temperature and light). Sensor data are collected when the LED is operating under normal conditions i.e., forward voltage 3.42 V and environment temperature is equal to room temperature 20°C. This data is then analysed to identify the mean values for the sensors data when the LED is operating normally. One LED is tested under the normal operating condition for 96.5 hours. Figure 6.5 shows the collected data under the normal operating condition. Table 6.1 details the mean values and variance of the data collected for all three sensors, when the applied voltage is 3.42 V. Hence the normal operating conditions can be defined in terms of sensor reading using the tabulated mean values.

144
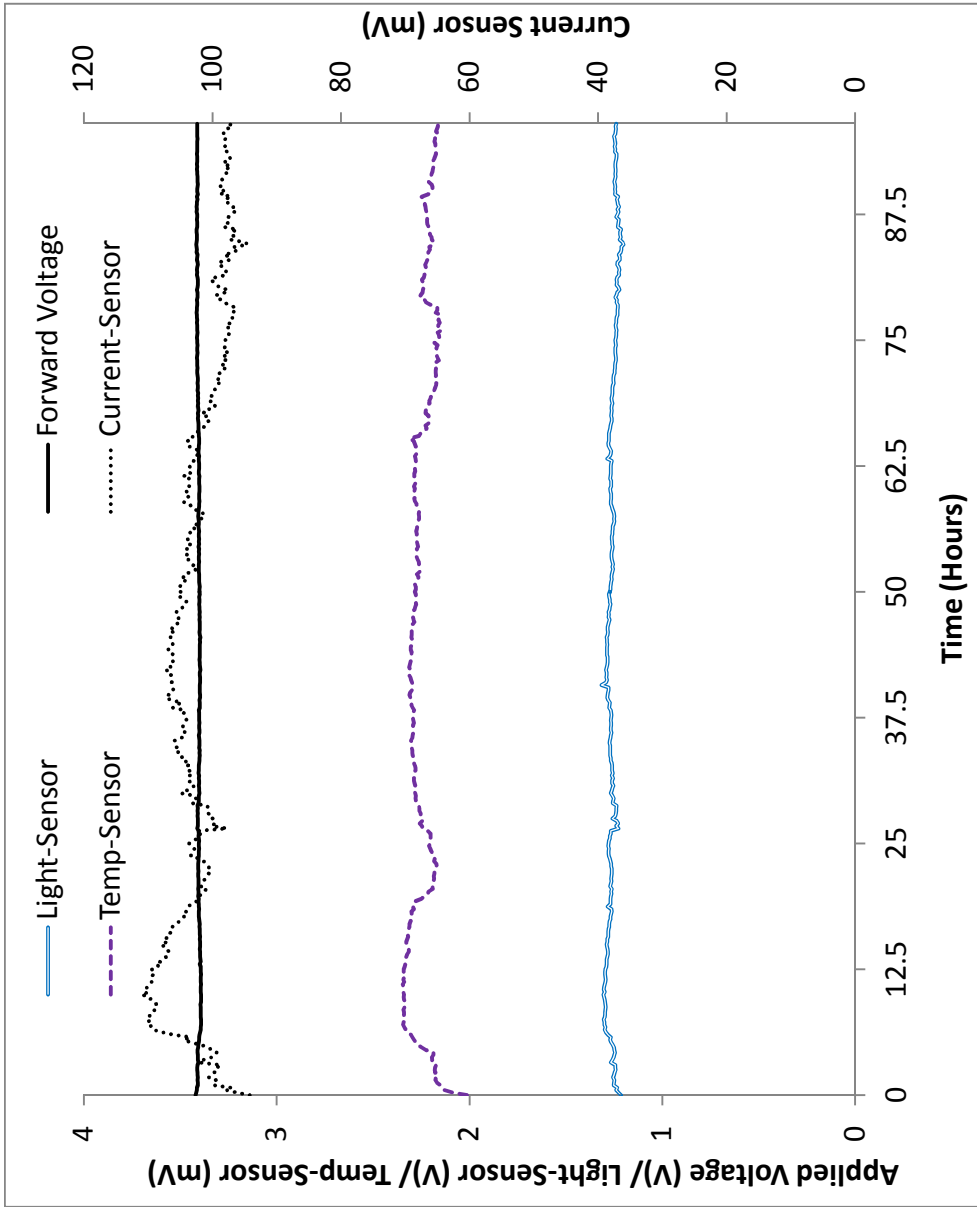
Figure 6.5: Sensor data for normal operating conditions
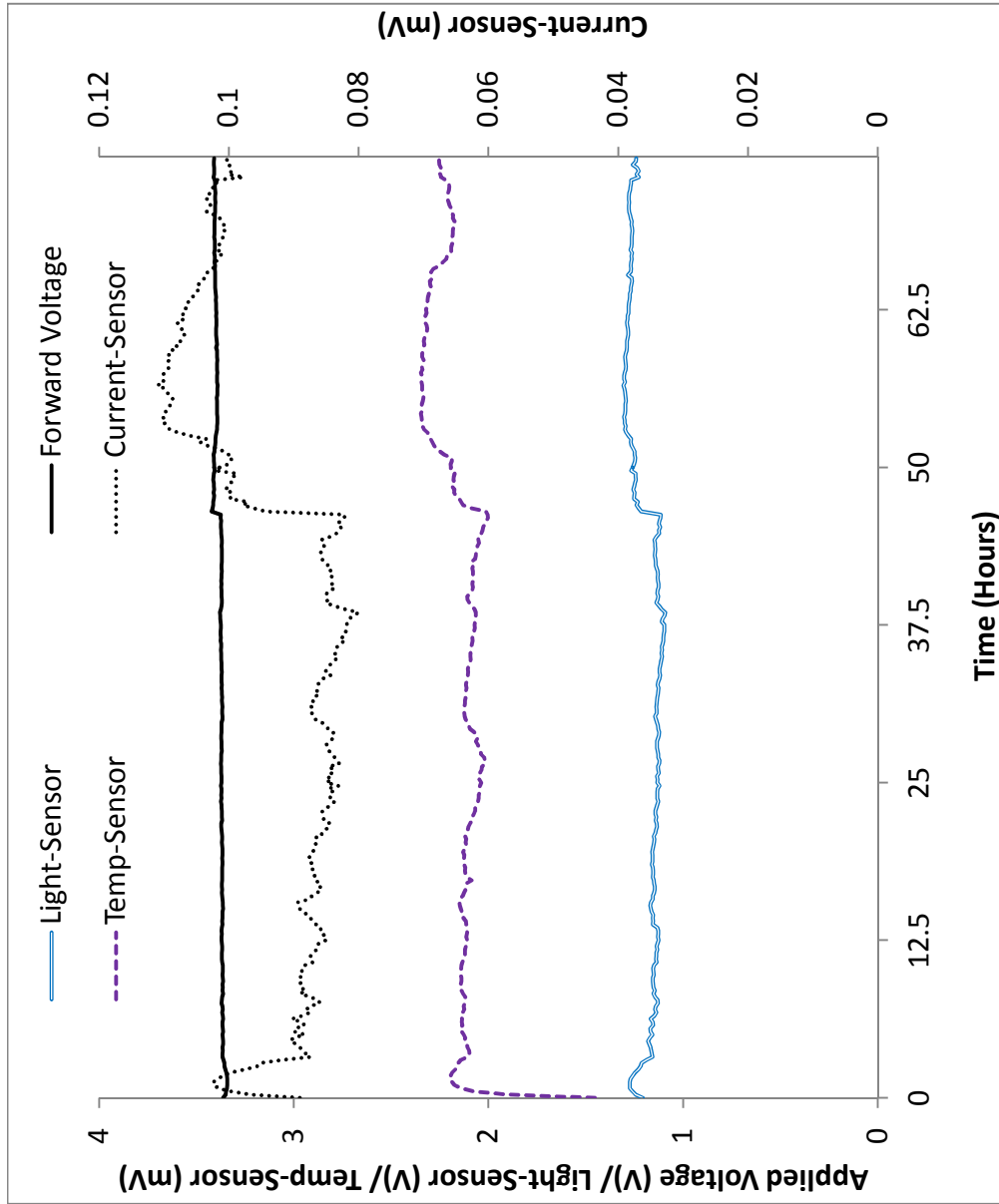
Figure 6.6: Sensor data shows the sensitivity of the LED to applied voltage

| Parameters | Mean Sensor Values | Variance | Real Values |
|---|---|---|---|
| Applied Voltage | 3.42 V | 0.00034 | 3.42 V |
| Light Output | 1.18 V | 0.00502 | Not Available |
| Board Temperature | 2.2 mV | 0.0088 | 42.7 °C |
| Forward Current | 0.09 V | 0.000069 | 0.35 A |

Table 6.1: Mean sensor readings for normal operating condition

Only one LED can be tested at a time using the available setup and the voltage needs to be adjusted manually to control the forward voltage to the LED. LEDs are very sensitive to the applied voltage and they also behave significantly different to each other. Figure 6.6 shows how the LED current profile changes with a small increases in the applied voltage. Almost a constant voltage of 3.37 V is applied to the LED and at time 46.5 hours the voltage is increased to 3.42 V. This shows at the normal operating conditions 0.05 V variation corresponds to more than 0.028 mV in the current sensor data which is equal to the actual value of 100 mA. These are the challenges of this experiment.

## 6.4 Data Collection – Accelerated Voltage Test

Accelerated life test (ALT) is carried out for the LEDs using the voltage as the acceleration parameter. Accelerated voltage is applied to LEDs in two different ways. First the applied voltage is increased in steps from the rated minimum voltage to the rated maximum voltage. In addition, constant level voltage of rated maximum voltage is applied from the start. These two different sets of data are used to develop and test the PHM approaches for the LEDs.

### 6.4.1 Voltage Increased in Steps

Figure 6.7 shows the sensor data for accelerated voltage test carried out for an LED. Applied voltage is increased with a step of 0.2 V every half an hour. Forward voltage profile of the LED is shown by the black straight line curve. As the voltage increases, all other sensor readings also increase. When voltage reaches a maximum value, LED starts to degrade gradually at a constant rate which is indicated by the light sensor reading in Figure 6.7 (blue double line). The test

shows that the LED starts to degrade after the forward voltage reaches 3.69 V. It should be noted that this voltage is 0.3 V less than the maximum rated voltage specified by the manufacturer. In this case, gradual light degradation is observed from 212 min and light output level reaches the failure value of 0.826 V. This failure value of 0.826 V for the light output is calculated from the 30% drop of the typical light output value (1.18 V) under normal operating condition which is reported in the Table 6.1.

A few LEDs demonstrated also catastrophic failures after a certain voltage level. The tests reveal that LEDs are very sensitive to voltage increases and absolute maximum rating varies for different LEDs. Hence, different LEDs can exhibit degradation at different forward voltage levels. Some LEDs failed before the applied voltage reaches the absolute maximum voltage of 3.99 V while some other LEDs operated above absolute limit specified by the manufacturer.

## 6.4.2 Maximum Rated Voltage Condition

In this test, the LEDs are supplied with the voltage which is very close to the absolute maximum rated voltage and data was collected for different LEDs. Figure 6.8 shows the data of an LED test carried out under a constant elevated voltage condition. LED starts to fail quickly as the forward current starts to drop gradually. Although similar voltages were applied to the LEDs, different LEDs exhibited different degradation and hence time taken to failure is different for different LEDs. Figure 6.8 shows that this particular LED failed at 108 minutes from the start of operation under the accelerated voltage condition. Failure is reported when the light output reaches its failure value of 0.826 V. Figure 6.9 shows the data for another LED tested under similar conditions. This particular LED failed at 170 minutes from the start of operation since the light output reaches the failure value of 0.826 V.
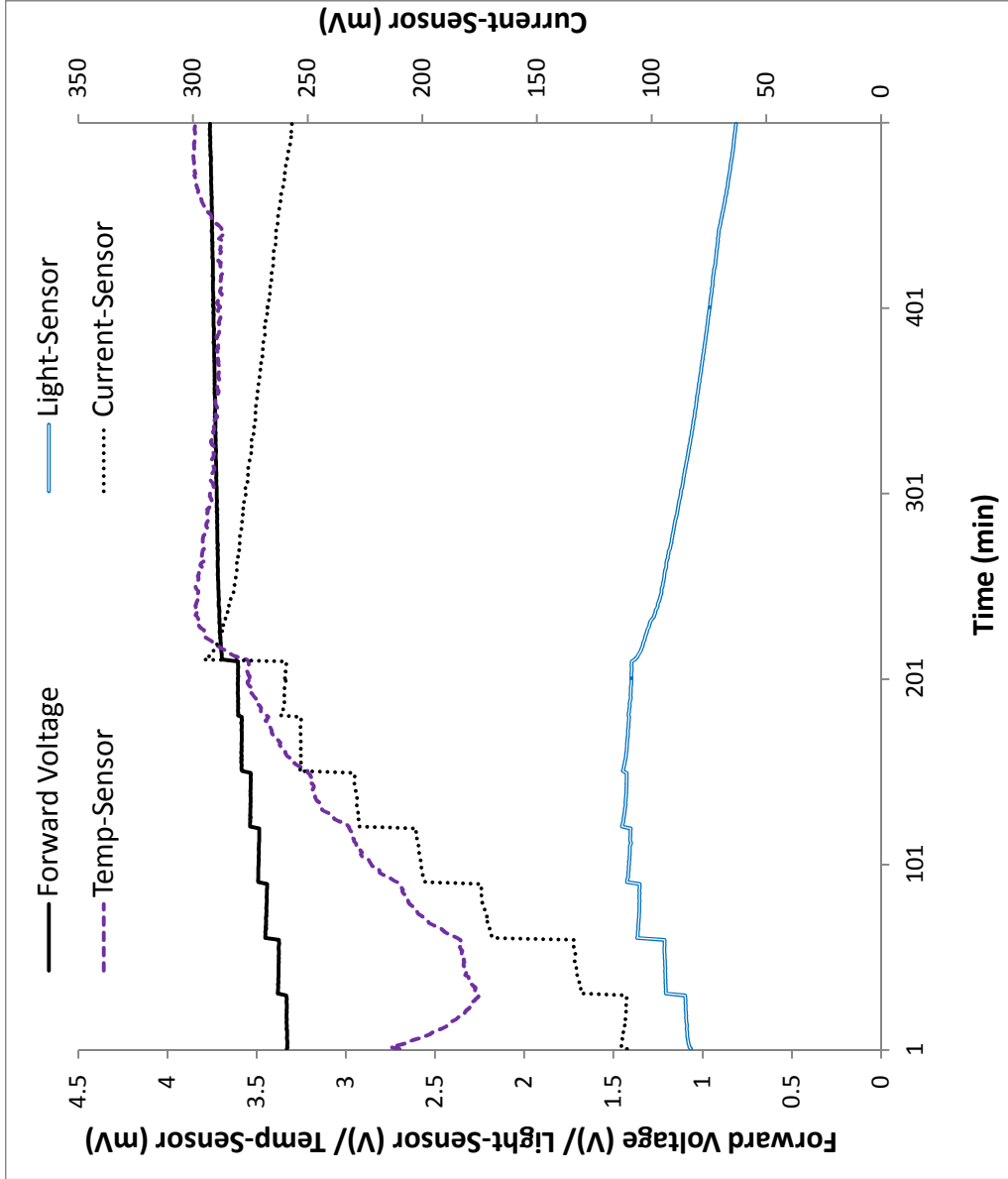
Figure 6.7: Sensor data for voltage increased in steps
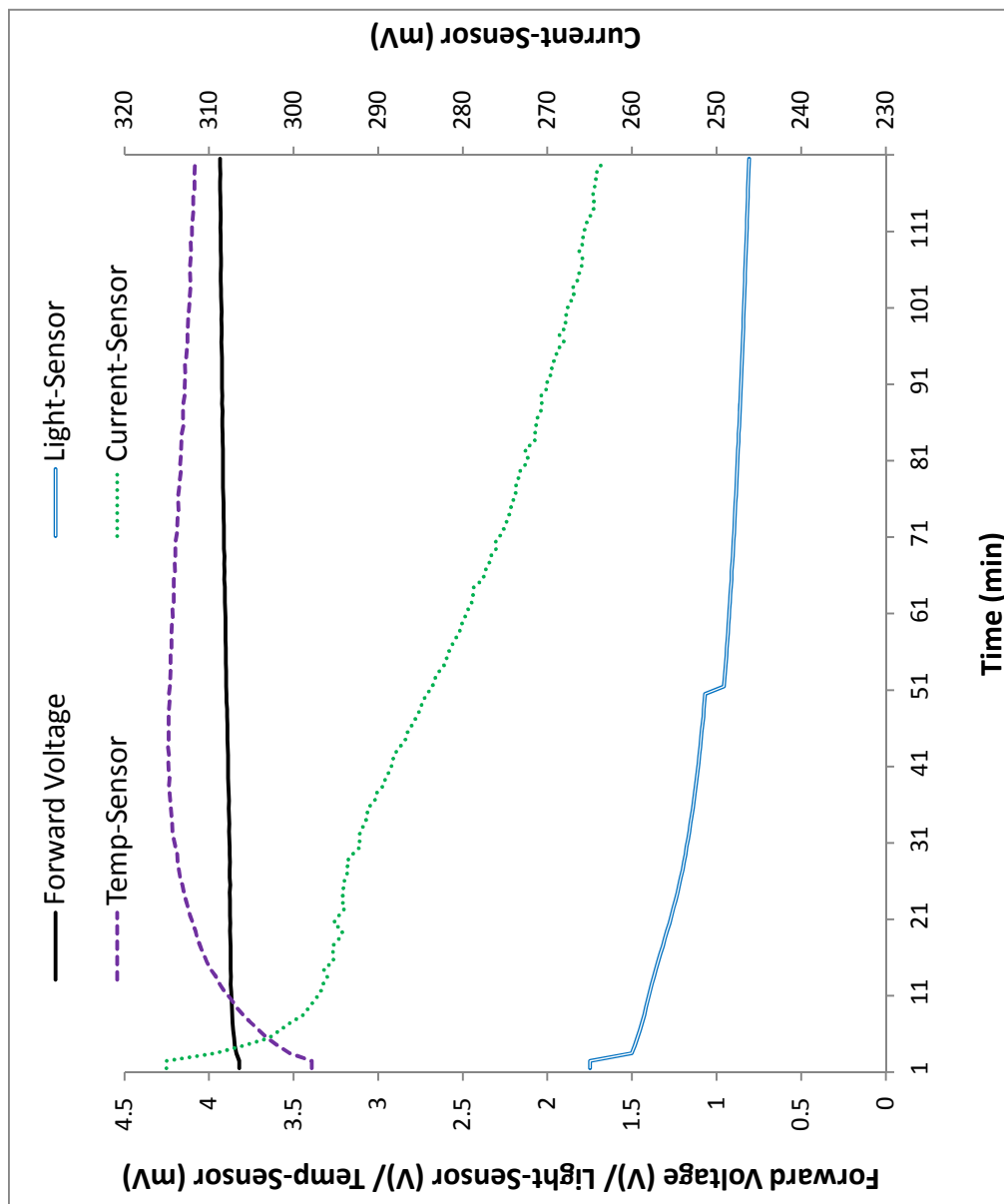
Figure 6.8: Sensor data for ALT (Voltage) at forward voltage of 3.83 V
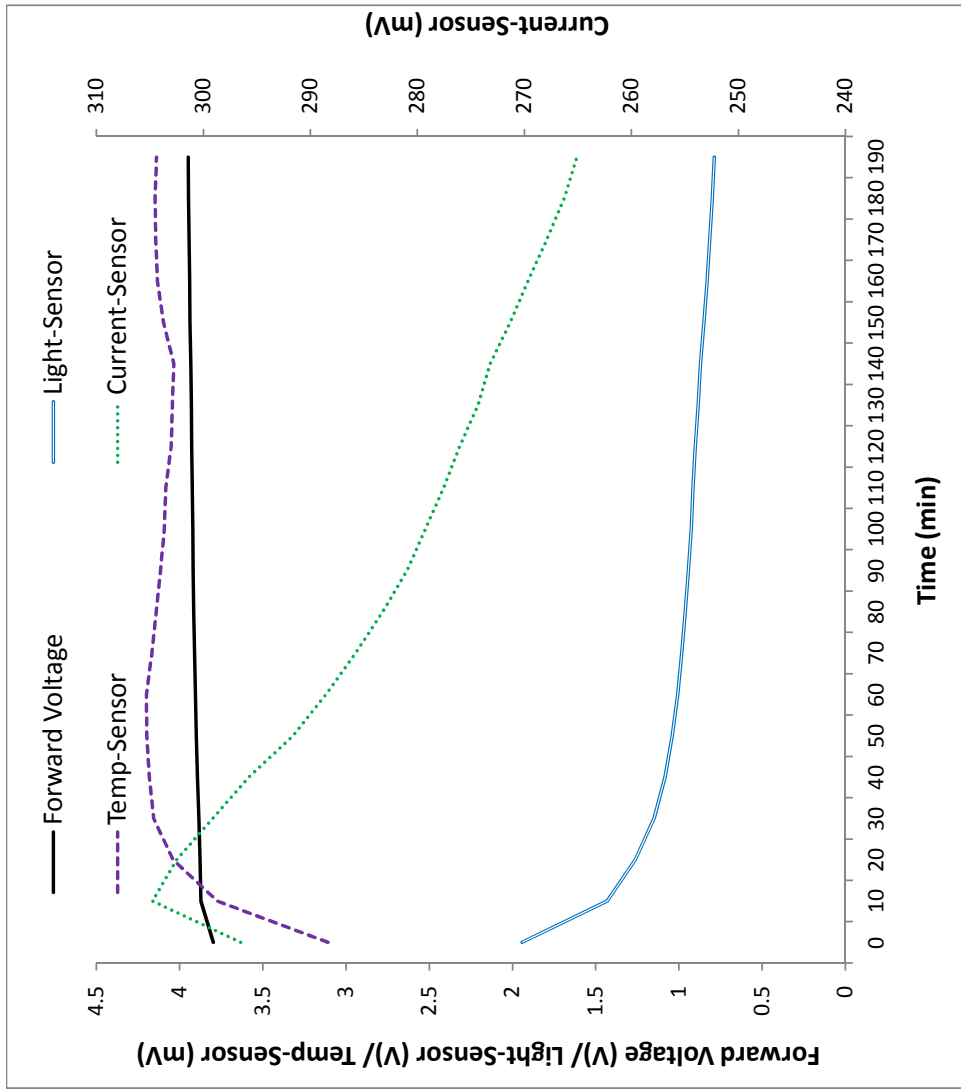
Figure 6.9: Sensor data for ALT (Voltage) at forward voltage of 3.87 V

## 6.5  Summary

This chapter has presented the experimental setup, detail account of the experiments and data collection. Data collected and presented in this chapter shows variations in the data based on applied voltage and failure time. It is also found out that the LEDs are very complex small systems which also behave significantly differently to each other.

# Chapter 7

# Results and Validation

## 7.1   Introduction

This chapter presents the results and validations for the techniques developed in chapter 5. Distance measures, logistic regression and neural network are investigated for data driven approach and results are reported. An empirical model for LED is developed and results are discussed. A fusion methodology to use the predictions from data driven and model driven approaches, to estimate RUL more accurately, is discussed and results are presented in this chapter. Results are presented under three different sections:

1. Data driven approach

2. Model driven approach

3. Fusion approach

## 7.2   Data Driven Approach

In this section we present the results from the data driven approaches and the respective validations. The following three approaches are developed and reported in chapter 5 for the diagnostics, prognostics and health monitoring of LEDs:

1. Distance measures

2. Logistic regression

3. Neural network

In particular these developed approaches can be used as a real-time prediction tools in the case when sensor data are available. The real-time implementations of these techniques for PHM are discussed in next chapter (chapter 8). Comparison of these approaches based on the accelerated ageing is also provided.

### 7.2.1 Distance Measure Approach

Data is obtained under both normal and accelerated stress conditions. Data collected from the normal operating voltage test is used to estimate the normal operating values in terms of the sensor readings and also used to estimate the respective distance measures such as Euclidean Distance (ED) and Mahalanobis Distance (MD). The data obtained from the accelerated voltage test is used to identify the threshold values for the ED and MD techniques, above which the LED will start to degrade. Figure 7.1 shows the ED and MD estimation based on the current and temperature sensor data under the normal operating voltage and temperature conditions. The normal operating conditions have been discussed in section 3 of chapter 6. The ED and MD calculations are based on equations 5.4 and 5.8 in chapter 5. The current and temperature sensor data used are from the data set shown in Figure 6.5 in page 145 in chapter 6. Since the weight of the current is very small compared to the weight of temperature sensor data, we propose a normalisation technique which is suitable to real-time systems. Current sensor data is normalised such that its mean value matches the mean value of the temperature data. Therefore the current sensor data in mV is divided by a factor of 40. This normalisation is more suitable to implement in real-time systems.

What is interesting in the above is the sensitivity of the MD method to small changes in the sensor readings. It is observed that the MD values increases when there is less correlation between the current and temperature sensor data. Table 7.1 summarises the observed minimum, maximum and mean values for both ED and MD under normal operating conditions. Under these conditions an LED typical lifetime will be an average of 50,000 hours. High values for ED and MD

154
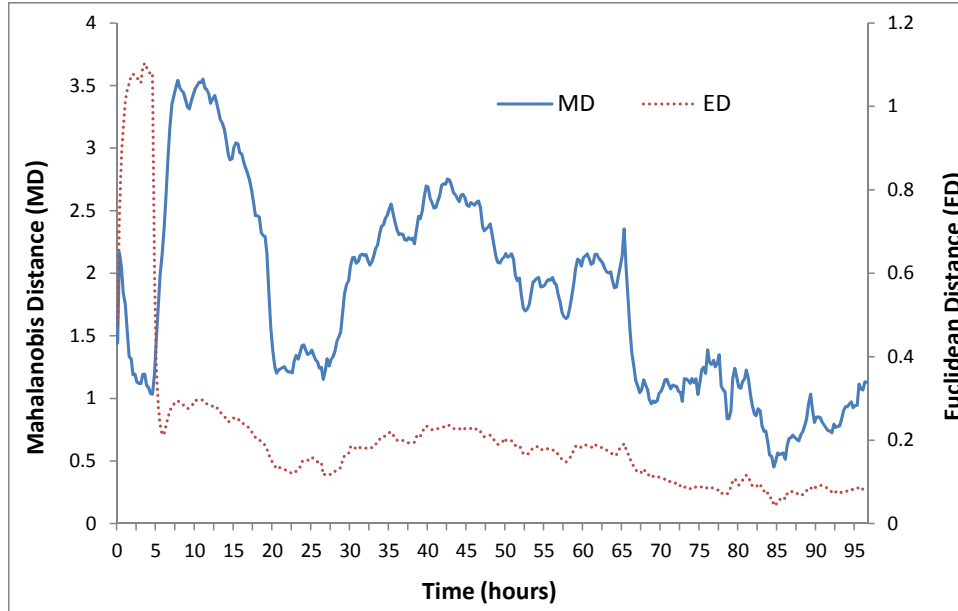
Figure 7.1: ED and MD estimation for normal voltage and temperature conditions

| Distance Measure | Minimum | Maximum | Mean Value |
|---|---|---|---|
| Euclidean Distance (ED) | 0.042 | 1.1 | 0.21 |
| Mahalanobis Distance (MD) | 0.45 | 3.55 | 1.8 |

Table 7.1: Observed minimum, maximum and mean values for ED and MD for normal conditions

are observed for first ten hours as the temperature and current start to stabilise in that period. As soon as current and temperature reach a stable value, both ED and MD become more stable. In this case, current sensor reading increases to 90 mV (i.e., 350 mA) which is the normal operating current, and temperature sensor reading increases to 42° C which is the normal operating board temperature.

To start the diagnostics and prognostics based on available sensor data, it is required to derive parameters that can be used to indicate different health state of the LED. For that purpose, we introduce the following parameters for the ED and MD methods:

1. Early warning threshold ($ED_{EWT}$ and $MD_{EWT}$)

2. Maximum values ($ED_{MAX}$ and $MD_{MAX}$)

3. Failure threshold ($ED_{FT}$ and $MD_{FT}$)

Early warning threshold (EWT) is used to indicate the starting of the degradation in the light output and failure threshold (FT) is used for the prognostics purpose. Maximum values are used to calculate the FT (i.e., $ED_{FT}$ and $MD_{FT}$) for different LEDs. This allows to compute different $ED_{FT}$ and $MD_{FT}$ values for different LEDs based on their observed corresponding maximum values ($ED_{MAX}$ and $MD_{MAX}$). If the ED or MD starts to decrease when the applied conditions are not changed, this process indicates the actual light degradation is taking place. For example, if ED and MD decreases from an observed maximum value of $ED_{MAX}$ and $MD_{MAX}$ receptively when the applied voltage condition is unchanged, this indicates the degradation in the light output. If ED and MD reaches FT values of $ED_{FT}$ and $MD_{FT}$ receptively, it can be assumed that the LED has failed (i.e., in this case, light output goes below the minimum require values of 0.826 V). This novel approach helps to incorporate the individual strength of the LEDs against the accelerated test conditions. Figure 7.2 shows the follow diagram of the developed distance measure approach for the real-time health monitoring of LEDs.

### 7.2.1.1 Early Warning Threshold ($ED_{EWT}$ and $MD_{EWT}$)

Data collected from the accelerated test is used to identify the EWT for MD and ED methods under accelerated ageing conditions, triggering light degradation. In this test the applied voltage is increased in steps from the initial of 3.29 V to a maximum of 3.99 V. This maximum voltage is also the absolute maximum forward voltage of the LED specified by the manufacturer. Note that the normal operational voltage that is required for the LED is 3.42 V. Data from the sensors are then analysed to identify the EWT for ED and MD (i.e, $ED_{EWT}$ and $MD_{EWT}$).

Figure 7.3 shows the voltage applied to a single LED and the readings from the current, light and temperature sensors. In addition to this, the graph also shows a horizontal red line at 0.826 V which represents a 30% drop in the light sensor from what its value would be when operating normally (i.e, light sensor reading should be around 1.18 V when the applied voltage is 3.42 V). Therefore if
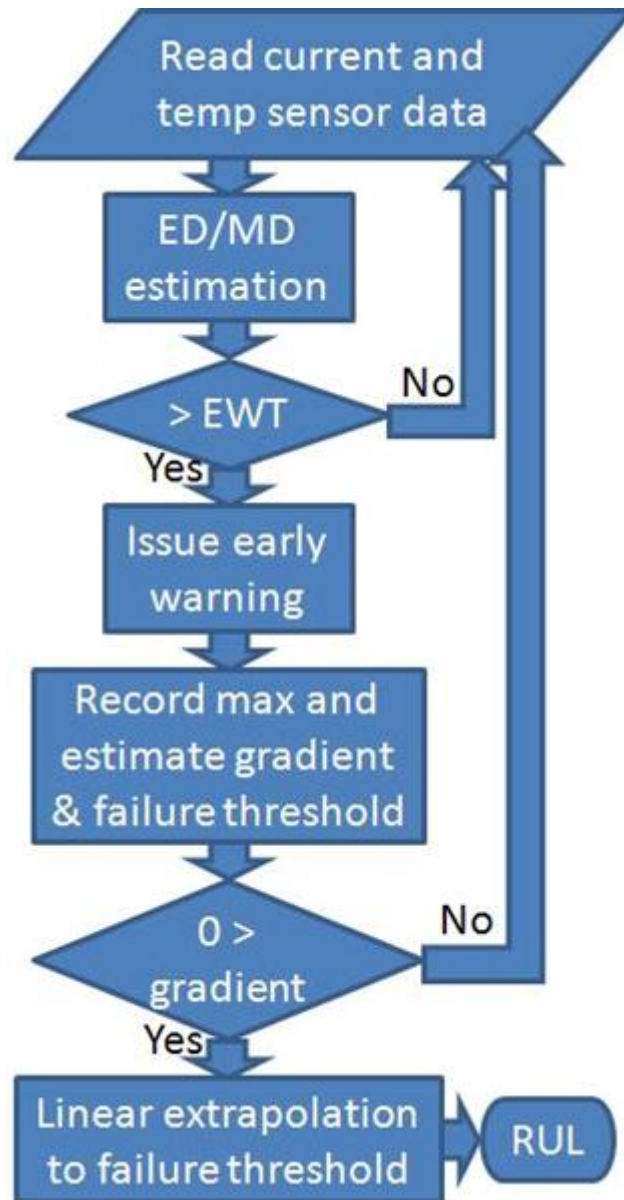
Figure 7.2: Distance measure approach for real-time health monitoring of LEDs

the light sensor reading goes below this horizontal line then we have a reduction in light output over 30% and hence a failure can be assumed.

In this case, the light sensor data starts to decrease with a gradual rate when the applied voltage increases to 3.99 V. This take places at 525 min and light sensor data reaches the 30% drop limit at 725 min. This reduction in the light sensor data is witnessed by the associated current and temperature reduction. In particular, when applied voltage is kept at an elevated level, current starts to decrease when actual degradation in the LED is taking place. This is because of the heat generated at the p-n junction.
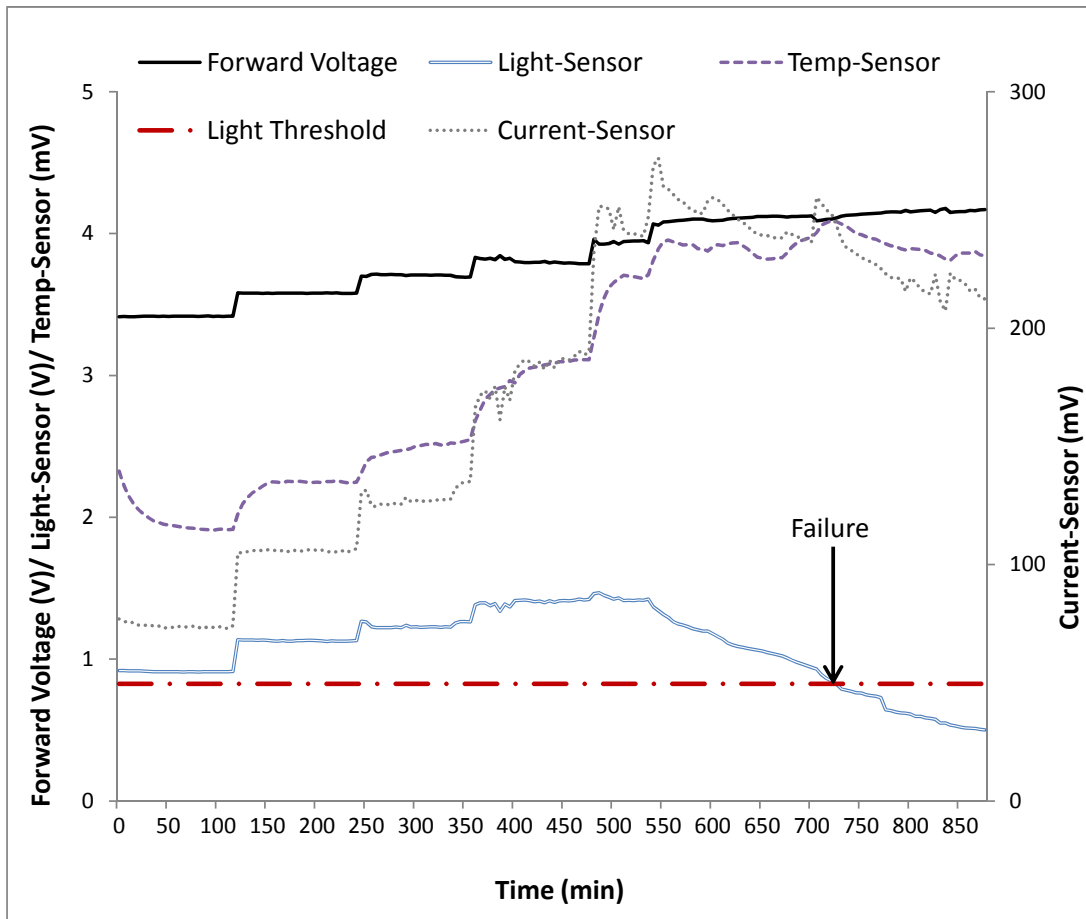


Figure 7.3: Sensor Data from Accelerated Voltage Test (Voltage Increased in Steps)

ED values are estimated using the current and the temperature sensor data shown in Figure 7.3. The light sensor readings are only used to observe the reduction in the light output power from the LED. Early warning threshold ($ED_{EWT}$) for this particular test data is 2.7. We would expect the light output to increase as the voltage increases. Hence, to calculate the EWT for the ED parameter we identify the point at which the light output starts to decrease continuously. This EWT represents the point in time at which the LED starts to degrade. Therefore, once a value for ED goes above this $ED_{EWT}$ the degradation in light output is taking place. Hence by monitoring the ED parameter we can diagnose when light output is degrading based on the monitored data from both temperature and current sensors. ED values are very high compared to the normal operating condition (see Table 7.1) and this indicates how far the LED is operating from its normal operating condition (i.e., overstress conditions). Figure 7.4 shows the estimated ED values graph for the data shown in Figure 7.3.

Similar analysis for MD approach is carried out to identify the EWT (i.e., $MD_{EWT}$). The same data set shown in Figure 7.3 is used for MD analysis. Figure 7.5 shows the estimated MD values graph for the data shown in Figure 7.3. For the MD method the light output is observed to decrease continuously from the MD value of 19, onwards. Hence the EWT for MD is 19, above which the light output is degrading. So, as with the ED method, by monitoring changes in current and temperature, we can use the MD calculation and its EWT to diagnose when light degradation starts.

The above was undertaken on ten different LED under the ALT (voltage increased in steps) and early warning threshold values (EWT) are calculated separately for each. From the calculated EWT for ED and MD for ten LEDs, early warning thresholds ($ED_{EWT}$ and $MD_{EWT}$) are selected as the minimum from the tested batch of 10 LEDs. Therefore for the following validation cases we use the minimum EWT from Table 7.2, which are $ED_{EWT} = 2.5$ and $MD_{EWT} = 17$.
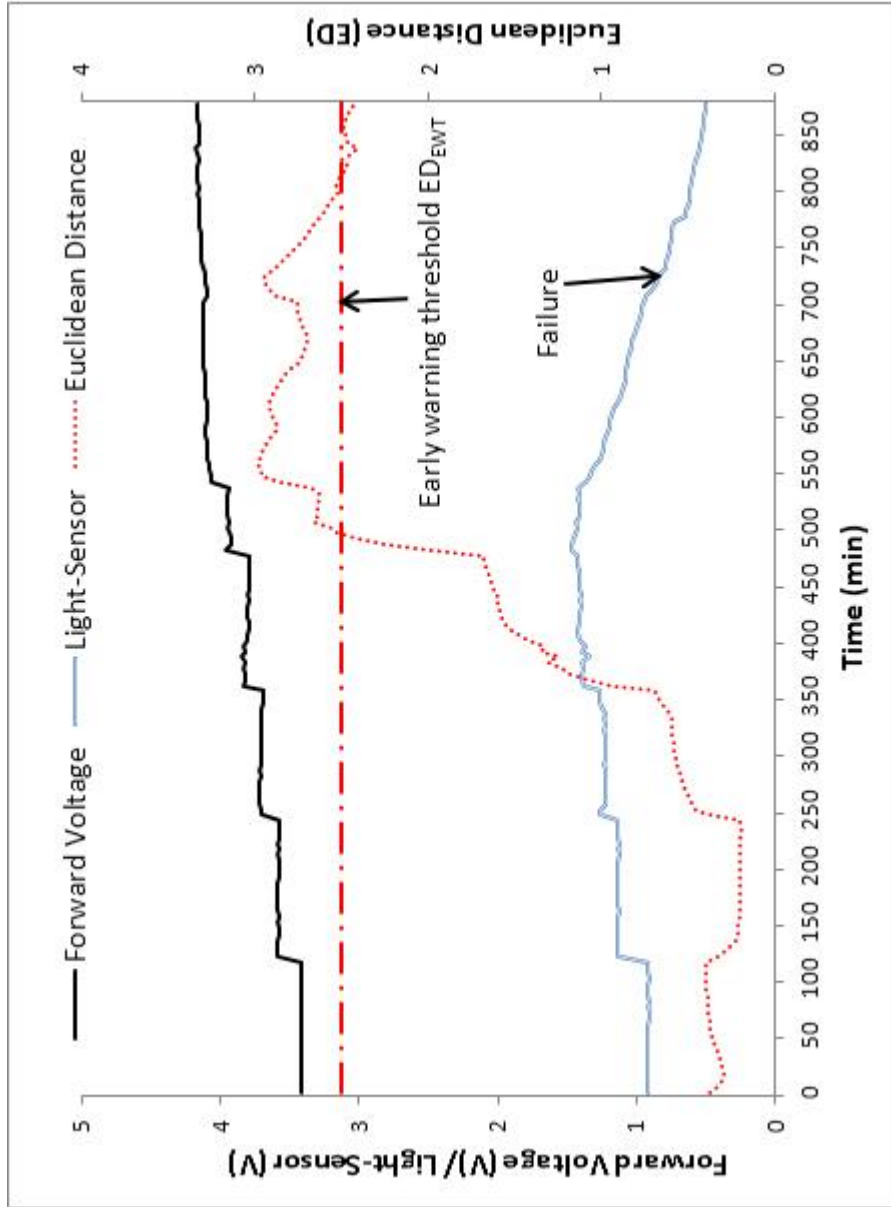
Figure 7.4: ED analysis for current and temperature sensor data shown in Figure 7.3
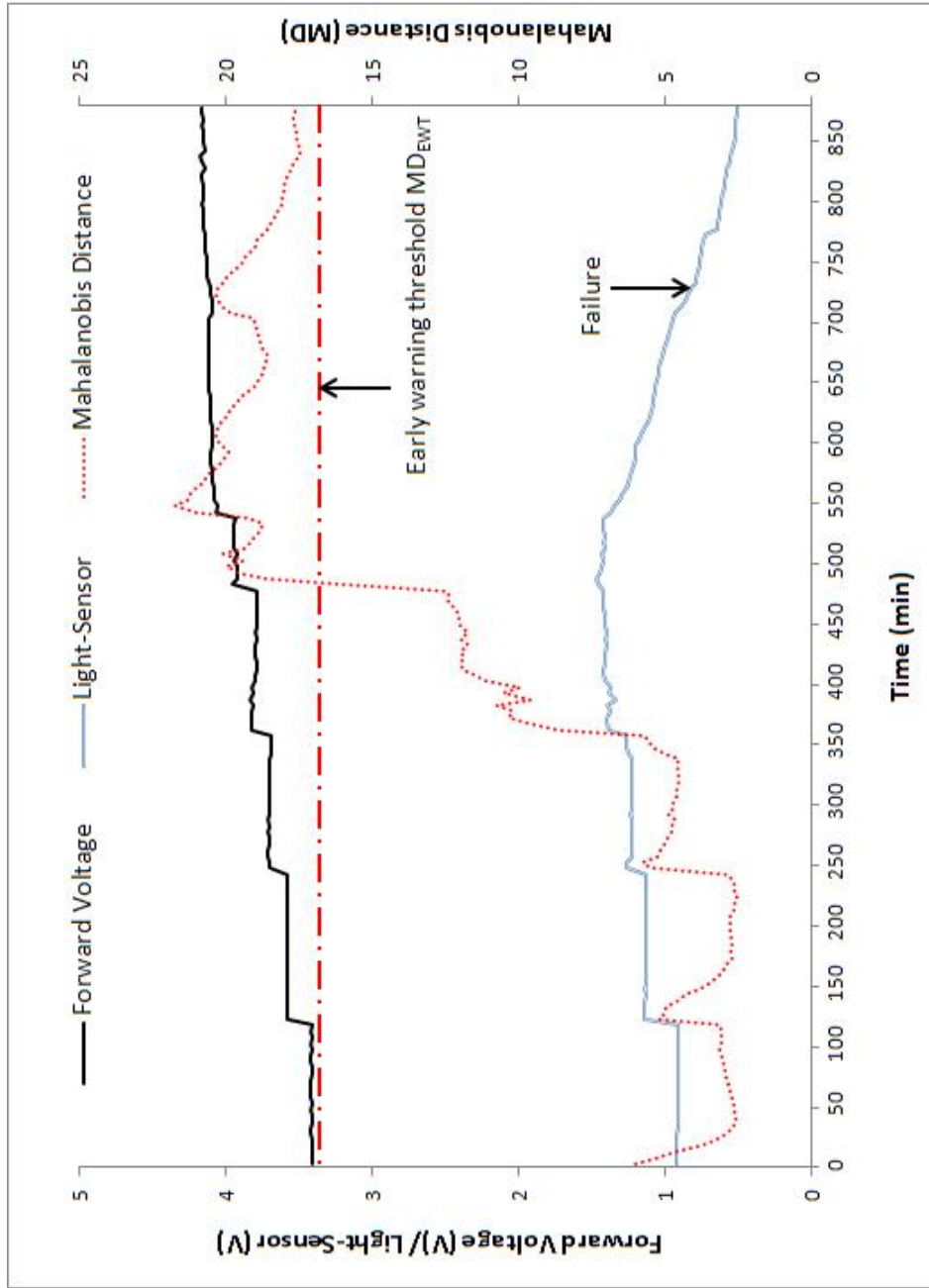
Figure 7.5: MD analysis for current and temperature sensor data shown in Figure 7.3

| LED No | $ED_{EWT}$ | $MD_{EWT}$ |
|--------|------------|------------|
| 1      | 2.6        | 20         |
| 2      | 2.6        | 22         |
| 3      | 2.5        | 17         |
| 4      | 2.5        | 18         |
| 5      | 2.5        | 17         |
| 6      | 2.6        | 18         |
| 7      | 2.5        | 17         |
| 8      | 2.7        | 19         |
| 9      | 2.8        | 23         |
| 10     | 2.7        | 22         |
| Min    | 2.5        | 17         |

Table 7.2: Early warning threshold for batch of 10 LEDs

### 7.2.1.2 Maximum Values ($ED_{MAX}$ and $MD_{MAX}$)

The values for ED and MD can be used to make predictions for the remaining useful life of LEDs. During light degradation both current and temperature values that are monitored decrease with time when the applied voltage to the LED does not change. This observation is made from the experiments. This will correspond to ED and MD parameters also decreasing over time (i.e., reach a maximum value and start to decrease). The observed maximum values for ED and MD vary for different LEDs, and they indicate different individual characteristics. In the case of the LED lighting systems, the extent of deviation or degradation (i.e., ED or MD) will not continuously increase until LED completely fails (i.e., light output drops to 70% which is light sensor reading of 0.826 V). As light output degrades to 70%, current will also decrease and this implies that the ED or MD should decrease to a certain level. Continuous constant rate of degradation in the light output can be observed in the rate of reduction in the ED and MD.

The approach proposed and developed here, the gradient of the ED and MD curves can be used to forecast the remaining useful life (RUL). To estimate the RUL using these gradients, it is required to have start and end values for ED and MD. The start ED and MD values for the prognostics are proposed as the observed maximum values, i.e., $ED_{MAX}$ and $MD_{MAX}$ under accelerated test condition. After these observed maximum values, ED and MD show gradual degradation

which corresponds to the light degradation in the LED. This is shown in Figure 7.4 for ED and Figure 7.5 for MD. Different values for $ED_{MAX}$ and $MD_{MAX}$ observed from the different tests.

### 7.2.1.3  Failure Threshold ($ED_{FT}$ and $MD_{FT}$)

ED and MD values that correspond to the failure of LEDs, i.e., when light output drops below 70% from the typical value, are defined using experimental data and referred as failure threshold (FT), i.e., $ED_{FT}$ and $MD_{FT}$, respectively. Almost linear reduction in the ED and MD is observed during the tests when the LED undergoes degradation process. Linear extrapolation of the ED and MD decreasing trend when light degrades, can be applied and used with the $ED_{FT}$ and $MD_{FT}$ to calculate the remaining useful life (RUL). This prediction for the RUL can be undertaken at any particular time point if the ED and MD curves are above the EWT (indicating possible degradation takes place) and the trend is decreasing when the applied voltage is unchanged. As new data becomes available over time, and ED and MD are re-calculated, their trends are adjusted and RUL predictions are re-calculated.

Test data obtained using ten LED devices are used to observe the respective values of ED and MD at the time when the power light output drops below 70% from the initial value (i.e., LED failure). Each LED was tested under slightly different accelerated voltage tests where the applied voltage was set to be in the range of 3.6 to 3.99 V. The aim is to obtain data for the relationship between the maximum ED and MD values (denoted by $ED_{MAX}$ and $MD_{MAX}$ respectively) observed at accelerated test conditions and the respective ED and MD failure thresholds (denoted by $ED_{FT}$ and $MD_{FT}$ respectively). It is observed that the values of ED and MD at LED failure, i.e., $ED_{FT}$ and $MD_{FT}$, are dependent on the elevated applied voltage level, respectively on the associated maximum value of ED and MD at that voltage level (i.e., $ED_{MAX}$ and $MD_{MAX}$). To capture the existing relationships between the maximum values of ED and MD, and the related ED and MD failure threshold, power law approximations from the available datasets are derived as follows:

$$ED_{FT} = 1.0912 \ \times ED_{MAX}{}^{0.8086} \tag{7.1}$$

$$MD_{FT} = 2.3105 \times MD_{MAX}{}^{0.6746} \tag{7.2}$$

#### 7.2.1.4 Real-Time Sequential Estimation of RUL

Since the data is collected periodically, RUL is estimated sequentially by estimating the mean trend of the ED and MD curves over time period when they exhibit decreasing trend and are over the respective early warning threshold. If $ED_t$ and $MD_t$ denote the ED and MD values obtained at the discrete time step $t$, then mean trend $m^{ED}{}_t$ of ED is calculated sequentially using the following equation:

$$m^{ED}{}_t = \frac{t-1}{t} m^{ED}{}_{t-1} + \frac{1}{t}(ED_t - ED_{t-1}) \tag{7.3}$$

where $m^{ED}{}_t$ is the mean trend at a given time step $t$ and the time step $t = 0, 1, 2, \ldots, n$ starting with $t = 0$ at the time when $ED_{MAX}$ and $MD_{MAX}$ are detected. In this study, the time steps are defined over intervals of one minute, i.e., the mean trend for ED and MD is calculated every minute following the observation of a decreasing trend of the ED and MD curves when ED and MD are above their respective threshold values.

Similarly, mean trend in the case of MD distance measure is defined as follows:

$$m^{MD}{}_t = \frac{t-1}{t} m^{MD}{}_{t-1} + \frac{1}{t}(MD_t - MD_{t-1}) \tag{7.4}$$

Once the mean trends above are available, they can be used to predict the future time point when the trends of the ED and MD intercept the respective failure threshold. This extrapolation of the trend provides a prediction for the remaining useful life. Using the approximations for computing the failure threshold (equations 7.1 and 7.2), and using sequential mean estimation for the ED and MD trends (equations 7.3 and 7.4), the RUL can be estimated from the following equations:

$$RUL_{ED} = \frac{ED_t - 1.0912 \times ED_{MAX}{}^{0.8086}}{m^{ED}{}_t} \tag{7.5}$$

$$RUL_{MD} = \frac{MD_t - 2.3105 \times MD_{MAX}^{0.6746}}{m^{MD}_t} \qquad (7.6)$$

### 7.2.1.5 Validation of Diagnostics Capability

This subsection details the validation of the diagnostics capability of the developed data driven PHM approach based on the distance measure techniques. As a first example, an accelerated voltage test data set (voltage increased in steps) is used for the demonstration here. Sensor data shown in Figure 7.6 is collected from the ALT and used to demonstrate both distance measure techniques in terms of their diagnostics capability. This data is collected from an accelerated voltage test, where the applied voltage is increased from the normal value and above the normal operating value over time. The LED used for this test is a Philipis Luxeon star, but from a different batch than that the batch of ten used to derive the EWT and FT. In this accelerated test the applied voltage is increased every 30 minutes by 0.2 V, i.e., we validate the PHM against a different voltage profile from the one used for establishing the threshold values in the two methods, i.e., EWT ($ED_{EWT}$ and $MD_{EWT}$) and FT (($ED_{FT}$ and $MD_{FT}$). In this test we can observe the light output has degraded by 30% after 485 minutes. We can also observe when the light begins to degrade which is after 145 minutes approximately. Note that the light sensor data here is used as benchmark against which the prediction from the methods will be judged.

Figure 7.7 demonstrates the ED technique for the data shown in Figure 7.6. It shows that using the defined EWT for ED ($ED_{EWT}$), an early warning for having a LED operating at conditions that lead to failure is given. ED is gradually increasing after it maximum healthy value of 1.1 (see Table 7.1 in page 155) as the applied voltage is increased gradually. In this case, the ED reaches the value of 2.5 which predicts the start of degradation in the light output. This is at time approximately 145 min. It takes another 340 minutes to degrade completely, i.e., to reach the light sensor reading of 0.826 Volts (i.e., 30% drop from the normal value of 1.18 V).

MD analysis of the test data shown in Figure 7.6, for the validation of the diagnostics capability of the MD method is shown in Figure 7.8. It shows that,
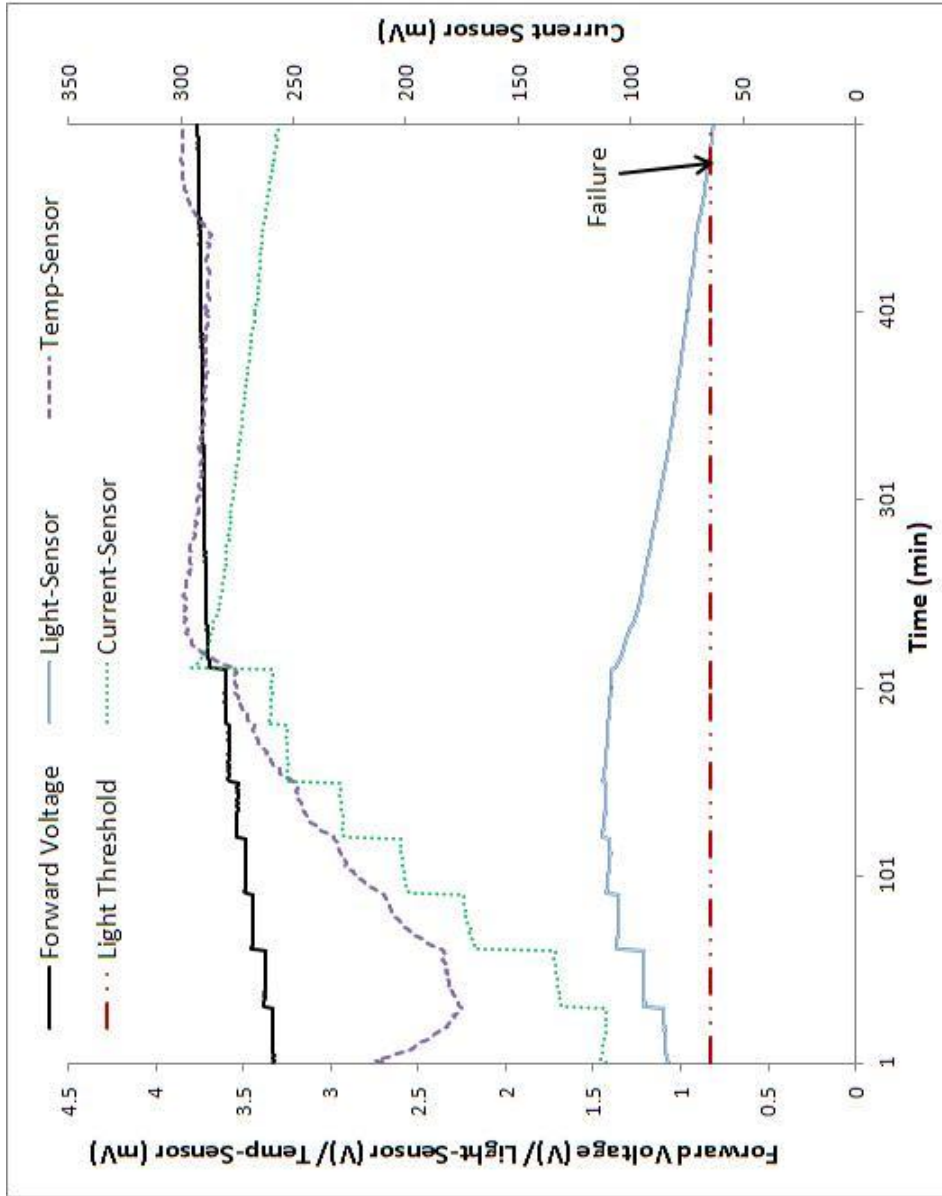
Figure 7.6: Sensor data from accelerated voltage (steps) test for validation
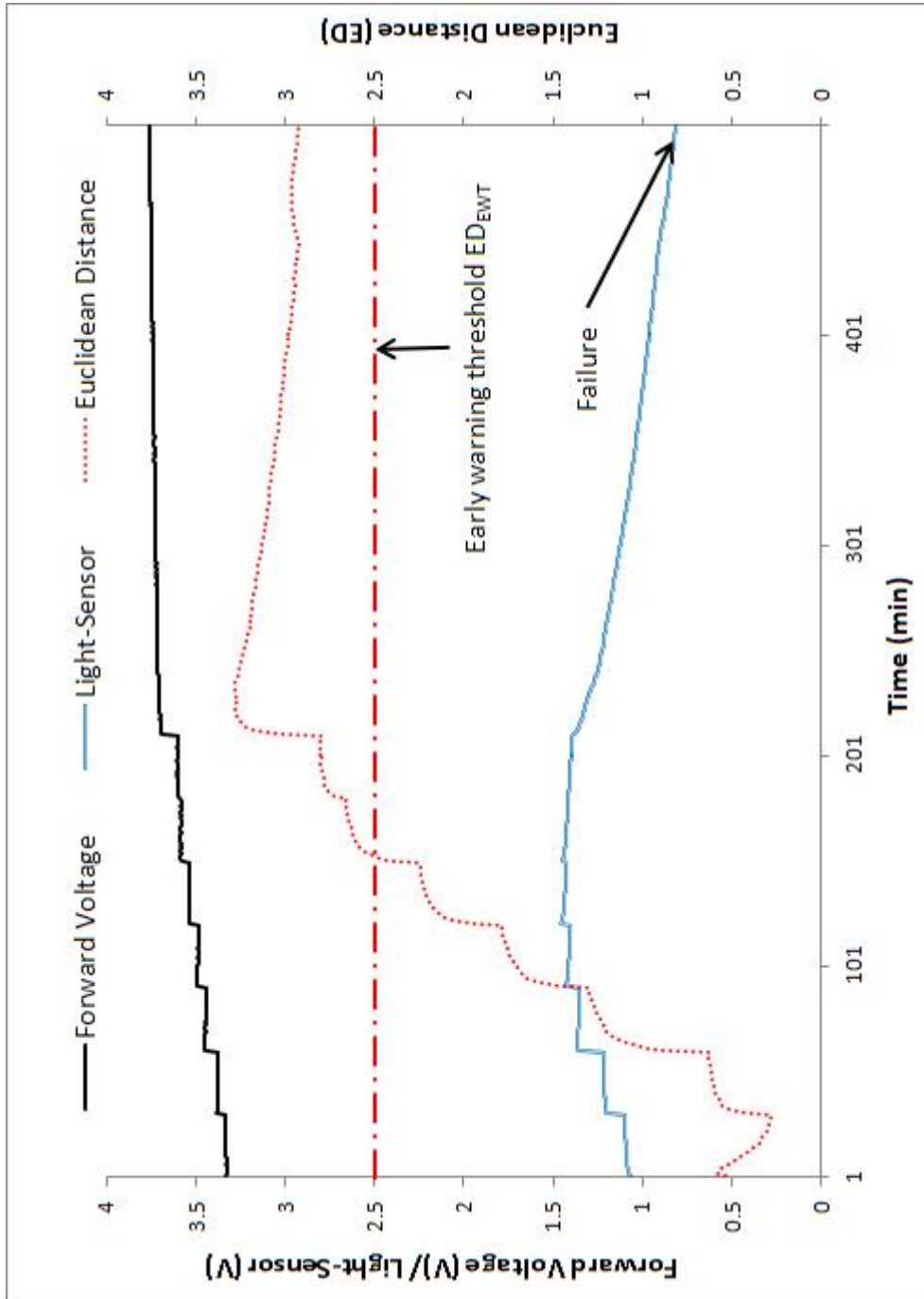
Figure 7.7: Demonstration of Euclidean distance measure technique for the data shown in Figure 7.6

an early warning can be given using established EWT for MD ($MD_{EWT}$). MD increases above the maximum values of 3.55 (see Table 7.1 in page 155) which is observed under normal operating conditions as the applied voltage is increased above the normal limit. In this case the MD reaches its EWT of 17 at 121 min indicates the start of degradation in the light output. It takes another 370 minutes to degrade completely. It is also noted that the MD values are very sensitive to the variations in the current and temperature values. When the voltage is increased to the next step, current reaches an almost stable value but temperature takes time to reach a stable value. This is observed in the variations in the MD values.

At time 443 min there is an increase in ED which corresponds to the temperature increases even though the current continuously decreases. But the MD continuously capture the degradation in the current even though the temperature is increased. Parameters which cause the degradation can be identified by monitoring the individual sensor readings (i.e., current or temperature) and their variation from the typical values. This can be done soon after anomalies detected in the ED and MD values. This information can be used further to analyse and identify the corresponding failure mechanism and the root cause of the degradation. Such study is not undertaken as part of this work as the main focus is on the data driven techniques and their diagnosis/prognostics capability.

Data collected under the constant elevated voltage test is used as the second example to validate approach for the constant voltage accelerated condition. For this case data shown in Figure 7.9 is used. In this case, voltage is kept constant at 3.83 V. Light sensor data starts to degrade from 1.77 V and reaches the failure criteria of 0.826 V after 248 min. Current sensor readings also show gradual reduction as the degradation in the LED continue. Temperature sensor readings start to increase initially and then start to reduces with the current sensor readings.

ED values for the data shown in Figure 7.9 is calculated using the normalised current and temperature sensor values. ED starts to increases suddenly as the higher voltage of 3.83 V is applied from the start. ED reaches its early warning threshold ($ED_{EWT}$) of 2.5 at 3 min after the LED is switched ON and hence the early warning can be provided when there is an abnormality is observed in the
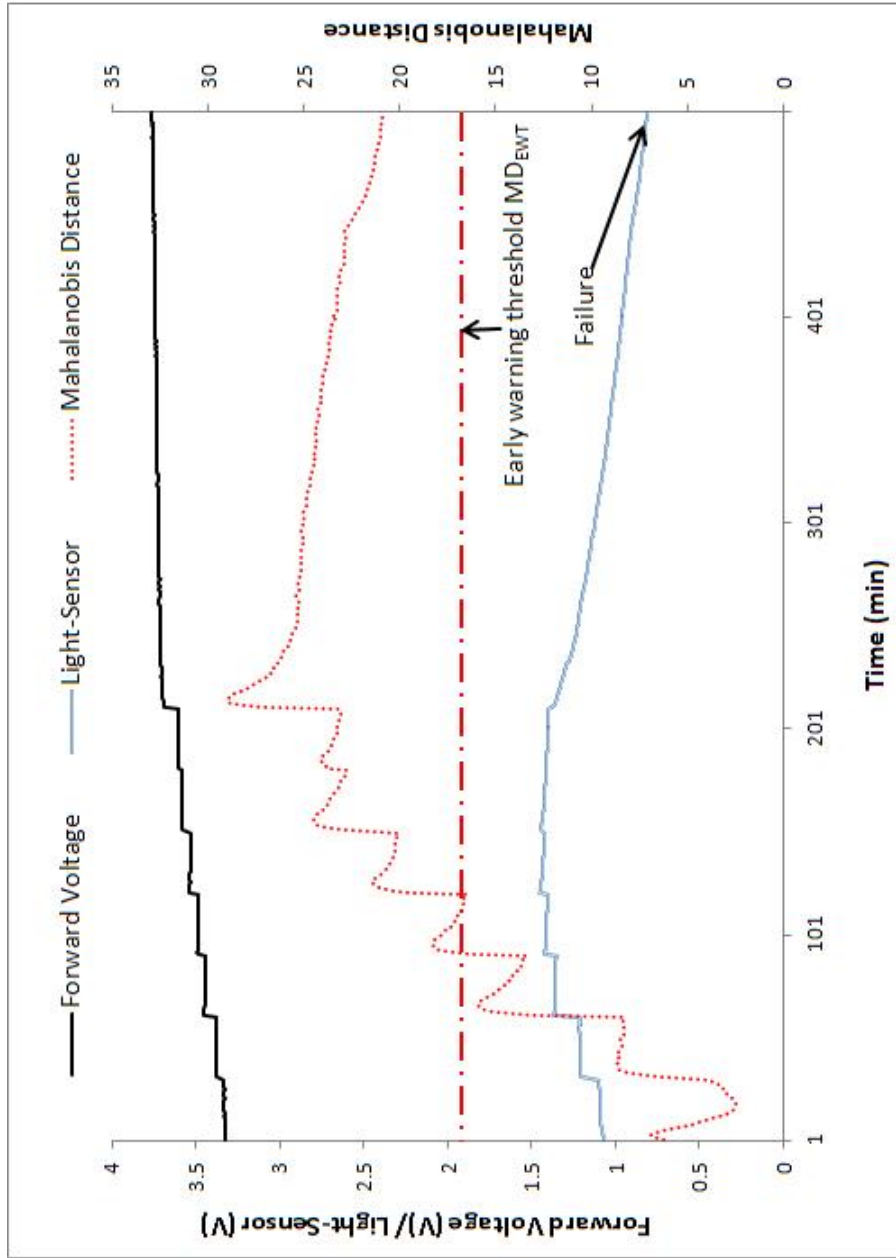
Figure 7.8: Demonstration of Mahalanobis distance measure technique for the data shown in Figure 7.6
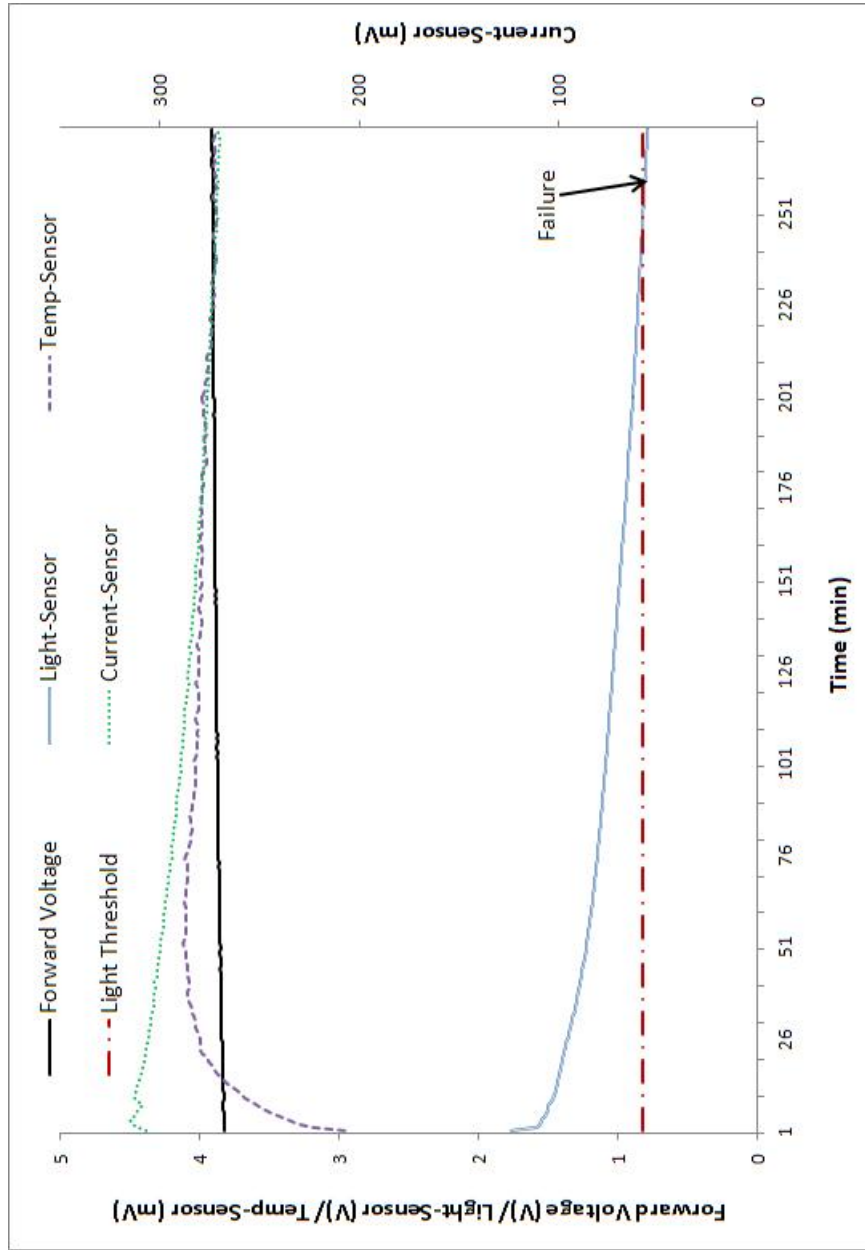
Figure 7.9: Sensor data from accelerated voltage (elevated constant) test for validation

ED values (i.e., after 3 min). ED reaches a maximum value of 3.62 and starts to reduces with the time. At the time of failure ED value reaches to 3.1. This reduction corresponds to the degradation in the light sensor output. Figure 7.10 shows the ED values and early warning threshold for accelerated voltage test data shown in the Figure 7.9.

MD value for test data shown in Figure 7.10 is calculated using the normalised current and sensor data. It shows the MD value goes above the early warning threshold ($MD_{EWT}$) of 17 soon after the LED is switched ON to the elevated voltage of 3.83 V. Therefore the early warning can be provided soon after the LED is switched ON. It also shows the MD value reaches a maximum values of 36 and reduces gradually to 23.2 when the LED fails. Figure 7.11 shows the MD values and early warning threshold for accelerated voltage test data shown in Figure 7.9.

### 7.2.1.6 Validation of Prognostics Capability

To demonstrate the predictions for RUL of an LED, the LED test data used for validation of diagnostics capability (see Figure 7.6) is used here as a first example. This data is collected from accelerated voltage test based on voltage increased in steps. Figures 7.7 and 7.8 illustrate how the ED and MD parameters change with time for the studied LED. In this case the $ED_{MAX}$ and $MD_{MAX}$ values used in the prognostics calculations are 3.28 and 28.81, respectively. The respective failure thresholds are: (i) $ED_{FL} = 2.85$ and (ii) $MD_{FL} = 21.7$. The failure thresholds are obtained from the approximations given in equations 7.1 and 7.2.

Sequential estimation of the mean of gradient of the ED and MD curves are carried out using the equations 7.3 and 7.4. This estimation starts when the ED and MD show a gradual reduction after a maximum values is observed under the voltage conditions is unchanged. These trends associated with ED and MD indicate the trend in the light output. Therefore these trends (i.e., for ED and MD) are used to predict the RUL. For example, RUL from the ED curve is the time taken to reach the failure threshold ($ED_{FL}$) of 2.85 and RUL from the MD curve is the time takes to reach the failure threshold ($MD_{FL}$) of 21.7 for Figures
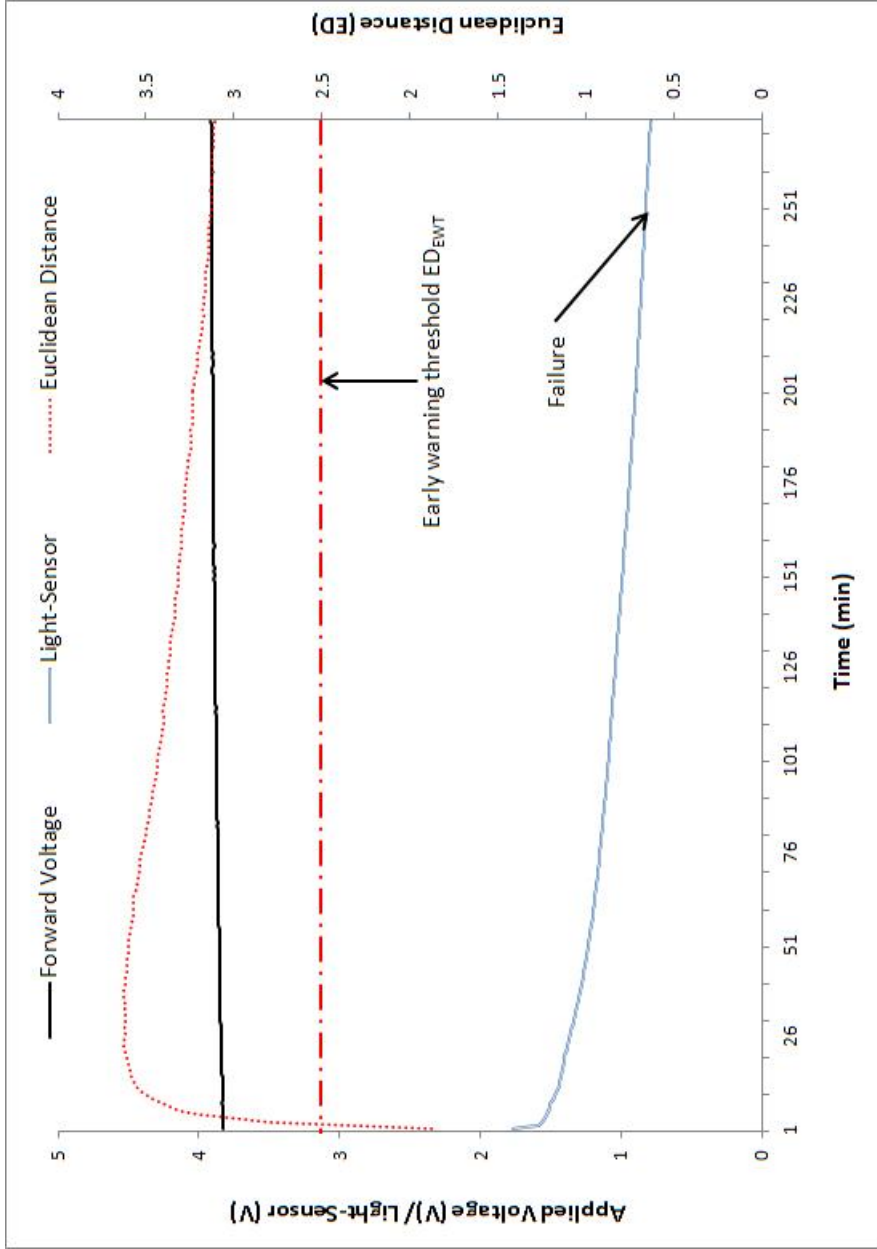
Figure 7.10: Demonstration of the Euclidean distance technique for the data shown in Figure 7.9
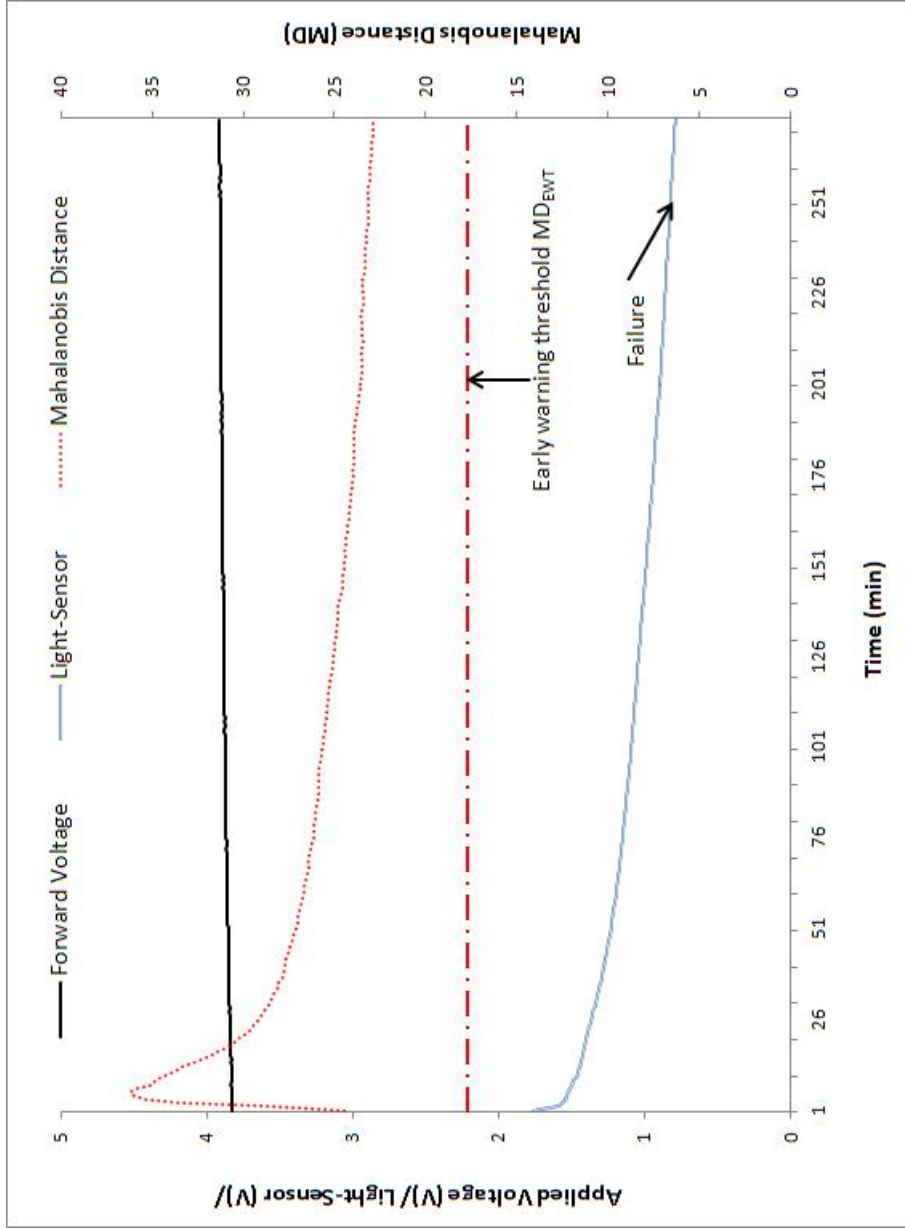
Figure 7.11: Demonstration of the Mahalanobis distance technique for the test data shown in Figure 7.9

| Time at which RUL prediction is made (min) | RUL from ED (min) | RUL from MD (min) | True RUL |
|:---:|:---:|:---:|:---:|
| 300 | 134 | 73 | 181 |
| 350 | 108 | 75 | 131 |
| 400 | 73 | 57 | 81 |
| 450 | 34 | 25 | 31 |

Table 7.3: RUL estimation from distance measures for voltage test (steps)

7.7 and Figure 7.8, respectively.

Table 7.3 shows a summary of prediction results for RUL at five different time points based on both ED and MD curves and using equations 7.5 and 7.6. For example, the predictions for RUL of the LED made at time 400 min estimate 73 min (Total lifetime = 473 minutes) and 57 min (Total lifetime = 457) from ED and MD data, respectively. The actual total lifetime for this LED is 481 min (i.e., true RUL at 400 min is 181 min). It is evident from Table 7.3 that with time the predictions become more accurate as more data is used in the calculation of the mean trends of ED and MD. In this case the results using ED data curve provide better predictions with time. On the other hand, the predictions based on the MD produce some fluctuation because MD is very sensitive to the correlation between the current and temperature data used to calculate the MD.

To demonstrate the predictions for data collected from the accelerated constant voltage test, an LED was subjected to this test. Drive voltage and sensor data shown in Figure 7.9 is used as the second example. Figures 7.10 and 7.11 detail the change with time of ED and MD values for the tested LED. In this case the $ED_{MAX}$ and $MD_{MAX}$ values used in the predictions are 3.63 and 36.1 respectively. The respective failure thresholds are: (i) $ED_{FL} = 3.10$ and (ii) $MD_{FL} = 25.5$. The failure thresholds are obtained from the approximations given in equations 7.1 and 7.2.

Sequential estimation of the mean of gradient of the ED and MD curves are carried out when the ED and MD show a gradual reduction after a maximum values is observed under the voltage conditions is unchanged. These trends associated with ED and MD indicate the trend in the light output. Therefore these trends (i.e., for ED and MD) are used to predict the RUL. For example, RUL

| Time at which RUL prediction is made (min) | RUL from ED (min) | RUL from MD (min) | True RUL |
|---|---|---|---|
| 50 | 260 | 39 | 196 |
| 100 | 109 | 19 | 146 |
| 150 | 82 | Failed | 96 |
| 200 | 51 | Failed | 46 |

Table 7.4: RUL estimation from distance measures for elevated constant voltage test

from the ED curve is the time takes to reach the failure threshold ($ED_{FL}$) of 3.10 and RUL from the MD curve is the time takes to reach the failure threshold ($MD_{FL}$) of 25.5 for Figures 7.10 and 7.11, respectively. The observed maximum values for ED and MD ($ED_{MAX}$ and $MD_{MAX}$) are different for the test data shown in Figure 7.6 and Figure 7.9, hence the failure threshold values ($ED_{FL}$ and $MD_{FL}$) for ED and MD are also different.

Summary of the prognostics predictions is shown in the Table 7.4 for RUL at four different time points. This is based on both ED and MD curves and using equations 7.5 and 7.6. The actual lifetime of this LED is 246 min. It is again showed from Table 7.4 that with time the ED predictions become more accurate as more data is used in the calculation of the mean trends of ED. But in the case of the MD, predictions are not much accurate as MD is sensitive to the correlation between the current and temperature sensor data in this case. Hence the results using ED data curve provide better predictions with time.

## 7.2.2 Logistic Regression Approach

Logistic regression approach is reported in chapter 5. Sensor data from the current and temperature are used for the logistic regression approach, hence three regression coefficients associated with the bias (constant), current and temperature have to be established. After these coefficient are estimated from a training data set, logistics regression can be used to predict the probability of an event. In this case, logistic regression is used to predict the probability for the event that the LED is healthy. Figure 7.12 shows both logistic regression and neural network approach for the real-time health monitoring of LEDs.
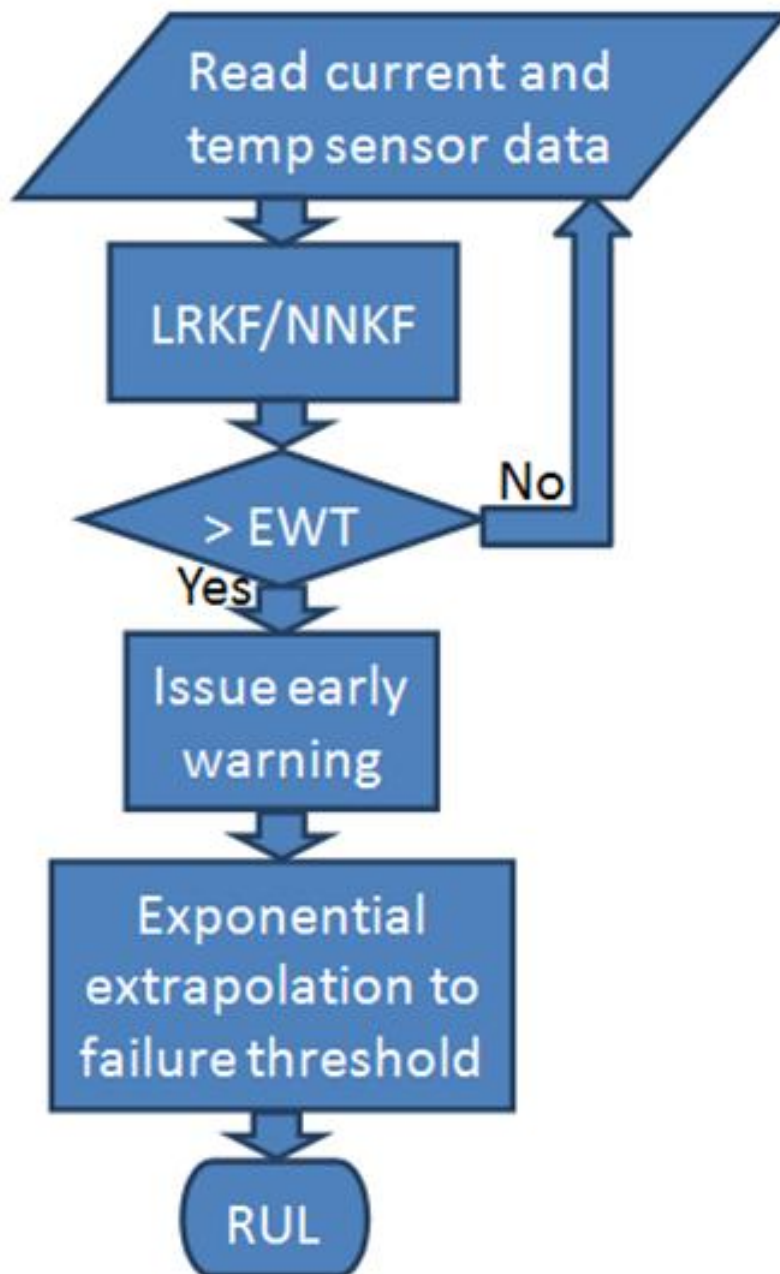
Figure 7.12: Logistic regression and neural network approaches for real-time health monitoring of LEDs

| Regression Coefficient | $\beta_0$ | $\beta_1$ | $\beta_2$ |
|:---:|:---:|:---:|:---:|
| Values | 33.6788 | 181.6766 | -21.4621 |

Table 7.5: Estimated logistic regression coefficients

### 7.2.2.1 Regression Coefficients ($\beta_0$, $\beta_1$ and $\beta_2$)

Logistic regression technique is trained using 918 data sets from the normal operating condition test and accelerated voltage test. Normal operating data sets are used to train the healthy status (1) and data sets from the failed LED (accelerated voltage test) are used to train the failed status (0). From these training data set the regression coefficients $\beta_0$, $\beta_1$ and $\beta_2$ of the logistic regression can be determined. In this case, the healthy light output data is classified and formatted as 0.99 and the failed light output data is classified and formatted as 0.01. Input data set (current and temperature sensor data for four LEDs) and corresponding target data (formatted LED status, i.e., 0.99 or 0.01) are solved for the regression coefficients using the equation 5.13. Table 7.5 shows the estimated regression coefficients for the logistic regression technique based on a regression model that takes current and temperature sensor data. Logistic regression model that takes the current and temperature sensor data as the input and provides the probability of an LED is to be healthy is shown by the following equation:

$$P\left(healthy\right) = \frac{1}{1 + \exp(-(33.6788 + 181.6766I - 21.4621T))} \quad (7.7)$$

where $I$ and $T$ are current and temperature sensor data. Probability of an LED is to be healthy, is estimated when new sets of data from the current and temperature sensors are available.

### 7.2.2.2 Real-Time Sequential Estimation of RUL

We developed a real-time sequential RUL estimation approach based on the observed exponential decay phenomenon. Although the LRKF provides probability of the healthy status of the LED, experimental result based on 10 LEDs shows that the LED fails when the LED's healthy status probability reaches 0.15 on average. This finding is used to estimate the remaining useful lifetime of the

177

LED under the accelerated voltage condition. Exponential decay can be fitted with the following equation:

$$R_0 = R_t e^{-At} \tag{7.8}$$

where the $R_0$ is the failure threshold value based on the filtered logistic regression output, $R_t$ is the starting value for the exponential decay, $A$ is the decay positive constant and $t$ is RUL. In this case we start the prognostics when the filtered logistic regression goes below the decision boundary which is 0.5. $R_0$ is determined from the average value of the failure thresholds for ten different LED tests. $R_0$ is established as 0.15. Hence the equation 7.7 can be modified as follow to estimate the RUL:

$$t = \frac{\ln \frac{R_t}{0.15}}{A_t} \tag{7.9}$$

where $t$ is the RUL, $R_t$ is the output from the logistic regression at the time of estimation (i.e., $t$) and $A_t$ is the mean exponential decay constant at the time step $t$. Exponential decay constant is determined for every time step and mean value of the exponential decay constant is estimated using the following equation:

$$A_t = \frac{t-1}{t} A_{t-1} + \frac{1}{t} \ln \frac{R_{t-1}}{R_t} \tag{7.10}$$

### 7.2.2.3   Validation of Diagnostics Capability

Test data set shown in Figure 7.13 is used to validate the logistic regression technique. This particular LED is failed after 625 minutes in operation. Current and temperature sensor data are fed into the logistic regression model and output is shown in Figure 7.14. Since noisy output is observed from the logistic regression model, we introduce a novel approach by introducing Kalman filter to filter the output data from the logistic regression model. Kalman filter is used to filter the noise and smooth the output of the logistic regression. Filtered output of the logistic regression using the Kalman filter is also shown in Figure 7.14. It is evident from Figure 7.14 that the Kalman filter is filtering the output data from the logistic regression model very effectively and provides a better approximate

curve for the diagnostics and prognostics of the LEDs.

Figure 7.15 shows voltage profile, light output, the filtered output from the logistic regression and the decision boundary. Output from the logistic regression is fed into first order Kalman filter to smooth the output. Filtered output from the logistic regression can be defined as the reliability number or the probability for the healthy LED. For example in Figure 7.15, at the start of the operation the probability is almost 1 (i.e., probability of healthy) and it starts to reduce when the degradation in the light output starts to take place (i.e., after 230 min). Probability reaches almost zero value when the LED completely fails. We also define a decision boundary where healthy probability is 0.5. It can also be used to indicate the probability of failure is 0.5. This decision boundary is used to indicate the probability of failure becomes greater that the probability of healthy. Figure 7.15 also shows that the logistic regression output reduces steeply from 230 minute and it reaches the decision boundary at 340 minute. This is because of the start of the degradation. Degradation in the light output is also observed from 230 minute onwards. After logistic regression reaches the decision boundary, it exhibits exponential decay. This phenomenon can be used to predict the remaining useful lifetime. The key advantage of this approach is that the prediction can be expressed in terms of probability.

### 7.2.2.4 Validation of Prognostics Capability

An accelerated test based on the gradually increased voltage is used as the first example to predict the RUL of the LED. This test case is discussed in Figure 7.3. Figure 7.16 shows the graph of the filtered logistic regression, voltage profile, light sensor output and decision boundary. The filtered output of the logistic regression reaches the decision boundary at 570 min and reaches the failure threshold at 715 min. Actual failure is observed at 725 min based on the light sensor output reading when reaches 0.826 V. Table 7.6 shows the predicted RUL of the LED, actual RUL and time of the prediction. Results show the logistic regression makes consistent prediction with the help of an appropriate filter and accurate threshold value for failure.

Data shown in Figure 7.6 is used as the second example to validate the re-
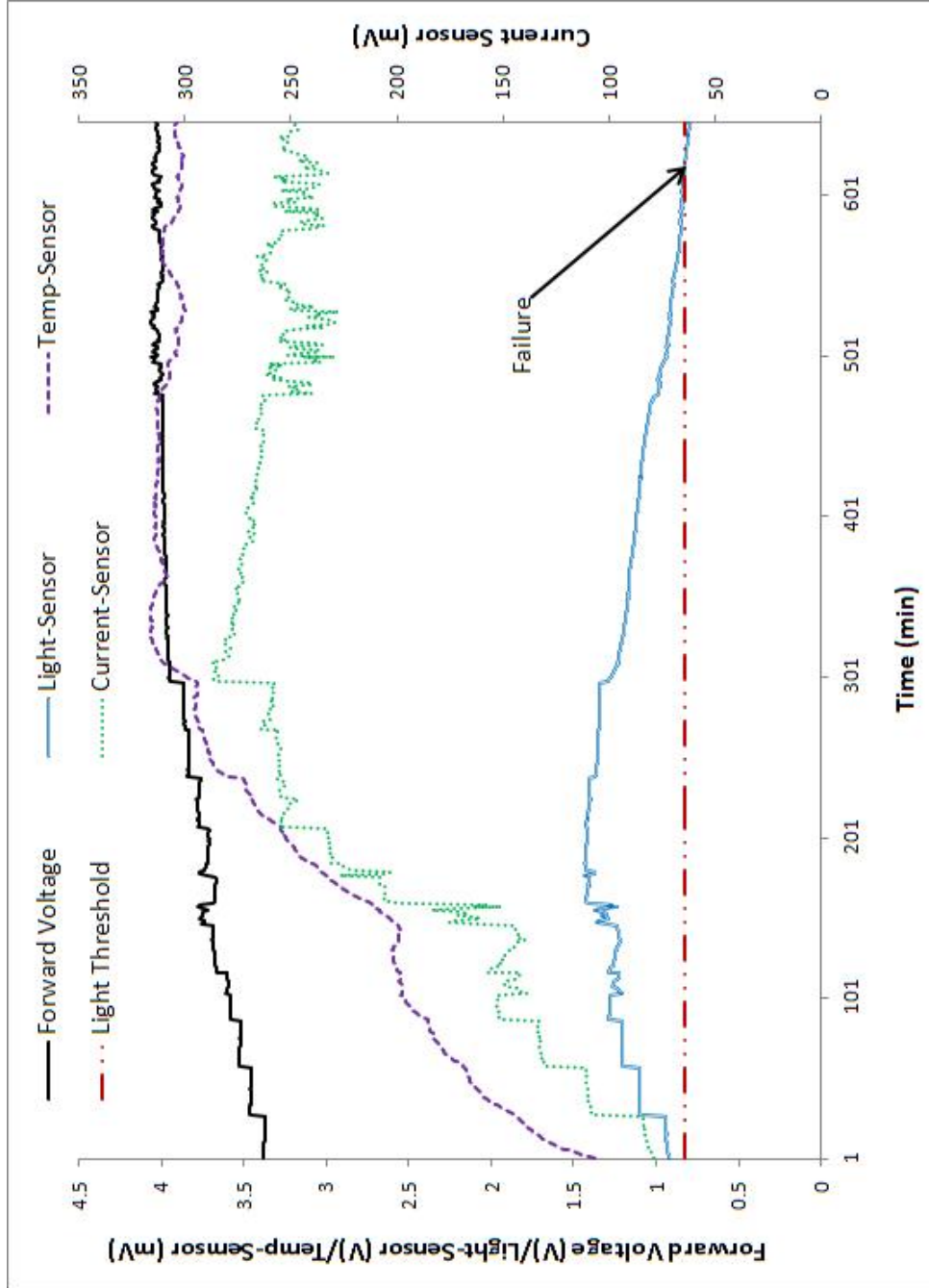
Figure 7.13: Sensor Data from Accelerated Voltage Test (Voltage Increased in Steps)
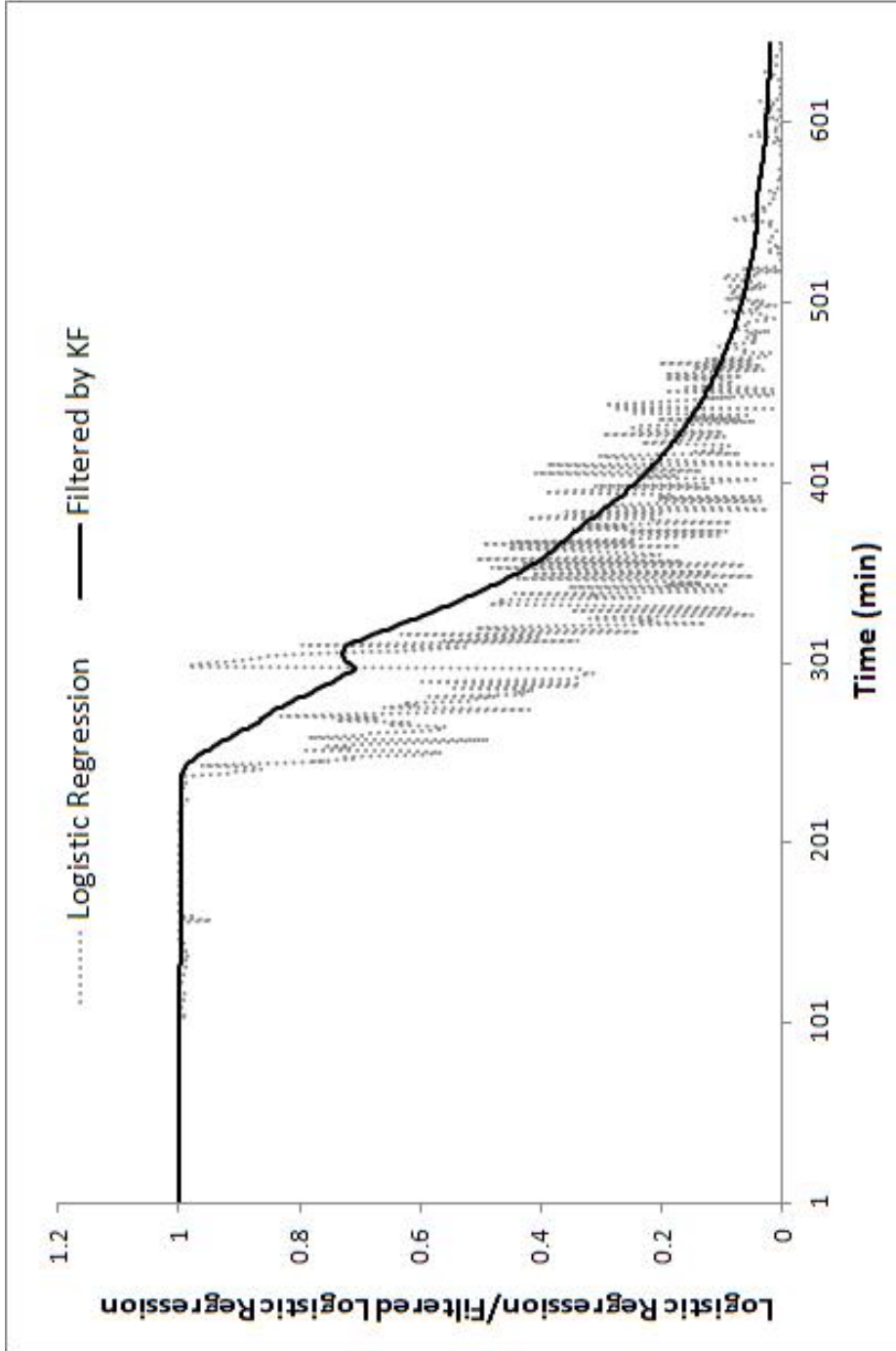
Figure 7.14: Output data from the logistics regression and Kalman filter for the data shown in Figure 7.13
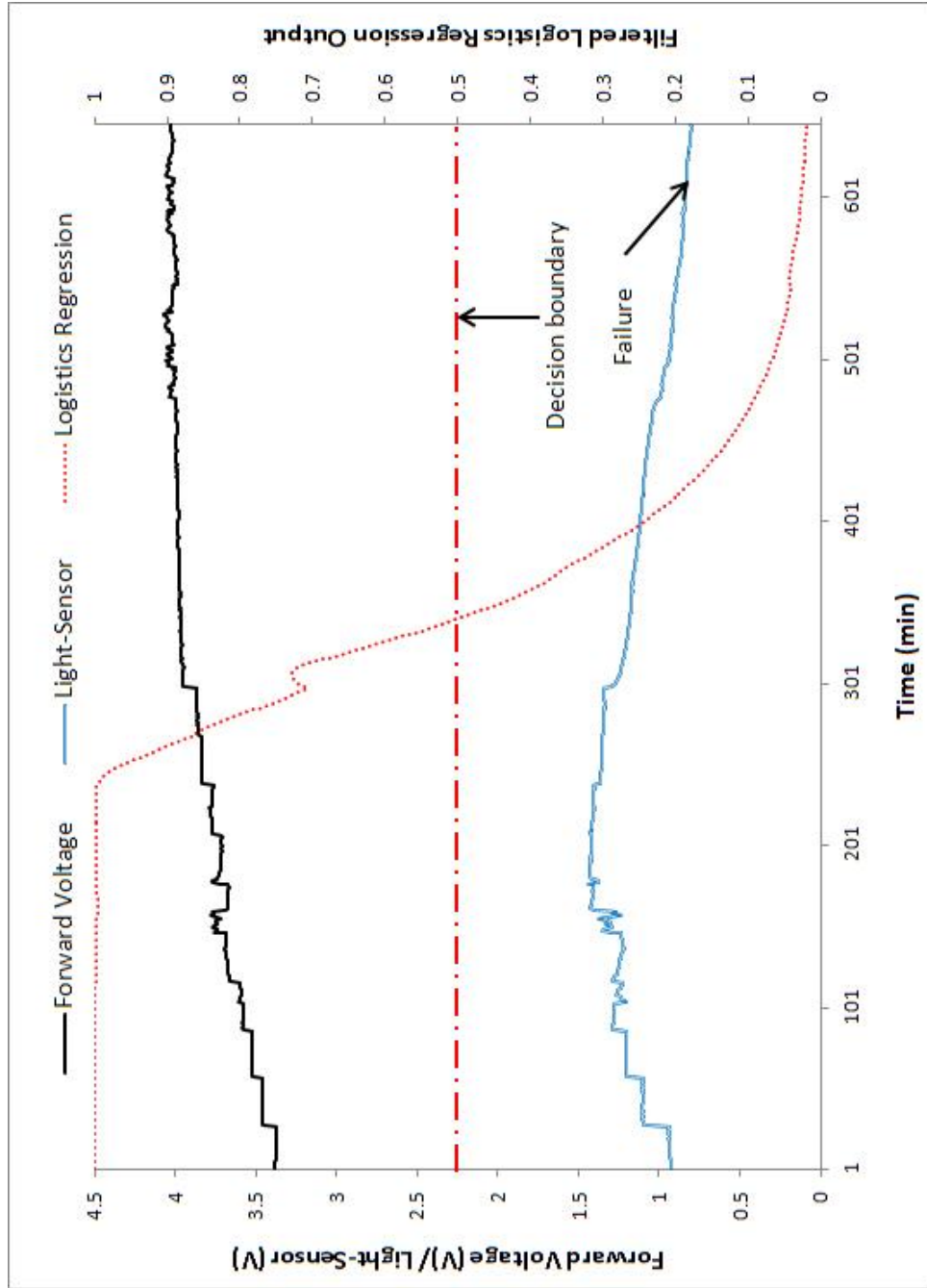
Figure 7.15: Filtered logistic regression curve for the test data shown in Figure 7.13
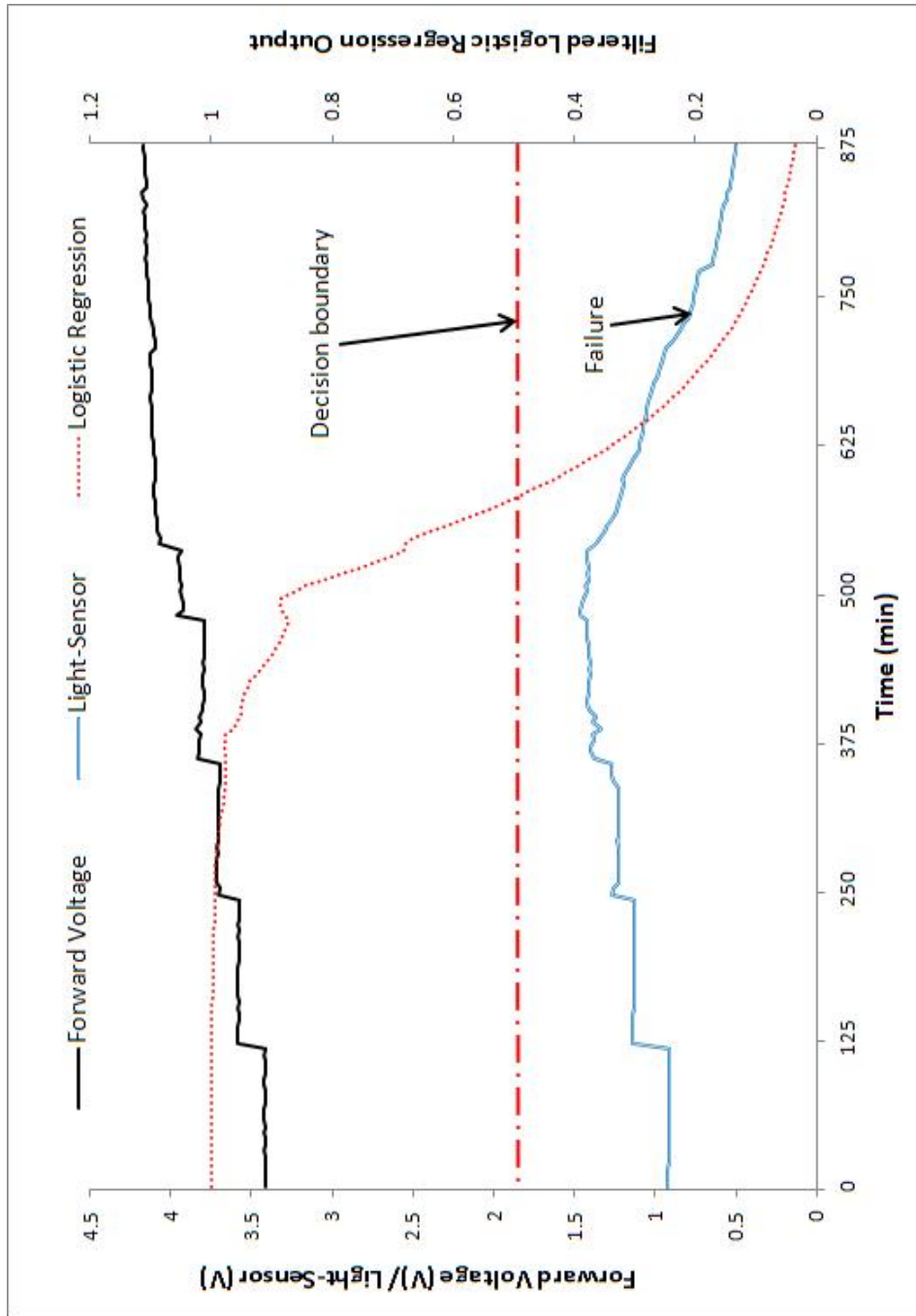
Figure 7.16: Filtered logistic regression curve for the test data shown in Figure 7.3

| Time at which RUL prediction is made (min) | RUL from Logistic Regression (min) | True RUL |
|---|---|---|
| 580 | 135 | 145 |
| 630 | 86 | 95 |
| 680 | 36 | 45 |

Table 7.6: RUL estimation from logistic regression and Kalman filter (LRKF) approach for the data shown in Figure 7.3

| Time at which RUL prediction is made (min) | RUL from Logistic Regression (min) | True RUL |
|---|---|---|
| 460 | 21 | 21 |
| 470 | 11 | 11 |
| 480 | 3 | 1 |

Table 7.7: RUL estimation from logistic regression and Kalman filter (LRKF) approach for the data shown in Figure 7.6

sults of the developed logistic regression and Kalman filter (LRKF) approach for the LED's health monitoring. Purpose of this demonstration is to compare the result with other techniques such as distance measures and neural network. This particular result shows that, although the degradation in the light output is not properly identified, failure can be predicted accurately. This approach uses two different techniques (i.e., logistic regression and Kalman filter) and both these techniques need to be trained properly to make more accurate diagnostics to identify the degradation on time. In additions to this we also have limited test data. Figure 7.17 shows the logistic regression graph for the data shown in Figure 7.6. In this case the steep reduction is observed in the later stage. LRKF shows the LED is healthy (with a probability of $\geq 0.9$) until 436 min. LRKF output suddenly drops to decision boundary of 0.5 at 456 min and drops to the failure threshold of 0.15 at 484 min. Actual failure is observed at 481 min. Table 7.6 shows the predicted and actual RUL at three different time interval at the last stage. It is evident from the Table 7.6 logistic regression with the help of an appropriate filter can used to predict the RUL more accurately.
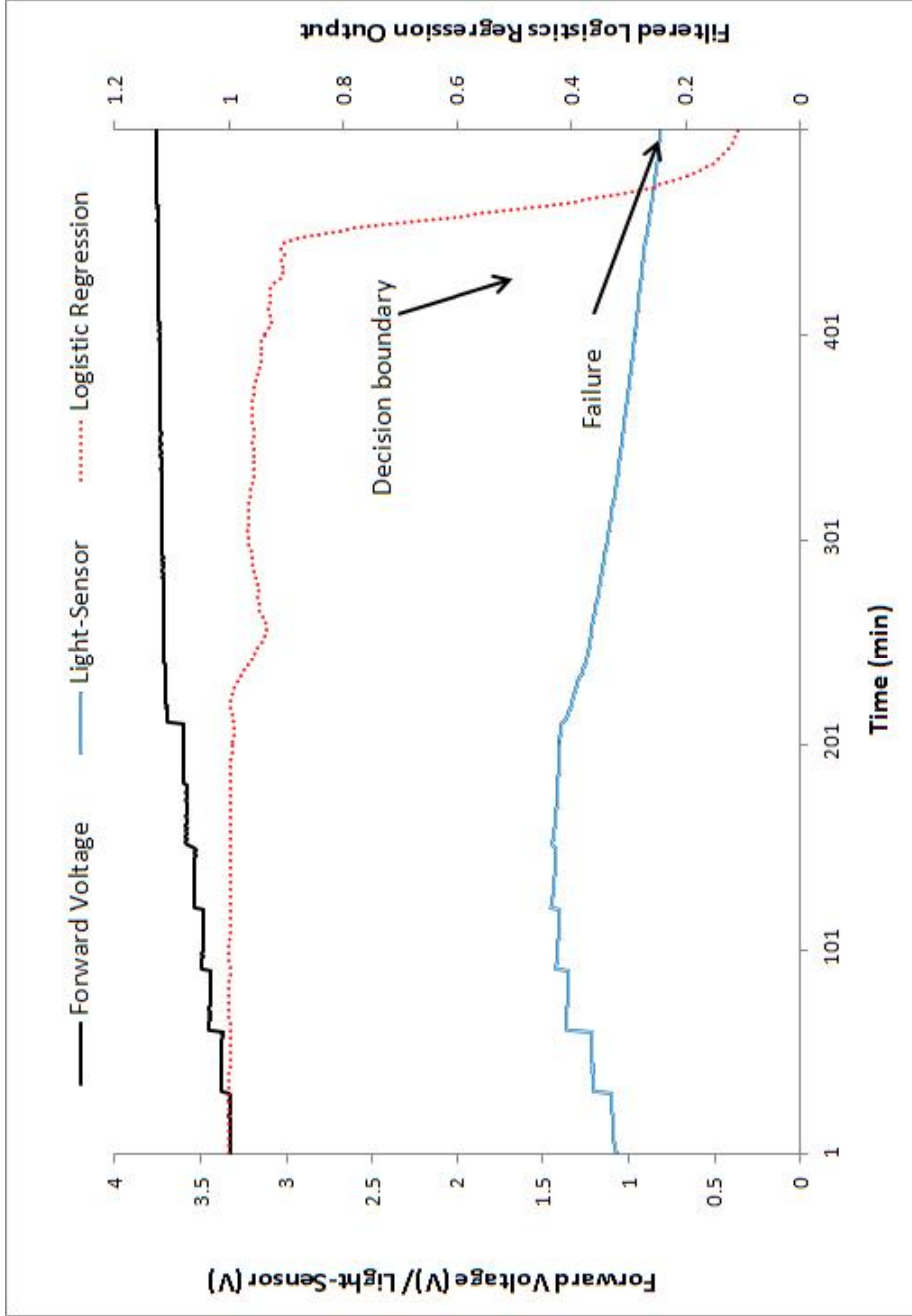
Figure 7.17: Filtered logistic regression curve for the LED test data shown in Figure 7.6

### 7.2.3 Neural Network

A neural network based approach is developed for the prognostics and health monitoring of LEDs and results are discussed here. A simple neural network with one hidden layer and two hidden neuron is developed and discussed in chapter 5. Figure 5.5 shows the developed neural network configuration for the prognostics and health monitoring of LEDs. Sensor data from the current and temperature are used as the input for the neural network approach. Hidden layer consists of two neurons and therefore 4 weight parameters and two biases need to be established. Output layer consists of one neuron and therefore two weight parameters and one bias need to be established. After these parameters are estimated from a training data set, neural network can be used to predict the probability of an event like logistic regression. In this case, neural network is used to predict the probability for the LED healthy status.

#### 7.2.3.1 Network Parameters

Data set used for the logistic regression is used to train the neural network in the Matlab environment. Built in neural network toolbox is used to develop and train the neural network in the Matlab environment. Figure 7.18 shows the neural network design in the Matlab environment using the built in neural network toolbox. In this case linear function is selected as the activation function of the hidden layer and sigmoid (logistic) function is selected as the activation function of the output layer. Number 2 in the input block indicates this neural network has two input parameter (i.e., current sensor and temperature sensor). Number 2 in the hidden layer indicates the hidden layer has two neurons. Each neuron in the hidden layer has a bias (which is a constant), weight parameters for the current sensor and the temperature sensor. Output from these two hidden neurons then fed into the neuron in the output layer, which also has its own weight parameters for the input and a bias.

After the neural network is trained in the Matlab environment, following weight parameters and bias parameters for the two neurons in the hidden layer and one neuron in the output layer are established (see Figure 5.5 in page 135) :
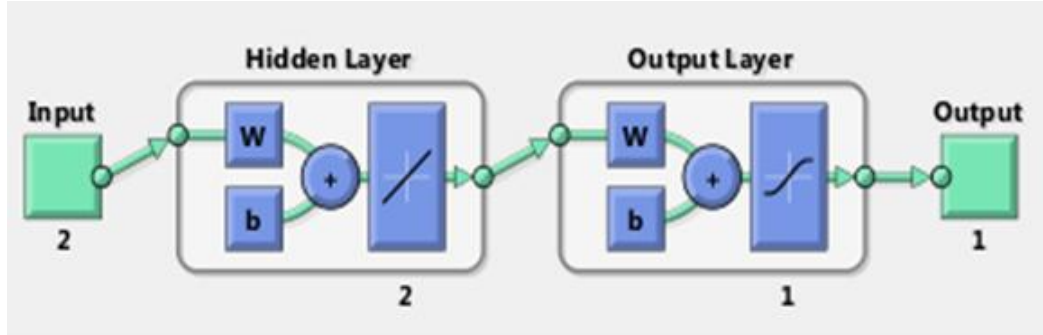
Figure 7.18: Neural network design in the Matlab environment

1. Weight matrix for the hidden layer is:

$$
\begin{bmatrix} w_{1,1} & w_{2,1} \\ w_{1,2} & w_{2,2} \end{bmatrix} = \begin{bmatrix} -2.2104 & 3.123 \\ 1.0512 & -5.7427 \end{bmatrix} \tag{7.11}
$$

2. Weight matrix for the output layer is:

$$
\begin{bmatrix} m_1 \\ m_2 \end{bmatrix} = \begin{bmatrix} -0.84 \\ 5.9476 \end{bmatrix} \tag{7.12}
$$

3. Bias matrix for the hidden layer is:

$$
\begin{bmatrix} b_1 & b_2 \end{bmatrix} = \begin{bmatrix} -0.25563 & 0.85434 \end{bmatrix} \tag{7.13}
$$

4. Bias to the output layer:

$$
\begin{bmatrix} b_3 \end{bmatrix} = \begin{bmatrix} 0.44004 \end{bmatrix} \tag{7.14}
$$

Data set used to train the logistic regression technique is used to train the neural network. This data set consists of 918 sample data. Input data has two columns for current and temperature sensor data (i.e., input data $918 \times 2$ matrix). Target data which indicates the healthy status of the LED, is formulated as healthy 0.99 and not healthy $= 0.01$ (i.e., target data is a column vector). These two data uploaded into the Matlab environment and neural network is trained using

neural network toolbox. Input and target data then divided into three groups using a random selection process which is a built in process in the neural network toolbox. 70% of the data is assigned as the training data set, 15% of the data is assigned for test and another 15% is assigned for the validation. Training data set is only used to established the network parameters such as the weights and biases. Test and validation data set are used to evaluate the performance of the network using the parameters which established from the training.

Mean squared error (MSE) is calculated for every iteration based on the calculated weights and biases. Forward and back propagation algorithms are used in the neural network toolbox to estimate the weights and biases such that MSE is minimised for a set of weights and biases. For every iteration weights and biases are adjusted. Figure 7.19 shows the performance measure of the neural network for every iteration (or epoch) based on the mean squared error. Figure 7.19 shows that the mean squared error is minimised to $6.0737 \times 10^{-7}$ for the set of weights and biases reported in the equations 7.11 to 7.14.
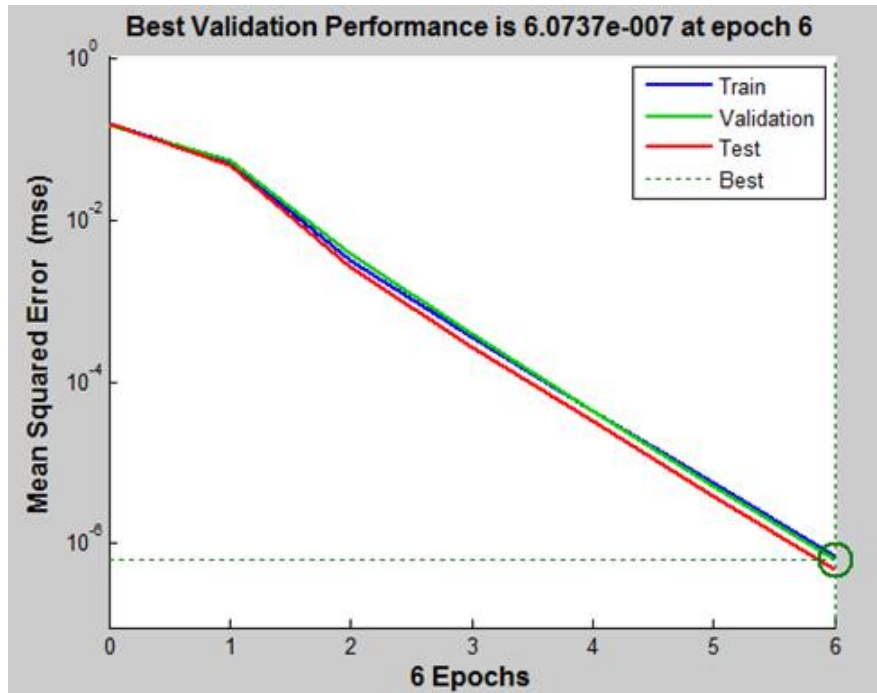


Figure 7.19: Performance of the neural network for every iteration or epoch

### 7.2.3.2 Real-Time Sequential Estimation of RUL

Similar to the LRKF approach, we developed a real-time sequential RUL estimation approach based on the observed exponential decay phenomenon. Although the NNKF provides probability of the healthy status of the LED, experimental result based on 10 LEDs shows that the LEDs fail when the LED healthy status probability reaches 0.03 on average. This finding is used to estimate the remaining useful lifetime of the LED under the accelerated voltage condition. Equations from 7.8 to 7.10 are used here to estimate RUL in real-time.

### 7.2.3.3 Validation of Diagnostics Capability

Figure 7.20 shows the neural network output for the LED test data shown in Figure 7.13. Neural network output is also filtered by the Kalman filter to get a smooth output like in the case of logistic regression technique. This particular neural network performs like the logistic regression technique discussed in the above section since the logistic regression is acting like a single neuron with an activation function of sigmoid (logistic) function. In the case of neural network, layers and neurons in a single layer can be increased to get a better performance. Activation function can also be selected such that the neural network gives better performance for the training data. This particular neural network has one hidden layer and hidden layer have two neurons with linear activation function. Activation function of the output layer is selected as the sigmoid function.

Similar to the logistics regression, the neural network output shows an exponential decay and this phenomenon can be used to estimate the remaining useful lifetime in real-time. Light output degradation can be diagnosed using neural network output. In Figure 7.20 the degradation starts to take place after 230 min and reaches the decision boundary of 0.5 at 317 min from the start of operation under the accelerated voltage condition.

Validation of Prognostics Capability Sequential estimation technique which is used for the logistics regression approach is used here to estimate the RUL based on filtered neural network output. When the neural network output goes below the decision boundary of 0.5, RUL estimation is carried out based on the estimated positive decay constant (equation 7.10).
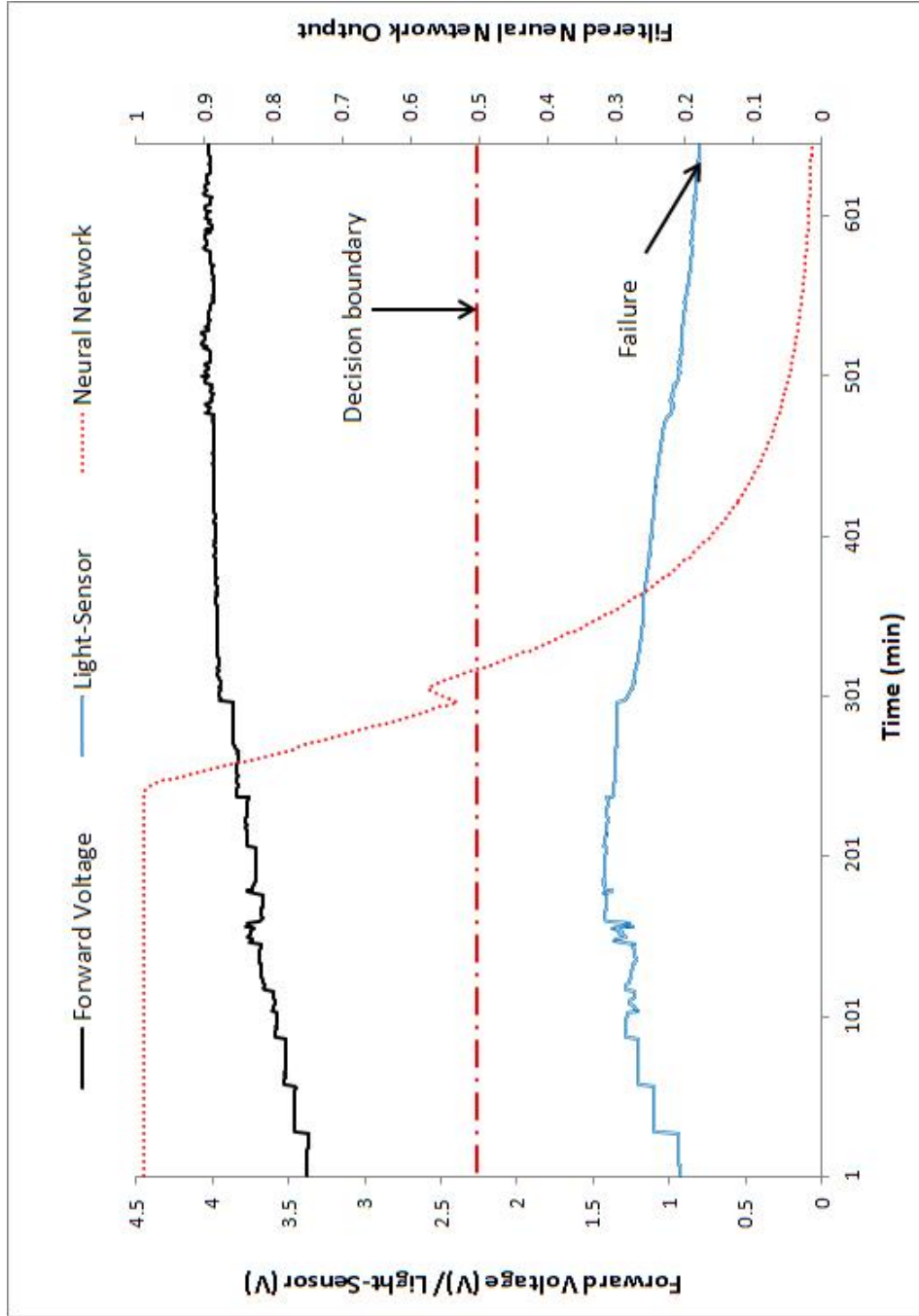
Figure 7.20: Filtered neural network curve for the LED test data shown in Figure 7.13

| Time at which RUL prediction is made (min) | RUL from Neural Network (min) | True RUL |
|:---:|:---:|:---:|
| 580 | 132 | 145 |
| 630 | 79 | 95 |
| 680 | 32 | 45 |

Table 7.8: RUL estimation from neural network and Kalman filter (NNKF) approach for the accelerated test data shown in Figure 7.3

Failure threshold value for the filtered neural network output is 0.03 observed from the ten LEDs tested under the accelerated voltage conditions (steps). Accelerated test data shown in Figure 7.3 is used as the first example to demonstrate the prognostics capability of the developed NNPF approach. Figure 7.21 shows the neural network output values for the test data shown in Figure 7.3. Steep reduction in the neural network output is observed after 485 min which indicates the start of the degradation in the light output.

Predicted RUL and true values for the RUL at three different time interval is tabulated in the Table 7.8. Result shows that the NNPF approach provides reasonable predictions for this particular test data based on the trained network parameters and Kalman filter settings.

Accelerated test data shown in Figure 7.5 is used as the second example to demonstrate and compare the results with other developed data driven approaches. Figure 7.22 shows the filtered neural network output for the data shown in Figure 7.5. Output graph shows similar performance to the logistic regression because similar settings are used to the Kalman filter. NNKF approach shows that the LED is healthy until 438 min (i.e., healthy probability is $\geq 0.9$) and drops to decision boundary which has the probability of 0.5 at 455 min. Healthy probability for LED failure criteria based on NNPF approach is 0.03 and output of NNPF approach drops to 0.03 at 478 min. Actual failure is observed based on the light output which drops to 0.826 V at 481 min.

RUL predictions are made at three different time intervals similar to other data driven approach developed in this work, and reported in the Table 7.9. It is evident from the Table 7.8 and Table 7.9 neural network can be used to estimate the RUL accurately with the help of an appropriate filter and accurate failure
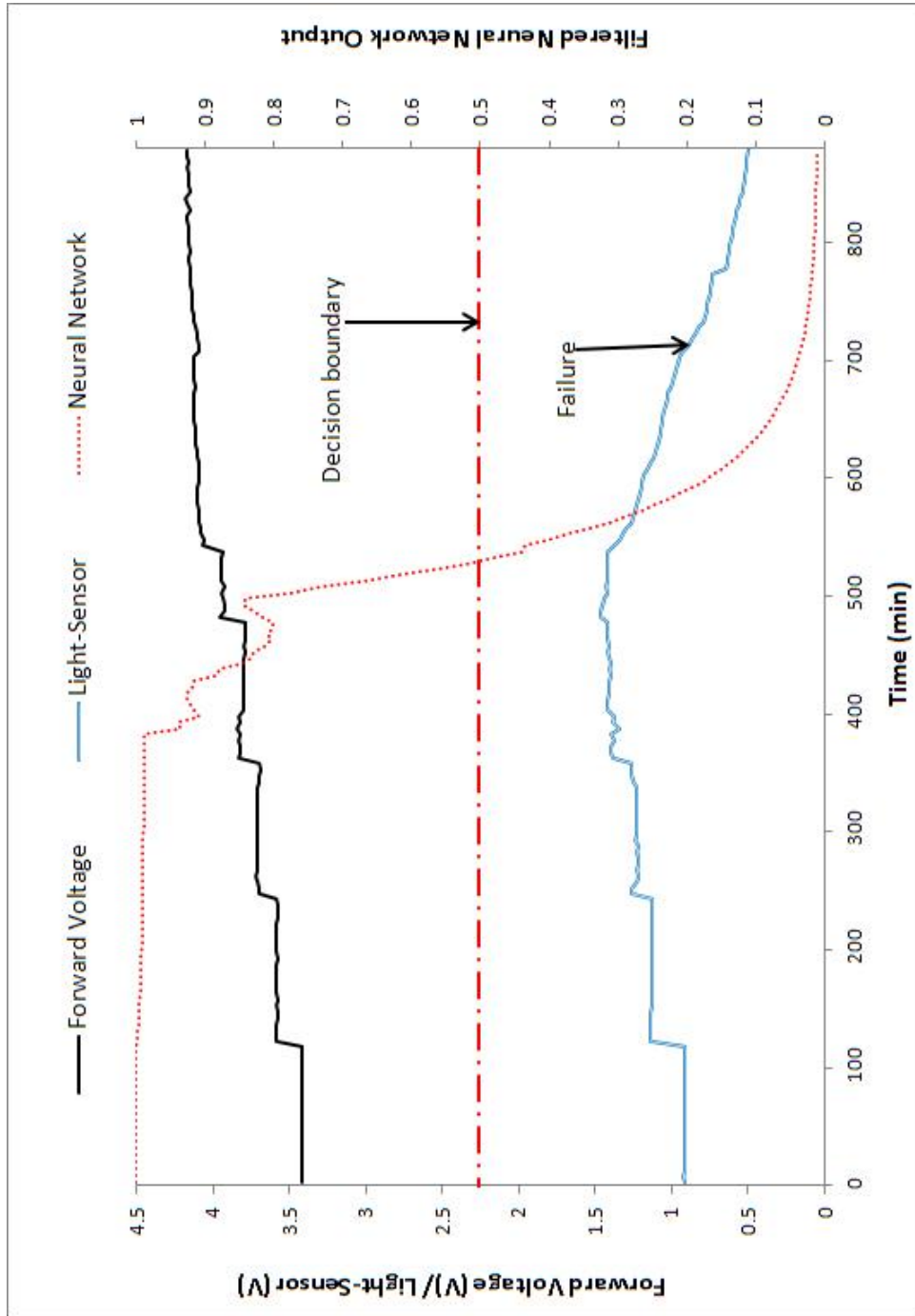
Figure 7.21: Filtered neural network output for the data shown in Figure 7.3
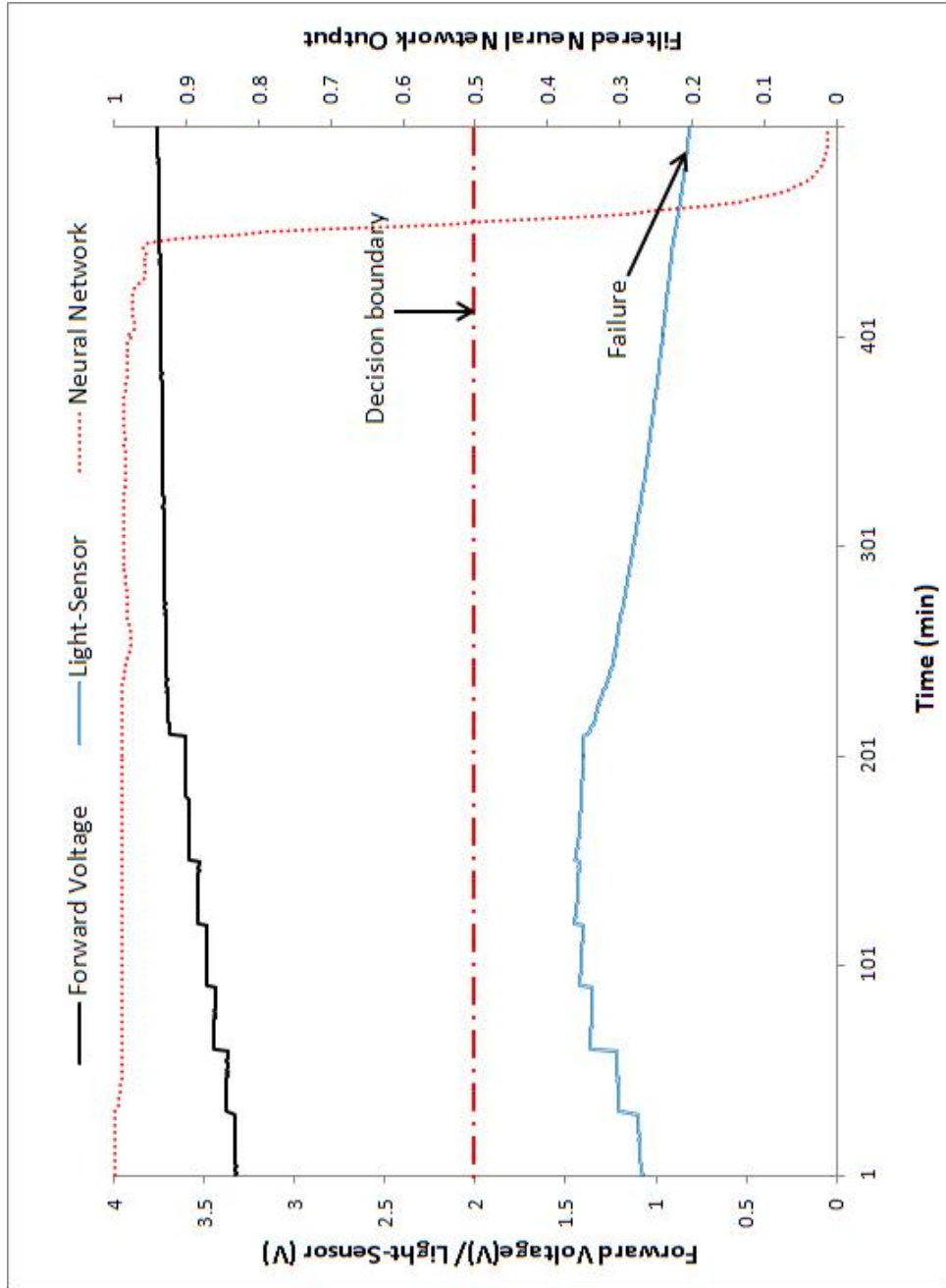
Figure 7.22: Filtered neural network output for the data shown in Figure 7.5

| Time at which RUL prediction is made (min) | RUL from Neural Network (min) | True RUL |
|---|---|---|
| 460 | 18 | 21 |
| 470 | 7.5 | 11 |
| 480 | Failed | 1 |

Table 7.9: RUL estimation from neural network and Kalman filter (NNKF) approach for the accelerated test data shown in Figure 7.5

threshold value. Neural network can also be further improved with the number of neurons in the hidden layer and also with number of layers in the network. Selection of activation function also plays critical role in optimising the neural network for the better performance.

## 7.2.4 Comparison of Data Driven Approach

Overall the data driven approaches developed and discussed above, provide good predictions for the anomaly detection and prognosis for the LEDs under the accelerated test conditions. Distance measure techniques (i.e., ED and MD) monitor the variation of the operating parameters from the typical operating values and use those values for the anomaly detection and failure predictions. MD uses the correlation between the data sets to compute the distance and hence MD shows sensitive variations particularly when there is a change in the operating condition. This behaviour sometime limits the prediction capability of the MD. ED on the other hand shows less variation compare to MD, in particular when the applied condition is changed.

Logistic regression based approach (LRKF) and neural network based approach (NNKF) provide consistent predictions particularly in the last stage of the LED's life. Neural network can be further improved by increasing the number of neurons in the hidden layer and increasing the number of layers between the input and output layers. In addition to this, both LRKF and NNKF can benefit from regularisation. Regularisation is a technique used in machine learning and statistical techniques to prevent the over fitting by introducing additional information into the error function. Further LRKF and NNKF can also be benefited by additional parameters such as applied voltage, power (i.e., $V \times I$) etc.

Hence both LRKF and NNKF are better approaches and they can be used to incorporate other operating or environmental conditions to get an optimised RUL estimations.

One dimensional Kalman filter is used in both approaches to smooth the output of the logistic regression and neural network. This provides benefit in terms of accurate predictions based on observed exponential decay. Statistically established setting for Kalman filter will provide better performance in terms of accuracy in predictions. Because of the time limitation, this work was limited to develop and demonstrate the approaches. Future work will focus on comparing the developed data driven approaches using a statistically accepted method.

## 7.3   Model Driven Approach

An empirical model based on V-I characteritics has been developed and discussed in chapter 5. Figure 5.8 shows the fitted model for the empirical data collected from the LED test under normal operating condition. In other words healthy LED can be defined by the emprical model fitted to the normal operating data. The empirical model can be expressed by the following equation:

$$I_{LED} = 1.84V_{LED} - 5.9432 \tag{7.15}$$

LEDs can be considered as a micro system which takes voltage as input. Current can be computed using the empirical model 7.10. Using the current sensor actual current through the LED can be determined. The difference between the model predictions for current and the actual current gives the residual. Residual can be used to estimate the damage in the LEDs. Based on acclerated voltage tests threshold value for the residual can be determined and used to diagnose and predict the failure in LEDs.

### 7.3.1   Failure Threshold

Failure threshold for the residual is established from ten tested LEDs. These LEDs are tested under accelerated voltage conditions that the voltage is increased

| LED No | Residual (V) at Normal Condition | Residual (V) at Failure | Deviation (V) |
|--------|----------------------------------|-------------------------|---------------|
| 1 | 0.03 | 0.18 | 0.13 |
| 2 | 0.03 | 0.15 | 0.12 |
| 3 | -0.01 | 0.11 | 0.12 |
| 4 | -0.04 | 0.09 | 0.13 |
| 5 | -0.02 | 0.11 | 0.13 |
| 6 | -0.01 | 0.12 | 0.13 |
| 7 | 0.01 | 0.13 | 0.12 |
| 8 | -0.01 | 0.11 | 0.11 |
| 9 | 0.01 | 0.14 | 0.13 |
| 10 | -0.01 | 0.10 | 0.11 |
| Average | -0.002 | 0.124 | 0.126 |

Table 7.10: Residual values under normal operating conditions (initial stage of the ALT) and at failures, and deviation in the residual

in steps of 0.2 V. Variation in the residual at the normal operating conditions and at the failure indicates the different characteristics of the LEDs. The deviation between the normal operating condition and the failure is estimated. An average value of this residual deviation between the normal operating condition and failure, is proposed as the maximum allowable deviation for the model driven approach developed in this work. Table 7.10 shows the different residual values and the deviations observed from the ten LEDs test under the accelerated test conditions where the voltage is increased in steps. The average deviation for the residual is established as 0.123 V. This maximum allowable deviation for the residual is used with the initial residual for the normal operating conditions to estimate the residual threshold. For example, for the LED no 1 the initial residual is observed as 0.05 and hence the residual threshold is estimated by adding the maximum allowable deviation of 0.123 V to the initial residual of 0.05, which is 0.128 V.

## 7.3.2   Sequential Mean Trend Estimation

From the experimental results, the almost a linear trend is observed in the residual curve under the accelerated test conditions. This finding is used to estimate the

RUL in real-time by estimating the trend of the curve every time. For a period of 10 min (i.e., using 10 sample data) the mean gradient is estimated sequentially using following equation:

$$m_t = \frac{t-1}{t}m_{t-1} + \frac{1}{t}(R_t - R_{t-1}) \tag{7.16}$$

Where $m_t$ is the mean gradient at time step $t$ and $R_t$ is the residual at time step $t$. RUL can be estimated using following equation:

$$RUL = \frac{R_{FT} - R_t}{m_t} \tag{7.17}$$

where the $R_{FT}$ is the failure threshold of the residual which is calculated from the maximum allowable deviation and the initial residual under normal operating conditions. This initial residual varies within the LED and hence incorporating the initial residual will be an advantage to the real-time RUL estimation.

### 7.3.3 Validation of Diagnostics Capability

Accelerated test data shown in Figure 7.3 is used to validate the diagnostics capability of the developed model driven approach. Residual is estimated and graph is shown in Figure 7.23. Residual graph shown in Figure 7.23, indicates the residual is kept at an almost constant value at 0.01 V at the initial stage when the LED is under normal operating voltage. This constant residual is the expected mean residual for this particular LED. Since the voltage is increased with the time, the residual is also increased because of the damage caused by the accelerated voltage condition. When the residual is increased, the light output degradation is observed and hence the residual is used as a damage estimator for the LED under the accelerated voltage condition. For this particular test data, the initial residual is 0.01 V and therefore the residual threshold is established as 0.136 V (i.e., 0.01 + 0.126). Figure 7.23 shows the degradation in the light output is detected using the continuous increase in the residual values. This particular LED residual value reaches the threshold of 0.136 V at 695 min. Actual failure is observed at 725 min.
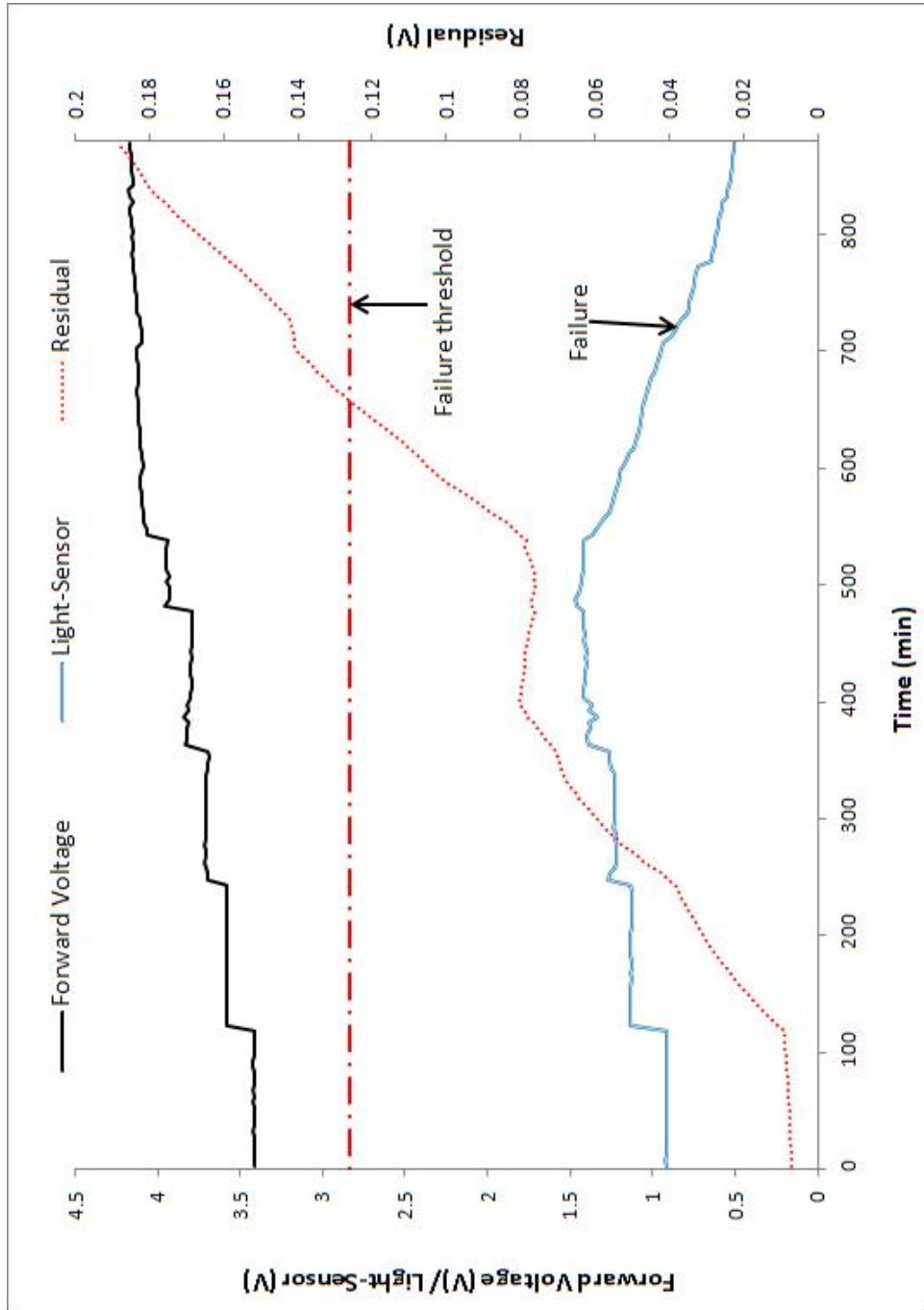
Figure 7.23: Current residual graph for the test data shown in Figure 7.3

| Time at which RUL prediction is made (min) | RUL from the Model (min) | True RUL |
|:---:|:---:|:---:|
| 500 | 77 | 119 |
| 550 | 32 | 69 |
| 600 | 29 | 19 |

Table 7.11: RUL estimation from empirical model driven approach for the accelerated test data shown in Figure 7.13

### 7.3.4 Validation of Prognostics Capability

Accelerated test data shown in Figure 7.13 is used to validate the prognostics capability of the developed empirical model driven approach for the LEDs. Figure 7.24 shows the residual graph for the test data shown in Figure 7.13. Under the accelerated stress conditions residual increases almost linearly and this behaviour is used to estimate the RUL. In this case (i.e., Figure 7.13), initial residual at the normal condition is observed as -0.01 V. Hence the failure threshold value for the residual is 0.116 V (i.e., $-0.01 + 0.126$). Predictions for RUL are made using the sequential mean gradient/trend estimation and linear extrapolation. Mean trend of the curve is estimated using 10 sample data.

Table 7.11 shows the three different predictions at three different times. It is evident from the Table 7.11 that the accuracy of the prediction increases with the time as more data and latest trend become available.

## 7.4 Fusion

Predictions made by the data driven approach and model driven approach are used to make best estimate for the RUL based on developed fusion approach. Kalman filter is used as discussed in chapter 5. Figure 7.25 shows estimated RUL curves for data driven, model driven and fusion approaches for the test data shown in Figure 7.15. In this example, RUL estimated from LRKF approach is used for the data driven approach. RUL estimated from the empirical model is used for the model driven approach. Kalman filter (see Appendix A) is used to estimate the best value for the RUL based on the estimated RULs from the data driven approaches. In this particular case, we assumed 20% error associated the
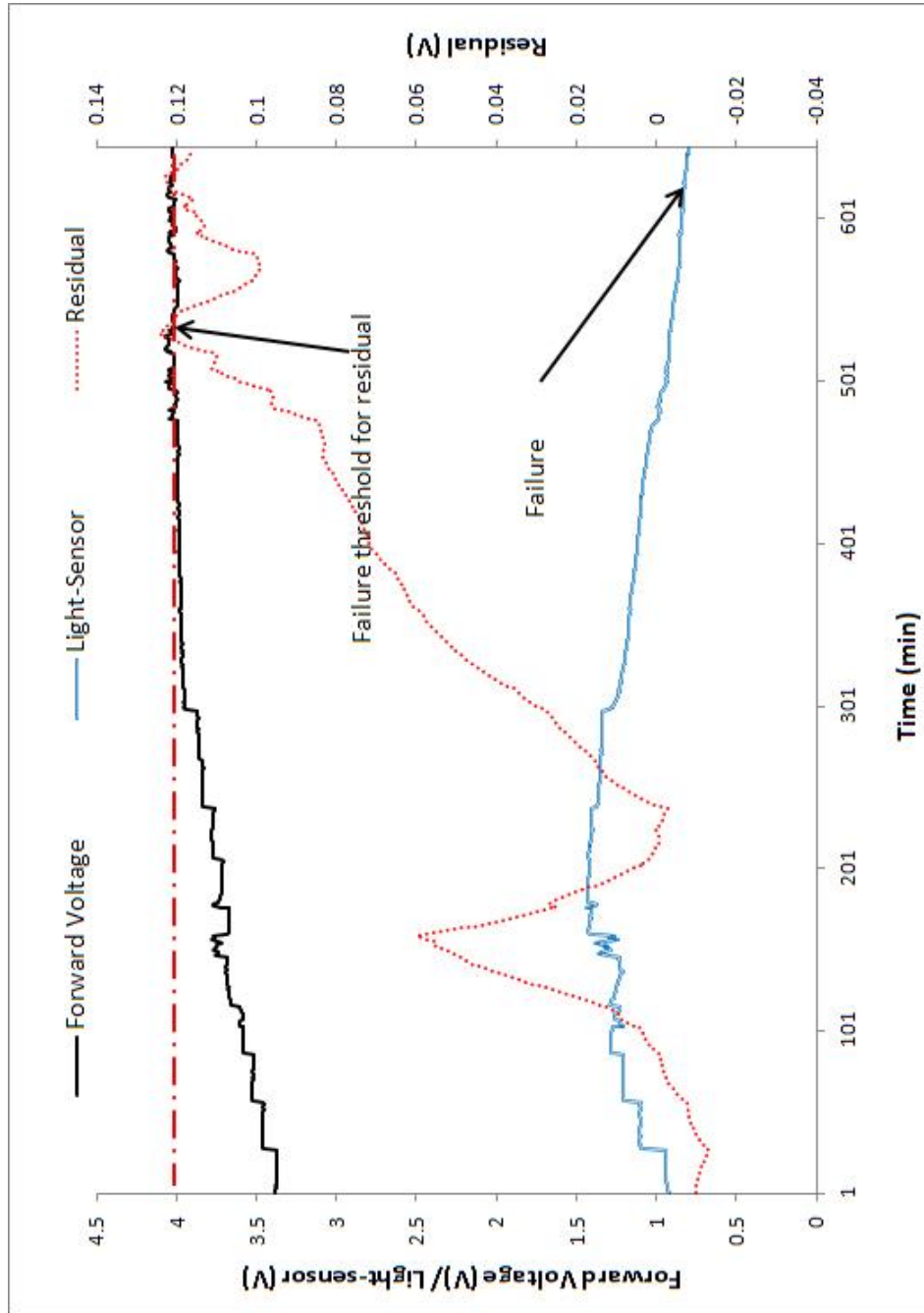
Figure 7.24: Current residual graph for the test data shown in Figure 7.13

| Time at which RUL prediction is made (min) | RUL from the LRKF (min) | RUL from the empirical model (min) | True RUL (min) |
|:---:|:---:|:---:|:---:|
| 500 | 49 | 65 | 52 |
| 550 | 19 | 43 | 23 |
| 600 | 7 | 24 | 10 |

Table 7.12: RUL estimation from the data driven (LRKF), empirical model driven and fusion approaches for the accelerated test data shown in Figure 7.15

RUL estimated by the data driven approach and 80% error associated with the RUL estimated by the model driven approach. It should be noted that these assumptions needs to be further investigated based on more tests. This has been identified as one of the potential future work.

Primary advantage of the fusion approach is that it can incorporate the predictions for RUL from both data driven and model driven approaches, and hence estimate a best value for RUL. Table 7.12 shows predicted values for RUL at three different intervals. Although the error parameters associated with the RULs estimated by the data driven and model driven approaches are not established theoretically and empirically, tabulated result in the table 7.12 shows the Kalman filter can be used to make best estimate for RUL, if the RUL estimates from the data driven and model driven approaches are available.
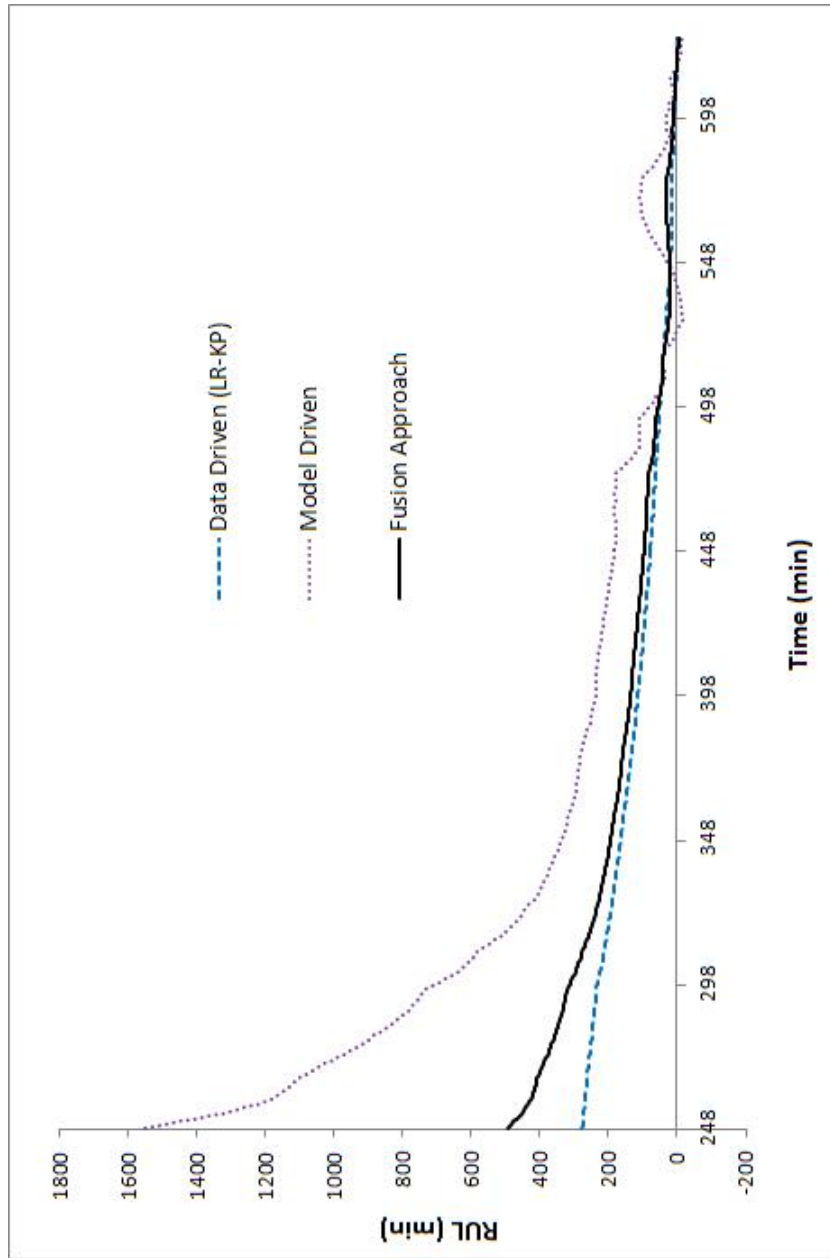
Figure 7.25: RUL predictions curve for the data shown in Figure 7.15

## 7.5   Summary

In this chapter we presented the results and validations for the developed approaches. Accelerated test data are used to validate the approaches. The validation results show that these approaches can be applied well in practice. Nevertheless, developed approaches can be further improved by doing more tests and establishing statistically proved diagnostics and prognostics parameters. For instance, early warning thresholds and failure thresholds for the ED and MD approaches can be further improved by doing more tests. Logistic regression and neural network based approaches can be further improved by introducing an additional regularisation parameter, adding more features, and collecting more data for training. Failure threshold value for the model driven approach can be further validated form more test data. Fusion approach can be used to make better prediction for RUL, if the error parameters associated with the RUL estimates made by the data driven and model driven approaches are available.

However, this chapter presented the details of the developed approaches to the data driven and model drive PHM for the LEDs with the validations and results. The developed approaches perform well under the presented accelerated test conditions. Incorporating two or more approaches together is another way to improve the performance. This integration of data and model driven approaches into a single fusion approach is out of scope but we attempted to demonstrate fusion approach using Kalman filter. Fusion approach which incorporates data driven and model driven approach can be developed further to get better performance.

# Chapter 8

# Real-Time Implementations

## 8.1  Introduction

Real-time systems are not just a high performance and fast computing systems. They are very deterministic and reliable computing system which meets its deadline with highest determinism for an extended period of time with high reliability. For example, if an event needs a response with an action exactly after one second, it can be achieved using a real-time system. Real-time system will respond to a particular event exactly after a certain time by programming the system. A passenger car airbag system is a good example for a real-time system which needs to activate the airbag within few microseconds after an accident occurred.

Real-time systems are designed to do certain things in particular operational and environmental conditions, no further performance or operations are necessary and therefore one real-time system will not be suitable for all applications. So the physical hardware design and the software design process should take account of all these aspects of an application. A real-time system can be a super computer to a low cost microcontroller. The flight control system (fly-by-wire) in an aircraft can be a super computer which needs to monitor many different things in real-time and at the same time actuate different actuators within a time limit to achieve its goals. On the other side a car airbag system for example can be programmed in microcontroller which needs to monitor few things and actuate the airbag. Again, it all depends on the application, requirements and operating

conditions.

Real-time systems are classified into four main categories:

1. Periodic real-time systems;

2. Non-periodic real-time systems;

3. Hard real-time systems;

4. Soft real-time systems.

Periodic real-time systems will have a continuous deterministic task. Acquiring sensor data is a periodic real-time task where sensor data is normally collected in every millisecond or nanosecond. Non periodic real-time systems will not have continuous tasks to respond but will have to respond to an event deterministically. Actuating the airbag is a non-periodic real-time task which is a time critical task. Airbag system is a perfect example for periodic and non-periodic tasks of a real-time system. It has to sense the accident periodically and actuate the airbag soon after the accident occurs. Hard real-time systems must meet the deadline precisely and failure to meet the deadline considered as a system failure and may lead to deaths, injuries, damage to environment and money lost. On the other hand soft real-time systems can tolerate the latency. This is often considered as poor quality of service.

Sometimes real-time systems are referred as embedded systems. Embedded systems are generally real-time systems which are embedded to other systems to control or monitor those particular systems. Engine control unit of a car is a real-time system and also an embedded system which is embedded into a car engine and performs real-time tasks.

In this work, PHM approaches are investigated for real-time implementation to make real-time assessment in the LEDs and make real-time RUL predictions. Implementation platforms for the realisation of the discussed PHM approaches in this work are divided into three main categories:

1. National Instruments' (NI) PXI real-time platform

2. National Instruments' (NI) FPGA

3. Microchip PIC32 Microcontroller

The remaining part of this chapter presents the details of the undertaken implementations and summary of the findings.

## 8.2 National Instruments' PXI Real-Time Platform

### 8.2.1 Hardware

National Instruments has developed many programmable controllers and systems for rapid prototyping and for the measurement and controls. PXI (PCI eXtensions for Instrumentation) is one of the rugged PC-based high performance platform for measurement and automation systems. These systems are used in many different applications such as manufacturing test, military and aerospace, machine monitoring, automotive, and industrial test. Figure 8.1 shows NI PXI system which consists of chassis, controller and modules. Implementation of the PHM approaches is carried out in the embedded controllers (NI PXI-8110) with a real-time OS (LabVIEW Real-Time). This particular embedded controller has 2.26 GHz Intel Core 2 Quad Q9100 quad-core processor. Figure 8.2 shows the NI PXI-8110 embedded controller.

### 8.2.2 Software

National Instruments also provides graphical systems to integrate the their software and hardware platforms. LabVIEW is the powerful system design software developed and patented by the National Instruments. There are many more tools developed over the years to achieve different tasks such as signal processing and control, mathematics, robotics, RF communication, sound and vibration, etc. LabVIEW environment enable add the hardware platforms into the projects. Software can be designed based on the added hardware platform and developed software can be deployed into the hardware platform very easily.

There are many tools developed into the LabVIEW environment which enable engineers to design, prototype and test the systems very easily. Figure 8.3 shows
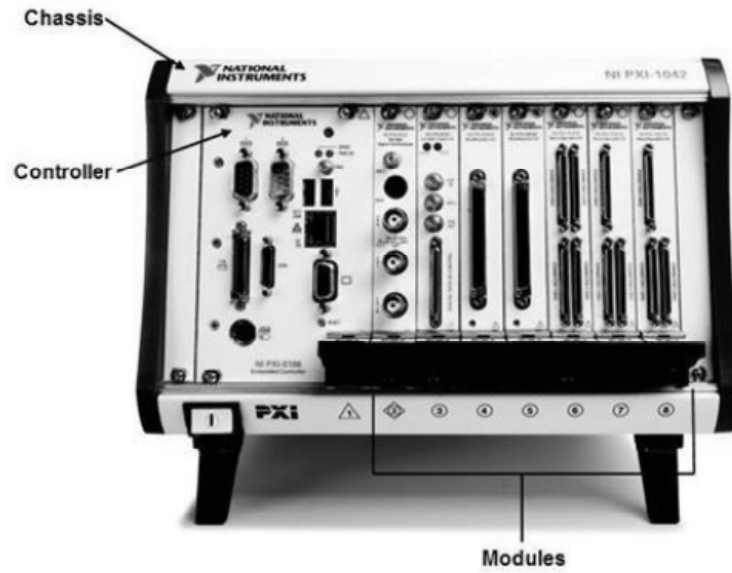
Figure 8.1: NI PXI system which consists of chassis, controller and modules [130]



Figure 8.2: NI PXI-8110 embedded controller [130]

the signal analysis tools which are provided with the LabVIEW environment. For example histogram tool can be used to analyse the signal and get the results such as mean, standard deviation etc., for the input signal. Figure 8.4 shows most of the available tool categories. For example mathematical tool have many sub tool sections such numeric, fitting, probability and statistics etc., for particular mathematical tasks. These sub categories have many individual tools which can be used in the block diagram of the design. Developers can also develop their own tools and used in their applications.
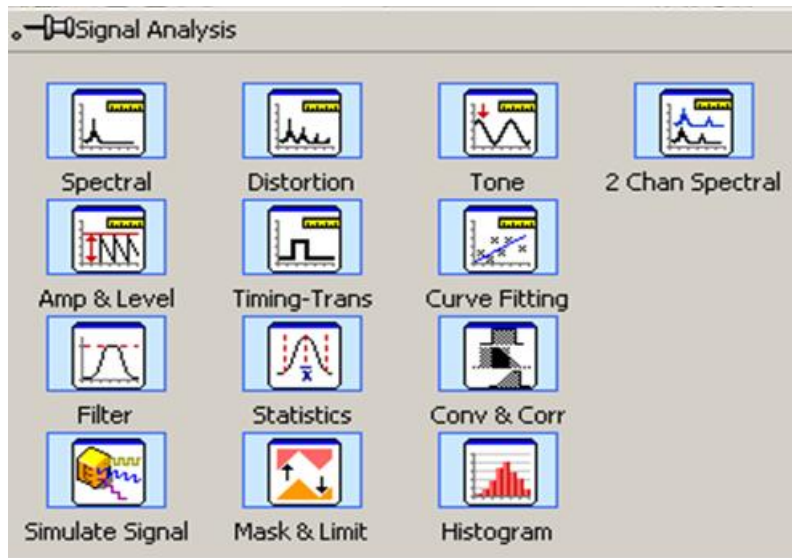


Figure 8.3: LabVIEW signal analysis tools

LabVIEW real-time software is the tool used to program the LabVIEW real-time hardware platforms such as embedded controller. Executable code then is transferred into the embedded controller. After that this real-time embedded controller can run as a standalone system.

### 8.2.3 Implementation of Data Driven Approach (Euclidean Distance)

The details of the data driven approach based on the Euclidean distance were discussed in chapters 5 and 7. This approach is required to estimate the ED
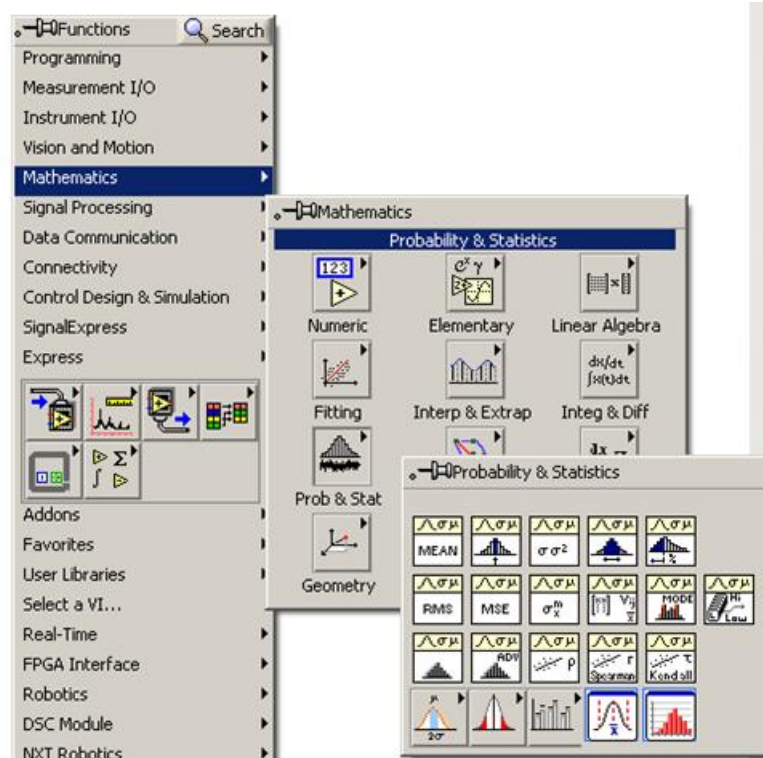
Figure 8.4: Various LabVIEW tools for mathematics, signal processing, robotics etc.

from the current and temperature sensors. This approach also requires the mean values for these sensor readings under normal operating conditions. From the sensor signal and mean values for current and temperature sensors (i.e., 0.09 and 0.00022 respectively), ED is calculated. Calculated ED data is then monitored for the early warning threshold ($ED_{EWT}$) of 2.5. Observed recent maximum value for ED is kept. If the ED goes above the early warning threshold, early warning is provided. If the ED goes above the early warning threshold and trend of the ED curve is negative, then the ED estimate at time step $t$, ($ED_t$) and observed maximum values for ED ($ED_{MAX}$) is passed into a loop to estimate the RUL. Failure threshold is estimated from the $ED_{MAX}$ and using the equation 7.1. Using the sequential mean trend for ED ($m^{ED}{}_t$), $ED_t$ and $ED_{FT}$, the RUL is estimated. Figure 8.5 shows the implementation of the ED approach in the LabVIEW real-time environment using the NI PXI-8110 as the real-time embedded hardware platform.

## 8.2.4 Implementation of Data Driven Approach (Mahalanobis Distance)

Mahalanobis distance based data driven approach was discussed in chapters 5 and 7. MD is estimated for current and temperature sensor data using the mean and standard deviations for the current and temperature sensor data under normal operating conditions. Estimated MD is then monitored for the early warning threshold ($MD_{EWT}$) of 17 and for a maximum value. If the MD goes above the early warning threshold of 17, early warning is provided. If the MD goes above the early warning threshold and trend of the MD curve is negative, then the MD estimate at time step $t$, ($MD_t$) and observed maximum values for MD ($MD_{MAX}$) is passed into a loop to estimate the RUL. Failure threshold for MD is estimated using equation 7.2. RUL is estimated using equation 7.6. Figure 8.6 shows the implementation of the MD approach into LabVIEW real-time environment.
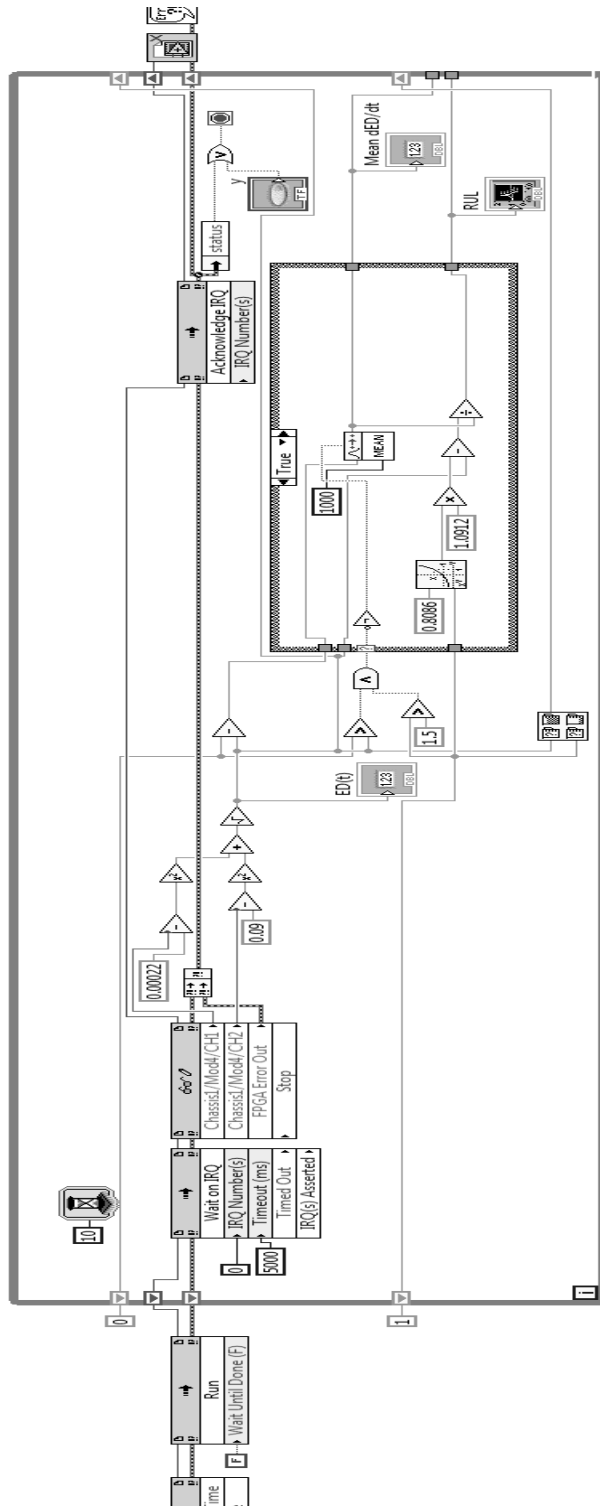
Figure 8.5: Implementation of Euclidean distance (ED) approach in the PXI real-time platform
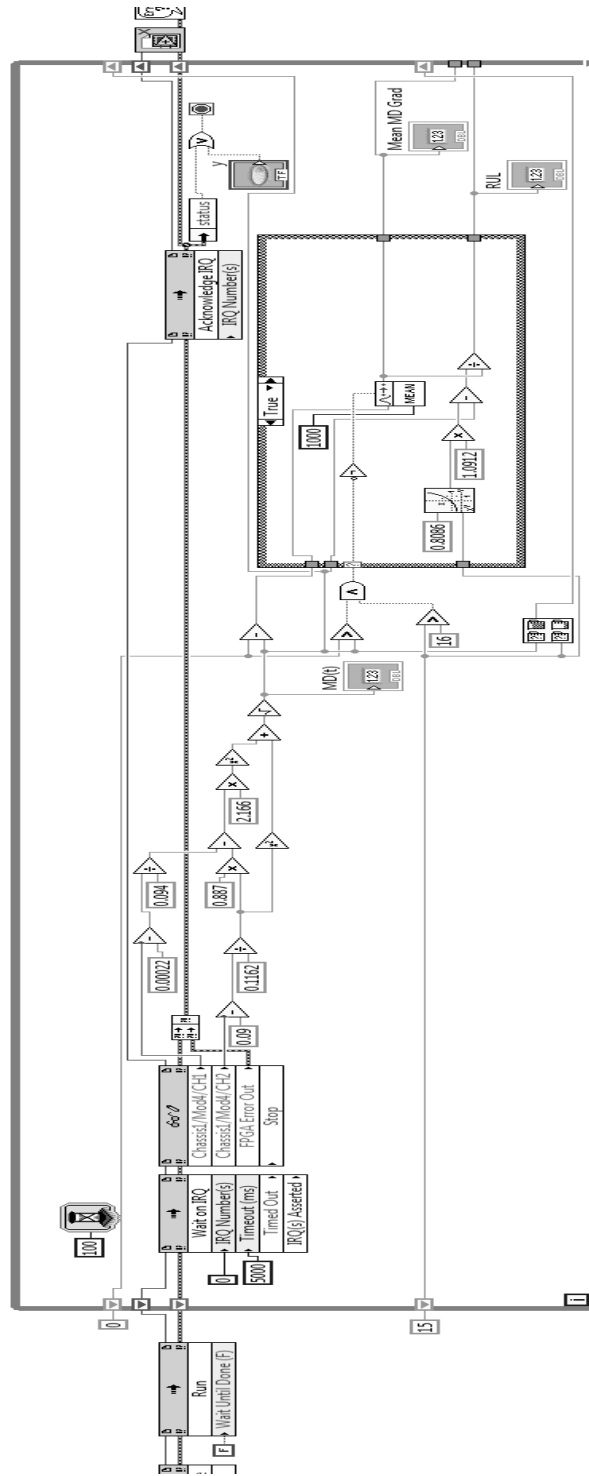
Figure 8.6: Implementation of Mahalanobis distance (ED) approach in the PXI real-time platform

### 8.2.5 Implementation of Data Driven Approach (LRKF)

Development of logistic regression based PHM approach was discussed in chapters 5 and 7. Logistic regression function is implemented for the current and temperature sensor data using the established regression coefficients reported in the Table 7.5. Output from the logistics function then filtered using Kalman filter with the noise coefficients of 11 and 0.022. Filtered signal from the logistics regression function is then monitored for the decision boundary. If the LRKF goes below the decision boundary of 0.5, output from the LRKF is passed into the loop which handling the RUL estimation. Mean exponential decay constant is estimated using built in mean function. Using this mean and failure threshold for logistic regression of 0.15, RUL is estimated. Main advantage of this approach is that probability of failure is reported with the estimated RUL. Figure 8.7 shows the implemented logistic regression and Kalman filter (LRKF) based data driven PHM approach in the LabVIEW real-time environment using the NI PXI-8110 as the real-time embedded hardware platform.

### 8.2.6 Implementation of Data Driven Approach (NNKF)

Neural network based PHM approach was developed and reported in chapters 5 and 7. Figure 5.5 shows the developed neural network. Weight and bias parameters are established from the training and reported in the equations 7.11, 7.12, 7.13 and 7.14. Using these neurons weights and biases, and selected activation functions (i.e., linear function for hidden layer and logistic (sigmoid) function for output layer) for hidden and output layers, neural network is implemented in the LabVIEW real-time environment. Output from the neural network is then passed into the Kalman filter with the noise coefficients of 11 and 0.022 to smooth the output. Filtered output from the neural network then monitored for the decision boundary of 0.5. If the output goes below the decision boundary early warning is provided and RUL loop is triggered for the lifetime estimation. Figure 8.8 shows the implemented neural network and Kalman filter (NNKF) based data driven PHM approach in the LabVIEW real-time environment using the NI PXI-8110 as the real-time embedded hardware platform.
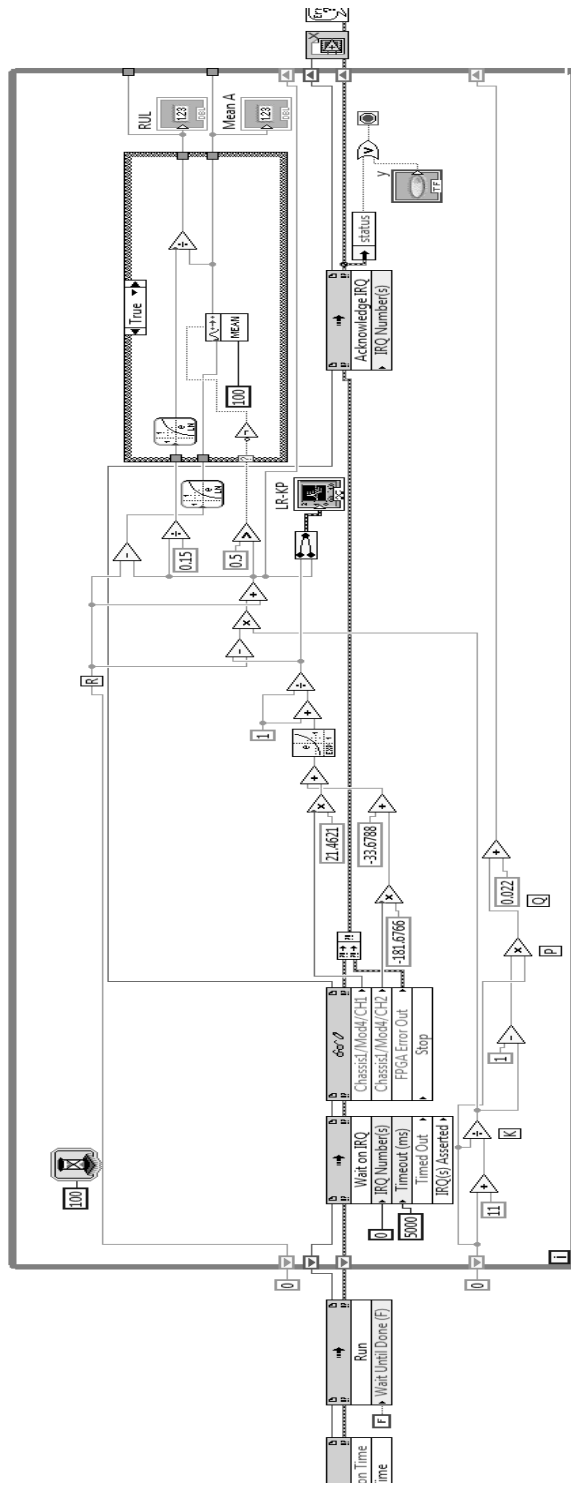
Figure 8.7: Implementation of logistic regression and Kalman filter (LRKF) approach in the PXI real-time platform
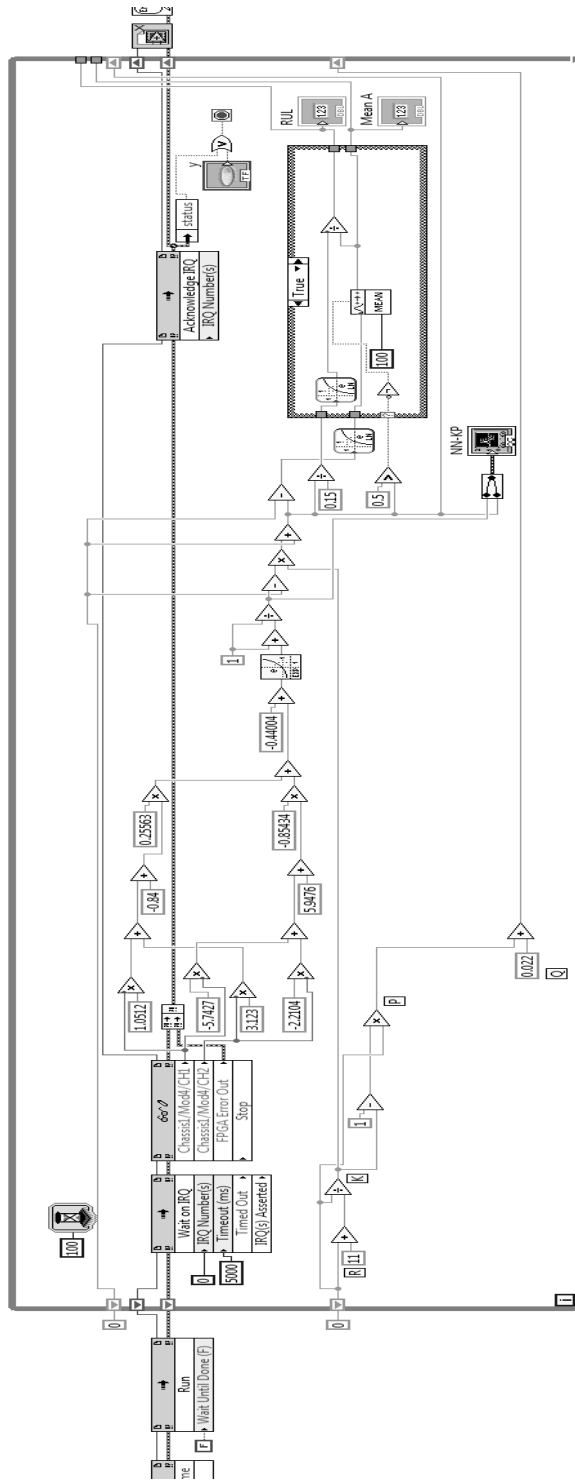
Figure 8.8: Implementation of neural network and Kalman filter (NNKF) approach in the PXI real-time platform

### 8.2.7   Implementation of Model Driven Approach

The developed empirical model is discussed in details in chapters 5 and 7. This empirical model uses sensor data for forward voltage and current. Developed model is used to predict the current using the forward voltage sensor value. Actual current value is known from the current sensor. Residual is then estimated from the model predicted value and actual sensor values for the forward current. Failure threshold for the residual is estimated by adding the maximum allowable deviation of 0.126 V to the initial observed for the particular LED. These data is then fed into RUL loop for the lifetime estimation. Mean trend of the residual curve, current residual and failure threshold for the residual are used to estimate the RUL using equation 7.17. Figure 8.9 shows the implemented linear model for the model driven PHM approach in the LabVIEW real-time environment using the NI PXI-8110 as the real-time embedded hardware platform.

## 8.3   National Instruments' FPGA

FPGA (Field Programmable Gate Arrays) is a reprogrammable or reconfigurable silicon chip which contains millions of logic gates. This enable engineers to program FPGA into different hardware block as required. For example, it can be programmed to work as a memory, digital filter, controller etc. Once it is programmed it does not need any software or operating system to run it. FPGAs configuration is generally defined by Hardware Description Language (HDL) or a schematic design. Then a bitfile is generated using electronic design automation (EDA) tool and a place-and-rout tool. Together the electronic design automation and the place-and-rout tools are called compiler which is FPGA company's proprietary. Figure 8.10 shows a sample structure of an FPGA. Figure 8.10 illustrates the key function blocks of the FPGA. Programmable interconnect is used to electronically program the logic cells. Most of the FPGAs have array of configurable logic blocks (CLB), programmable interconnects, I/O blocks, lookup tables (LUT) and flip-flops. Compiler will find the required number of CLB, I/O, LUT etc and compile the HDL into bitfile to map the circuit into the FPGA. Finally FPGA will run like configured hardware. Manufacturers also supply compilers,

Figure 8.9: Implementation of model driven approach in the PXI real-time platform
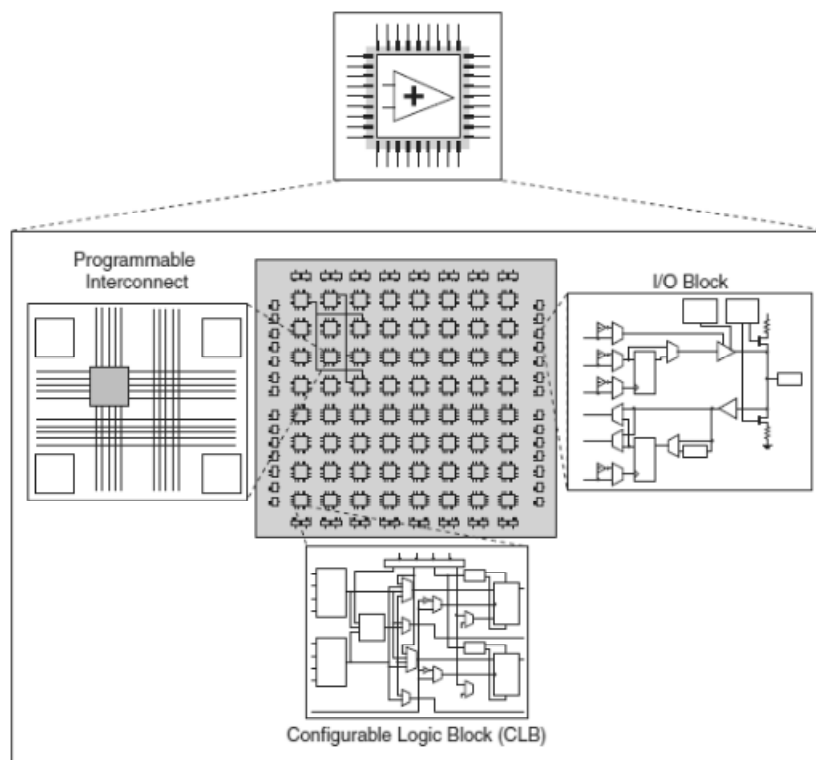
Figure 8.10: Sample structure of an FPGA [130]

development tools and very high level graphical tools which enable the designers not to worry about HDL or any low level programming. For this thesis, National Instruments' LabVIEW FPGA is used to program the PHM approaches discussed in this work. Figure 8.11 shows a traditional real-time system which consists of operating system, driver APIs and application software. Figure 8.12 shows a LabVIEW FPGA systems which shows all the calculations are performed at the hardware level. Because all the calculations and processes are handled by the hardware cells, FPGA is more reliable than the traditional real-time system. This is the main advantage of the FPGA over a traditional real-time system.
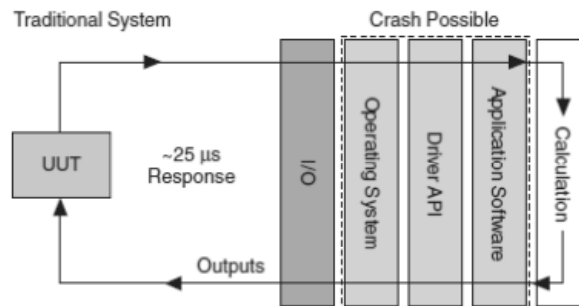


Figure 8.11: Traditional real-time systems [130]
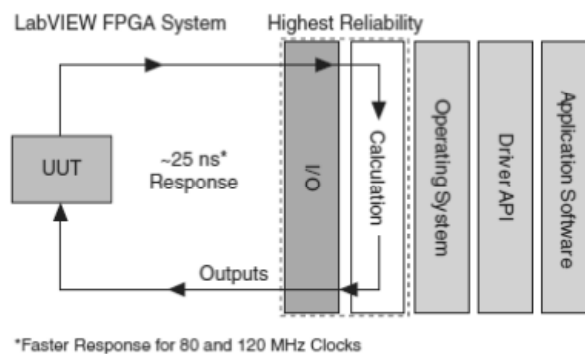


Figure 8.12: LabVIEW FPGA system [130]

Another key advantage of the FPGA is the parallelism, which enables an FPGA to run several parallel loops at the same time. Two independent parallel

loops are shown in Figure 8.13. In this exapmple, loop one has three inputs A, B and C. At the first logic cell A and B are added together and passed to the next logic cell to multiply with C. Result from this manipulation is then transferred to the output pin F. Second loop also have three inputs X, Y and M. X and Y are added in the first cell and result is passed to the second cell. At the second cell the result from the first cell and M are added together. Final manipulation results from the second logic cell from the second loop which is sent to the output pin Z. First and second loops shown in the Figure 8.13 do not depend each other, hence both loops are executed simultaneously.

Main disadvantage of the the FPGA is that it does not support floating point arithmetic and therefore we have to rely on fixed point arithmetic. LabVIEW FPGA is designed to handle floating point arithmetic using the fixed point arithmetic. This has been already built in by the NI. But it requires more logic cells to convert a floating point into fixed point and do the manipulations. Developed approaches for data driven and model driven PHM of the LEDs require floating point arithmetic. This is one main limiting factor for the implementation of these approaches in the LabVIEW FPGA environment. In this work, NI PXI-7851R multifunction reconfigurable input output (RIO) with Virtex-5 LX30 FPGA is used to implement the PHM approaches developed in this thesis.

### 8.3.1 Implementation of Data Driven Approach (Euclidean Distance)

Euclidean distance based data driven approach is implemented in the FPGA using the LabVIEW FPGA module. The implementation is similar to the implementation in the real-time system (NI PXI), but here fixed point arithmetic is used using built in functions. Each arithmetic function block has two inputs and one output. These inputs and output are configured such that they represent the number of bits for before the digit and after the digit. Figure 8.14 shows the implemented Euclidean distance based data driven PHM approach in LabVIEW FPGA environment.

Figure 8.15 shows the summary of device utilisation for the Euclidean distance based approach. Summary shows that 56.2% of the DSP48s blocks are used for
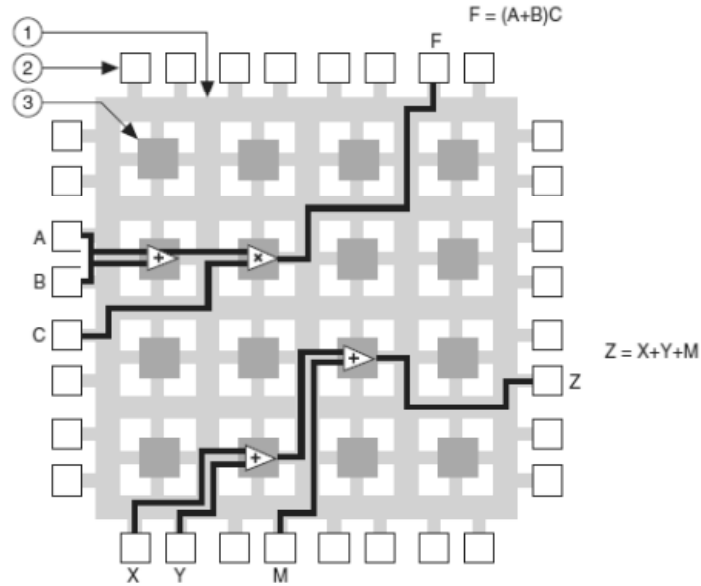
Figure 8.13: Parallel implementation in FPGA using separate logic cells [130]

this implementation (i.e., 18 out of 32 DSPs are used). DSPs are the most utilised devices in the FPGA. Other devices used for this implementation are total slices 30.1%, registers 15.0% and LUTs 17.6%. None of the block RAMs are used for this implementation. Clock speed used by the components and maximum clock speed are also shown in Figure 8.15. Compilation time for this design is 11.01 minutes.

## 8.3.2 Implementation of Data Driven Approach (Mahalanobis Distance)

Mahalanobis distance based data driven approach is designed and implemented in the LabVIEW FPGA environment. Figure 8.16 shows the implemented Mahalanobis distance based data driven PHM approach in LabVIEW FPGA. Number of arithmetic blocks required for this design is high compared to the design of the ED approach discussed and implemented in the above section. When the designed is compiled for the LabVIEW hardware, compiler finds difficult to fit this design into the available FPGA logic cells. Figure 8.17 shows the summary
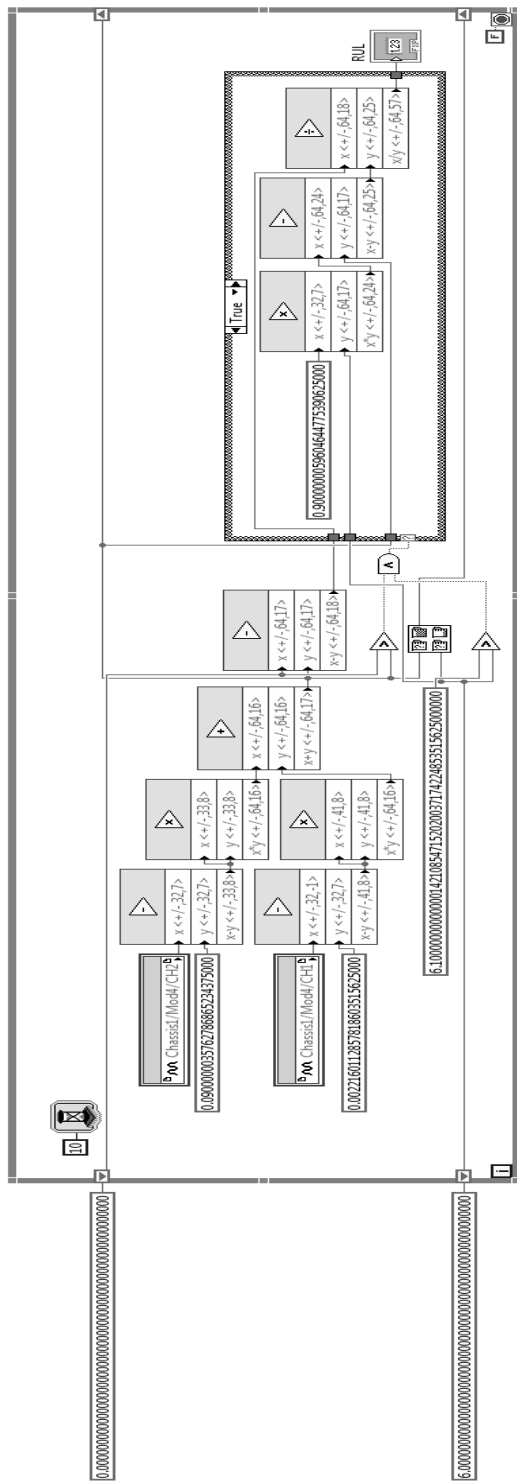
Figure 8.14: Implementation of Euclidean distance (ED) approach in the LabVIEW FPGA

```
Device Utilization
--------------------------
Total Slices: 30.1% (1444 out of 4800)
Slice Registers: 15.0% (2875 out of 19200)
Slice LUTs: 17.6% (3380 out of 19200)
DSP48s: 56.2% (18 out of 32)
Block RAMs: 0.0% (0 out of 32)

Timing
--------------------------
ReliableClk40 (Used by non-diagram components): 40.02 MHz (307.31 MHz maximum)
MiteClk (Used by non-diagram components): 33.00 MHz (102.75 MHz maximum)
40 MHz Onboard Clock: 40.02 MHz (49.13 MHz maximum)

Start Time: 15:06:04
End Time: 15:17:05
Total Time: 00:11:01
```
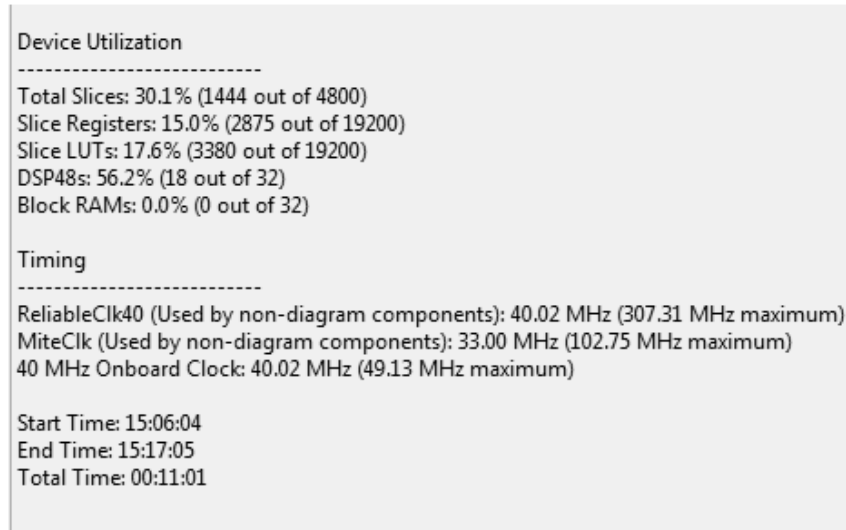
Figure 8.15: Device utilisation summary for the implemented ED approach

of device utilisation for the Mahalanobis distance based approach. Error message says that too many DSPs are required to accommodate this design.

This shows that the PHM algorithms need to be considered with respect to the available hardware platform. For example, in this case ED based approach can be deployed into the LabVIEW FPGA system and MD based approach can not be deployed in the LabVIEW system. Hence hardware platform plays a critical role in selecting a suitable algorithm for a PHM system.

Other two data driven approaches for LED's PHM can not be implemented in the LabVIEW FPGA platform as they (i.e., LRKF and NNKF) require more block functions (such as addition, multiplication ec.,) compare to that of the MD approach. This is another disadvantage of the FPGAs. FPGA's space are limited and they can accommodate certain number of functions as their logic cells are limited to a certain number. Because of this disadvantage FPGAs are called space limited devices.

### 8.3.3 Implementation of Model Driven Approach

Developed empirical model was discussed in details in chapters 5 and 7 and implemented in the LabVIEW FPGA. Design of this approach is similar to the design

Figure 8.16: Implementation of Mahalanobis distance (MD) approach in the LabVIEW FPGA

```
Compilation failed due to a Xilinx error.

Details:
ERROR:TclTasksC:process_077: Failed to complete. Please inspect the log and report files.false
    while executing
"process run "Map""
    (file "C:\NIFPGA\jobs\O2K69xj_rYTw6YC\map.tcl" line 7)


ERROR:Pack:2310 - Too many comps of type "DSP48E" found to fit this device.
ERROR:Map:237 - The design is too large to fit the device.  Please check the
    Design Summary section to see which resource requirement for your design
    exceeds the resources available in the device. Note that the number of slices
    reported may not be reflected accurately as their packing might not have been
    completed.
    NOTE:  An NCD file will still be generated to allow you to examine the mapped
    design.  This file is intended for evaluation use only, and will not process
    successfully through PAR.
Mapping completed.
See MAP report file "toplevel_gen_map.mrp" for details.
Problem encountered during the packing phase.
Design Summary
--------------
Number of errors  :  2
Number of warnings : 131
Process "Map" failed

Start Time: 09:47:19
End Time: 09:59:01
Total Time: 00:11:42
```

Figure 8.17: Device utilisation summary for the implemented MD approach

in the LabVIEW real-time system but the fixed point arithmetic is used. Figure 8.18 shows the implemented linear model for the model driven PHM approach in the LabVIEW FPGA system.

Device utilisation summary illustrates that 30.9% of total slices, 15.1% of registers, 19.1 of the LTUs and 21.9% of the DSPs are used for this LabVIEW FPGA design. Total compilation time for this implementation is 11.44 minutes. Figure 8.19 shows the device utilisation summary for the model driven implementation in the LabVIEW FPGA.

## 8.4 PIC Microcontroller

Generally microcontroller is considered as a small computer on a single integrated circuit. They consist of CPU, memory, I/O interface etc. Microcontrollers are used in embedded systems which monitor and control other systems such as automobiles, remote control, medical devices etc. There are many different types microcontrollers available in the market. Some applications are developed using the real-time operating systems (RTOS) such VxWorks, RTLinux, QNX, etc. Embedded C is mostly used to develop the applications.

Figure 8.20 shows typical microcontroller architecture which consists of CPU, ROM, RAM, I/O peripherals, timbers, counters and other interfaces. There are also application specific microcontrollers which are used for specific applications. PIC microcontrollers are manufactured by Microchip and is one of the widely used microcontrollers. Figure 8.21 shows a PIC32 microcontroller architecture. In this work, PIC18F4550 is investigated to implement the developed approaches. Application can be developed using embedded C in the MPLAB environment which is designed to program the PIC microcontrollers. C18 compiler is used to convert the embedded C into the assembly code then into the machine code.

Figure 8.18: Implementation of model driven approach in the LabVIEW FPGA
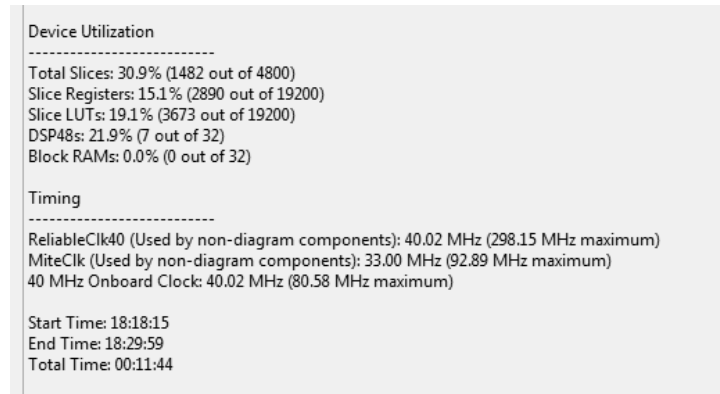
Figure 8.19: Device utilisation summary for the implemented model driven approach
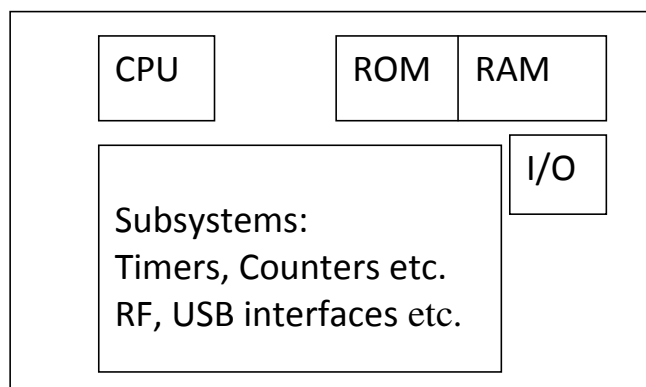


Figure 8.20: Microcontroller architecture
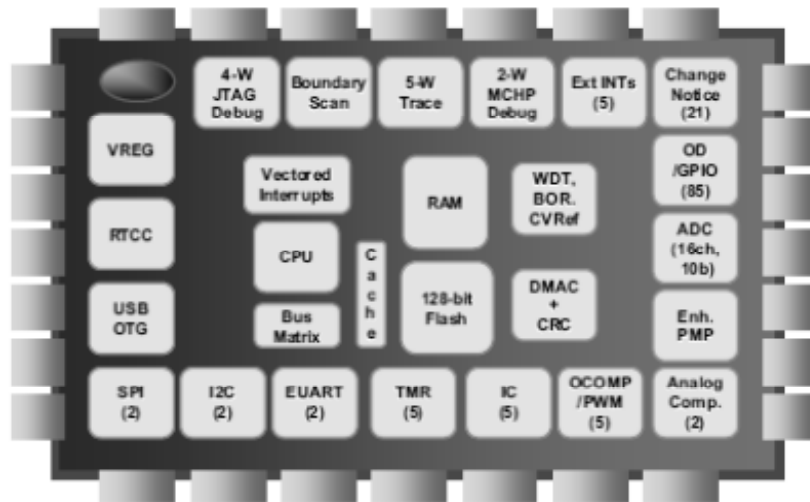
Figure 8.21: PIC32 architecture [131]

## 8.5  Summary

This chapter discussed the implementations of the developed PHM approaches in the different hardware platforms. Developed approaches are implemented in LabVIEW real-time platform which is NI PXI-8110 embedded controller and details are presented in this work. LabVIEW FPGA is also used for implementations but only ED and model driven approaches are implemented because of the space limitation of the particular FPGA (Vertex-5) used in this work.

Another popular implementation option is the microcontrollers. PIC microcontrollers have been investigated for the implementation of the developed approaches. Although it understood most of the developed approaches could be implemented with no or small modifications. For instant, logistic (sigmoid) function used in the logistic regression and neural network need to be approximated to a linear function. This approximation may under-perform the approaches. However, this should be considered for the future work.

# Chapter 9

# Conclusion and Future Work

## 9.1 Conclusion

This thesis has discussed data driven and model driven PHM approaches for real-time health monitoring and prognostics of high power LEDs. The PHM framework developed in this programme relies on sensor data such as forward voltage, forward current and temperature. The results from the undertaken experiments show that both data driven and model driven techniques for PHM can be used to detect when unusual changes in the expected performance of an LED start to take place, and can successfully provide an early warning if light output degrades and approaches the failure limit. In addition to the diagnostics capabilities of the data driven and model driven approaches, prognostics capability was also developed and demonstrated. The potential of the studied approaches to predict remaining useful life of an LED was established.

For the distance measure techniques, the accuracy of the prognostics calculations improves with time as more data to perform the sequential estimation of the ED and MD trends becomes available. In addition, embedding the temperature sensors very close to the junction has shown to improve the temperature measurement in all situations; hence the approach will become more accurate. The ED technique is found to be more suitable for this application as it involves less mathematical operations and requires less computational time compared to the MD technique. The undertaken tests have indicated that the ED curves are generally less sensitive to noise in the monitored parameters and when test condi-

tions (i.e. applied voltage) change. This is an important finding as manipulation of noisy data would otherwise require additional filtering.

For the logistic regression approach, the accuracy of the prediction depends on the Kalman filter and the proposed decision boundary. The filtered output of the logistic regression gives the probability of healthy state of the LED, which is a great advantage. Logistic regression based approach makes better consistent predictions than the distance measure approach. In addition to the RUL prediction capability, logistic regression can also be used to detect the anomalies i.e., when unusual changes in the expected performance starts to take place.

Neural network approach discussed in this thesis is similar to the logistic regression approach but have the advantage of choice for activation function and number of neurons. This gives the neural network more flexibility to fit the training data more accurately. Every neuron in the neural network can be treated as a logistic regression function and hence neural network can be considered as a combination of many logistic regression with different set of regression coefficients. But the activation function of the neurons in a particular layer can be selected from a number of different functions such logistic function, linear function etc. The developed neural network and Kalman filter (NNKF) based approach for the LED PHM makes similar consistent predictions to the logistic regression and the Kalman filter (LRKF) based predictions. Similarly logistic regression approach, accuracy of the neural network approach discussed in this work depends on the Kalman filter and the established threshold.

Model driven approach for the LED PHM discussed in this work was also demonstrated. Accuracy of the predictions depends on the failure threshold based on evaluated residual values. Linear extrapolation technique is used to predict the RULs. The techniques discussed in this work are shown to have good predictive and detection capability. The accuracy of the predictions can be further improved by establishing statistically proved threshold values for the failure, and by increasing the sample size used in the derivation of sensor data.

Real-time implementation of the discussed approaches show both data driven and model driven approaches discussed in this work can be implemented in real-time platforms to monitor the health of the systems or products based on sensor data and empirical models. In the case of the LED application, data driven

approaches can be implemented in microcontroller based real-time systems with minor approximations and model driven approach can be implemented in microcontroller based real-time system directly to monitor the health of the LED lighting systems. For example, logistic regression and neural network based approaches might require approximation for the sigmoid or the logistic function to implement in the microcontroller, if it is possible to make reasonable predictions based on the approximations. The neural network can be further improved by adding more neurons and hidden layers.

The data driven PHM presented in this paper can be applied to other semiconductor devices such as microprocessors to monitor the real-time health and do the prognostics by embedding suitable sensors (i.e., temperature, accelerometer, vibration, humidity etc.,) into those semiconductor devices. This will allow the semiconductor devices to have a built-in embedded health and usage monitoring capabilities.

## 9.2    Future Work

Further study is required to generalize this result for harsh operating conditions which are not considered in this work such as high and low room temperatures which will affect the board temperature etc. This will require controlling the current and temperature independently. Further experiments are also necessary to integrate other parameters which affect the LED life, into a generalized approach of LED health monitoring under harsh operating conditions.

Studied data driven and model driven prognostics algorithms can be implemented in any LED lighting systems along with the LED driver to monitor the reliability and report the risk of failure in advance. Future research in this real-time data driven prognostics systems will focus on the development and deployment of an intelligent LED driver to monitor and improve the remaining useful life of LEDs based on discussed data driven and model driven approaches. In particular, motivation of the future research is to implement and test these approaches in a microcontroller. Embedding temperature and current sensors into an LED package will make this implementation possible and will also make the

temperature measurement more accurate.

Future work can also focus on improving the accuracy of the studied data driven and model driven approaches by establishing statistically proved threshold values for each approach, and smoothing constant for the logistic regression and the neural network based approaches. Future research in these real-time PHM systems will aim at the development of hybrid or fusion approach for real-time health monitoring and prognostics of LEDs based on developed data driven and model driven approaches.

A specific topic that requires further studies is the failure related to discolouration of the LED die or LED encapsulate. More tests need to be carried out to establish the relationship between the sensor values and light colour.

# Appendix A - Algorithms and Programs

## Kalman Filter

General form of KP is given below [132]: Prediction step based on physical or process model:

$$x_{k+1}^- = Ax_k + v \tag{1}$$

where $A$ is the state transition matrix, $\hat{x}_k$ is the state of the system at time step $k$, $v$ is the Gaussian noise with zero mean and $\hat{x}_{k+1}^-$ is the predicted state of the systems based on the state transition matrix and Gaussian noise. Covariance matrix of the state estimate $\hat{x}_{k+1}^-$ is given by:

$$P_{k+1}^- = AP_kA^T + Q \tag{2}$$

where $P_k$ is the covariance matrix of the state estimate at time step $k$ and $Q$ is the covariance matrix of the noise $v$. The measurement is linearly related to the state of the system by the matrix $H$ and associated with some error is given by:

$$z_{k+1} = Hx_k + R \tag{3}$$

where $R$ is the measurement error/noise covariance matrix. Kalman gain for the time step $k+1$ is then estimated as follows:

$$K_{k+1} = P_{k+1}^- H^T \left[ H P_{k+1}^- H^T + R \right]^{-1} \tag{4}$$

Then the state of the system is updated from the estimated Kalman gain as follows:

$$x_{k+1} = x_{k+1}^- + K_{k+1} \left[ z_{k+1} - H x_{k+1}^- \right] \tag{5}$$

Covariance matrix of the state estimate is updates as follows:

$$P_{k+1} = (1 - K_{k+1} H) P_{k+1}^- \tag{6}$$

## Particle Filter

A pseudo code of particle filter algorithm based on sequential important sampling (SIS) is given below [118]:

$$\left[ \{ x_k^i,\ w_k^i \}_{i=1}^{N_s} \right] = SIS \left[ \{ x_{k-1}^i,\ w_{k-1}^i \}_{i=1}^{N_s}, z_k \right] \tag{7}$$

$$for\ i = 1:\ N_s$$

$$- Draw\ x_k^i\ \sim\ q(x_k | x_{k-1}^i,\ z_k) \tag{8}$$

$$- Assign\ a\ weight, w_k^i$$

$$END\ for$$

$\{ x_k^i,\ w_k^i \}_{i=1}^{N_s}$ is a random measure which characterise the posterior density, $p(x_{0:k} | z_{1:k})$, where $\{ x_{0:k}^i,\ i = 0, \ldots, N_s \}$ is a set of support points with associated weights

$\{w_k^i, \ i = 0, \ldots, N_s\}$ and $x_{0:k} = \{x_j, \ j = 0, \ldots, k\}$ is the set of all states up to time $k$. The weights are normalised such that $\sum_i w_k^i = 1$. The weight is chosen using the principle of important sampling and $q(.)$ is the important density. Weight is assigned such that [118]:

$$w_k^i \ \propto \ w_{k-1}^i \ \frac{p\left(z_k \mid x_k^i\right) p(x_k^i | x_{k-1}^i)}{q(x_k^i | x_{k-1}^i, z_k)} \tag{9}$$

# Matlab Code − Kalman Filter

```
clear
norcur = csvread(filename);
length = 1361;
Q = 1;
R = 1; % Adjust R for Degree of Damping

    for n = 1: 1: length;

    z(n) = norcur(n);

    end;

    for n = 1: 1: length;

    index(n) = n;

    end;

    Pmin1 = 0;

    K = 1

    Xhat(1) = norcur(1) + K*(z(1) - norcur(1))
```

```
P = (1-K)*Pmin1

Pmin = P + Q

Xhatmin(1) = Xhat(1)

for n = 2: 1: length;

K = 1/(n+1);

Xhat(n) = Xhatmin(n-1) + K*(z(n) - Xhatmin(n-1));

P = (1-K)*Pmin;

Pmin = P + Q;

Xhatmin(n) = Xhat(n);

end;
```

# References

[1] E. F. Schubert. *Light Emitting Diodes*. Cambridge University Press, 2006. ix, x, 33, 34, 65, 73, 74

[2] Roland Haitz, Fred Kish, Jeff Taso, and Jeff Nelson. The case for a national research program on semiconductor lighting. In *Annual Forum of the Optoelectronics Industry Development Association*, pages 1–22, 1999. ix, 35, 36

[3] Roland Haitz and Jeffrey Y. Tsao. Solid-state lighting: The case 10 years after and future prospects. *Physica Status Solidi (A)*, 208:17–29, 2011. ix, 36, 37

[4] Audi and Car Body Design. Audi: light and design, December 2008. ix, 38, 39, 40

[5] Viknesh Vijayenthiran. A look at the new led headlights on the lexus ls600h, May 2007. ix, 40

[6] Ookaboo. Virgin america airbus a320 economy class enhanced cabin with led lighting, December 2009. ix, 41

[7] Boeing. Show highlights 2012, December 2011. ix, 42

[8] Randy Tinseth. Bsi: Seattle, April 2009. ix, 42

[9] Atg Airports. Airfield lighting control systems and runway lighting and portable lighting. ix, 43

[10] Green Bright. Led refrigeration lighting project, August 2009. ix, 44

[11] Philips. Lighting food. brightening faces, January 2011. ix, 44, 45

[12] Meditech Asia. Surgical operating lights: The new era in operating room lighting. ix, 46

[13] Tylene Levesque. Led traffic lights take to taiwan, October 2007. ix, 46

[14] TAPCO. Intelligent traffic systems. ix, 47

[15] Traffic Technology Today. Led traffic message boards. x, 47

[16] Ed Ebrahimian. Best practice: Led street lighting system, February 2011. x, 48, 49

[17] THE CLIMATE GROUP. China's clean revolution, November 2011. x, 48, 49

[18] Ed Hare. Failure analysis of LEDs. Technical report, Failure Analysis and Scanning Electron Microscopy - SEM Lab, 2004. x, 66, 67, 68, 69, 70, 71, 72, 73, 75

[19] Liang Tang, Gregory J. Kacprzynski, Kai Goebel, Abhinav Saxena, Bhaskar Saha, and George Vachtsevanos. Prognostics-enhanced automated contingency management for advance autonomous systems. In *Proceeding of 2008 International Conference on Prognostics and Health Management (PHM)*, pages 1–9, 2008. 2, 78

[20] Herbert Hecht. Why prognostics for avionics? In *Proceeding of IEEE Aerospace Conference*, pages 1–6, 2006. 2

[21] Herbert Hecht. Prognostics for electronic equipment: An economic perspective. In *Proceeding of Reliability and Maintainability Symposium (RAMS)*, pages 165–168, 2006. 2

[22] Jeung-Mo Kang, Jae-Wook Kim, Jeong-Hyeon Choi, Du-Hyun Kim, and Ho-Ki Kwon. Life-time estimation of high-power blue light-emitting diode chips. *Microelectronics Reliability*, 49:1231–1235, 2009. 3, 25, 26

[23] Guo Weling, Jia Xuejiao, Yin Fei, Cui Bifeng, Gao Wei, Liu Ying, and Yan Weiwei. Characteristics of high power LEDs at high and low temperature. *Journal of Semiconductors*, 32:1–3, 2011. 3, 22, 28

[24] Nadarajah Narendran and Yimin Gu. Life of LED-based white light source. *Display Technology*, 1:167–171, 2005. 4, 22, 24, 124

[25] Nikhil Vichare, Peter Rodgers, Valerie Eveloy, and Michael Pecht. Environment and usage monitoring of electronic products for health assessment and product design. *Quality Technology and Quantitative Management*, 4:235–250, 2007. 13, 16

[26] Jose R. Celaya, Abhinav Saxena, Philip Wysocki, Sankalita Saha, and Kai Goebel. Towards prognostics of power MOSFETs: Accelerated aging and precursors of failure. In *Proceeding of Annual Conference of the Prognostics and Health Management Society*, pages 1–10, 2010. 13, 82

[27] Vasilis A. Sotiris, Peter Tse, and Michael Pecht. Anomaly detection through a bayesian support vector machine. *Journal of Transaction on Reliability*, 1:1–11, 2010. 13, 79

[28] Jose R. Celaya, Abhinav Saxena, Sankalita Saha, and Kai F. Goebel. Prognostics of power MOSFETs under thermal stress accelerated aging using data-driven and model-based methodologies. In *Proceeding of Annual Conference of the Prognostics and Health Management Society*, pages 1–10, 2011. 13, 14, 15, 81, 112

[29] Kai Goebel, Bhaskar Saha, and Abhinav Saxena. A comparision of three data-driven techniques for prognostics. In *Proceeding of 62nd Meeting of the Society for Machinery Failure Prevention Technology (MFPT)*, pages 119–131, 2008. 14, 81, 100, 105

[30] Mark A. Schwabacher. A survey of data-driven prognostics. In *Proceeding of InfoTech@Aerospace Conference, American Institute of Aeronautics and Astronautics*, pages 1–5, 2005. 14, 100

[31] Mark A. Schwabacher and Kai Goebel. A survey of artificial intelligence for prognostics. In *Proceeding of AAAI Fall Symposium*, pages 1–8, 2007. 14, 100

[32] Niranjan Roy and Ranjan Ganguli. Filter design using radial basis function neural network and genetic algorithm for improved operational health monitoring. *Applied Soft Computing*, 6:154–169, 206. 14

[33] Hoon Sohn, Keith Worden, and Charles R. Farrar. Novelty detection under changing environment conditions. In *Proceeding of SPIE's 8th International Symposium on Smart Structures and Material*, pages 1–11, 2001. 14, 15

[34] Setu Madhavi Namburu, Mark Wilcutts, Shunsuke Chigusa, Liu Qiao, Kihoon Choi, and Krishna Pattipati. Systematic data-driven approach to real-time fault detection and diagnosis in automotive engines. In *Proceeding of IEEE Autotestcon*, pages 59–65, 2006. 15

[35] Setu Madhavi Namburu, Shunsuke Chigusa, Danil Prokhorov, Liu Qiao, Kihoon Choi, and Krishna Pattipati. Application of an effective data-driven approach to real-time fault diagnosis in automotive engines. In *Proceeding of IEEE Aerospace Conference*, pages 1–9, 2007. 15

[36] Bo Ling, Michael Khonsari, and Ross Hathaway. Data-driven roller bearing diagnosis using degree of randomness and laplace test. In *Proceeding of Annual Conference of the Prognostics and Health Management Society*, pages 1–8, 2009. 15, 81

[37] Bor Yann Liaw, Ganesan Nagasubramanian, Rudolph G. Jungst, and Daniel H. Doughty. Modeling of lithium ion cells-a simple equivalent-circuit model approach. *Solid State Ionics*, 175:835–839, 2004. 15, 114

[38] Chetan Kulkarni, Gautam Biswas, Xenofon Koutsoukos, Kai Goebel, and Jose Celaya. Physics of failure models for capacitor degradation in dc-dc converters. In *Proceeding of The Maintenance and Reliability Conference (MARCON)*, pages 1–13, 2010. 15, 112

[39] Lorenzo Borello, Matteo Dalla Vedova, Giovanni Jacazio, and Massimo Sorli. A prognostic model for electrohydraulic servovalves. In *Proceeding of Annual Conference of the Prognostics and Health Management Society*, pages 1–12, 2009. 15, 112

[40] Matthew J. Daigle and Kai Goebel. A model-based prognostics approach applied to pneumatic valves. *International Journal of Prognostics and Health Management*, 8:1–16, 2011. 15, 112

[41] Jianhui Luo, Madhavi Namburu, Krishna Pattipati, Liu Qiao, and Masayuki Kawamoto ans Shunsuke Chigusa. Model-based prognostic techniques. In *Proceeding of IEEE Systems Readiness Technology Conference : Autotestcon*, pages 1–11, 2003. 15, 16

[42] Jianhui Luo, Krishna R. Pattipati, Liu Qiao, and Shunsuke Chigusa. Model-based prognostic techniques applied to a suspension system. *IEEE Transactions on Systems, Man, and Cybernetics - Part A: Systems and Humans*, 38:1156–1168, 2008. 15, 16

[43] Bhaskar Saha, Kai Goebel, and Jon Christophersen. Comparison of prognostic algorithms for estimating remaining useful life of batteries. *Transactions of the Institute of Measurement  Control*, 31:293–308, 2009. 16, 17

[44] Jose R. Celaya, Chetan Kulkarni, Gautam Biswas, Sankalita Saha, and Kai Goebel. A model-based prognostics methodology for electrolytic capacitors based on electrical overstress accelerated aging. In *Proceeding of Annual Conference of the Prognostics and Health Management Society*, pages 1–9, 2011. 17, 111, 112

[45] Shunfeng Cheng and Michael Pecht. A fusion prognostics method for remaining useful life prediction of electronic products. In *5th Annual IEEE International Conference on Automation Science and Engineering*, pages 102–107, 2009. 17, 18, 107, 108, 119

[46] Nishad Patil, Diganta Das, Chunyan Yin, Hua Lu, Chris Bailey, and Michael Pecht. A fusion approach to IGBT power module prognostics. In

*10th International Conference Thermal, Mechanical and Multi-Physics simulation and Experiments in Microelectronics and Microsystems, EuroSimE*, pages 1–5, 2009. 18

[47] Jiuping Xu and Lei Xu. Health management based on fusion prognostics for avionics systems. *Journal of Systems Engineering and Electronics*, 22:428–436, 2011. 19, 119

[48] Dheeraj Bansal, David J. Evans, and Barrie Jones. A real-time predictive maintenance systems for machine systems. *International Journal of Machine Tools Manufacture*, 44:759–766, 2004. 20

[49] Ioannis A. Raptis and George Vachtsevanos. An adaptive particle filtering-based framework for real-time fault diagnosis and failure prognosis of environmental control systems. In *Proceeding of Annual Conference of the Prognostics and Health Management Society*, pages 1–8, 2011. 20

[50] Jurgen Remmlinger, Michael Buchholz, Markus Meiler, Peter Bernreuter, and Klaus Dietmayer. State-of-health monitoring of lithium-ion batteries in electric vehicles by on-board internal resistance estimation. *Journal of Power Sources*, 196:5357–5363, 2011. 20, 21

[51] Juha Voutilainen, Jussi Putaala, Markku Moilanen, and Heli Jantunen. A prognostic method for the embedded failure monitoring of solder interconnections with 1149.4 test bus architecture. *Microelectronics Journal*, 40:1069–1080, 2009. 21, 22

[52] Nadarajah Narendran, Yimin Gu, Lalith Jayasinghe, Jean Paul Freyssinier, and Yiting Zhu. Long-term performance of white LEDs and systems. In *First International Conference on white LEDs and solid state lighting*, pages 174–179, 2007. 22

[53] N. Narendran, Y. Gu, J. P. Freyssinier, H. Yu, and L. Deng. Solid-state lighting: failure analysis of white LED. *Journal of Crystal Growth*, 268:449–456, 2004. 22, 23, 24

[54] Nadarajah Narendran, L. Deng, R. M. Pysar, Y. Gu, and H. Yu. Performance characteristics of high-power light-emitting diodes. In *Third International Conference on Solid State Lighting*, pages 93–99, 2004. 22

[55] Eugene Hong and Nadarajah Narendran. A method for projecting useful life of LED lighting systems. In *Third International Conference on Solid State Lighting*, pages 267–275, 2004. 22

[56] Lalith Jayasinghe, Tianming Dong, and Nadarajah Narendran. Is the thermal resistance coefficient of high-power LEDs constant? In *Seventh International Conference on Solid State Lighting*, 2007. 22, 125

[57] Lalith Jayasinghe, Yimin Gu, and Nadarajah Narendran. Characterization of thermal resistance coefficient of high-power LEDs. In *Sixth International Conference on Solid State Lighting*, 2006. 22, 125

[58] ASSIST. LED life for general lighting. *ASSIST Recommendation*, 1, 2005. 22, 23, 61

[59] ASSIST. Recommendations for testing and evaluating white LED light engines and integrated LED lamps used in decorative lighting luminaires. *ASSIST Recommendation*, 4, 2009. 22, 23

[60] Gang Niu, Ming Lu, Daniel Lau, and Michael Pecht. Prognostics-based qualification for LED lighting systems. In *International Microsystems, Packaging and Assembly and Circuit Technology Conference*, pages 1–4, 2009. 22

[61] Jiajie Fan, K. C. Yung, and Michael Pecht. Physics-of-failure-based prognostics and health management of high-power white light-emitting diode lighting. *IEEE Transaction on Device and Material Reliability*, 11:407–416, 2011. 22, 26, 27, 66, 68

[62] M. Meneghini, L. Trevisanello, C. Sanna, G. Mura, M. Vanzi, G. Meneghesso, and E. Zanoni. Hight temperature electro-optical degradation of InGaN/GaN HBLEDs. *Microelectronic Reliability*, 47:1625–1629, 2007. 22, 24, 29

[63] Cher Ming Tan, Boon Khai Eric Chen, Gan Xu, and Yuanjie Liu. Analysis of humidity effects on the degradation of high-power white LEDs. *Microelectronic Reliability*, 49:1226–1230, 2009. 22, 25, 29

[64] S. I. Chan, W. S. Hong, K. T. Kim, Y. G. Yoon, J. H. Han, and J. S. Jang. Accelerated life test of high power white light emitting diodes based on package failure mechanisms. *Microelectronics Reliability*, 51:1806–1809, 2011. 22, 28, 29

[65] Daniel L. Barton, Marek Osinski, Piotr Perlin, Petr G. Eliseev, and Jinhyun Lee. Single-quantum well InGaN green light emitting diode degradation under high electrical stress. *Microelectronic Reliability*, 39:1219–1227, 1999. 22, 29

[66] M. Meneghini, S. Podda, A. Morelli, R. Pintus, L. Trevisanello, G. Meneghesso, M. Vanzi, and E. Zanoni. Hight brightness GaN LEDs degradation during dc and pulsed stress. *Microelectronic Reliability*, 46:1720–1724, 2006. 22, 29

[67] Moon-Hwan Chang, Diganta Das, P. V. Varde, and Michael Pecht. Light emitting diodes reliability review. *Microelectronics Reliability*, 52:762–782, 2012. 27, 37, 63, 66, 67, 68, 73, 121

[68] X. A. Cao, P. M. Sandvik, S. F. LeBoeuf, and S. D. Arthur. Defect generation in InGaN/GaN light-emitting diodes under forward and reverse electrical stress. *Microelectronics Reliability*, 43:1987–1991, 2003. 29

[69] Jae-Seong Jeong, Jin-Kyu Jung, and Sang-Deuk Park. Reliability improvement of InGan LED backlight module by accelerated life test (alt) and screen policy of potential leakage LED. *Microelectronics Reliability*, 48:1216–1220, 2008. 29

[70] E. Nogueira, M. Vazquez, and N. Nunez. Evaluation of AlGaInP LEDs reliability based accelerated tests. *Microelectronics Reliability*, 49:1240–1243, 2009. 29

[71] M. Vazquez, N. Nunez, E. Nogueira, and A. Borreguero. Degradation of AlInGaP red LEDs under drive current and temperature. *Microelectronics Reliability*, 50:1559–1562, 2010. 30

[72] F. K. Yam and Z. Hassan. Innovative advances in LED technology. *Microelectronics Journal*, 36:129–137, 2005. 33

[73] McKinsey & Company. Lighting the way: Perspectives on the global lighting market, July 2011. 35

[74] LEDs Magazine. Cree reports rd result of 231 lm/w efficacy for white led, May 2011. 36

[75] John F. Van Derlofske and Michele McColgan. White LED sources for vehicle forward lighting. In *Proceedings of SPIE: Solid State Lighting II*, pages 195–205, 2002. 37

[76] Wikipedia. Headlamp, September 2012. 38

[77] NGLIA. LED luminaire lifetime: Recommendations for testing and reporting. Technical report, Next Generation Lighting Industry Alliance with U. S. Department of Energy, 2011. 60, 62, 124

[78] IES. Approved meothd: Measuring lumen maintenance of led light sources. Technical report, Illuminating Engineering Society, 2008. 61, 124

[79] Guoguang Lu, Shaohua Yang, and Yun Huang. Analysis on failure modes and mechanisms of LED. In *8th International Conference on Reliability, Maintainability and Safety ICRMS 2009*, pages 1237–1241, 2009. 65, 66

[80] David S. Meyaard, Qifeng Shan, Qi Dai, Jaehee Cho, E. Fred Schubert, Min-Ho Kim, and Cheolsoo Sone. On the temperature dependence of electron leakage from the active region of GaInN/GaN light-emitting diodes. *Applied Physics Letters*, 99:1–3, 2011. 66

[81] Nikhil M. Vichare, Peter Rodgers, and Michael G. Pecht. Methods for binning density estimation of load parameters for prognostics and health

management. *International Journal of Performability Engineering*, 2:149–161, 2006. 77, 78, 93, 97

[82] Michael G. Pecht. A prognostics and health management roadmap for information and electronics-rich systems. *IEICE Fundamentals Review*, 3:25–32, 2010. 79, 81, 116

[83] Michael Pecht and Sachin Kumar. Data analysis approach for systems reliability, diagnostics and prognostics. In *Pan Pacific Microelectronics Symposium*, pages 1–9, 2008. 81

[84] Carl S Byington, Matthew Watson, and Doug Edwards. Data-driven neural network methodology to remaining life predictions for aircraft actuator components. In *IEEE Aerospace Conference*, pages 1–10, 2004. 81

[85] Mohammed A. Alam, Michael H. Azarian, Michael Osterman, and Michael Pecht. Progostics of failures in embedded planer capacitors using model-based and data-driven approaches. *Journal of intelligent Material Systems and Structures*, 22:1293–1304, 2011. 81, 112

[86] Chaitanya Sankavaram, Bharath Pattipati, Anuradha Kodali, Krishna Pattipati, Mohammad Azam, Sachin Kumar, and Michael Pecht. Model-based and data-driven prognosis of automotive and electronic systems. In *5th Annual IEEE Conference on Automation Science and Engineering*, pages 96–101, 2009. 81, 112

[87] Michael G. Pecht. *Prognostics and Health Management of Electronics*. John Wiley & Sons, 2008. 81, 82, 90, 91, 92, 97, 98, 99, 112, 116, 119

[88] Abhinav Saxena, Kai Goebel, Don Simon, and Neil Eklund. Damage propagation modeling for aircraft engine run-to-failure simulation. In *International Conference on Prognostics and Health Management*, pages 1–9, 2008. 82

[89] Bhaskar Saha and Kai Goebel. Prognostics HIL testbed. In *Aviation Safety 2009 IVHM Posters*, pages 1–1, 2009. 82, 112

[90] Bhaskar Saha and Kai Goebel. Model adaptation for prognostics in a particle filtering framework. *International Journal of Prognostics and Health Management*, 6:1–10, 2011. 82, 112

[91] Markos Markou and Sameer Singh. Novelty detection: a review. *Signal Processing*, 83:2481–2521, 2003. 83, 85, 92, 97, 101, 110

[92] David A. Clifton, Lei A. Clifton, Peter R. Bannister, and Lionel Tarassenko. Automated novelty detection in industrial systems. *Studies in Computational Intelligence*, 116:269–296, 2008. 83, 90

[93] V. N. Vapnik. *Statistical Learning Theory*. Wiley-Interscience, 1998. 83, 101

[94] Christopher M. Bishop and Michael E. Tipping. Variational relevance vector machines. In *Proceedings of the 16th Conference on Uncertainty in Artificial Intelligence*, pages 46–53, 2000. 83

[95] Varun Chandola, Arindam Banerjee, and Vipin Kumar. Anomaly detection: A surevey. *ACM Computing Surveys*, 41:15:1–58, 2009. 84, 93, 97, 98, 102

[96] Hyunseok Oh, Michael H. Azarian, and Michael Pecht. Estimation of fan bearing degradation using acoustic emission analysis and Mahalanobis distance analysis. In *The Applied System Health Management Conference*, pages 1–12, 2011. 85

[97] Gang Niu, Daniel Lau, and Michael Pecht. Prognostics and health management for next generation LED lighting systems. *Microelectronics Reliability*, 50:132–139, 2009. 85

[98] Lei Nie, Michael H. Azarian, Mohammadreza Keimasi, and Michael Pecht. Prognostics of ceramic capacitor temperature-humidity-bias reliability using Mahalanobis distance analysis. *Circuit World*, 33:21–28, 2007. 85

[99] R. De Maesschalck, D. Jouan-Rimbaud, and D. L. Massart. The Mahalanobis distance. *Chemometrics and Intelligent Laboratory Systems*, 50:1–18, 2000. 85

[100] G. E. P. Box and S. L. Andersen. Permutation theory in the derivation of robust criteria and the study of departures from assumption. *Journal of the Royal Statistical Society*, 17:1–34, 1955. 85, 86

[101] Stephen J. Roberts. Novelty detection using extreme value statistics. In *IEE Proceedings on Vision, Image and Signal Processing*, pages 124–129, 1999. 90, 92

[102] Hyoung J. Lee and Stephen J. Roberts. On-line novelty detection using the kalman filter and extreme value theory. In *19th International Conference on Pattern Recognition*, pages 1–4, 2008. 90

[103] Suyash P. Awate, 2006. Adaptive Nonparametric Markov Models and Information-Theoretic Methods for Image Restoration and Segmentation. 90, 91

[104] Dit-Yan Yeung and Calvin Chow. Parzen-window network intrusion detectors. In *16th International Conference on Pattern Recognition*, pages 385–388, 2002. 92, 93

[105] Shyam Boriah, Varun Chandola, and Vipin Kumar. Similarity measures for categorical data: A comparative evaluation abstract. In *In SIAM Data Mining Conference*, pages 243–254, 2008. 98

[106] Yongqiang Tang. Size and power estimation for the Wilcoxon-Mann-Whitney test for ordered categorical data. *Statistics in Medicine*, 30:3461–3470, 2011. 98

[107] Arthur L. Samuel. Some studies in machine learning using the game of checkers. *IBM Journal of Research and Development*, 44:206–226, 2000. 98

[108] A. Blum and T. Mitchell. Combining labeled and unlabeled data with co-training. In *Proceedings of the Eleventh Annual Conference on Computational Learning Theory*, pages 92–100, 1998. 99

[109] Christopher M. Bishop. *Pattern Recognition and Machine Learning.* Springer, 2007. 99, 100, 105, 107, 108, 109, 110

[110] Jihong Yan, Muammer Koc, and Jay Lee. A prognostics algorithm for machine performance assessment and its application. *Production Planning Control*, 15:796–801, 2004. 100

[111] Michael I. Jordan and Christopher M. Bishop. *Neural networks*. CRC Press, 1997. 100, 101

[112] Christopher J. C. Burges, 1998. A Tutorial on Support Vector Machines for pattern recognition. 102, 103

[113] Michael E. Tipping. Sparse Bayesian learning and the relevance vector machine. *Journal of Machine Learning Research*, 1:211–244, 2001. 105

[114] Carl Edward Rasmussen and Christopher K. I. Williams. *Gaussian Processes for Machine Learning*. MIT Press, 2006. 105

[115] C. K. I. Williams, 1997. Prediction with Gaussian processes: from linear regression to linear prediction and beyond. 105

[116] Xiaobin Tan and Hongsheng Xi. Hidden semi-Markov model for anomaly detection. *Applied Mathematics and Computing*, 205:562–567, 2008. 108

[117] R. E. Kalman. A new approach to linear filtering and prediction problem. *Transaction of the ASME-Journal of Basic Engineering*, 82:35–45, 1960. 110

[118] M. Sanjeev Arulampalam, Simon Maskell, Neil Gordon, and Tim Clapp. A tutorial on particle filtering for online nonlinear/non-Gaussian Bayesian tracking. *IEEE Transaction on Signal Processing*, 50:174–188, 2002. 111, 112, 235, 236

[119] Pradeep Lall, Ryan Lowe, and Kai Goebel. Prognostics using Kalman-filter models and matrics for risk assessment in BGAs under shock and vibration loads. In *Electronic Components and Technology Conference*, pages 889–901, 2010. 111

[120] Marcos E. Orchard and George J. Vachtsevanos. A particle-filtering approach for on-line fault diagnosis and fault prognosis. *Transaction of the Institute of Measurement and Control*, 31:221–246, 2009. 111

[121] Marcos E. Orchard, Liang Tang, and George J. Vachtsevanos. A combined anomaly detection and failure prognosis approach for estimation of remaining useful life in energy storage devices. In *Annual Conference of the Prognostics and Health Management Society*, pages 1–7, 2011. 112, 119

[122] Marcos E. Orchard, Biqing Wu, and George J. Vachtsevanos. A particle filtering framework for failure prognosis. In *Proceeding of World Tribology Congress III*, pages 1–2, 2005. 112

[123] Guangfan Zhang, Chiman Kwan, Roger Xu, Nikhil Vichare, and Michael Pecht. A enhanced prognostic model for intermittent failure in digital electronics. In *IEEE Aerospace conference*, pages 1–9, 2007. 112

[124] Jayanth Srinivasan, Sarita V. Adve, Pradip Bose, Jude Rivers, and Chao-Kun Hu, 2003. RAMP: A Model for reliability aware microprocessor design. 117, 118

[125] Arvind Sai Sarathi Vasan and Michael Pecht. Investigation of stochastic differential models and a recursive nonlinear filtering approach for fusion-prognostics. In *Annual Conference of the Prognostics and Health Management Society*, pages 1–3, 2011. 119

[126] IES. Approved meothd: Electrical and photometric measurements of solid-state lighting products. Technical report, Illuminating Engineering Society, 2008. 124

[127] IES. Projecting long term lumen maintenance of led light sources. Technical report, Illuminating Engineering Society, 2011. 124

[128] Y. Xi and E. F. Schubert. Junction-temperature measurement in GaN ultra-violet light-emitting diodes using diode forward voltage method. *APPLIED PHYSICS LETTERS*, 85:2163–2165, 2004. 124

[129] Yangang Xi, Thomas Gessmann, Jingqun Xi, Jong Kyu Kim, Jay M. Shan, E. Fred Schubert, Arthur J. Fischer, Mary H. Crawford, Katherine H. A. Bogart, and Andrew A. Allerman. Junction temperature in ultraviolet light-emitting diodes. *Japanese Journal of Applied Physics*, 44:7260–7266, 2005. 126

[130] National Instruments. Labview fpga course manual, May 2009. xiii, xiv, 207, 218, 219, 221

[131] Microchip. Pic32, May 2009. xiv, 229

[132] Raul Rojas, 2003. The Kalman Filter. 234